UNIVERSITÉ CATHOLIQUE DE LOUVAIN
FACULTY OF SCIENCE, DEPARTMENT OF GEOGRAPHY
EARTH AND LIFE INSTITUTE
GEORGES LEMAÎTRE CENTRE FOR EARTH AND CLIMATE RESEARCH

STUDY OF THE VARIATIONS IN THE ANTARCTIC SNOW ACCUMULATION AND ITS LINKS WITH CLIMATE CHANGE IN THE SOUTHERN HEMISPHERE OVER THE PAST CENTURIES

DOCTORAL DISSERTATION PRESENTED BY

QUENTIN DALAIDEN

IN PARTIAL FULFILLMENT OF THE
REQUIREMENTS FOR THE DEGREE OF
DOCTOR IN SCIENCES

THESIS COMMITTEE:

Prof. Hugues Goosse (Supervisor)	Université catholique de Louvain
Prof. Marie-Laurence De Keersmaecker (Chair)	Université catholique de Louvain
Dr. Jan Lenaerts	University of Colorado, Boulder, USA
Prof. Thierry Fichefet	Université catholique de Louvain
Dr. Hubert Gallée	Université de Grenobles Alpes, France
Prof. Qiuzhen Yin	Université catholique de Louvain

LOUVAIN-LA-NEUVE
APRIL 2021

Je voudrais dans un premier temps remercier mon promoteur de thèse Hugues Goosse qui m'a offert l'opportunité de travailler sur un sujet plus que fascinant, ainsi qu'un accompagnement idéal tout au long de cette thèse. Hugues, merci pour ton optimisme, ta bonne humeur au quotidien, ton enthousiasme et pour les nombreuses discussions plus intéressantes les unes que les autres. Merci d'avoir fait naître des collaborations et opportunités scientifiques stimulantes.

I would also like to thank Jan Lenaerts who started to help me from the early beginning of my thesis. Jan, thank you for the great expertise from which I learnt a lot and for taking the time and energy to read and participate in my work since the beginning. I would also like to thank Liz Thomas from who I learnt much about ice cores and their use.

I would like to thank the other committee members, Thierry Fichefet, Qiuzhen Yin and Hubert Gallée for the careful reading of my manuscript and for their relevant comments that definitively improved the quality of the present work. Je remercie également Marie-Laurence de Keersmaecker d'avoir encadré la défense de thèse dans une atmosphère conviviale.

Un grand merci à Dominique et Monique pour tout ce qu'elles ont fait et font pour nous, et qui rend notre quotidien tellement plus appréciable au Mercator.

Je voudrais également remercier le Fonds de la Recherche Scientifique (F.R.S.-FNRS) qui a financé cette thèse de doctorat. Le projet Mass2Ant est également remercié.

Je ne pourrais oublier de remercier l'ensemble de mes collègues pour la bonne ambiance qui règne au bureau, et bien entendu, hors bureau.

Finalement, je voudrais remercier mes proches pour le soutien avec une dédicace toute particulière à J.

Contents

Contents iii

List of abbreviations v

1 Introduction 1
- 1.1 The Antarctic Ice Sheet . . . 2
- 1.2 Snow accumulation on the Antarctic Ice Sheet . . . 4
- 1.3 Current surface climate changes in the Antarctic . . . 11
- 1.4 The Antarctic snow accumulation from ice cores . . . 14
- 1.5 Climate models and future Antarctic snow accumulation . . . 15
- 1.6 Objectives and outlines of this thesis . . . 19
- 1.7 Data and methods . . . 24

2 Snow accumulation-surface temperature relationship 33
- 2.1 Introduction . . . 34
- 2.2 Data: model simulations and observations . . . 37
- 2.3 Methods . . . 41
- 2.4 Results . . . 43
- 2.5 Discussion and conclusions . . . 54

3 West Antarctic climate reconstruction over the past 200 years 59
- 3.1 Introduction . . . 60
- 3.2 Data assimilation method . . . 63
- 3.3 Results and discussion . . . 72
- 3.4 Conclusions . . . 91

4 Snow accumulation increase explained by storms systems 95
- 4.1 Introduction . . . 96
- 4.2 Methods . . . 98

4.3 Results . . . 102
4.4 Discussion . . . 109

5 Conclusions and perspectives 111
5.1 Main achievements . . . 111
5.2 General conclusions . . . 114
5.3 Perspectives . . . 116

A Supplement to Chapter 2 119
A.1 Statistical surface temperature reconstructions from Stenni et al. [2017] . . . 119
A.2 Defining uncertainties associated with proxy data used during data assimilation process . . . 120
A.3 Present-day AIS SMB simulated by GCMs . . . 120
A.4 Supplementary figures . . . 122
A.5 Supplementary tables . . . 136

B Supplement to Chapter 3 141
B.1 Supplementary figures . . . 141

C Supplement to Chapter 4 145
C.1 Role of tropical climate modes of variability on snow accumulation changes . . . 145
C.2 Impact of ozone depletion on Antarctic snow accumulation changes over the last decades . . . 146
C.3 Evaluation of the Antarctic snow accumulation as simulated by selected ESM/GCMs . . . 146
C.4 Evaluation of the *P–E* from the moisture budget . . . 147
C.5 Antarctic moisture budget using climate model simulations . . . 149
C.6 Supplementary figures . . . 150
C.7 Supplementary tables . . . 169

D List of publications related to the thesis 173

References 175

List of abbreviations

AIS	Antarctic Ice Sheet
AP	Antarctic Peninsula
ASL	Amundsen Sea Low
AWS	Automatic Weather Station
CC	Clausius-Clapeyron
CE	Common Era
CESM	Community Earth System Model
CMIP	Coupled Model Intercomparison Project
CMIP5	Coupled Model Intercomparison Project Phase 5
CMIP6	Coupled Model Intercomparison Project Phase 6
DA	Data assimilation
DML	Dronning Maud Land
EAIS	East Antarctic Ice Sheet
ECMWF	Centre for Medium-Range Weather Forecasts
ENSO	El-Niño Southern Oscillation
EPE	Extreme Precipitation Event
ESM	Earth System Model
GCM	General Circulation Model
GrIS	Greenland Ice Sheet
IPCC	Intergovernmental Panel on Climate Change
IPO	Interdecadal Pacific Oscillation
MB	Mass balance
MSA	Methan sulphonic acid
NCAR	National Center for Atmospheric Research
NSIDC	National Snow and Ice Data Center
PMIP3	Paleoclimate Modelling Intercomparison Project Phase 3
RACMO	Regional Atmospheric Climate MOdel
SAM	Southern Annular Mode

SAT	Surface air temperature
SH	Southern Hemisphere
SMB	Surface mass balance
SST	Sea surface temperature
TRW	Tree-ring width
WAIS	West Antarctic Ice Sheet

1

Introduction

According to the latest report of the Intergovernmental Panel on Climate Change (IPCC) on the Ocean and Cryosphere [IPCC, 2019], the global climate is currently undergoing deep changes that are unprecedented in the context of the past two millennia (Fig. 1.1). As reported by the European Centre for Medium-Range Weather Forecasts (ECMWF), 2020 has been 1.25°C warmer than the pre-industrial period. Albeit 2020 was a La-Niña year, which tends to cool the global climate, it is ranked as the second warmest year after 2016, an El-Niño year [ECMWF, 2021].

The global surface warming is only one element of climate change. Over the past decades, for instance, the Earth has witnessed stronger heatwaves [e.g., Schär et al., 2004], Arctic sea-ice extent reduction [Comiso, 2012], deep modification in the global hydrological cycle [Held and Soden, 2006], melting of mountain glaciers [Marzeion et al., 2014], unprecedented bush fires [e.g., Abram et al., 2021], etc... Albeit climate change is observed mostly everywhere, polar regions are particularly vulnerable because of several feedback [e.g., Goosse et al., 2018], in particular the well-known temperature-albedo feedback. Consequently, polar regions are warming faster than anywhere else [Post et al., 2019]. Additionally, polar regions are key components of the climate system as a whole. One example among others is the increasing contribution of the Greenland and Antarctic ice sheets to the global sea-level rise [Shepherd et al., 2020; Rignot et al., 2019]. However, their exact contribution to the global sea-level rise for the 21st century is highly uncertain [e.g., Pattyn and Morlighem, 2020]. It has been estimated that the recent Antarctic snow accumulation increase has partly offset the 20th century sea-level rise [Medley and Thomas, 2019]. It is projected to continue over the 21st century. Though, the underlying mechanisms of the Antarctic snow accumulation

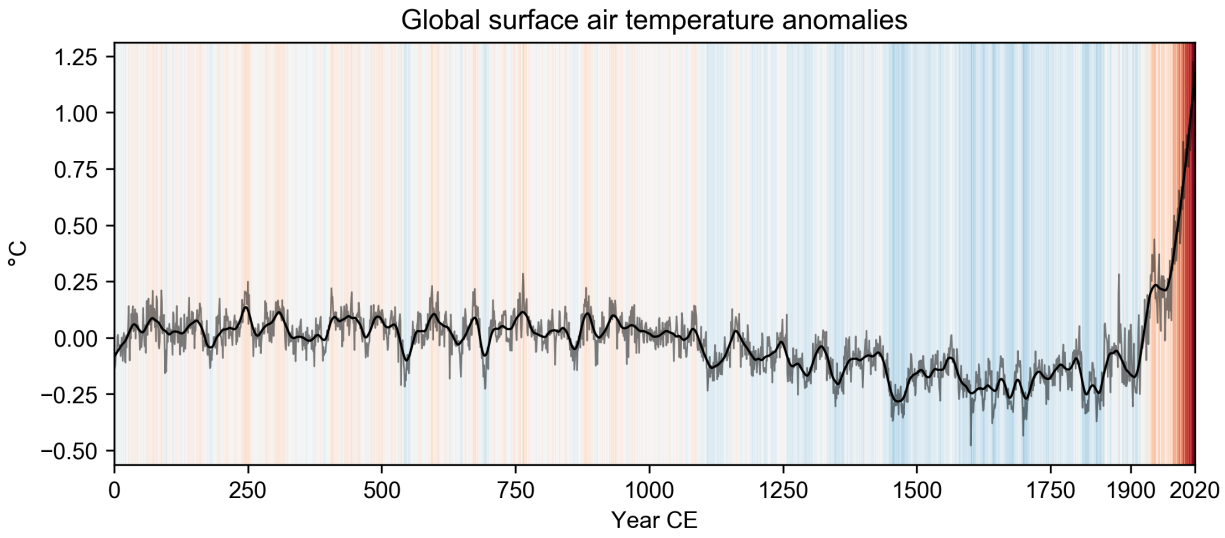


Figure 1.1: *Anomalies of global surface air temperature over the Common Era. For the 1–1849 CE period, the surface temperature reconstruction from Neukom et al. [2019] based on various paleoclimate records (mostly tree-ring width records) is represented. Afterwards, the HadCRUT version 5 dataset [Osborn et al., 2021], which combines all the available surface air temperature observations is used. Anomalies are computed using the 20th century as reference. The thin gray line is the annual mean while the thick black line corresponds to the 30-year smoothed annual time-series using a lowess filter. The colored background represents the anomaly of global surface air temperature; red (blue) corresponds to a positive (negative) anomaly.*

increase are poorly understood, limiting our confidence in the contribution of the Antarctic Ice Sheet to the future sea-level rise. In this context, the present thesis sheds light on the mechanisms that govern the snow accumulation in Antarctica. The Antarctic Ice sheet, the Antarctic snow accumulation along with its variability over the past centuries and for the future are introduced below.

1.1 The Antarctic Ice Sheet

The largest single mass of ice on Earth is located in the Southern Hemisphere and approximately centred on the South Pole (Fig. 1.2). Owing to its size, this ice mass is more commonly defined as an ice sheet, i.e., the Antarctic Ice Sheet (AIS). Through time, the Antarctic continent has received a large amount of snowfall that has accumulated as a result of the extreme cold weather. The fresh snow, compressed by its own weight, is then converted to ice. Over years and years, the glacier originally situated on the most elevated regions, and thus also the coldest areas (i.e., the Plateau), expanded through the entire continent towards the coasts, to ultimately covers 98% of the continent at present [Fretwell et al., 2013]. The

thickness of the ice sheet decreases from the Plateau (maximum thickness: 4776 m) to the coast, with an average thickness of 2160 m [Fretwell et al., 2013]. At the coastline, the ice sheet flows towards the Southern Ocean to form floating ice connected to the ice sheet, called ice shelves. Today, the AIS covers 14 10^6 km^2, which is about 450 times the area of Belgium. The complete melting of the AIS would represent a global sea-level rise of 57 m [Fretwell et al., 2013].

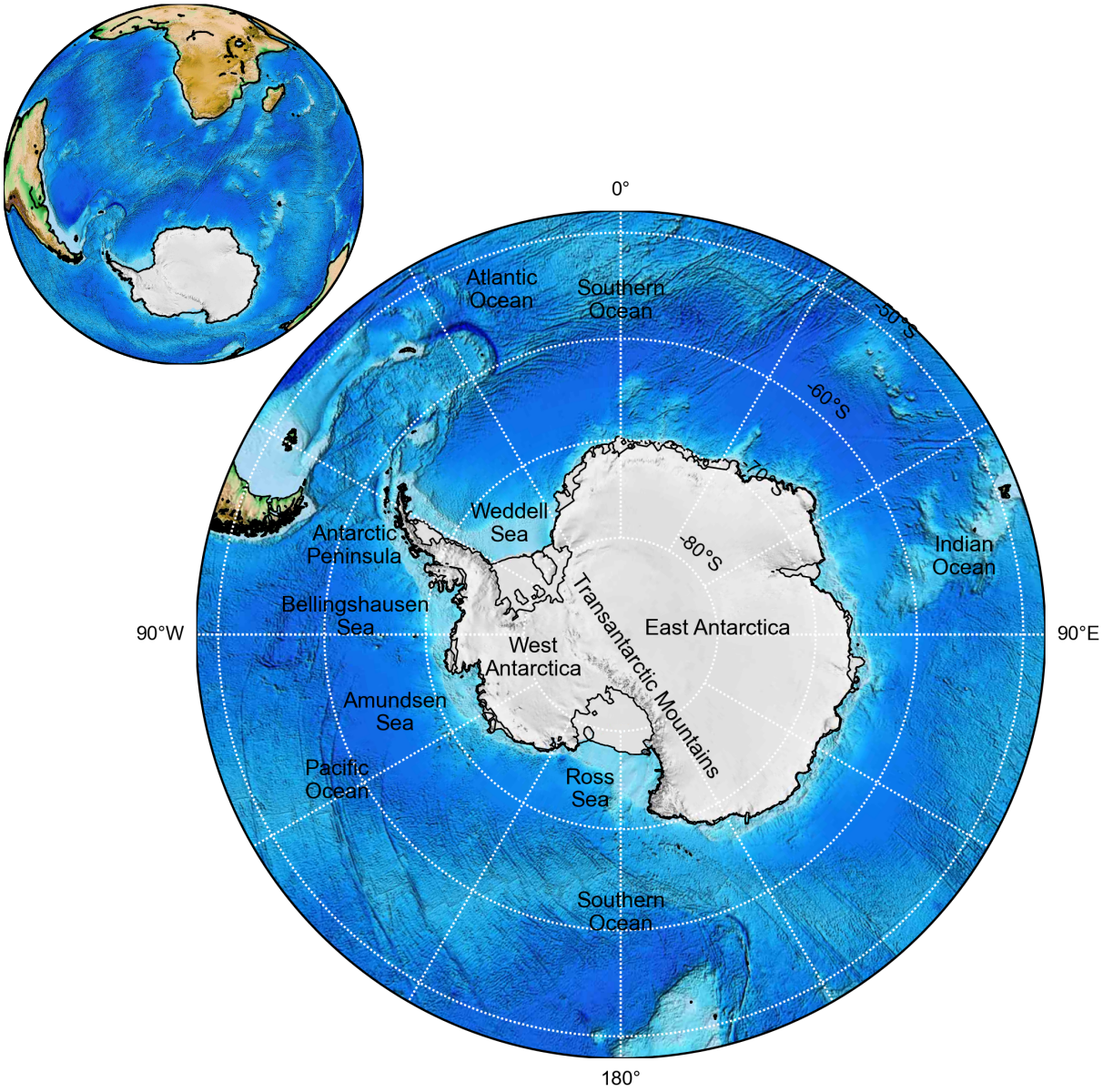


Figure 1.2: *Geographical position of the Antarctic Ice Sheet and the main place names cited in the manuscript. Background map from NOAA National Geophysical Data Center [2009].*

The AIS is usually divided into three regions: West Antarctica, East Antarctica and the Antarctic Peninsula (AP).

- West Antarctica is separated from East Antarctica by the Transantarctic Mountains (Fig. 1.2). This region includes the two largest Antarctic ice shelves, namely the Ross and Ronne-Filchner ice shelves, situated in the Ross Sea and the Weddell Sea sectors, respectively. West Antarctica has an average altitude of around 850 m, making this region prone to important marine air intrusions [Nicolas and Bromwich, 2011a].
- East Antarctica is situated at the East of the Transantarctic Mountains (approximately between 30°W and 165°E). Its coastline roughly follows the 62°S meridian (Fig. 1.2). The altitude of East Antarctica is much higher than West Antarctica and characterized by the presence of the Antarctic Plateau. It covers most of East Antarctica and lies between 2000 m and 4100 m. The name of Plateau comes from the relatively low variations in elevation over this region, that looks like a flat desert where it snows infrequently [e.g., Bromwich, 1988; Palerme et al., 2017a]. In contrast, coastal areas in East Antarctica display a strong variability in elevation due to the presence of ice rises [Matsuoka et al., 2015]. This results in complex interactions between winds and topography. Like West Antarctica, the coastal regions of East Antarctica are substantially subject to marine air intrusions, while the Antarctic Plateau is almost not influenced by these features [e.g., Vannitsem et al., 2019].
- The Antarctic Peninsula is the northward extension of the Antarctic continent towards South America (Fig. 1.2). Its average altitude is 1500 m. Due to the strong variation in elevation over a few kilometres, the Antarctic Peninsula is often perceived as an ice wall rising from the ocean. This region is thus subject to foehn effects, which results in large amounts of snowfall [e.g., van Wessem et al., 2016].

1.2 Snow accumulation on the Antarctic Ice Sheet

The mass balance (MB) of an ice sheet is defined as the difference between the mass gain and the mass loss. The ice sheet reaches its equilibrium when the former equals the later. The AIS gains mass at its surface (referred to as surface mass balance; SMB) and loses mass by ice discharge (D) at its margins when the ice flux crosses the grounding line [Lenaerts et al., 2019]. At that point, the ice starts to float on the ocean. These floating ice platforms connected to the ice sheet are called ice shelves. Over the grounded ice sheet, MB = SMB - D. Ice shelves loss mass not only through icebergs but also by the basal melting due to marine warm water intrusions [Depoorter et al., 2013]. As ice shelves float, MB changes in the ice shelf have no direct impacts on the sea-level. Note that SMB and snow accumulation terms are used interchangeably throughout the manuscript.

Several components contribute to SMB as sketched in Figure 1.3. Ice sheets, including the AIS, mainly gain mass at their surface through snowfall [Palerme et al., 2014; Souverijns et al., 2018], which accumulates over time. Additionally, some areas of the AIS, in particular the Antarctic Plateau, gain mass through diamond dust (riming) [Ricaud et al., 2017]. The main sink of the snow accumulation over the AIS is through a turbulent moisture flux [e.g., van Lipzig et al., 2004; Lenaerts et al., 2012], called sublimation. This process directly depends on the moisture content of the air as well as the wind strength that causes the turbulence resulting in a mixing of the first atmospheric layers. Surface mass lost is also observed when the meltwater – generally resulting from the absorption of solar radiation [e.g., Van den Broeke et al., 2005] – is not retained by the firn (thin fresh layer of snow before snow is compacted and transformed into ice), resulting in runoff towards the ocean. At present, this process is not much seen over the AIS since the majority of meltwater refreezes in the firn. Finally, near-surface winds can influence the SMB in two different ways. Firstly, winds can redistribute snow over the continent (snow erosion and deposition), which it is referred as to blowing snow [e.g., Palm et al., 2018]. Secondly, when snow is transported by the winds, it can potentially be sublimated [Déry and Yau, 1999; Bintanja, 1998], which results in an ice loss. Blowing snow-related processes especially occur during the winter when the near-surface winds are the strongest [e.g., Lenaerts et al., 2010].

All processes taken together, the SMB can be written as follows [Lenaerts et al., 2019]:

$$SMB = P - SU_s - ER_{ds} - SU_{ds} - RU \tag{1.1}$$

where P stands for total precipitation (liquid and solid), SU_s corresponds to the surface loss by sublimation and evaporation – in effect, evaporation is very limited –, ER_{ds} and SU_{ds} are the erosion/deposition and sublimation induced by the near-surface winds (i.e., the blowing snow), respectively, and finally, RU is the meltwater runoff.

The resulting spatial distribution of the Antarctic SMB under present-day conditions is displayed in Figure 1.4. This shows that the Antarctic SMB is roughly everywhere positive – albeit some areas can display negative SMB values temporarily due to local processes. The Antarctic SMB is characterized by a strong negative gradient between the coastal regions, with the highest positive values, and the Antarctic Plateau, with the lowest positive values (Fig. 1.4). At first order, the spatial distribution of SMB nearly follows the spatial distribution of the near-surface air temperature, which is mainly determined by the topography. Consequently, the overall SMB gradient can be explained by the warm coastal regions and cold interior of the AIS, that are therefore characterized by more and less snowfall, respectively, following the Clausius-Clapeyron relationship.

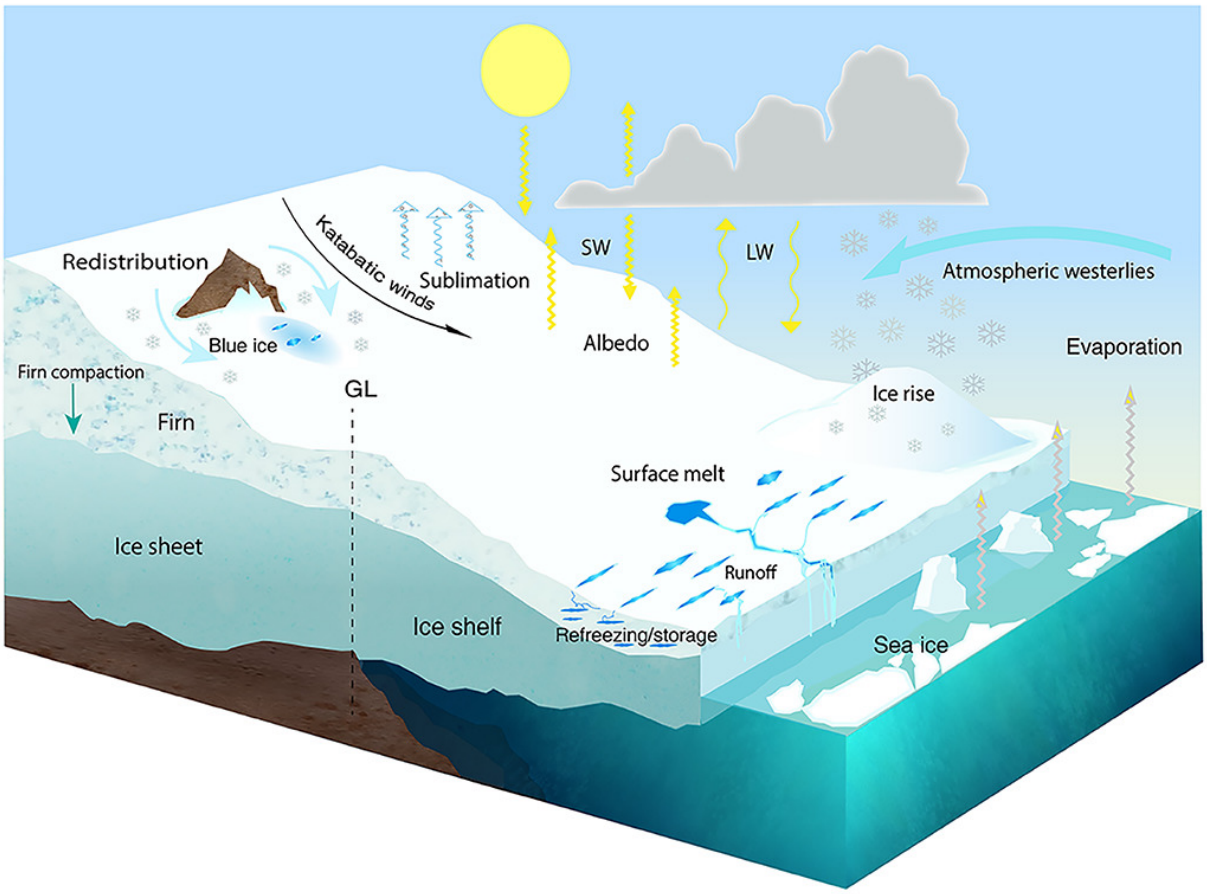


Figure 1.3: *Main relevant surface processes impacting the surface mass balance of the Antarctic Ice Sheet. Figure from Lenaerts et al. [2019].*

However, the near-surface air temperature cannot explain the SMB spatial pattern as a whole. The SMB spatial distribution is also closely related to the interactions between topography and winds [Fyke et al., 2017] (Fig. 1.5). For instance, the western part of the Antarctic Peninsula is on the path of the westerly winds (windward side). Due to the strong elevation gradient in this region, the rising air produces a large amount of snowfall as the moisture content of the air is converted into snow by adiabatic cooling [e.g., van Wessem et al., 2016]. On the contrary, the eastern part of the Antarctic Peninsula (leeward side) receives a smaller amount of snowfall since the air has already lost its moisture content during the uplift. This phenomenon is also observed in a lesser extent along the coasts of East Antarctica because of the presence of ice rises, in particular in the Dronning Maud Land region, as shown by Lenaerts et al. [2014].

When integrated over the whole AIS, the Antarctic SMB corresponds to about 2200 Gt year^{-1}, according to the best estimates [Agosta et al., 2019]. Therefore, even small changes in the Antarctic SMB would have a significant impact on the global sea-level rise.

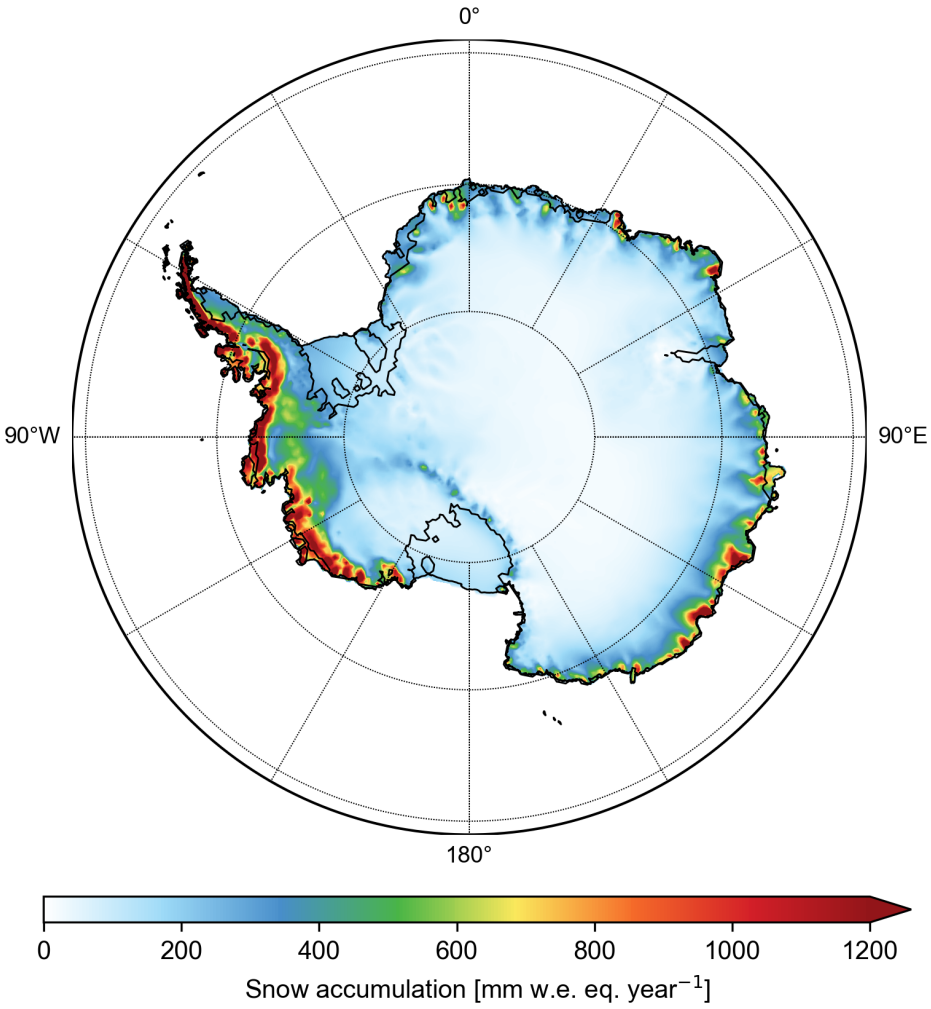


Figure 1.4: *Mean Antarctic snow accumulation over the 1979–2016 CE period (in mm w.e. eq. year^{-1}). Data from the Regional Atmospheric Climate MOdel specifically designed for surface processes in polar regions [van Wessem et al., 2018].*

The main source to SMB is precipitation [Palerme et al., 2014; Souverijns et al., 2018], particularly snowfall as liquid precipitation is very infrequent over the AIS [e.g., Palerme et al., 2014]. At present, the snowfall variability virtually explains all the spatial and interannual variability of the SMB [van Wessem et al., 2018; Agosta et al., 2019]. Overall, to explain the variability of the SMB, the drivers of snowfall must be examined predominantly.

The lower troposphere above the AIS contains little moisture because of the strong cold conditions. As a result, snowfall is strongly governed by the meridional humidity transport from the mid-latitudes to the high-latitudes of the Southern Hemisphere. Therefore, the winds, and more generally the atmospheric circulation, are the main driver of Antarctic snowfall [Bromwich, 1988]. Antarctic snowfall is generally generated from low-pressure systems, most widely called storm systems. Although the storms travel from West to East embedded in the general

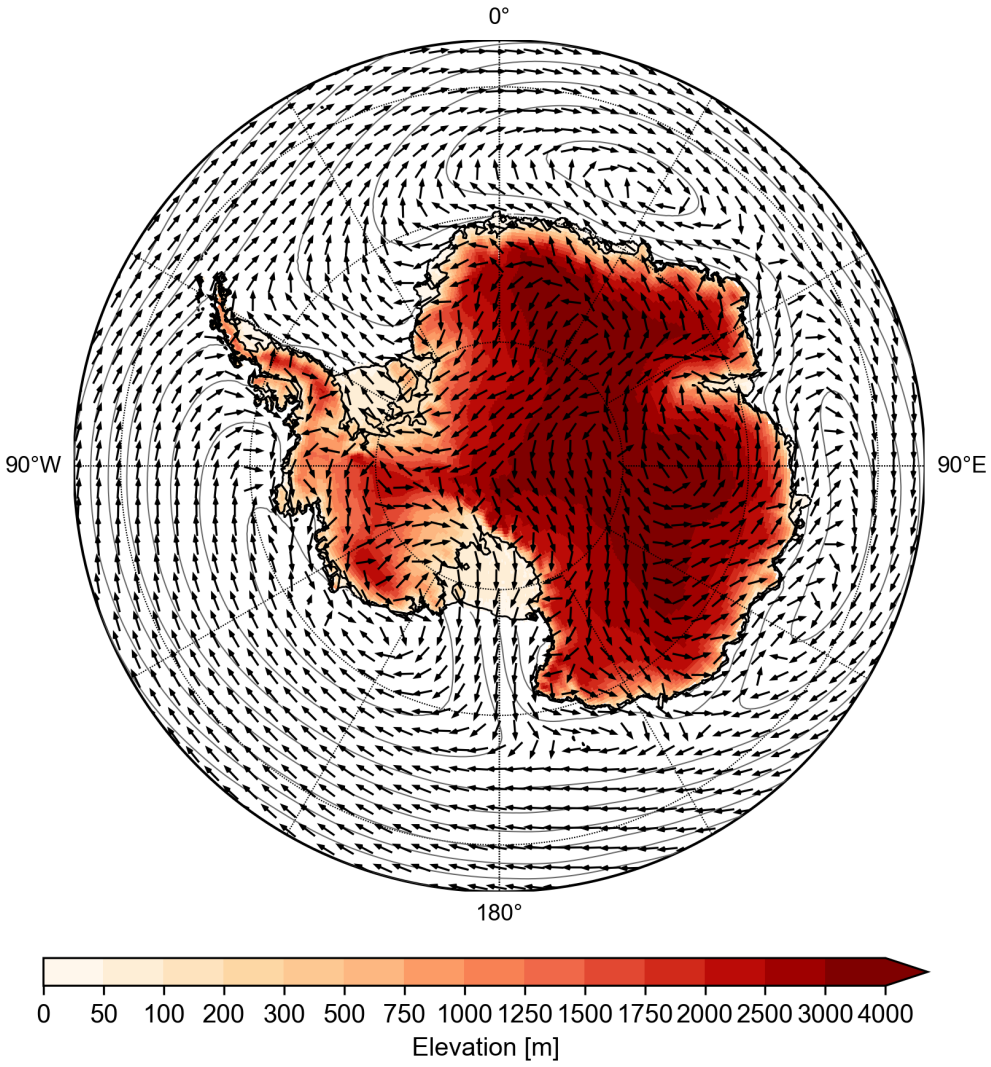


Figure 1.5: *Mean direction of near-surface winds over 1979–2019 CE from the ERA5 reanalysis. The background represents the Antarctic elevation (in m).*

westerly flow, they are also influenced be easterly winds close to the continent and can follow complex paths. This general West-East movement forms a roughly zonal low-pressure belt around the continent.

Three climatological low-pressures emerge within the circumpolar low-pressure belt (Fig. 1.6). This results in a zonal wave three (ZW3) pattern [Raphael, 2004]. One is situated in the South Atlantic Ocean, in front of the Dronning Maud Land region at around 20°E. The second is found along the Wilkes Land Coast at around 170°E. Finally, the Amundsen Sea Low (ASL) pressure is located off Amundsen Sea coasts in the West Antarctic sector (on average centred around 90°W). The ASL is one of the deepest climatological low-pressure systems observed on Earth and exhibits large spatial and temporal variability [Lachlan-Cope et al., 2001]. Furthermore, the ASL is characterized by a substantial storm density [e.g., Turner et al., 2013; Raphael et al., 2016].

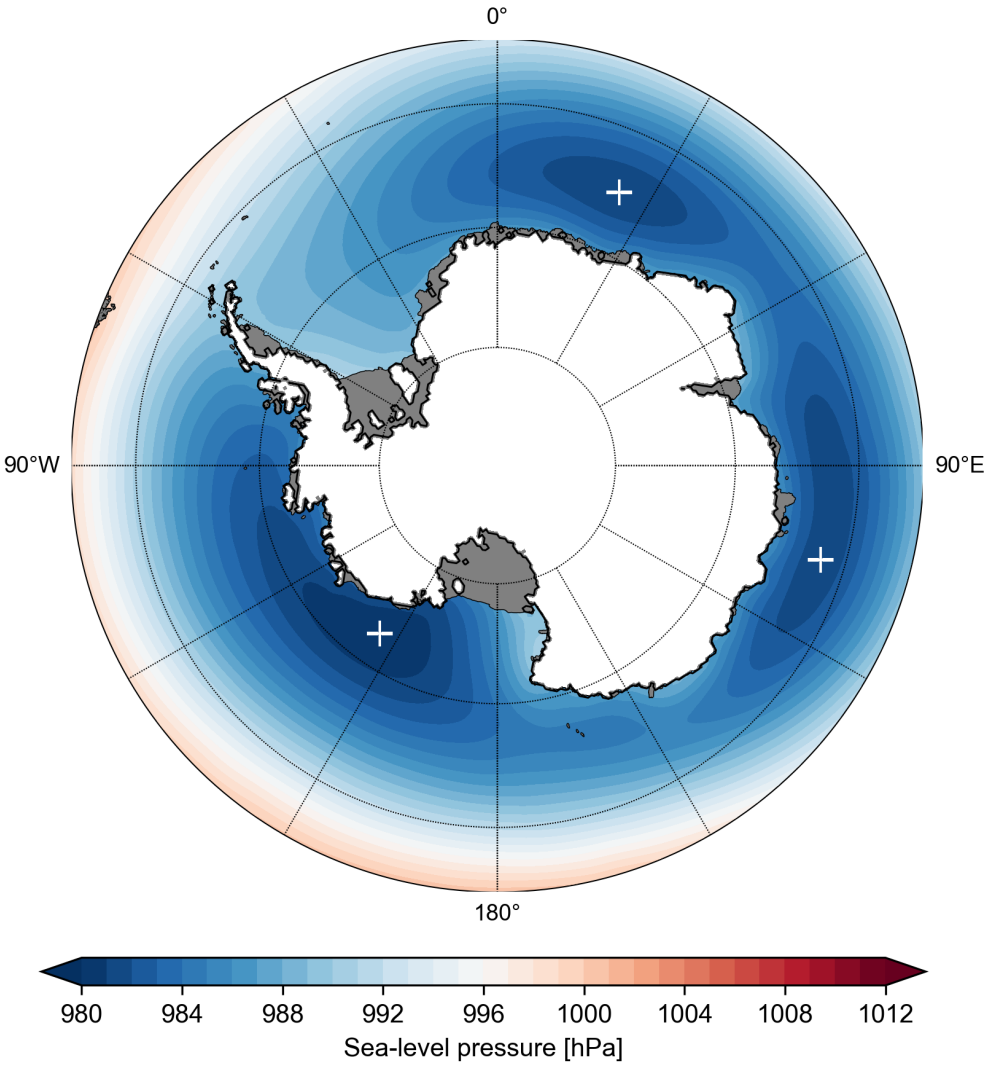


Figure 1.6: *Mean sea-level pressure (in hPa) over 1979–2019 CE in the ERA5 reanalysis. White crosses mark the three climatological low-pressure systems around the Antarctic.*

Large-scale atmospheric modes also influence the Antarctic snowfall variability [Krinner et al., 2014; Marshall et al., 2017], and more generally the Antarctic climate [e.g., Marshall and Thompson, 2016]. The Southern Annular Mode (SAM) is the dominant large-scale mode of atmospheric variability in the Southern Hemisphere at the interannual timescale. SAM represents the strength and the latitudinal position of the westerly winds (Westerlies), corresponding to the storm track (i.e., narrow zone within the storms evolve) as well [e.g., Marshall, 2003; Fogt and Marshall, 2020]. When the SAM is in its positive phase, the Westerlies strengthen and move south, towards Antarctica. At the opposite, in its negative phase, the Westerlies weaken and move north, away from Antarctica. Variations in the SAM is associated with a snow redistribution between regions [e.g., van den Broeke and van Lipzig, 2004]. The most notable fingerprint of the SAM on the Antarctic SMB is a dipole in the West Antarctic sector because of its impact on the strength

and position of the ASL [e.g., Turner et al., 2013; Raphael et al., 2016]. During SAM+ conditions, the ASL is deeper than in SAM- conditions. This results in a snow accumulation increase over the Antarctic Peninsula and the eastern part of West Antarctica while the western part of West Antarctica, including the Ross Ice Shelf receives a smaller amount of snowfall [e.g., Marshall et al., 2017]. However, the SAM has no significant effect on the integrated Antarctic-wide SMB [Medley and Thomas, 2019] since a regional snow accumulation increase is generally associated with a regional snow accumulation decrease elsewhere because of the winds-topography interactions [Fyke et al., 2017].

The Southern Ocean surrounding the Antarctic continent is often seen as an obstacle to interactions between Antarctica and more northward regions. However, an increasing scientific literature suggests that the mid-latitudes and tropical climate variability exerts a major influence on the Antarctic climate [e.g., Clem et al., 2016; Fogt et al., 2011; Schneider et al., 2012; Holland et al., 2019] and thus also on snow accumulation [e.g., Marshall and Plumb, 2007; Thomas et al., 2008; Clem et al., 2016; Goodwin et al., 2015]. Those kinds of connections are referred to as teleconnections [e.g., Yuan et al., 2018]. In particular, the El-Niño Southern Oscillation (ENSO), which is the largest mode of climate variability observed on Earth at the interannual timescale, affects strongly the West Antarctic climate [e.g., Goodwin et al., 2015; Turner, 2004; Holland et al., 2019]. High sea surface temperatures (SSTs) in the Pacific Ocean induce a heat convection, which results in the formation of Rossby waves. When these waves reach Antarctica, this in turn modifies wind patterns in the West Antarctic sector, and therefore the amount and distribution of Antarctic snowfall. Additionally, other large-scale atmospheric modes of tropical variability also impact the Antarctic climate at longer timescales than ENSO. This is the case for instance of the Interdecadal Pacific Oscillation (IPO) [e.g., Clem et al., 2020]. IPO has a larger latitudinal extension than ENSO and a period of around 30 years [e.g., Salinger et al., 2001].

In addition to the atmospheric circulation, the sea surface conditions also control the Antarctic snow accumulation [e.g., Kittel et al., 2018; Krinner et al., 2014]. In particular, the AIS is surrounded by a thin layer of sea-ice at the surface of the Southern Ocean which can reach an extent of 20 10^6 km^2 in winter but only 3 10^6 km^2 at the end of the summer over the present-day conditions [Parkinson, 2019]. The direct influence of sea-ice on SMB is related to its impact on atmosphere-ocean surface interactions. When ice covers the ocean, it prevents the moisture enrichment of the air through evaporation. On the contrary, open water enhances the air moisture content, which potentially increases snowfall on the Antarctic continent. Based on this mechanism, Goosse et al. [2021] showed that snow accumulation records have the potential to detect large polynyas (large-open water areas within the sea ice pack) in the Weddell Sea.

The majority of snowfall events occur during the winter season [e.g., Lenaerts et al., 2012] when the storms are the most frequent and the strongest. Short-lived synoptic events, also called Extreme Precipitation Events (EPEs), account for a large part of the interannual variability of snowfall in some areas of the Antarctic [Turner et al., 2019b]. Specifically, increasing scientific literature analyzes the impact of atmospheric rivers on the Antarctic climate. Atmospheric rivers are thin and long atmospheric tongues, which usually originate from mid-latitudes/tropical regions and thus contain a large amount of moisture. Atmospheric rivers are generated by positives anomalies in sea surface temperatures in the tropics that enhances the evaporation over the oceans. They are often associated with the cold zone of an extratropical cyclone [Zhu and Newell, 1994]. When reaching the Antarctic coastal regions, these atmospheric rivers discharge their moisture content in the form of snow, during a couple of days [Gorodetskaya et al., 2014]. Unlike storm systems, which are more intense and frequent in winter, atmospheric rivers do not have a seasonal cycle [e.g., Gorodetskaya et al., 2014; Wille et al., 2019].

1.3 Current surface climate changes in the Antarctic

The observed surface climate changes (e.g., near-surface air temperature, snow accumulation and sea-ice extent) in the Antarctic since the 1950s are strongly coupled [Fan et al., 2014; Goosse et al., 2009]. Therefore, to understand the past surface climate changes in the Antarctic, in particular snow accumulation, the system has to be analyzed in a holistic way. Over the satellite era (from 1979 onwards), the high-latitudes of the Southern Hemisphere have experienced major changes in their surface climate [e.g., Jones et al., 2016] (Fig. 1.7). Both West Antarctica and Antarctic Peninsula display large warming over the 1979–2014 CE period while, over the same period, East Antarctica displays a cooling on average. This strong West-East asymmetry in near-surface air temperature has been observed since 1958 [Nicolas and Bromwich, 2014], and the underlying mechanisms are still investigated [e.g., Jun et al., 2020]. In contrast, albeit some regions display a significant trend in snow accumulation such as the Dronning Maud Land region [Lenaerts et al., 2013], the AIS-wide snow accumulation is quite stable over the satellite era [e.g., Agosta et al., 2019; van Wessem et al., 2018]. This could be related to the higher internal variability of snow accumulation compared with near-surface air temperature, which requires longer time-series for detecting long-term changes [e.g., King and Watson, 2020]. Regarding the sea surface conditions, an overall sea-ice expansion has been observed over the instrumental period, but with important regional differences [Parkinson, 2019]. The most pronounced sea-ice expansion is noticed in the Ross Sea sector, while the Amundsen-Bellingshausen Sea sector presents a sea-ice reduction.

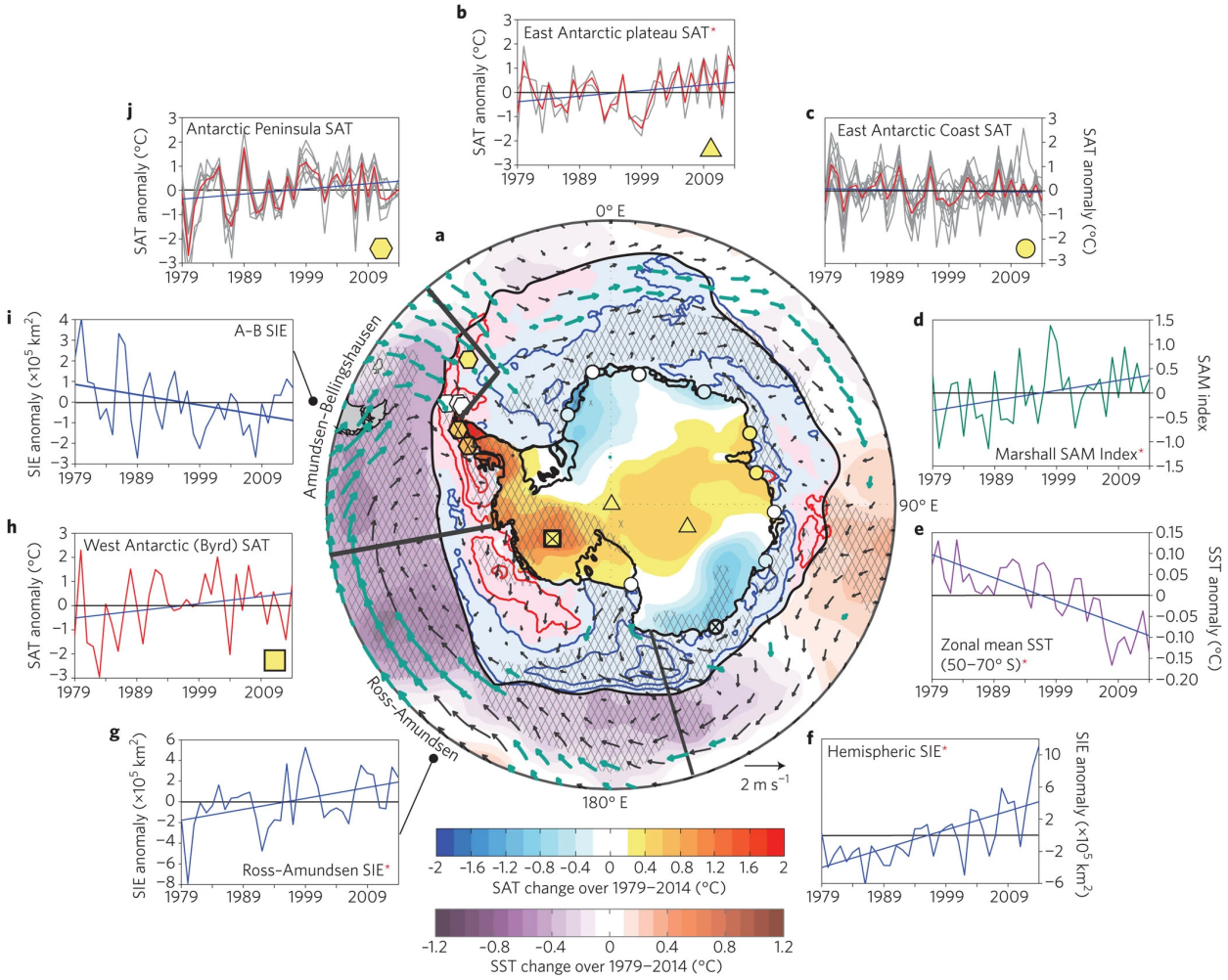


Figure 1.7: *(**a**) Observed linear trends in the Antarctic over 1979–2014 for the continental surface air temperature (SAT) and sea surface temperature (SST), sea-ice concentration (contour at 10% level of the sea-ice concentration; positive and negative trends are represented in blue and red, respectively) and near-surface winds (vectors). Hatching represents significant trends at 95% level. Surrounding plots represent time-series of SAT for different Antarctic regions (**b**, **c**, **j** and **h**; red lines correspond to the mean of all the local time-series; in °C), the SAM index (**d**; unitless), zonal mean SST (**e**; in °C), total Antarctic sea-ice extent (SIE; **f**; in $10^5 km^2$), SIE in the Ross-Amundsen Sea sector (**g**; in $10^5 km^2$) and SIE in the Amundsen-Bellingshausen Sea sector (**i**; in 10^5 km^2). Figure from Jones et al. [2016].*

The surface climate changes are widely attributed to wind changes [e.g., Jones et al., 2019; Bromwich et al., 2013; Lefebvre and Goosse, 2008; Lenaerts et al., 2013; Dotto et al., 2020]. Since the mid-1970s, the SAM has displayed a positive linear trend, which means that the Westerlies are southward shifted and stronger. According to Thompson et al. [2011a], this positive trend is a forced response that can be primarily attributed to the stratospheric ozone depletion and, to a lesser extent, the increase in greenhouse gases. The positive trend is particularly significant during the summer season. The largest impact of the SAM on the atmospheric circulation around the Antarctic is found in the Pacific sector, where the ASL is located. Although the ASL is also modulated by the tropical variability in the Pacific through the tropical-polar teleconnections [Schneider et al., 2012; Ding et al., 2011; Fogt and Wovrosh, 2015], the ASL tends to intensify when the SAM is in a positive phase [e.g., Clem et al., 2016]. This leads to an enhanced northerly airflow over the Antarctic Peninsula and the eastern part of West Antarctica resulting in a surface warming, usually associated with an increased snow accumulation. Conversely, the western part of West Antarctica displays a surface cooling associated with decreased snow accumulation [e.g., Marshall and Thompson, 2016]. This process can also explain the opposite sea-ice trend over the instrumental era between the Ross Sea and Amundsen-Bellingshausen Sea sectors [e.g., Lefebvre and Goosse, 2008; Turner et al., 2016b]. In addition to the thermodynamic response, the deepening of the ASL results in a sea-ice compaction towards the Antarctic Peninsula in the Amundsen-Bellingshausen Sea sector and in a sea-ice expansion in the Ross Sea sector because of the wind-induced sea-ice movement (i.e., the wind stress) [e.g., Hosking et al., 2013; Raphael et al., 2019].

In addition to the changes observed at the surface, the Antarctic ice shelves are thinning since the 1990s at an accelerated pace [Rignot et al., 2013]. Albeit this mass loss has no direct impact on the global sea-level, ice shelves stabilize the AIS, and thus controls the AIS mass balance [e.g., Hooke, 2005]. For this reason, ice shelves are often termed the "gatekeepers" of the AIS. The thinning of ice shelves mainly results from a basal melting occurring at the ice shelf-ocean interface [e.g., Paolo et al., 2015; Rignot et al., 2013]. More specifically, this melting is caused by the intrusions of warm water masses, in particular from the Circumpolar Deep Water, into the ice shelf cavities. This ice shelf thinning may lead to a grounding line retreat [e.g., Dutrieux et al., 2014]. The strongest ice shelf thinning is observed in the West Antarctic sector [Jacobs et al., 2011]. Under the present-day conditions, the temperature of the water originating from the CDW can be 2-4°C above the sea water freezing point when reaching the ice shelf cavities in the Amundsen Sea [Dotto et al., 2020]. Several studies have suggested a substantial contribution of wind changes for explaining the enhanced intrusions of these warm water masses that cause the increased ice shelf melting in that sector over the past decades [e.g., Donat-Magnin et al., 2017; Deb et al., 2018; Dotto

et al., 2020; Steig et al., 2012; Thoma et al., 2008]. For instance, the intensification of the eastward winds at the ice shelf break linked to the recent positive trend in the SAM may have enhanced the inflow of warm water masses towards the cavities [Holland et al., 2019]. In addition, the intensification and the southward displacement of the Westerlies have increased the Ekman pumping towards the ice shelves. This results in an upwelling of warm water that leads to the ice shelf thinning.

1.4 The Antarctic snow accumulation from ice cores

The satellite period is too short to understand the Antarctic snow variability and its links with the surrounding climate. Actually, the Antarctic climate displays a large internal climate variability compared to the other regions on Earth [e.g., Jones et al., 2016; Turner et al., 2019a; Jones et al., 2019; Previdi and Polvani, 2016]. Consequently, this makes difficult the detection of long-term changes on short timescales [e.g., Jones et al., 2016; Previdi and Polvani, 2016; King and Watson, 2020]. To study the climate variability before the instrumental and satellite era, we need to rely on paleoclimate records.

Ice cores are valuable paleoclimate records for reconstructing the past climate in the Antarctic beyond the instrumental era [e.g., Masson-Delmotte et al., 2008; Steig and Neff, 2018]. Among all the elements analyzed within an ice core, the stable isotopes of the water composition have been used since decades for estimating the past climate variability [e.g., Epstein et al., 1953; Craig, 1961; Dansgaard, 1964]. In particular, the ratio between the heavy stable isotope ($H_2^{18}O$) and the light stable isotope of oxygen in water ($H_2^{16}O$), referred to as $H_2^{16}O/H_2^{18}O$, is strongly affected by changes in the hydrological cycle. The fractionation, which is defined as the process whereby the isotopic composition of the water is modified by a change in the physical state, takes place during the condensation and evaporation. As these two processes are directly influenced by temperature, the change in the water isotopic ratio is strongly region-dependent. The water isotopic ratio measured in ice cores thus depends on the source regions. The water isotopic ratio is also altered through exchanges between the oceans and atmosphere [e.g., Galewsky et al., 2016] as well as changes in the moisture source regions [e.g., Holloway et al., 2016a]. Therefore, the change in the water isotopic ratio, referred to as $\delta^{18}O$, represents a valuable tracer of the activity in the hydrological cycle. As the hydrological cycle is closely related to the atmospheric temperature, ice core $\delta^{18}O$ records have been used for decades to reconstruct surface air temperatures [e.g., Craig, 1961; Dansgaard, 1964; Jouzel et al., 1997; Stenni et al., 2017].

More recently, interest has grown for the ice core snow accumulation records as they enable to contextualize the snow accumulation variability of the instrumental era into a longer time perspective. Annual snow accumulation rates from ice

cores are estimated based on the physical distance between suitable age markers, such as seasonal variations in the stable isotopic composition (oxygen and hydrogen) of the snow or sea salt sulfate concentrations McConnell et al. [2002]; Herron [1982]. Over the AIS, the available ice core snow accumulation records are spatially heterogeneous [e.g., Thomas et al., 2017]. For estimating past regional and continental-wide snow accumulation changes from ice cores, it is necessary to synthesize all available records. For this purpose, Medley and Thomas [2019] provided a spatially complete reconstruction of Antarctic snow accumulation changes spanning the past two centuries by interpolating the local snow accumulation records. The interpolation scheme is based on the spatial snow accumulation coherence derived from an atmospheric reanalysis. Based on their gridded ice core-based snow accumulation reconstruction, Medley and Thomas [2019] have shown that the AIS-wide snow accumulation has increased since the 19th century at an accelerating pace, but with strong regional differences, both in amplitude and sign (Fig. 1.8). For instance, while the most pronounced increase is found over the Antarctic Peninsula and eastern part of West Antarctica over the 1957–2000 CE period, the western part of West Antarctica has experienced a snow accumulation decrease during the same period. Additionally, East Antarctica is characterized by areas displaying either snow accumulation increase or decrease. Since the snow accumulation trends are highly spatially dependent, this suggests that the atmospheric circulation is key. The SAM explains more than 80% of the spatial variability in snow accumulation trends over 1957–2000 [Medley and Thomas, 2019]. However, the SAM is not associated with a continental-wide change [van den Broeke and van Lipzig, 2004], as mentioned earlier, a snow accumulation increase induced by wind anomalies somewhere is always counteracted by a snow accumulation decrease elsewhere [Fyke et al., 2017]. Therefore, Medley and Thomas [2019] have not excluded the general climate warming for explaining the AIS-wide snow accumulation trend, as it presents a more homogeneous spatial fingerprint than the wind pattern changes. However, the physical mechanisms for explaining this Antarctic-wide increase are still not fully understood [Lenaerts et al., 2019].

1.5 Climate models and future Antarctic snow accumulation

Climate models are useful tools to better understand the climate changes as they include a representation of the main physical processes that govern the climate system [Schneider and Dickinson, 1974]. The first climate models were standalone Atmospheric General Circulation Models (AGCMs) [Trenberth, 1992; Goosse, 2015]. Thereafter, these atmospheric models have been coupled to an Oceanic General Circulation Models (OGCMs), together forming General Circulation Models (GCMs). Over the past decades, GCMs have become increasingly complex by incorporating more climate components such as the land surface, sea-

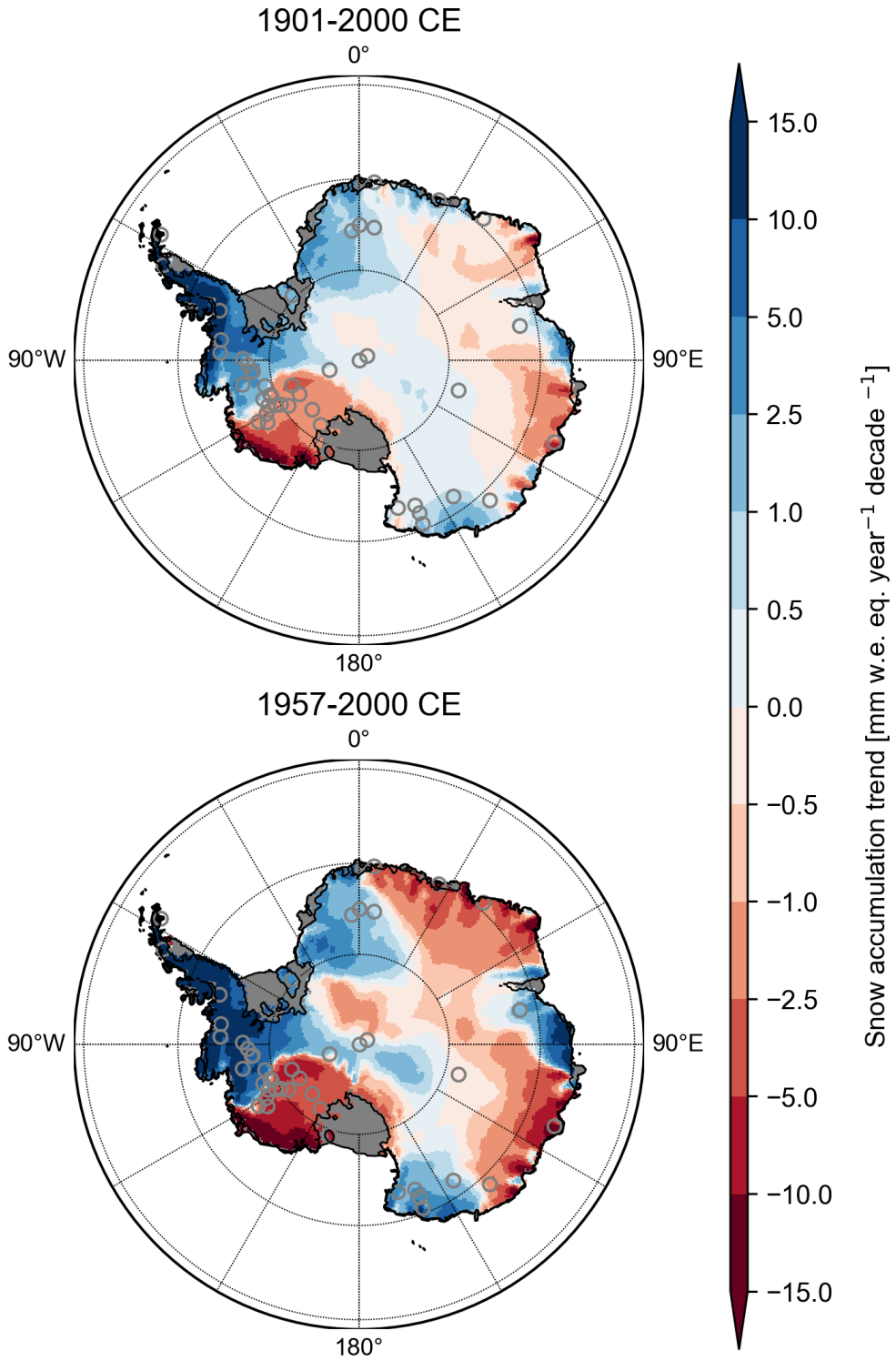


Figure 1.8: *Linear trends in the Antarctic snow accumulation from the ice core-based reconstruction of Medley and Thomas [2019] for the 1901–2000 CE and 1957–2000 CE periods (in mm w.e. eq. year^{-1} decade^{-1}).*

ice, atmospheric chemistry, and more recently ice sheet for some of them [e.g., Vizcaíno et al., 2013; van Kampenhout et al., 2020]. When climate models also include chemical and biological processes (for example the carbon cycle), they are referred to as Earth System Models (ESMs), even exceeding the complexity of the GCMs, only based on the climate physics [Goosse, 2015; Trenberth, 1992]. As the physics is consistent within all the climate system components in the GCMs or ESMs, their use in analyzing the Antarctic snow accumulation is particularly relevant to identify the processes that govern the snow accumulation variability. For instance, climate models are used for detecting the response of snow accumulation to an external forcing, for instance the ozone depletion [e.g., Lenaerts et al., 2018]. Additionally, ensembles of climate model realizations, which differ by small differences in the atmospheric initialization, allow to assess the impact of the natural fluctuations of the climate system on the Antarctic snow accumulation variability [e.g., Kay et al., 2015; Previdi and Polvani, 2016]. In this thesis, we regularly make use of the ESM from the National Center for Atmospheric Research (NCAR), the Community Earth System Model (CESM). CESM is one of the first ESMs to display good performance in simulating the Antarctic surface climate, including the snow accumulation [Lenaerts et al., 2016; Fyke et al., 2017; Agosta et al., 2015]. However, it is important to keep in mind that, like for other ESMs, CESM is not able to reproduce the fine scale ($< \sim$25 km) processes because of its coarse resolution.

Complementary to the GCMs/ESMs, Regional Climate Models (RCMs) have been used since the 2000s to provide estimations of the Antarctic snow accumulation and its components [Bromwich et al., 2004; van de Berg et al., 2006], as well as to understand the snow accumulation variability. The observations of snow accumulation are relatively sparse, their spatial distribution is heterogeneous over the AIS and the spatial snow accumulation variability is large. As a consequence, spatial interpolation from those observations fails to correctly reproduce the high-snow accumulation zones. For that reason, RCMs have become popular to estimate the snow accumulation of the AIS. In contrast to global climate models, RCMs are designed to simulate the climate over a specific region, here the polar regions. More specifically, these polar-oriented RCMs are based on an atmospheric model coupled to a land model that includes a snow model to represent the interactions between the atmosphere and the snowpack through a snow model. RCMs are forced at their lateral boundaries by a climate reanalysis or GCMs/ESMs. Since RCMs focuses on a limited area, they can run at a higher spatial resolution than the GCMs/ESMs, typically between 15-30 km over the entire AIS [van Wessem et al., 2018; Agosta et al., 2019] and even 5 km for sub-Antarctic regions such as the West Antarctic Ice Sheet [Lenaerts et al., 2017] and the Antarctic Peninsula [van Wessem et al., 2016]. Small-scale processes such as the orographic precipitations are thus better reproduced than in the GCMs/ESMs. In contrast to global

climate models, no long simulation performed with a RCM exists for Antarctica. This hinders their use for analyzing the snow accumulation variability over long timescales. To combine the high spatial resolution of the RCMs with the large-scale interactions (i.e., with other regions), ESMs with a refined grid over the AIS are promising tools as demonstrated by van Kampenhout et al. [2018] over the Greenland Ice Sheet.

Climate models have their own physics and biases so that their results can differ from each other. In this context, the Coupled Model Intercomparison Project Phase 5 (CMIP5) aims to compare GCM/ESM results. On average, all the GCMs/ESMs in CMIP5 simulate a positive trend in the SAM over the past decades, as observed [Swart et al., 2015; Zheng et al., 2013]. However, CMIP5 models are not able to capture the observed West-East asymmetry in surface air temperature trend over the second half of the 20^{th} century. Instead, they simulate on average a spatially uniform warming over the Antarctic continent [Jones et al., 2019; Klein et al., 2019]. Concurrently with the Antarctic-wide surface warming, CMIP5 models display an overall decrease in Antarctic sea-ice extent since 1979, and are thus not able to reproduce the increase observed since 1979 [Zunz et al., 2013]. This data-model discrepancy may arise from the underestimation of the contribution of the natural variability relatively to the forced variability, in models [e.g., Neukom et al., 2018]. Actually, when analyzing an ensemble of simulations performed with the same model but slightly different initial conditions show, for instance, a surface warming in West Antarctic and no change in East Antarctica [Klein et al., 2019]. The same result has been noticed for sea-ice extent as well, with some simulations showing an Antarctic sea-ice extent increase [Zunz et al., 2013; Roach et al., 2020]. This indicates that natural variability plays a large role in the Antarctic climate changes over the past few decades. Additionally, other studies [e.g., Bintanja et al., 2013; Swart and Fyfe, 2013; Rye et al., 2020] have suggested an important role of the increased ice shelf melting over the past decades [Rignot et al., 2013] that results in a decrease in ocean surface density. This freshening has increased the ocean stratification and reduced the heat input from deeper layers to the surface. This can lead to a general surface cooling over the Southern Ocean that turns in a sea-ice extent expansion.

As for Antarctic snow accumulation, Palerme et al. [2017b] have shown that the CMIP5 models reproduce the mean Antarctic snowfall rate well over the present-day conditions when compared to the best observations. However, due to their coarse resolution (typically $\sim$50-100 km at the 60°South parallel), these models underestimate snow accumulation in coastal regions and overestimate it over the Antarctic Plateau. Furthermore, in agreement with the surface warming, almost all models show a positive trend in both snowfall (on average: 2.3 mm per decade) and snow accumulation (on average: 1.9 mm per decade) over the 1956–2005 period.

The studies cited above evaluating the Antarctic climate over the past decades are not based on the latest CMIP phase (i.e., CMIP6) since their simulations have been released only recently. However, recent studies analyzing the performance of the CMIP6 models in simulating the Antarctic climate indicate limited improvements relative to CMIP5 models although the inter-model spread is reduced in CMIP6 compared to CMIP5 [Roach et al., 2020; Bracegirdle et al., 2020a; Roussel et al., 2020]. Therefore, the conclusions drawn from CMIP5 models are likely also valid for CMIP6 models.

Climate models projections for the end of the 21st century suggest an Antarctic-wide snow accumulation increase due to enhanced snowfall [Frieler et al., 2015; Lenaerts et al., 2016; Ligtenberg et al., 2013; Palerme et al., 2017b], which will partly counteract the sea-level rise induced by land ice melting. Several studies [Grieger et al., 2016; Krinner et al., 2014] have indicated that the dynamic contribution (i.e., the wind changes) to the projected snow accumulation increase is almost negligible compared to the thermodynamic contribution (i.e., the atmospheric warming). This projected increase is, in fact, directly related to the strong correlation between snow accumulation and near-surface air temperature. The water vapour pressure, which determines the maximum moisture content in the air, increases with temperature (i.e., the Clausius-Clapeyron relationship). Therefore, in a warmer climate as projected by climate models for the end of the century relative to present-day conditions, more snowfall is expected, and thus ultimately more snow accumulation. According to Frieler et al. [2015], for every degree of warming, the Antarctic snow accumulation increases by approximately 5%. Although the runoff will increase as well with the higher near-surface air temperature, Ligtenberg et al. [2013] have suggested a minor contribution to the Antarctic snow accumulation compared to snowfall, for the end of the century. Additionally, atmospheric warming reduces the sea-ice cover, enhances the evaporation of the open water by increasing the atmosphere-ocean transfers. Although the sea-ice cover reduction can lead to an intensification of the katabatic winds [Gallée and Schayes, 1994; van Lipzig et al., 2002; Kittel et al., 2018], and therefore prevents the moisture transport from the oceans to the continent, the overall sea-ice cover reduction will contribute to more snow accumulation over the AIS [e.g., Lenaerts et al., 2016; Krinner et al., 2008].

1.6 Objectives and outlines of this thesis

Ice core snow accumulation records suggest that the AIS has gained mass at its surface over the past century [Medley and Thomas, 2019]. This increase has thus mitigated the sea-level rise induced by the dynamical AIS loss. Accordingly, the Antarctic snow accumulation increase is projected to continue over the 21st century. Several studies have suggested the atmospheric warming to be the main

driver of this AIS-wide snow accumulation increase [e.g. Medley and Thomas, 2019; Frieler et al., 2015; Palerme et al., 2017b; Lenaerts et al., 2016; Kittel et al., 2021]. However, regional snow accumulation trends over the past century suggest that the atmospheric warming is not the only driver of snow accumulation changes since regional increases are not always associated with surface warming. This has been confirmed by several studies [e.g., Philippe et al., 2016; Goursaud et al., 2019; Medley et al., 2018; Fudge et al., 2016; Altnau et al., 2015] that have shown that the relationship between snow accumulation and near-surface air temperature strongly varies from one location to another. Consequently, the underlying mechanisms of snow accumulation increase are still unclear. This limited understanding of the drivers of snow accumulation changes hampers our ability to assess the future contribution of the Antarctic snow accumulation to the 21st century sea-level rise.

Ice core records represent the main source of observations for estimating the variability of snow accumulation over past centuries (section 1.4). However, ice core records provide information on the past variability at local scale. Given that the network of ice core records is highly spatially heterogeneous, it is very challenging to estimate the snow accumulation over the entire AIS from those records. Consequently, different methods have been proposed to produce a spatially complete snow accumulation reconstruction based on ice core records. Recent studies [Medley and Thomas, 2019; Wang et al., 2019] have combined the information from ice core snow accumulation records with global atmospheric reanalysis using a kriging interpolation, which is based on the spatial structure given by the global atmospheric reanalysis. However, this method presents several drawbacks. The weights calculated for interpolating the snow accumulation from ice core records are calibrated over a very short period. In addition to making these weights prone to potential issues regarding the stationarity in time [Brown et al., 2017], the short calibration period may lead to an important uncertainty in the resulting weights because of the inherent noise in observations (undersampling of the relationship). Finally, such a method only provides a reconstruction for the field of interest (i.e., the snow accumulation). This method does not allow analyzing in a consistent framework the drivers of the snow accumulation variability such as wind changes.

Over the past decades, data assimilation has been increasingly employed in paleoclimatology [e.g., Goosse et al., 2009; Widmann et al., 2010; Steiger et al., 2017; Hakim et al., 2016; Klein et al., 2019]. This method aims at reconstructing the past climate variability using paleoclimate records combined with the dynamic constraints given by climate models. Through data assimilation, the temporal and local climate information provided by paleoclimate records is spread in space and propagated to other variables by using the spatial co-variance and co-variance among variables, respectively, as given by the climate model. In other words, by incorporating for instance ice core snow accumulation records in the data assimi-

lation, not only the snow accumulation is reconstructed but potentially also all the variables simulated by the model such as the atmospheric temperature, winds and even the sea-ice cover. The multivariate data assimilation-based reconstruction thus ensures a dynamical consistency in space and between variables, as long as the climate model used in the data assimilation reproduces well the climate of the region. Therefore, in contrast with statistical methods as used for instance by Medley and Thomas [2019] and Wang et al. [2019], data assimilation-based reconstructions also allow analyzing in a consistent way the dynamical links between climate variables. Consequently, the data assimilation approach provides a framework for which reconstructing several climate fields is obtained in a natural way as it directly relies on the climate physics of the model. Such a method also does not assume a stationary relationship between the assimilated records and the climate, unlike most of the statistical methods. This is particularly relevant as several studies have highlighted important time-dependent relationships, for example between surface air temperature and δ^{18}O [e.g., Klein et al., 2019]. Finally, the data assimilation approach offers much more flexibility to combine different sources of proxies, as well as different types of records, while taking into account their uncertainties [e.g., Hakim et al., 2016].

In addition to snow accumulation, other ice core records have the potential to provide useful information on the past snow accumulation variability, in particular the δ^{18}O records recently synthesized by Stenni et al. [2017], in a similar way as snow accumulation records [Thomas et al., 2017]. This is particularly relevant as the network of snow accumulation records is relatively sparse and spatially heterogeneous over the AIS. Ice core δ^{18}O records have been extensively used for reconstructing the past surface air temperature [e.g., Masson-Delmotte et al., 2008]. Since snow accumulation is related to surface air temperature [e.g., Frieler et al., 2015], the snow accumulation reconstruction could be improved by using the ice core δ^{18}O records. For this purpose, data assimilation is especially appropriate as this method is able to combine various types of paleoclimate records.

In contrast to snow accumulation, δ^{18}O is not a standard variable simulated by climate models. However, over the past years, several long simulations performed with isotope-enable climate models have been made available. A direct comparison between model results and δ^{18}O data is thus possible, without the need to first reconstruct near-surface air temperature from δ^{18}O data. This is of great interest as several studies have raised concern in the use of ice core δ^{18}O records for reconstructing near-surface air temperature. The changes in moisture origin [e.g., Holloway et al., 2016a] and precipitation seasonality [e.g., Sime et al., 2008; Sime et al., 2019], as well as other processes, may indeed alter the δ^{18}O-temperature relationship over time [e.g., Jouzel et al., 1997; Goursaud et al., 2019].

By combining all the available ice core δ^{18}O records on Earth with an isotope-enable climate model based on a data assimilation method, Steiger et al. [2017]

have shown that δ^{18}O has the potential to inform on the past variability of other variables than the local surface air temperature, such as the atmospheric circulation, and in a much lesser extent precipitation. Additionally, Klein et al. [2019] have reconstructed regional surface air temperature from the regional δ^{18}O composites of Stenni et al. [2017] with two isotope-enabled climate models over the last two millennia using also a data assimilation approach. They have concluded that the temperature signal in the ice core δ^{18}O records is too limited for correctly reconstructing the surface air temperature and recommended using other temperature-sensitive records, for instance snow accumulation records.

In this context, the present thesis aims at better understanding the drivers of the Antarctic snow accumulation variability at the interannual to multi-decadal timescale for the regional and continental scales. A particular attention is paid to the respective role of thermodynamic processes, i.e., influences of atmospheric temperature and sea-ice cover, and of dynamic processes, i.e., changes in the winds patterns. In addition to improving our knowledge on the snow accumulation variability, the thesis aims at providing past estimates of variables that cannot be directly observed such as the surface air temperature, atmospheric circulation and sea-ice cover in the Antarctic. This is achieved by making regularly use of data assimilation to take advantage of both ice cores snow accumulation and δ^{18}O records and climate models. Specifically, the thesis addresses the following main question:

How is the Antarctic snow accumulation over the past centuries related to changes in atmospheric temperature, winds and sea-ice extent and how those links can help us to better reconstruct past changes in accumulation and their drivers?

In order to answer the overarching question, the thesis is divided in three chapters treating the following lines:

1. Examining the relationship between Antarctic snow accumulation and surface air temperature over past centuries in ice core-based reconstructions and climate models (Chapter 2, published in *The Cryosphere*).

2. Investigating the interest of using information from ice core data for better reconstructing and understanding surface climate changes in the Antarctic over the last 200 years (Chapter 3, submitted to *Climate Dynamics*).

3. Determining the physical mechanisms that are responsible for the Antarctic snow accumulation increase observed over the 20$^{\text{th}}$ century and projected for the end of the 21$^{\text{st}}$ century (Chapter 4, published in *Communications Earth&Environment*).

The main objective of Chapter 2 is to use the relationship between snow accumulation and surface air temperature to obtain a better reconstruction of both variables at large spatial scale over the past centuries. To this end, the relationship is first examined in the ice core-based reconstructions and climate model simulations over the last millennium for the seven geographically distinct Antarctic regions. Since ice cores do not record surface temperature but δ^{18}O, simulations performed with isotope-enabled climate models are also analyzed, to make a direct comparison between model results and the variable that is recorded in ice cores, i.e., δ^{18}O and snow accumulation. Based on this analysis, we then reconstruct snow accumulation and surface air temperature over the past centuries. We employ a data assimilation method (see section 1.7 for the description of the method) that fuses the regional ice core-based reconstruction of snow accumulation [Thomas et al., 2017] and δ^{18}O [Stenni et al., 2017] with several isotope-enabled climate models. We thus take advantage of the co-variance between the assimilated variables (i.e., snow accumulation and δ^{18}O from ice core records) as given by the model. The benefit of using an isotope-enable climate model is that the δ^{18}O records can be directly assimilated without the need to first reconstruct surface air temperature from δ^{18}O using a statistical method.

In Chapter 3, we concentrate on the region of West Antarctica, to study the dynamic relationships between multiple climate variables at a smaller spatial scale. In particular, the smaller scale allows the atmospheric circulation and sea-ice cover from ice core records to be investigated, on the contrary to Chapter 2. The aim is to reconstruct the past surface climate changes in the West Antarctic sector over the past two centuries in order to improve our understanding of the drivers of snow accumulation changes in West Antarctica at the interannual and multi-decadal timescales. Indeed, as surface climate changes in that region are strongly coupled to each other [Fan et al., 2014; Goosse et al., 2009], by studying the climate in a holistic way, our understanding of snow accumulation variability will be improved. We focus on West Antarctica for two reasons. 1) More ice cores are available in West Antarctica compared to East Antarctica. 2) Large climate changes in multiple variables have been observed over the past few decades, in particular, a widespread surface warming [Steig et al., 2009; Nicolas and Bromwich, 2014], a major thinning of ice shelves [e.g., Pritchard et al., 2012], as well as strong and spatially contrasted snow accumulation changes, i.e., a surface mass gain in the Antarctic Peninsula and the eastern part of West Antarctica, and a surface mass loss in the western part of West Antarctica [Medley and Thomas, 2019; Wang et al., 2019]. In this chapter, we are assessing to which extent changes in the atmospheric circulation and sea-ice extent can explain the snow accumulation variability over the last two centuries. A special focus is given to the ASL, which has been suggested to be a major contributor to surface climate changes in the West Antarctic sector. For this purpose, we provide a spatially complete climate

reconstruction for the main surface variables over the past two centuries at the interannual timescale based on a data assimilation approach. We rely on the same data assimilation method as in Chapter 2 but adapted for local ice core records instead of regional ice core-based reconstructions.

Finally, the strong link between surface air temperatures and snow accumulation leads to two questions that are addressed in Chapter 4. The first concerns the origin of this link: is it due to a change in wind patterns that affect simultaneously temperature and precipitation changes (i.e., dynamic origin) or is it simply related to a thermodynamic response of the system (i.e., Clausius-Clapeyron relationship)? The second question asks whether the relative importance of thermodynamic and dynamic processes is the same at all timescales and for all periods. Therefore, the main goal of Chapter 4 is to analyze the dynamic and thermodynamic processes responsible for changes in the Antarctic hydrological cycle and more specifically to explain the Antarctic-wide snow accumulation increase in recent decades and projected for the end of the 21st century. To this end, we compute a moisture budget for the atmosphere over the Antarctic for the 20th and 21st centuries. This moisture budget allows distinguishing the contribution of the three main mechanisms that control the Antarctic snow accumulation variability, namely i) the thermodynamic processes, which referred to snow accumulation changes induced by air temperature changes (i.e., the Clausius-Clapeyron relationship); ii) the large-scale dynamics; and iii) the synoptic-scale dynamics related to the short-lived storm systems embedded within the large-scale dynamics. This moisture budget is applied to the ECMWF ERA-Interim reanalysis [Dee et al., 2011], which is one of the best reanalysis for studying the Antarctic surface climate [e.g., Gossart et al., 2019a], and to model simulations covering the 20th and 21st centuries performed with the ESMs/GCMs that simulate at best the Antarctic surface climate.

Main conclusions and contributions of the thesis are then discussed in Chapter 5, as well as perspectives.

1.7 Data and methods

Throughout the thesis, a large panel of data are used including instrumental observations, paleoclimate observations, atmospheric reanalyses, remote sensing as well as general and regional climate model outputs. Most of analyses presented in the thesis are based on GCM/ESM outputs. Although their spatial resolution is relatively coarse, their use is justified by the fact that we are mainly interested in large-scale processes and regional changes. Those simulations are also the only ones available for the timescales studies here. However, the performance in simulating the Antarctic climate of the ESMs/GCMs selected in the thesis is assessed

by using the polar-oriented Regional Atmospheric Climate MOdel (RACMO) [van Wessem et al., 2018]. All those data are presented in Tab. 1.1.

Most of the methods used in the thesis are explained in the chapters where they are employed.Given the importance of data assimilation throughout the thesis (Chapters 2 and 3), the general data assimilation method used in the thesis is described below.

Table 1.1: *Overview of the observations and climate model simulations used throughout the thesis.*

Dataset	Period	Reference
Instrumental observations		
Near-surface air temperature from Automatic Weather Stations	1958 CE to present	Turner et al. [2004]
Gridded near-surface air temperature over Antarctica	1958–2012 CE	Nicolas and Bromwich [2014]
Global gridded surface air temperature and precipitation	1901–2012 CE	Sheffield et al. [2006]
Global gridded sea surface temperature (ERSST.v5)	1854 CE to present	Huang et al. [2017]
Marshall SAM index	1958 CE to present	Marshall [2003]
Antarctic sea-ice concentration	1979 CE to present	Parkinson [2019]
Atmospheric reanalyses		
ERA-Interim	1979–2018 CE	Dee et al. [2011]
ERA5	1979 CE to present	Hersbach et al. [2020]
Paleoclimate observations		
Antarctic ice core snow accumulation records	1000–2010 CE	Thomas et al. [2017]
Antarctic ice core δ^{18}O records	1–2010 CE	Stenni et al. [2017]
Southern Hemisphere tree-ring width records	900–2006 CE	Emile-Geay et al. [2017]
Paleoclimate reconstructions		
Regional Antarctic snow accumulation composites	1000–2010 CE	Thomas et al. [2017]

Regional Antarctic δ^{18}O composites	1–2010 CE	Stenni et al. [2017]
Regional Antarctic surface air temperature composites	1–2010 CE	Stenni et al. [2017]
Regional Antarctic surface air temperature composites	1–2010 CE	Klein et al. [2019]
SAM index from a multi-proxy database	1000–2000 CE	Abram et al. [2014]
Position of the winter sea-ice edge at 146°W in the Amundsen Sea sector	1702–2010 CE	Thomas and Abram [2016a]
Position of the winter sea-ice edge in the Bellingshausen/Amundsen Sea sector (70°–100°W)	1901–1990 CE	Abram et al. [2010]
Gridded Antarctic snow accumulation over the grounded ice sheet	1800–2000 CE	Medley and Thomas [2019]
Gridded Antarctic pressure variability	1905–2013 CE	Fogt et al. [2019]
Global climate model simulations		
ACCESS1-3	1950-2100 CE	Bi et al. [2013]
BCC-CSM1-1	850–2005 CE	Wu et al. [2014]
CCSM4	850–2005 CE	Gent et al. [2011]
CESM1-CAM5	850–2005 CE	Otto-Bliesner et al. [2015]
CESM1-LE	1920–2100 CE	Kay et al. [2015]
CESM2	1850–2100 CE	Danabasoglu et al. [2020]
CSIRO-Mk3L-1-2	850–2005 CE	Rotstayn et al. [2010]
GISS-E2-R	850–2005 CE	Schmidt et al. [2014]
HadCM3	850–2005 CE	Turner et al. [2006]
IPSL-CM5A-LR	850–2005 CE	Dufresne et al. [2013]

MPI-ESM-P	850–2005 CE	Stevens et al. [2013]
MRI-CGCM3	850–2005 CE	Yukimoto et al. [2012]
NorESM1-M	1950–2100 CE	Bentsen et al. [2013]
Global isotope-enable climate model simulations		
ECHAM5-MPI/OM	800–2000 CE	Sjolte et al. [2018]
ECHAM5-wiso	1873–2011 CE	Steiger et al. [2017]
iCESM1	850–2005 CE	Brady et al. [2019]
iHadCM3	1851–2003 CE	Turner et al. [2016b]; Tindall et al. [2009]; Sime et al. [2008]
Sensitivity experiments with a global climate model		
Ozone depletion sensitive experiments performed with CESM1-CAM5	1950–2005 CE	Landrum et al. [2017]
Regional Antarctic climate model simulations		
RACMO2 (snow accumulation and its components)	1979–2016 CE	van Wessem et al. [2018]

Overall, the goal of data assimilation is to estimate the state of the climate system, in particular the climate variables of interest, according to the available observations (Fig. 1.10). The initial state of the climate system is called the prior. A probabilistic approach for describing the state of the climate system is used as proposed by van Leeuwen [2009]. Each variable of the climate system is estimated by a probability density function (pdf), which is described in a discrete way using a set of model states called particles.

The data assimilation used in the thesis relies on a particle filter. For this purpose, the Bayes' theorem provides an ideal framework. We define $\mathbf{x}^p$ as the model state for all the variables to be reconstructed (i.e., the prior) averaged over the assimilation period (for instance one year, as in the thesis) and $\mathbf{y}$, the available observations used to update the prior at the same time resolution. According to the Bayes' theorem, the probability to observe $\mathbf{x}^p$ given the observations $\mathbf{y}$ is:

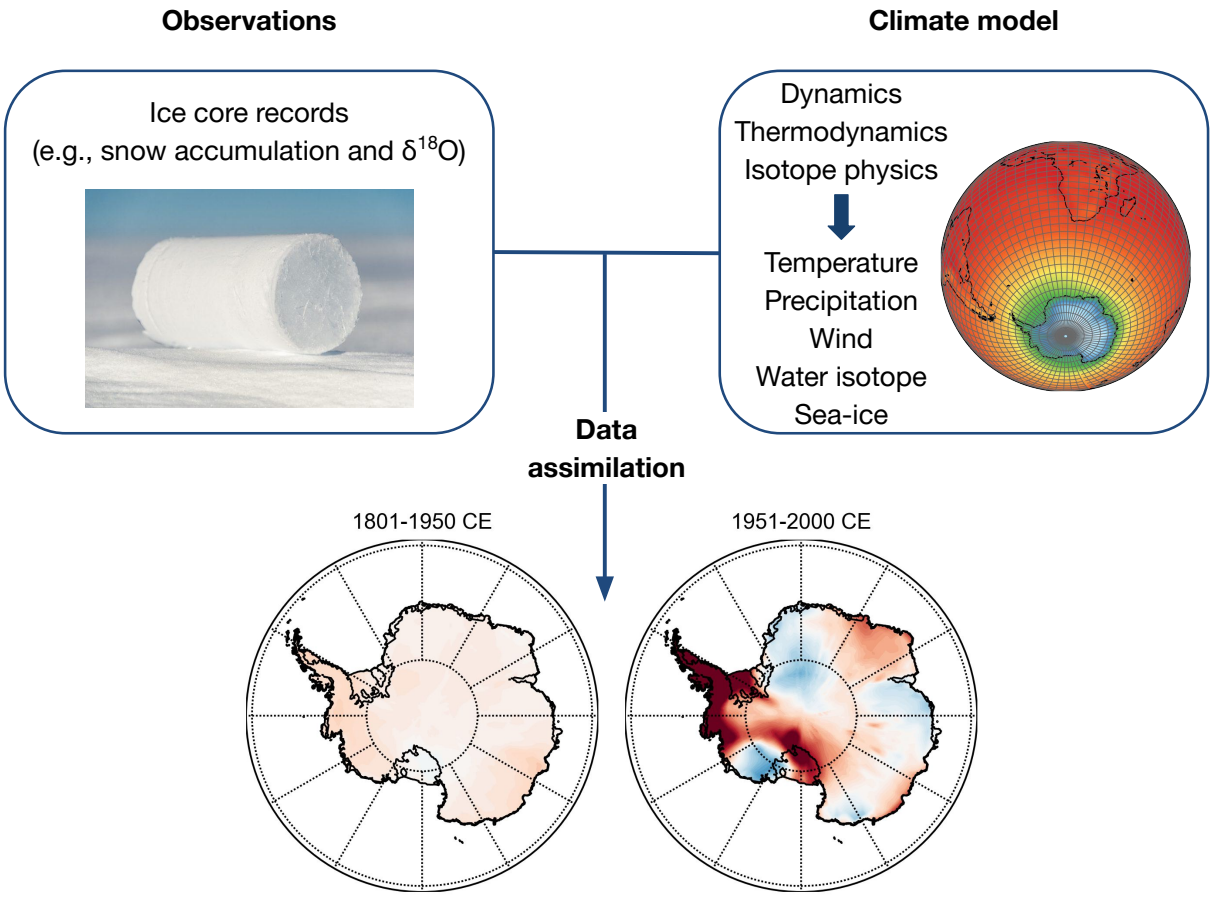


Figure 1.9: *The principle of data assimilation in paleoclimatology: optimally combining the information from paleo records (here ice core records) with the physics of the climate models. The maps below represent the anomalies of near-surface air temperatures for the 1801–1950 CE and 1851–2000 CE periods relative to the 19th century in the reconstruction provided in Chapter 3. The red (blue) color corresponds to a positive (negative) anomaly. Darker colors stand for greater anomalies. Figure inspired by Hakim et al. [2016]. Ice core picture taken from https://www.bel-antar2018.be.*

$$p(\mathbf{x}^p|\mathbf{y}) = \frac{p(\mathbf{y}|\mathbf{x}^p)p(\mathbf{x}^p)}{p(\mathbf{y})} \tag{1.2}$$

$p(\mathbf{x}^p|\mathbf{y})$ is called the posterior pdf, i.e., the updated pdf according to the available observations. The posterior represents the climate reconstruction. $p(\mathbf{y}|\mathbf{x}^p)$ corresponds to the conditional probability of observations $\mathbf{y}$ given the prior $\mathbf{x}^p$, i.e., the likelihood. The likelihood is assumed to be Gaussian:

$$p(\mathbf{y}|\mathbf{x}^p) = K^{-1} exp\left[-\frac{1}{2}\left(\mathbf{y} - H(\mathbf{x}^p)\right)^T R^{-1}\left(\mathbf{y} - H(\mathbf{x}^p)\right)\right] \tag{1.3}$$

where K^{-1} is a normalization constant – to ensure that the integrated posterior pdf over all particles is equal to one–, H is the function that maps the prior to the observational phase space, which is also called the observation operator (i.e., the mapping). For instance, H can be a linear interpolation of the value of the model results at the location of the available observations, or simply an operator that selects the model grid point in which the assimilated observations is located. In paleoclimatology, a more sophisticated model that simulates the proxy is often required for a comparison between the climate model outputs and the proxy record [e.g., Dee et al., 2015]. Such a model is called a Proxy System Model (PSM) [e.g., Evans et al., 2013]. R corresponds to the error covariance matrix representing the errors associated with the observations. In addition, R encompasses the error related to the mapping (i.e., the observation-model inconsistency). This observation-model inconsistency mainly arises from the fact that observations are representative of small-scale processes that are unresolved in the the climate model because of the coarse spatial resolution (the so-called representativeness error) [e.g., Oke and Sakov, 2008; Janjić et al., 2018]. R is assumed to be diagonal, meaning that we suppose that the errors are independent. Finally, T is a matrix transpose.

The method proposed by van Leeuwen [2009] approximates the prior pdf by a discrete distribution that is built from independent model states, called particles. This approach is referred to as the particle filtering. For complex systems, the required number of particles is higher than for simple systems. Throughout the thesis, the data assimilation period is one year. The prior is drawn by selecting N years in an existing long-term climate model ensemble of simulations. In contrast with the standard sequential data assimilation method that propagates the information forward in time (i.e., online data assimilation [e.g., Goosse, 2017; Perkins and Hakim, 2017]), the offline data assimilation method that we used here (also called no-cycling method) is based on a fixed prior for all the reconstructed years. In this thesis, we are mainly interested in atmospheric processes. The offline method is adequate since the predictability of the climate for atmospheric processes at the interannual timescale is relatively low because of the chaotic nature of the atmosphere. As shown by Matsikaris et al. [2015], online methods do not outperform offline methods for reconstructing the hydroclimate, which is mainly governed by atmospheric processes. In this framework, the prior pdf can be written as follows:

$$p(\mathbf{x}^p) = \frac{1}{N} \sum_{i=1}^{N} \delta \left(\mathbf{x}^p - \mathbf{x}_i^p \right) \tag{1.4}$$

where N and δ correspond to the number of particles and to a kernel density, respectively. Before the assimilation, we assume that each particle has the same probability. By combining Eqs. (1.2) and (1.4), the posterior pdf can re-written as:

$$p(\mathbf{x}^p|\mathbf{y}) = \frac{1}{N}\sum_{i=1}^{N} w_i \delta\left(\mathbf{x}^p - \mathbf{x}_i^p\right) \tag{1.5}$$

with,

$$w_i = \frac{p(\mathbf{y}|\mathbf{x}_i^p)}{\sum_{j=1}^{N} p(\mathbf{y}|\mathbf{x}_j^p)} \tag{1.6}$$

By combining Eqs. (1.3) and (1.6), we obtain:

$$w_i = \frac{exp\left[-\frac{1}{2}\left(\mathbf{y} - H(\mathbf{x}_i^p)\right)^T R^{-1}\left(\mathbf{y} - H(\mathbf{x}_i^p)\right)\right]}{\sum_{j=1}^{N} exp\left[-\frac{1}{2}\left(\mathbf{y} - H(\mathbf{x}_j^p)\right)^T R^{-1}\left(\mathbf{y} - H(\mathbf{x}_j^p)\right)\right]} \tag{1.7}$$

where, w_i is the weight attributed to the particle i depending on its likelihood calculated with the available observations. Therefore, if a particle is closer (less close) to the observation, it gets a higher (lower) weight. In the manuscript, we consider the mean of the posterior as the reconstruction. It is computed as the weighted mean of all the particles:

$$\overline{p(\mathbf{x}^p|\mathbf{y})} = \sum_{j=1}^{N} w_i \mathbf{x}_i^p \tag{1.8}$$

As the particles are not modified – only their weights are modified –, the dynamics of the climate is fully respected. Since the prior includes all the climate fields simulated by the model, the 500-hPa geopotential height can be, for instance, reconstructed from the assimilation of observed surface air temperature by relying on the co-variance between the two variables in the model, as long as a co-variance between the assimilated variable and the analyzed variable exists.

In practice, the data assimilation process is performed over the entire period on which observations are available. As we use an offline data assimilation method, each year (i.e., the timestep of the data assimilation) is reconstructed independently.

To summarize the data assimilation procedure (Fig. 1.10):

1. The fixed prior is estimated by selecting N particles from different years of an ensemble of simulations. This prior contains all the variables to be assimilated and analyzed.

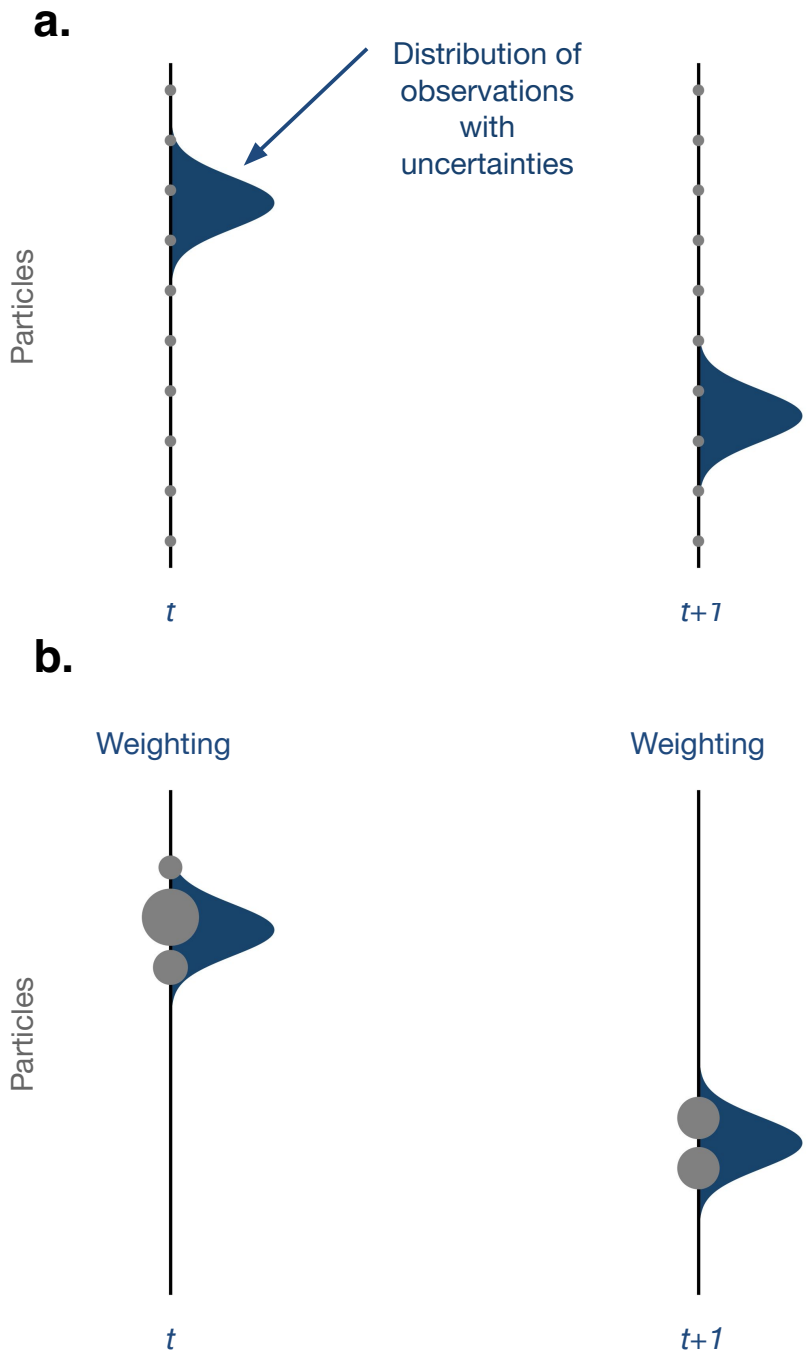


Figure 1.10: *(**a**) Weights of particles before the data assimilation procedure for two specific time t and t+1. The vertical axis corresponds to the model states while the horizontal axis represents the time. Here the prior is estimated with ten particles (gray bullets). The size of the bullets corresponds to the weight assigned to each particle (equal weight for all the particles). The blue distribution corresponds to the distribution of the observations with the associated uncertainties (i.e., related to R). (**b**) Weighting of the particles after the data assimilation procedure. Each particle receives a weight proportional to their likelihood knowing the observations. Particles with a zero weight have been removed from the figure.*

2. Based on the available observations at each timestep of the data assimilation (i.e., one year), the prior is updated by computing the likelihood between each particle and the observation. Depending on the likelihood, a weight is assigned to each particle.

3. Then, the final reconstruction is defined as the weighted mean of the particles (i.e., the weighting).

4. This process is repeated from the first year to the last year of observations.

2

How useful is snow accumulation in reconstructing surface air temperature in Antarctica? A study combining ice core records and climate models

Abstract

Improving our knowledge of the temporal and spatial variability of the Antarctic Ice Sheet (AIS) Surface Mass Balance (SMB) is crucial to reduce the uncertainties of past, present and future Antarctic contribution to sea level rise. An examination of the surface air temperature–SMB relationship in model simulations demonstrates a strong link between the two. Reconstructions based on ice cores display a weaker relationship, indicating a model-data discrepancy that may be due to model biases or to the non-climatic noise present in the records. We find that, on the regional scale, the modelled relationship between surface air temperature and SMB is often stronger than between temperature and δ^{18}O. This suggests that SMB data can be used to reconstruct past surface air temperature. Using this finding, we combine isotope-enabled model SMB and δ^{18}O outputs with ice-core observations through a data assimilation procedure, to generate a new surface air temperature reconstruction over 1800–2010 CE. Although an independent evaluation of the skill is difficult because of the short observational time series, this new reconstruction outperforms the previous reconstructions for the continental-mean temperature that were based on δ^{18}O alone. The improvement is largest for the East Antarctic region, where the uncertainties are particularly large. Finally, using the same data assimilation method as for the surface air temperature reconstruction, we provide a spatial SMB reconstruction for the AIS over the last two centuries

This chapter is based on: Dalaiden, Q., Goosse, H., Klein, F., Lenaerts, J.T.M., Holloway, M., Sime, L., and Thomas, E.R. (2020). How useful is snow accumulation in reconstructing surface air temperature in Antarctica? A study combining ice core records and climate models, *The Cryosphere*, **14**, 1187–1207, https://doi.org/10.5194/tc-14-1187-2020. Supplementary materials are in Appendix A.

showing large variability in SMB trends at regional scale, with an increase (0.82 Gt year^{-2}) in West Antarctica over 1957–2000 CE and a decrease in East Antarctica during the same period (-0.13 Gt year^{-2}). As expected, this is consistent with the recent reconstruction used as a constraint in the data assimilation.

2.1 Introduction

The spatial coverage of climate observations in Antarctica and the Southern Ocean is sparse [e.g., Jones et al., 2016; Neukom et al., 2018]. Consequently, the climate dynamics of the high southern latitudes are still poorly understood, leading to large uncertainties in the processes governing climate variability [Church et al., 2013]. Since around 1995 CE, the contribution to the global sea level rise from the ice sheets – Greenland Ice Sheet (GrIS) and the Antarctic Ice Sheet (AIS) – has strongly increased, and are slowly outpacing the contributions from mountain glaciers and ocean thermal expansion [Shepherd et al., 2018b]. The GrIS has been dominating the ice sheet contribution so far [Rignot et al., 2019], but AIS mass loss has increased fivefold in 2012–2017 CE relative to 1992–1997 CE, with current AIS mass loss values that approach those of the GrIS.

The (grounded) AIS Mass Balance (MB) is the difference between the surface mass balance (SMB) and the solid ice discharge [Lenaerts et al., 2019; Fyke et al., 2018]. Reliable estimates of AIS MB and its relationship with internal climate variability and transient climate forcing are needed to constrain future climate and sea level projections [Bamber et al., 2018]. The current AIS MB is negative [Rignot et al., 2019] because of large values of ice discharge (IMBIE team, 2018).

The SMB is defined as the difference between the incoming and outgoing mass at the surface of the ice sheet. In Antarctica, the main source term of the SMB, and its interannual variations, is precipitation in the form of snow [e.g., Lenaerts et al., 2012; Agosta et al., 2019]. Unlike Greenland, AIS surface melt is small, and most surface melt water refreezes in place, not contributing to SMB [Trusel et al., 2015; Kuipers Munneke et al., 2012]. As a result, the surface sublimation and sublimation of blowing snow are the main sink terms of the AIS SMB [e.g., Frezzotti et al., 2013; van Wessem et al., 2018].

Ice cores provide information on past changes in surface air temperature and SMB across Antarctica on time scales of centuries to millennia [e.g., Stenni et al., 2017; Thomas et al., 2017]. In particular, it has become standard to reconstruct past temperature changes from water stable isotopes, and in particular δ^{18}O [e.g., Jouzel, 2003; Masson-Delmotte et al., 2006]. However, ice core studies suffer from several limitations: 1) the ice core network is still relatively sparse, despite recent coordinated international drilling efforts [Thomas et al., 2017; Stenni et al., 2017]; 2) annually resolved surface air temperature and SMB records are not available from extremely dry areas, such as the East Antarctic Plateau; 3) changes in pre-

cipitation seasonality [e.g., Sime et al., 2008], moisture origin [e.g., Holloway et al., 2016a] and other processes can modify the expected relationship between $\delta^{18}O$ and surface air temperature [e.g., Jouzel et al., 1997; Klein et al., 2019]. Combined, these factors lead to large uncertainties in the reconstruction of surface air temperatures.

Until recently, AIS SMB had been considered to display no significant trends since the mid-twentieth century [Monaghan et al., 2006; Frezzotti et al., 2013]. Based on recent work, this hypothesis has been revised: using a larger ice core network (PAGES2k database), Thomas et al. [2017] and Medley and Thomas [2019] have shown that AIS SMB has increased significantly since 1900, albeit with important regional differences. The Antarctic Peninsula has witnessed a considerable SMB increase during the twentieth century [e.g., Thomas et al., 2015; Goodwin et al., 2016], as well as some regions of Dronning Maud Land [e.g., Philippe et al., 2016; Lenaerts et al., 2013; Medley et al., 2018; Shepherd et al., 2012]. In contrast, other regions of Droning Maud Land are subjected to a SMB decrease over the recent past [Schlosser et al., 2014; Altnau et al., 2015]. All these studies point out the need to densify the ice-core network over Antarctica, but also to retrieve more insight in what is driving the trends in AIS SMB and its spatial signatures. For the latter, output of climate model simulations can be very useful [e.g., Lenaerts et al., 2018].

In the last decade, outputs of several climate model simulations that cover the last millennium has become available [Schmidt et al., 2011]. Thus far, model evaluation has been mainly focussed on surface air temperature [PAGES 2k-PMIP3 group, 2015]. These results have shown discrepancies in AIS surface air temperature between climate model simulations and reconstructions during the last millennium. In contrast to climate model results, surface air temperature reconstructions show no clear warming over the 20^{th} century at the continental scale [Goosse et al., 2012; Stenni et al., 2017; PAGES 2k-PMIP3 group, 2015; Neukom et al., 2018]. This mismatch can be explained by an overestimation of the response of climate models to external forcing, or the strong natural variability occurring in Antarctica or an underestimation of the signal in proxy-based reconstructions, or by a combination of all those [Jones et al., 2016; Neukom et al., 2018]. Unlike temperature changes, modelled AIS SMB variations over the past millennium are poorly documented.

In a warmer climate, AIS SMB is expected to increase due to higher snowfall associated to the greater moisture holding capacity at higher air temperature [e.g., Lenaerts et al., 2016]. Taken alone, this straightforward thermodynamical effect would mitigate the sea level rise [Huybrechts et al., 2004; Krinner et al., 2007; Frieler et al., 2015]. According to Frieler et al. [2015], the observed sensitivity of Antarctic snowfall accumulation to surface air temperature was about 5% K^{-1} during the 1960–1999 CE period. Based on climate model simulations, this sensitivity

is expected to increase in future with an estimated conversion value of 7.4% K^{-1} for the end of the 21st century (2080–2099) [Palerme et al., 2017b]. The link between surface air temperature and SMB has been confirmed for small regions at the centennial time scale (200 years) [e.g., Oerter et al., 2000; Medley et al., 2018] and on longer time scales (glacial-interglacial) [e.g., Frieler et al., 2015] for the full AIS using climate models and ice cores. However, some studies using surface air temperature reconstructions based on δ^{18}O data [Fudge et al., 2016; Altnau et al., 2015; Philippe et al., 2016; Goursaud et al., 2019] suggest that this SMB-surface air temperature relationship is not always positive and varies spatially and temporally. These results suggest that in some regions, especially along the AIS coasts, the SMB variability is dominated by large-scale atmospheric circulation rather than by thermodynamic processes (such as the Clausius-Clapeyron relation), limiting the correlation with δ^{18}O.

The first goal of this study is to document the relationship between surface air temperature and SMB in Antarctica on a regional scale using climate models and ice-core records over the two past centuries and over the last millennium. The final goal is to use the covariance between both variables to reconstruct past changes over the last two centuries by using a data assimilation procedure. All reconstruction methods depend on the number and quality of the input data. However, while the statistical methods classically used to infer past surface air temperature [e.g., Stenni et al., 2017] rely on the length of the calibration period, on the quality of the record during this period, and on the stationarity of the link between the proxy and the variable of interest, which can be strong assumptions in the case of the δ^{18}O-temperature relationship [Klein et al., 2019], data assimilation does not. In recent years, data assimilation has become a standard procedure in paleoclimatology to optimally combine the information from model results and proxies and to provide estimates of past climate states [e.g., Hakim et al., 2016; Widmann et al., 2010; Goosse et al., 2010; Matsikaris et al., 2015; Steiger et al., 2014]. Nevertheless, Antarctic SMB to the best of our knowledge has never been assimilated in a climate model. The biggest advantage of using data assimilation is that it takes into account information brought by both SMB and δ^{18}O without making the strong assumptions that the statistical methods do. Additionally, using the covariance between them might lead to better estimates of past changes in the two variables, particularly when proxy records are scarce and few instrumental data are available, which is the case for the Antarctica. The resulting reconstructions will have the benefit of being compatible with the physics of the climate system as represented by the models.

2.2 Data: model simulations and observations

2.2.1 Global climate model simulations

The climate model simulations selected for this study are those for which the required variables (i.e., precipitation and sublimation/evaporation) are available for the last millennium from the PMIP3-CMIP5 database [Otto-Bliesner et al., 2009; Taylor et al., 2012]. In addition to these simulations, the CESM1-CAM5 model simulations covering the last millennium [Otto-Bliesner et al., 2015] are also used. The characteristics and references of each model are described in Tab. A.1. All these GCMs use the GMTED2010 elevation dataset [Danielson and Gesch, 2011] as topography, adapted to their spatial horizontal resolution. The simulations are driven by both natural (orbital, solar and volcanic) and anthropogenic (greenhouse gases, land use, aerosol and ozone) forcings through the last millennium [Schmidt et al., 2011, 2012]. Except for CESM1-CAM5, CSIRO- Mk3L-1-2 and MPI-ESM-P, the simulations do not cover the entire millennium. Historical simulations covering 1851-2005 CE were launched independently of simulations covering 850-1850 CE (referred to as past1000 experiment). In order to obtain results over the full millennium, we adopt the approach from Klein and Goosse [2018] and merge the first ensemble members (r1i1p1) of the past1000 experiment with the corresponding ensemble members of the historical experiment. Although not continuous, there is no large discrepancy between the two merged simulations [e.g., Klein and Goosse, 2018].

Simulations performed with the isotope-enabled climate models, ECHAM5-MPI/OM [Sjolte et al., 2018], ECHAM5-wiso [Steiger et al., 2017] and iHadCM3 [Tindall et al., 2009; Holloway et al., 2016b] are also analyzed. These simulations allow for a direct comparison with observed water isotope content. ECHAM5/MPI-OM is a fully coupled General Circulation Model (GCM). The simulation used here covers the 800–2000 CE period forced by natural and anthropogenic forcing [Sjolte et al., 2018]. The horizontal resolution of the atmospheric model is $3.75^\circ \times 3.75^\circ$. The simulation of ECHAM5-wiso, which only includes an atmospheric component, was performed by Steiger et al. [2017] and covers the 1871–2011 CE period at $\sim 1^\circ$ resolution. The model is driven by the sea surface temperature and sea ice from the Rayner et al. [2003] dataset. Due to a lack of Antarctic sea ice data before 1973, this dataset is based on historical climatologies of sea ice concentration for the 1871–1973 CE period, with no interannual variability. Finally, iHadCM3 is the version of HadCM3 (fully coupled climate model) [e.g., Turner et al., 2016a] which has an explicit representation of the water isotopes. The resolution of the atmospheric model is $3.75^\circ \times 2.5^\circ$. While only one simulation is available for ECHAM5-MPI/OM and ECHAM5-wiso, we have an ensemble of seven iHadCM3 simulations spanning the industrial period from 1851 to 2003 CE. The initial conditions for

each of these simulations correspond to different years in the pre-industrial control simulation of the iHadCM3 model. Comparisons of the results of these three isotope-enabled models with modern δ^{18}O observations indicate that they all reproduce the main characteristics of the spatial distribution of the isotopic composition of precipitation over Antarctica including the latitudinal distribution (negative δ^{18}O gradient from the coasts to the Plateau). According to Tindall et al. [2009] and Sime et al. [2008], the small biases in δ^{18}O (for example, an underestimation of the spatial δ^{18}O variability in rugged areas) in the iHadCM3 simulation mainly come from the coarse horizontal resolution of the model and not from the isotopic model itself. ECHAM5-wiso and ECHAM5/MPI-OM display an overall underestimation of δ^{18}O in Antarctica but reproduce well the general Antarctic δ^{18}O pattern [Goursaud et al., 2018; Klein et al., 2019, see reference of each model for more details].

Klein et al. [2019] has recently described an evaluation of Antarctic surface air temperature in reconstructions and model simulations over the last millennium. In accordance with Abram et al. [2016], they highlighted the early onset of industrial warming simulated by the PMIP/CMIP models, which is not observed in the δ^{18}O-based temperature reconstructions of Stenni et al. [2017]. This suggests that the Antarctic surface air temperatures simulated by the models are too sensitive to the anthropogenic forcing.

2.2.2 The regional climate model RACMO2 simulation

The evaluation of AIS SMB simulated by GCMs for the present period (1979–2005 CE) is mainly based on the results of the regional atmospheric climate model RACMO2.3p_2 (RACMO2 hereafter) covering the entire AIS over 1979–2016 CE [van Wessem et al., 2018]. This is because 1) the SMB observations are very sparse on the AIS [Favier et al., 2013]; 2) the interannual (year-to-year) variability is different between observations and GCMs given that the latter are freely-evolving coupled models. Consequently, the comparison can be only made on multi-decadal time scales (> 20 years), which drastically reduces the availability of observations; 3) unlike observations, RACMO2 provides a complete SMB field over the entire AIS; and, finally, (4) RACMO2 has been extensively evaluated against available measurements and displays a very good agreement [e.g., van Wessem et al., 2018; Lenaerts et al., 2012]. In an intercomparison of AIS SMB from reanalysis, atmospheric models and observations, Wang et al. [2016] showed that the RACMO2 model best fits the recent AIS SMB observations compared to all other available datasets.

RACMO2 combines the physics package of the European Centre for Medium-Range Weather Forecasts [ECMWF, 2008] integrated Forecast System and the hydrostatic dynamics of the High Resolution Limited Area Model (HIRLAM) [e.g.,

Unden et al., 2002]. RACMO2 is specially adapted to polar regions since it includes the interactions between the atmosphere and the multi-layered snow model that calculates physical processes occurring in the firn: meltwater production, percolation, runoff, refreezing, as well as snow grain size and resulting snow albedo [Greuell and Thomas, 1994; Ettema et al., 2010]. RACMO2 also includes a drifting snow scheme simulating the interactions between the near-surface air with snow [Lenaerts et al., 2010]. All the SMB components are explicitly calculated by this regional model on a 27 km resolution grid. The Digital Elevation Model of Bamber and Griggs [2009] is taken as reference of the Antarctic topography. ERA-Interim reanalysis data [Dee et al., 2011] are used to force the regional model at its lateral boundaries. For more details on RACMO2, see van Wessem et al. [2018].

2.2.3 Snow accumulation database from Antarctica2k

The annually resolved Antarctica2k (Ant2k) snow accumulation database [Thomas et al., 2017] is used for the evaluation of AIS SMB simulated by GCMs before 1979 CE. The estimate of the SMB from ice cores is based on the physical distance between suitable age markers within the ice core. The age markers used depend on the timescale of interest ranging from glacial cycles (e.g. bulk changes in isotopic compositions) to seasonal variations reflected by changes in stable water isotopes, while volcanic eruptions can inform on decadal to millennial timescales [Dansgaard and Johnsen, 1969]. Once the age markers are identified, since the firn density generally increases with depth in the ice core, it is necessary to consider those variations to convert the age and depth to mass [van Den Broeke et al., 2008]. Doing so, SMB is converted to meters of water equivalent based on measured density and corrected for the vertical strain rate effect – the differential vertical velocity with depth leading to layer thinning with depth [Thomas et al., 2017].

This database is composed of 79 records that are assigned to seven geographical regions (Fig. 2.1) with distinctly different climates. East Antarctica above 2000 m elevation constitutes the East Antarctica Plateau (EAP). West Antarctica is separated into two parts: the Antarctic Peninsula (AP) and the West Antarctica Ice Sheet (WAIS), with a division at 88° W. The coastal region of East Antarctica is divided into four regions: Victoria Land (VL; 150-170° E), the Wilkes Land Coast (WL; 70-150° E), Dronning Maud Land (DML; 15° W-150° E) and the Weddell Sea Coast (WS; 15-60° E). For each region, this database covers the past 1000 years except for EAP, AP and DML, for which the period covered is 1240–2005 CE, 1703–2010 CE and 1737–2010 CE, respectively. Hereafter, West Antarctica is composed of WAIS and AP, while East Antarctica comprises all of the other regions. Since some Antarctic regions lack long-term data, the SMB reconstruction for the whole Antarctic ice sheet is only available from 1737 CE. This regional SMB

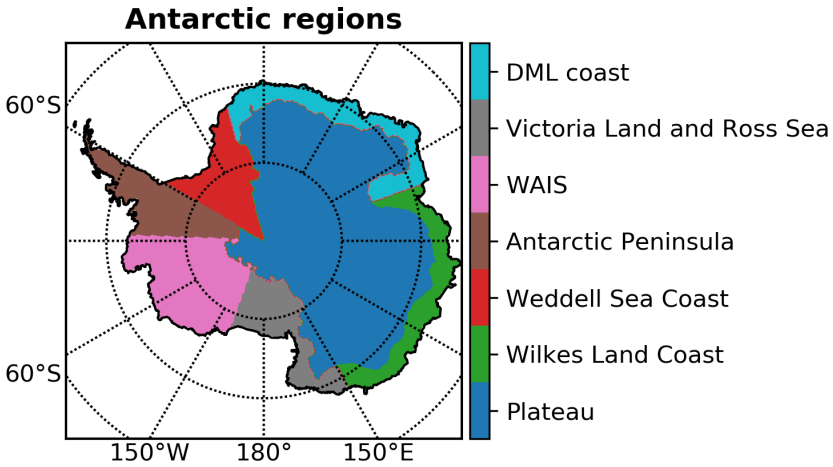


Figure 2.1: *Antarctic regions used in this study. The definitions of the regions are those of Thomas et al. [2017].*

reconstruction has been compared to RACMO2, concluding that the reconstruction captures a large proportion of the regional spatial SMB variability as defined by RACMO2 for the 1979–2010 CE period [Thomas et al., 2017].

2.2.4 Water stable isotopes records and surface air temperatures reconstructions from Antarctica2k

Stenni et al. [2017] built δ^{18}O regional composites from 112 individual ice cores compiled in the framework of the PAGES Antarctica2k working group for similar seven Antarctic subregions as in Thomas et al. (2017; see Sec. 2.2.3) over the last two millennia. Based on those δ^{18}O composites, they reconstructed regional surface air temperatures over the last two millennia based on the statistical relationship between δ^{18}O and surface air temperature. Three methods have been used to scale the δ^{18}O composites. The second reconstruction (*borehole* reconstruction) is used throughout this study for two reasons: 1) this is not based on surface air temperature observations, which are used here to estimate the skill of the reconstructions which would have led to a bias; 2) because it is based on more information, the borehole reconstruction is expected to be more accurate (see section A.1 for details). The temporal resolution is the same as for the δ^{18}O composites: 10 years over 0–1800 CE and 5 years over 1800–2010 CE.

2.3 Methods: Reconstructing SMB and surface air temperatures using data assimilation

2.3.1 Data assimilation method: a particle filter using fixed ensembles

Data assimilation optimally combines observations (proxy data in our case) and climate model states. Two types of data assimilation methods are usually applied in paleoclimatology. First, online methods follow standard sequential data assimilation approaches, in which the analysis at a single time step depends on the state at the previous step. Information is thus propagated forward in time. However, because data assimilation requires a large ensemble of model simulations (tens to hundreds), for paleoclimate reconstructions, performing online data assimilation with complex climate models such as the ones participated in the CMIP5 (as used here) becomes impractical. Second, when working with so-called offline methods, ensemble members are constructed from existing model simulations, which is of great interest in terms of computation time compared to online methods. Here, ensemble members are constructed by individual years and not by independent model simulations. Therefore, in contrast to online methods, offline methods do not maintain temporal consistency. However, when the predictability on inter-annual time-scales is limited, such as surface air temperature or precipitation because of the dominant role of their chaotic nature, online methods do not outperform offline ones [Matsikaris et al., 2015]. Indeed, offline methods have provided skilful data assimilation-based reconstructions for various types of data [e.g., Steiger et al., 2017; Klein and Goosse, 2018; Hakim et al., 2016]. Nevertheless, the online approach is preferred when focussing on ocean dynamics because of the ocean long memory [e.g., Goosse, 2017; Pendergrass et al., 2012].

The offline data assimilation method applied in this study is based on a particle filter [e.g., van Leeuwen, 2009; Dubinkina et al., 2011] using fixed ensembles from climate model outputs. The implementation described in Dubinkina et al. [2011] is identical to previous studies [e.g., Klein and Goosse, 2018]. Hence, only a brief description of the methodology will be given here. At each time step of the data assimilation procedure (yearly, see Sec. 2.3.2), each ensemble member, called particle, is compared to the proxy-based reconstruction by computing its likelihood, assumed here to be Gaussian, taking into account data uncertainties (see Dubinkina et al. [2011] for details). Depending on its likelihood, each particle receives a weight. Then, all the weights are multiplied by the number of particles and rounded to the nearest integer toward negative infinity by ensuring that the sum of the weights equals the number of particles throughout the data assimilation process (see Dubinkina et al. [2011] for details). Considering all particles weights, we can compute a weighted average, providing a reconstruction for this time step. In

this study, the ensemble members are derived from the three isotope-enabled climate model outputs ECHAM5-MPI/OM, ECHAM5-wiso and iHadCM3, presented at Section 2.2.1. These models have been chosen because they explicitly simulate δ^{18}O. Because iHadCM3 offers an ensemble of seven simulations, while the other isotope-enable models have only a single realization, we mainly focus on the iHadCM3 outputs in the main manuscript. The results from the other models are shown in Appendix A and provide similar conclusions to the ones obtained with iHadCM3. Using an ensemble allow us estimating the contribution of internal variability over the last century and the range provided by this ensemble is larger than the one given by the other two models, increasing the probability of finding model results close to the assimilated records during the data assimilation process. Additionally, iHadCM3 ensemble provides a more realistic Antarctic surface air temperature and snow accumulation over recent past than the ECHAM5-MPI/OM simulation (Fig. A.8) [Klein et al., 2019].

2.3.2 Experiment design

Data assimilation is used in this study to reconstruct surface air temperature and SMB by taking advantage of the covariance between these variables. They are assimilated together as well as separately in three different experiments. In the first experiment, the seven subregion composites of δ^{18}O data [Stenni et al., 2017] are used to constrain model results. Assimilating δ^{18}O instead of surface air temperature potentially accounts for the non-stationary and the non-linearity of the stable oxygen ratios–surface air temperature link [Masson-Delmotte et al., 2008; Klein et al., 2019]. For the second experiment, the SMB reconstruction for the seven subregions [Thomas et al., 2017] is used in the data assimilation process. Finally, both δ^{18}O and SMB are taken into account together in the last experiment. This allows us to estimate independently the consistency of the SMB and surface air temperature reconstructed between the various records and model results. In addition, our experiments allow us to assess the information acquired on surface air temperature by assimilating SMB, and on SMB by assimilating δ^{18}O. In all the experiments, as we are interested in the year-to-year variability and that the ice core snow accumulation records are annually-resolved, we assimilate annual-mean proxies. All modelled δ^{18}O are precipitation-weighted as this quantity is most similar to the one measured in ice cores.

Since the amount of ice cores is limited before 1800 CE (both for δ^{18}O and for SMB), which drastically decreases the quality of the regional composites [Thomas et al., 2017], the experiments are performed on the 1800–2010 period. Contrary to the SMB composites, which have an annual resolution, the composites of δ^{18}O are 5-year averages. Consequently, the δ^{18}O data have been interpolated linearly over the studied period to match the temporal resolution of the SMB reconstruction.

However, as recommended by Stenni et al. [2017], the results are analyzed only for the 5-year averages. This temporal averaging reduces uncertainties in dating and the noise induced by non-climatic processes [e.g., Laepple et al., 2018; Fan et al., 2014].

In order to assess the skill of our data assimilation-based surface air temperature reconstructions, we evaluate them at first with the reconstructions of Stenni et al. [2017]. But this is biased since they are only based on δ^{18}O and we cannot thus evaluate the added value brought by SMB data and model physics in the data assimilation experiments. Therefore, independent data is needed to properly assess the potential of SMB and δ^{18}O in reconstructing surface air temperature. This is done here using the surface air temperature reconstruction from Nicolas and Bromwich [2014], which is based on surface air temperature records and not on δ^{18}O data, over the 1958–2010 CE period. SMB estimates are also available for the last decades [e.g., Medley et al., 2014], but they cover a too short period or have a too small spatial coverage to provide an independent validation of our reconstruction. It is thus not possible to estimate if the assimilation of SMB and δ^{18}O measurements provides an improvement for this field.

2.4 Results

2.4.1 Reconstructed and simulated SMB changes over the last centuries

The AIS SMB over the last millennium has been estimated for each GCM by computing the difference between precipitation and sublimation/evaporation. Runoff is assumed to be negligible as surface meltwater generally refreezes in the cold firn [Magand et al., 2008; Kuipers Munneke et al., 2012]. Our short evaluation of SMB simulated by GCMs over the present-day (see section A.3) suggests that the selected GCMs (including the isotope-enable models) display reasonable SMB climatology when compared to RACMO outputs.

Before the 19th century, all GCMs simulations are characterized by large decadal variability, but no long-term trend (Fig. 2.2). A positive trend, albeit initiated at different times, is shown at the end of the simulation (around 1950 CE). All models agree on an AIS SMB increase from $\sim$1975 onwards, which is consistent with the SMB reconstruction of Thomas et al. [2017]. However, the contrast in the SMB trends between East Antarctica and West Antarctica is clearly stronger in the reconstruction based on ice cores than in GCMs on average. Indeed, over the last decades (1950–2000), the ice core SMB reconstruction shows a large increase for West Antarctica (25.6 Gt year^{-1} per decade) and a small decrease (-3.6 Gt year^{-1} per decade) for East Antarctica, while, on average, the GCMs simulate a strong SMB increase in both regions (8.9 $\pm$ 9.2 Gt year^{-1} per decade and 14.2 $\pm$ 13.5 Gt

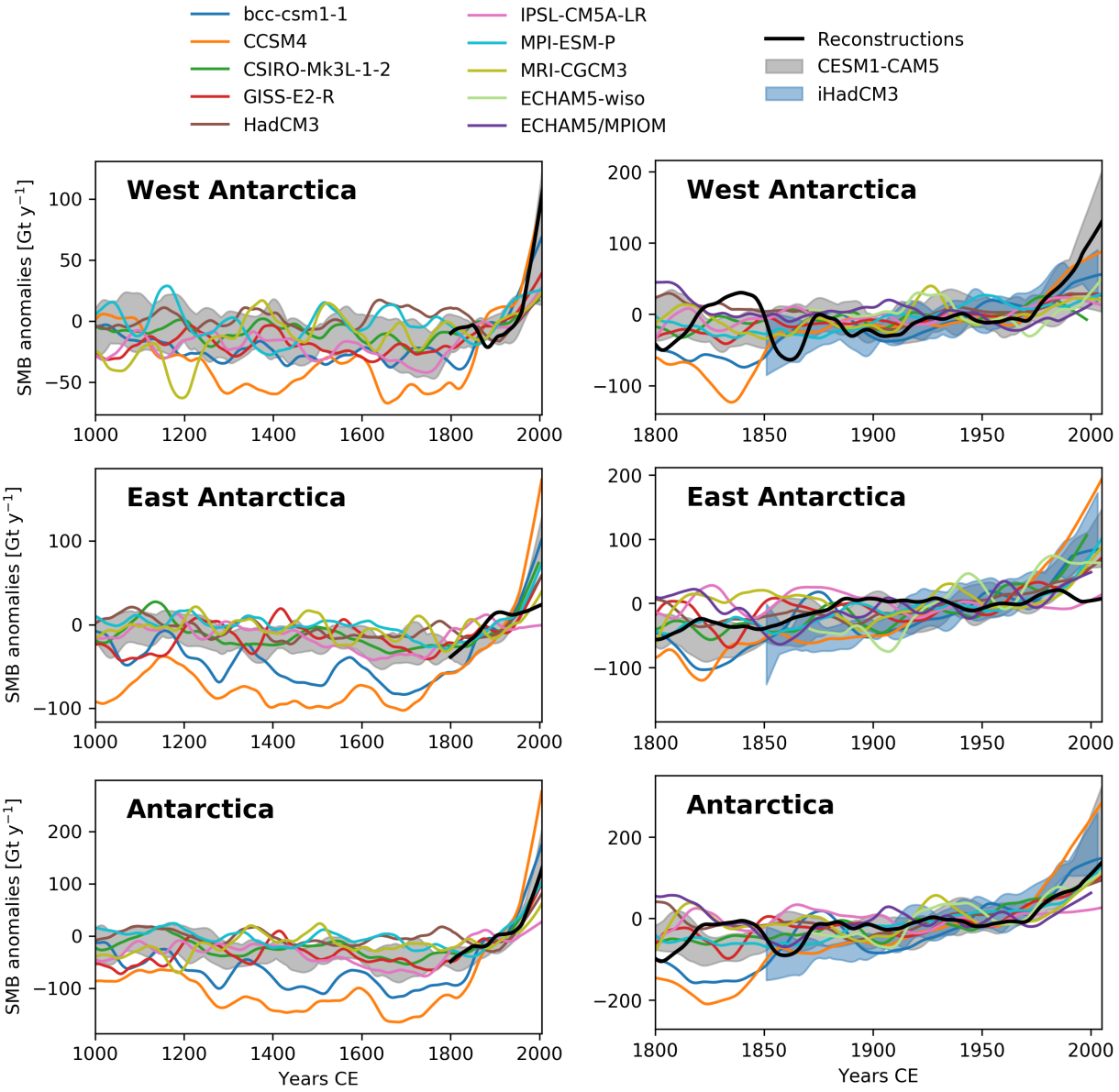


Figure 2.2: *Surface Mass Balance anomalies [Gt y^{-1}] simulated by the GCMs (Tab. A.1) and snow accumulation reconstructions [Thomas et al., 2017] during 1000 to 2005 CE and during 1800 to 2005 CE for West Antarctica, East Antarctica and Antarctica as a whole. Anomalies are relative to the 1871–2000 period. The shaded area corresponds to the range of the CESM1-CAM5 simulations. For visibility, data has been smoothed with a 100-year moving average for the last millennium and a 30-year moving average for the last 200 years. The equivalent for the seven subregions is given on Fig. A.1.*

year^{-1} per decade respectively; Figs. 2.2 and 2.3 and Tab. A.2). When analyzing the ensemble of simulations performed with CESM1-CAM5, the ensemble mean also shows a relatively homogeneous increase, but some simulations display a contrast between East Antarctica and West Antarctica close to the one observed in the reconstruction (Fig. 2.3). This suggests that internal variability has a dominant contribution in the current Antarctic SMB changes and might explain why the observed contrast between East and West Antarctica is only present in a few simulations.

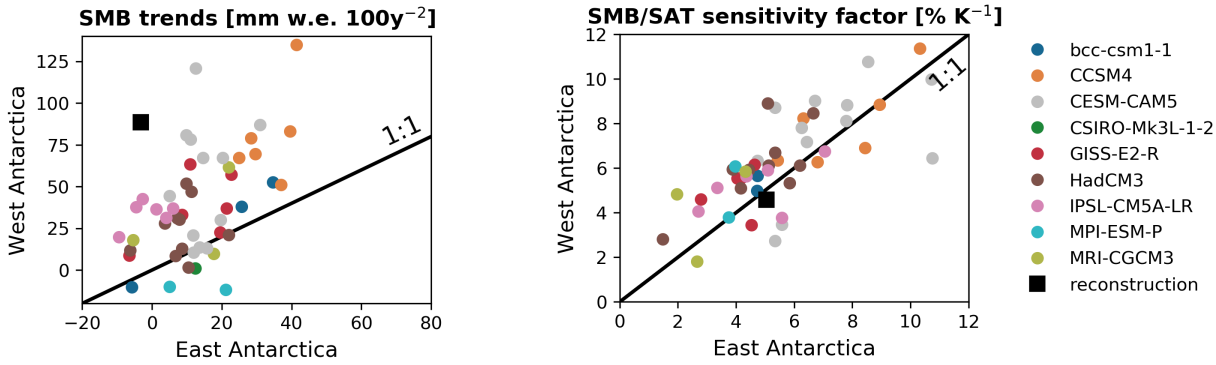


Figure 2.3: *(left) Comparison between the reconstructed and the simulated SMB trends (mm w.e./100y^{-2}) over the period 1950–2000 CE in West Antarctica (y axis) and East Antarctica (x axis). (right) As on the left but for SMB/SAT sensitivity factors (% K^{-1}). For the reconstruction, data from Thomas et al. [2017] and Nicolas and Bromwich [2014] are used.*

2.4.2 Relationship between SMB and surface air temperatures in Antarctica

Averaged across all GCMs, the relationship between SMB and surface air temperature is positive for each Antarctic region (Fig. 2.4). A very similar result is obtained when the annual mean surface air temperature and SMB derived from the RACMO2 simulation over the recent period (1979–2016) are used. The regional correlations are much weaker for the reconstructions based on ice cores than those obtained from model outputs (Fig. 2.4). These results are also true for detrended times series, indicating that this modelled link is valid at the inter-annual time-scale (not shown).

To quantify more precisely the link between surface air temperature and SMB in model outputs and reconstructions, the SMB sensitivity to temperature – defined as the slope of the linear fit between surface air temperature (SAT) and SMB – has been calculated. Firstly, the GCMs and reconstruction [i.e., Thomas et al., 2017; Nicolas and Bromwich, 2014] suggest that this sensitivity is similar for both West

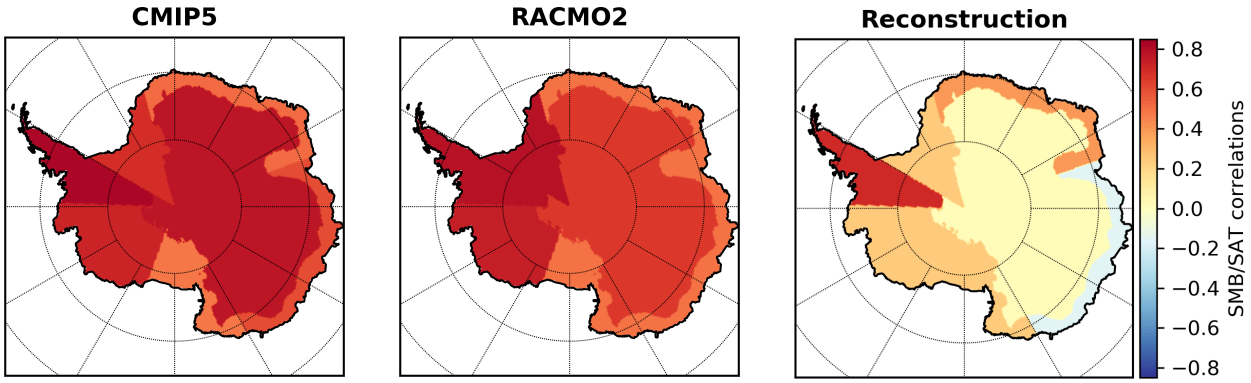


Figure 2.4: *5 yearly correlations (r) between SMB and surface air temperature for seven Antarctic regions (see Fig. 2.1 for geographical definitions) for GCMs over 1850–2000 CE (left), for RACMO2 over 1979–2016 CE (center) and for ice core reconstructions [Thomas et al., 2017; Stenni et al., 2017] over 1850–2000 CE (right). For the CMIP5 models and RACMO2, their correlations are all statistically significant (p-value<0.05). For the reconstructions, the statistically significant (p-value<0.05) correlations are obtained for the Antarctic Peninsula and Dronning Maud Land Coast. See Fig. A.2 for the correlations for each CMIP5 model.*

Antarctica and East Antarctica over the 1950–2000 CE period (Fig. 2.3). Secondly, on average over the entire continent, this sensitivity reaches 3.6 % K^{-1} in ice cores-based reconstructions for the 1850–1949 period. According to these reconstructions, this sensitivity has increased a lot for the recent period (1950–2005; 15.52 % K^{-1}), confirming the findings of Frieler et al. [2015]. However, Frieler et al. [2015] do not obtain such an increase in SMB sensitivity (only $\sim$+40%). Additionally, this recent increase found here in the reconstructions is not represented by the GCMs: on average, the simulated sensitivity of SMB to surface air temperature is 5.0 $\pm$ 1.1 % K^{-1} over 1850–1949 CE and 5.4 $\pm$ 2.0 % K^{-1} over 1950–2005 CE. When looking at the regional scale over 1850–2005 CE, the average SMB sensitivity over all models for West Antarctica (6.8 % K^{-1}) is in good agreement with the one deduced from the reconstructions (8.0 % K^{-1}; Fig. 2.5), while for East Antarctica, the sensitivity of the model mean is higher than the one obtained from the reconstructions (6.2 % K^{-1} and 2.1 % K^{-1} respectively). The very low SMB sensitivity in the reconstructions for East Antarctica, especially on the Antarctic Plateau (0.5 % K^{-1}) is somewhat unexpected, given that this region is continental and thus less affected by synoptic activities than coastal areas [Monaghan and Bromwich, 2008]. Actually, when using the observed surface air temperatures [e.g., Nicolas and Bromwich, 2014] instead of the reconstructed ones of Stenni et al. [2017], the Antarctic SMB sensitivity to temperature is strongly increased (4.02 % K^{-1} for the 1958–2010 CE period), and thus closer to the resulting sensitivity found in the GCMs (5.4 $\pm$ 2.0 % K^{-1} for the 1950–2005 CE period).

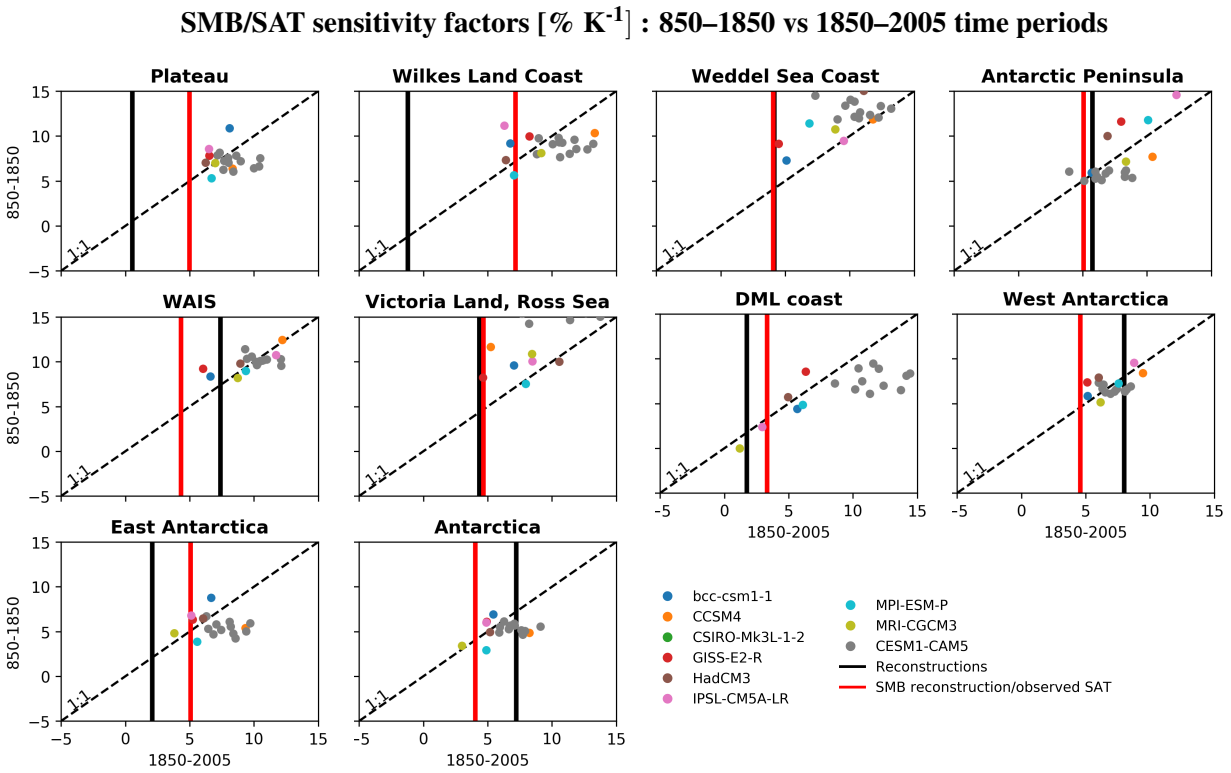


Figure 2.5: *SMB sensitivity to Surface Air Temperature (SAT) over the 850–1850 CE and the 1850–2005 CE periods for each Antarctic region (see Fig. 2.1 for geographical definitions) for GCM outputs. Additionally, the SMB-δ^{18}O sensitivity for ice cores based-reconstructions [i.e., Thomas et al., 2017; Stenni et al., 2017] over 1850–2005 CE is represented by a solid black vertical line while a solid red vertical line represents the SMB-observed surface air temperature sensitivity [i.e., Thomas et al., 2017; Nicolas and Bromwich, 2014] over 1960–2010 CE. For the CESM1-CAM5 model, the 12 simulations are plotted as grey points.*

In the study of Neukom et al. [2018], the authors argue that the data sampling, the noise in proxy data and the deficiencies in the reconstruction methods can partly explain the discrepancy between models and reconstructions for the surface air temperature during the last millennium, especially for the southern hemisphere. The spatial coverage of the surface air temperature and SMB reconstructions based on ice cores is poor, in particular for East Antarctica [Stenni et al., 2017; Thomas et al., 2017]. Moreover, due to the low snow accumulation in some regions, the uncertainties of the reconstruction are large for both surface air temperatures and SMB, leading to noise in the time series [Stenni et al., 2017; Thomas et al., 2017; Frezzotti et al., 2007]. Since the SMB reconstruction is only based on direct snow accumulation measurements, this is expected to be more accurate than the δ^{18}O-based temperature reconstruction, which is built by assuming a stationary link between δ^{18}O and surface air temperature. Because a lot of processes (such as precipitation seasonality or moisture origin) can signif-

icantly modify this relationship over time [e.g., Jouzel et al., 1997; Sime et al., 2008], this is computed over a short calibration period, but this might be too short to be representative [Klein et al., 2019]. Consequently, all these processes could explain the large differences between models and proxy-based reconstructions in the estimation of SMB sensitivity to surface air temperatures.

2.4.3 SMB and surface air temperature reconstructions from data assimilation

The high correlation values obtained between SMB and surface air temperatures in GCMs suggest that we can potentially use SMB to reconstruct Antarctic surface air temperature. The analysis of isotope-enabled model results reinforces this hypothesis (Fig. 2.6): the iHadCM3 outputs show high correlations between these two variables. For most regions, the link between surface air temperature and SMB (r=0.70 on average over the seven subregions for the 1850–2000 CE period) is higher than that between surface air temperatures and δ^{18}O (r=0.55 on average over the seven subregions for the 1850–2000 CE period). This is consistent with the observations: the regional correlations between SMB from ice cores [e.g., Thomas et al., 2017] and the observed surface air temperatures [i.e., Nicolas and Bromwich, 2014] are high for several regions over the 1960–2010 CE period (using 5-year averages as for Stenni et al. [2017]). In particular, this correlation for East Antarctica is 0.82 (statistically significant). The results with the outputs of ECHAM5-wiso and ECHAM5/MPI-OM are a bit more nuanced than those from iHadCM3 (Fig. A.3). The results of ECHAM5-wiso and ECHAM5/MPI-OM confirm this strong link between SMB and temperature but, in contrast to iHadCM3, the correlations are not systematically higher than between δ^{18}O and temperature. When analyzing the long ECHAM5/MPI-OM simulation (800–2000 CE), the relationship between SMB and surface air temperature is generally higher than between δ^{18}O and surface air temperature but the difference is small. For some regions, the SMB-surface air temperature link is much higher than the δ^{18}O-surface air temperature link but it is weaker for other regions. Compared to the δ^{18}O-surface air temperature link, the SMB-surface air temperature is also less spatially variable (minimum regional correlation is 0.54 against 0.07 for the δ^{18}O-surface air temperature link).

2.4.3.1 Surface air temperatures reconstruction

When constraining the model with the SMB reconstruction of Thomas et al. [2017], the obtained surface air temperature reconstruction is less well correlated with the reconstruction of Stenni et al. [2017] than for the data assimilation reconstruction constrained by only the δ^{18}O (Fig. 2.7). However, the difference is relatively small,

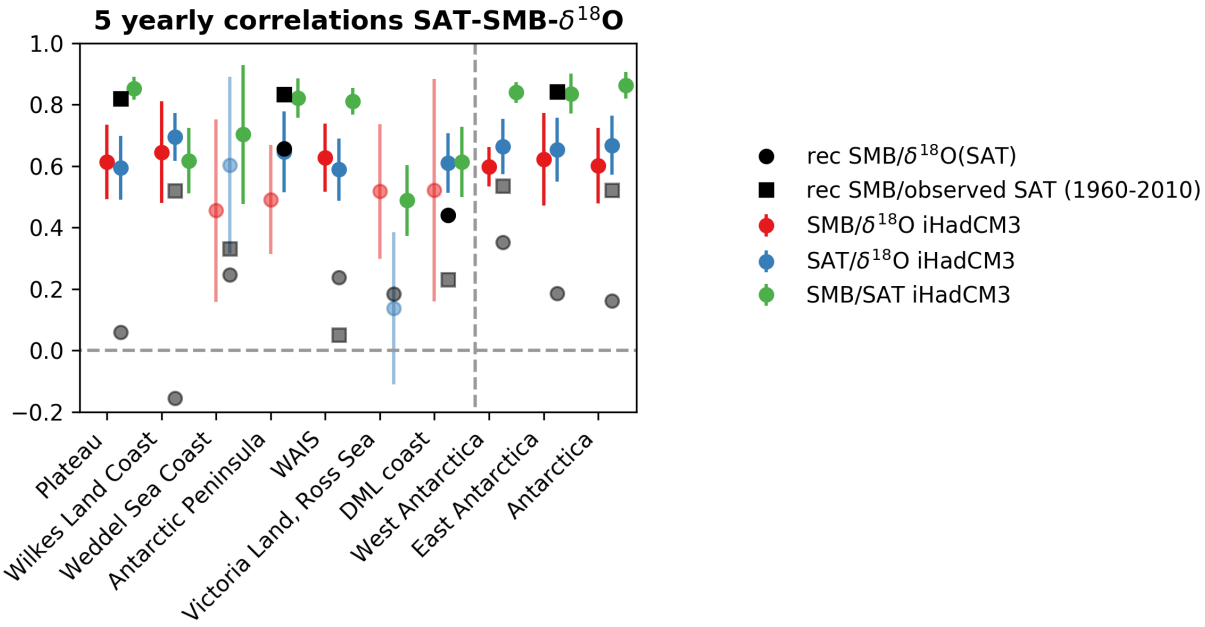


Figure 2.6: *5 year correlations between SMB and δ^{18}O, surface air temperature and δ^{18}O, and SMB and surface air temperature for the seven Antarctic regions over 1850–1995 CE period from the iHadCM3 outputs. The error bars correspond to the range (maximum and minimum) of the iHadCM3 simulations while the dot is the mean of the simulation ensemble. In black circles, the correlation between the SMB ice core reconstructions from Thomas et al. [2017] and the δ^{18}O of Antarctic ice cores aggregated for the seven Antarctic regions [Stenni et al., 2017]. In black squares, the correlation between the SMB reconstructions from Thomas et al. [2017] and the observed surface air temperatures aggregated for the seven Antarctic regions [Nicolas and Bromwich, 2014]. This latter dataset covers only the 1960–2010 CE period (5-year averages). Non-significant correlations (p-value>=0.05) are shown in pale.*

despite the fact that SMB and surface air temperatures are more strongly correlated in models than in the ice core reconstruction (0.86 for iHadCM3 against 0.16 for ice cores; Fig. 2.6). When compared to observed surface air temperature over the 1958–2010 CE period [i.e., Nicolas and Bromwich, 2014], the surface air temperature reconstruction of Stenni et al. [2017] as well as the reconstruction when only δ^{18}O is assimilated is in good agreement with the observed surface air temperatures for West Antarctica (Tab. 2.1, coefficient correlations are 0.79 and 0.69 respectively, both statistically significant) but not for East Antarctica (coefficient correlations are 0.10 and 0.13 respectively, both not statistically significant).

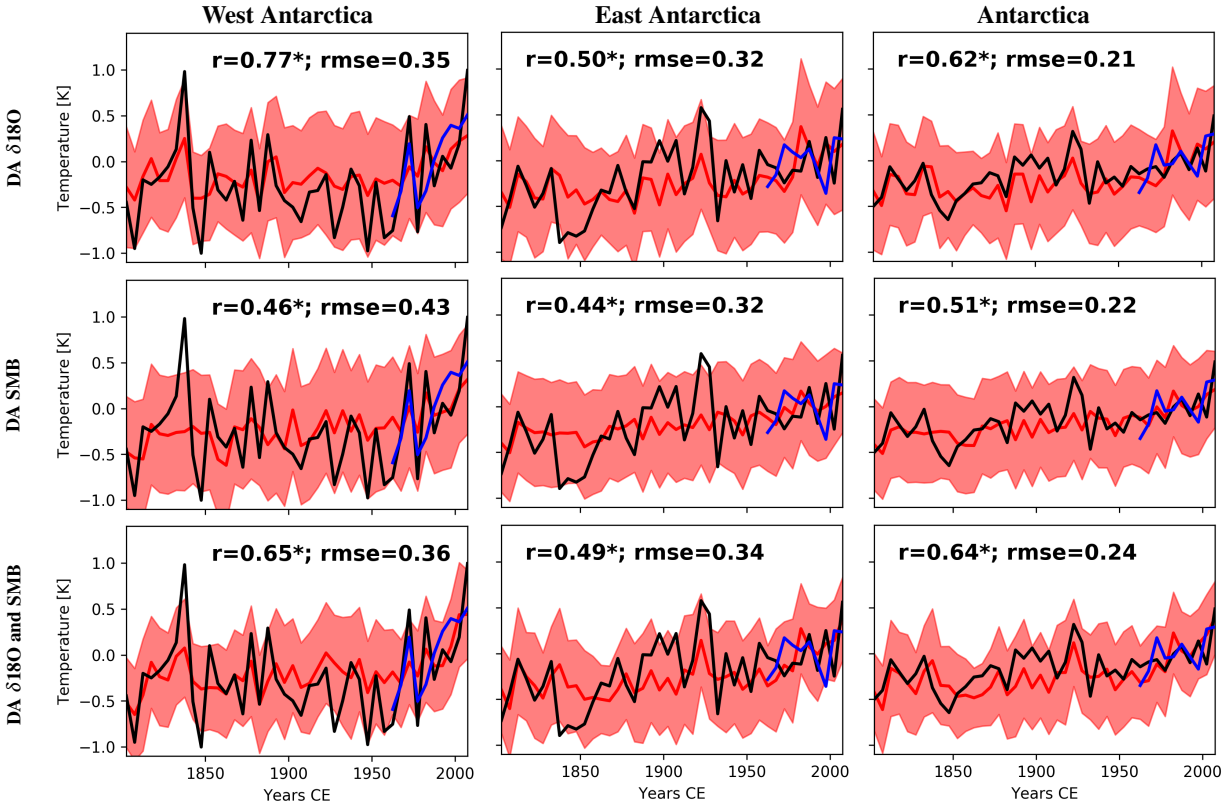


Figure 2.7: *Reconstructed temperatures (5-year mean) for West Antarctica, East Antarctica and for Antarctica as a whole from data assimilation experiment (red) using the iHadCM3 outputs and $\delta^{18}O$ [Stenni et al., 2017] and SMB reconstruction [Thomas et al., 2017] as constrain in the data assimilation process. The period is 1800–2010. The surface air temperature reconstruction of Stenni et al. [2017] are represented in black and those from Nicolas and Bromwich [2014] are in blue. DA $\delta^{18}O$ (first row) is the data assimilation experiment using only the $\delta^{18}O$ data to constrain the model while DA SMB (second row) uses the SMB reconstruction and DA $\delta^{18}O$ and SMB (third row) uses both. For each experiment and each region, the correlation (r) between the reconstruction based on ice cores (in black) and that based on data assimilation is computed (in red). The shaded areas represent $\pm$ 1 standard deviation of the model particles. Stars represent the statistically significant correlation (p-value<0.05).*

Table 2.1: *5-year mean correlations between the three surface air temperature reconstructions from data assimilation experiments using the ECHAM5-MPI/OM, ECHAM5-wiso and iHadCM3 outputs and the statistical reconstruction of Stenni et al. [2017], with the surface air temperature reconstructions from Nicolas and Bromwich [2014] over the 1958–2010 CE period for West Antarctica, East Antarctica and Antarctica as a whole. Stars represent statistically significant correlations (p-value<0.10). DA stands for data assimilation.*

	West Antarctica			East Antarctica			Antarctica		
	ECHAM5-MPI/OM	ECHAM5-wiso	iHadCM3	ECHAM5-MPI/OM	ECHAM5-wiso	iHadCM3	ECHAM5-MPI/OM	ECHAM5-wiso	iHadCM3
DA δ^{18}O	0.57*	0.78*	0.69*	0.19	0.08	0.13	0.50	0.47	0.34
DA SMB	0.40	0.52	0.55	0.27	0.53	0.60*	0.28	0.58*	0.65*
DA δ^{18}O and SMB	0.53	0.65*	0.72*	0.34	0.48	0.61*	0.59*	0.71*	0.73*
Stenni et al. [2017]		0.79*			0.10			0.57*	

In contrast to the data assimilation experiment, in which only δ^{18}O is assimilated, the skill of the surface air temperature reconstruction is almost identical for both regions in the data assimilation experiment where only SMB is assimilated: r=0.55 (p-value<0.1) for West Antarctica and r=0.60 (p-value<0.1) for East Antarctica. Assimilating SMB thus provides a more spatially robust temperature reconstruction than when assimilating δ^{18}O. When both δ^{18}O and SMB are taken into account in the data assimilation process, the skill of the surface air temperature reconstructions for the two sub-Antarctic regions is higher (r=0.72 and 0.61 for West Antarctica and for East Antarctica respectively, both significant) than when assimilating separately the δ^{18}O or the SMB. Moreover, the only reconstruction that provides statistically significant results for all the regions (West, East and the entire Antarctica; p-value<0.1) is when both δ^{18}O and SMB are assimilated, implying that assimilating both proxies offers more robust results than only assimilating one of them.

When looking at the linearly detrended time series, our final reconstruction (i.e., when δ^{18}O and SMB are assimilated) displays a null correlation with observed surface air temperature (p-value=0.99) for West Antarctica, but the correlation remains high for East Antarctica (r=0.60; p-value=0.07). During the 1958–2012 CE period, a significant warming is observed in West Antarctica while no significant change is noticed for East Antarctica [Nicolas and Bromwich, 2014]. Consequently, data assimilation tends to reproduce the warming for West Antarctica and the inter-annual variability for East Antarctica, explaining our different results between the original and detrended time series. Additionally, as well as our reconstruction based on only δ^{18}O, the correlation of the detrended δ^{18}O-based temperature reconstruction of Stenni et al. [2017] with the observed one for East Antarctica is non-significant and negative suggesting that SMB constitutes a better proxy than δ^{18}O for surface air temperatures, at least at the inter-annual time-scale (see Tab. A.3).

Regarding surface air temperature trends over the last two centuries, our reconstructions displays an increase of 0.02°C per decade for West Antarctica and 0.023°C per decade for East Antarctica, which finally leads to an increase of 0.022°C per decade for Antarctica as a whole (all statistically significant). For the 1961–2010 CE period, our reconstruction is able to simulate the observed contrast between West and East Antarctica (0.22 °C per decade (significant) and 0.053 °C per decade (not significant), respectively, for Nicolas and Bromwich [2014] compared with 0.1 °C per decade and 0.06 °C per decade, respectively, for our reconstruction, both significant). The resulting contrast in our reconstruction is thus less large than observed (see Tab. A.4 for details). However, because of the short time period considered, these values can highly vary depending on the time interval chosen (not shown).

2.4.3.2 SMB reconstruction

Constraining the model with the δ^{18}O data leads to a poor SMB reconstruction, especially for West Antarctica (correlation coefficient of 0.29; Fig. 2.8). Moreover, the constraint derived from observed δ^{18}O on SMB is weak as illustrated by the large error band of the reconstruction (estimated by the weighted variance of the particles with non-zero weight). When assimilating both δ^{18}O and SMB, the SMB reconstruction is in good agreement with the reconstruction of Thomas et al. [2017] as expected.

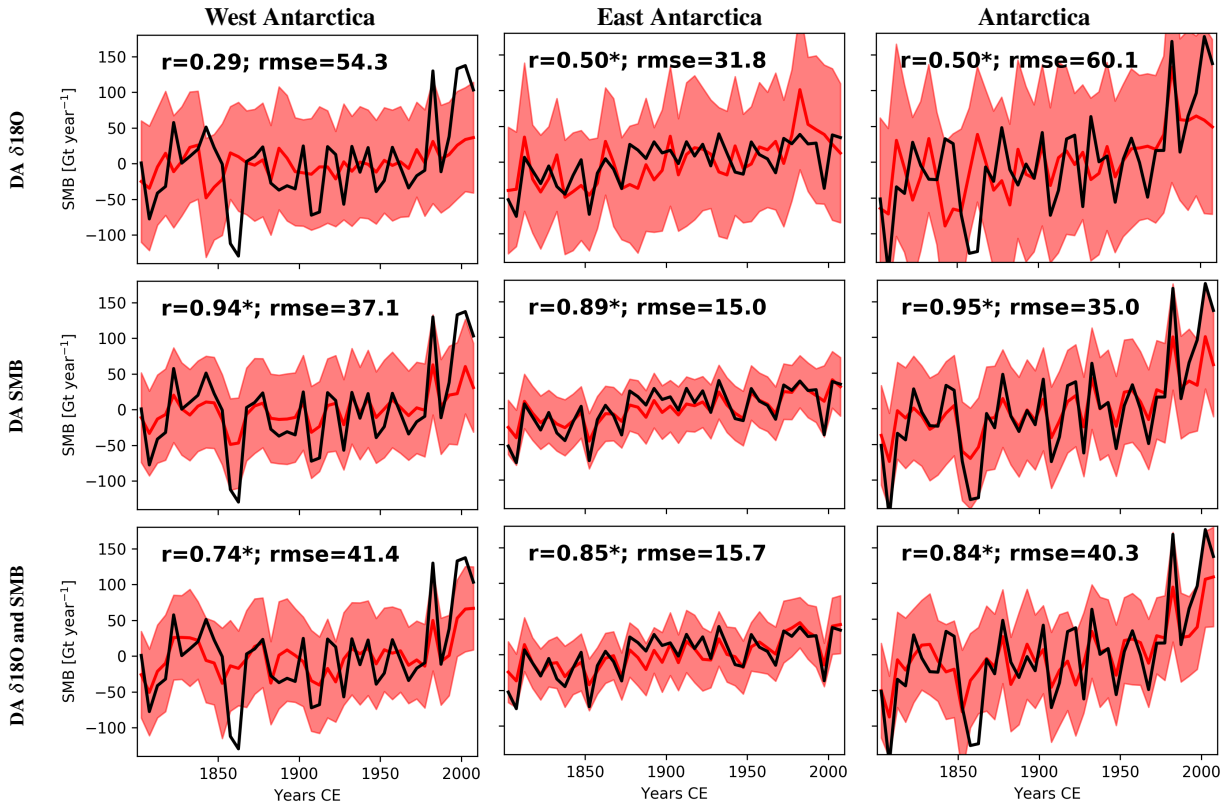


Figure 2.8: *Reconstructed SMB (5-year mean) for West Antarctica, East Antarctica and Antarctica as a whole from data assimilation experiment using the iHadCM3 outputs and δ^{18}O [Stenni et al., 2017] and SMB reconstruction (in black) [Thomas et al., 2017] as constrain in the data assimilation process. The period is 1800–2010 CE. DA δ^{18}O (first row) is the data assimilation experiment using only the δ^{18}O data to constraint the model while DA SMB (second row) uses the SMB reconstruction and DA δ^{18}O and SMB (third row) uses both. For each experiment and each region, the correlation (r) between the reconstruction based on ice cores (in black) and that based on data assimilation is computed (in red). The shaded areas represent $\pm$ 1 standard deviation of the model particles. Stars represent the statistically significant correlation (p-value<0.05).*

According to this data assimilation-based SMB reconstruction, the grounded AIS SMB (i.e., SMB over the AIS excluding ice shelves) has increased at a 0.26

$\pm$ 0.05 Gt year^{-2} pace (p-value<0.05) during the 1801–2000 CE period (Tab. 2.2) and 0.70 $\pm$ 0.45 Gt year^{-2} (p-value>0.05) for the 1957–2000 CE period. Over this latter period, West Antarctica has witnessed a significant increase of 0.82 $\pm$ 0.40 Gt year^{-2} while East Antarctica displays a decrease of 0.13 $\pm$ 0.33 Gt year^{-2} (p-value>0.05). Unlike West Antarctica, the non statistical significance of the SMB trend for East Antarctica might imply that internal variability currently plays a large role in the SMB variability there [e.g., Jones et al., 2016]. However, if we focus on the shorter 1979–2000 CE period, a significant decrease is obtained for East Antarctica (-3.3 $\pm$ 0.87 Gt year^{-2}; p-value <0.05) while it is still positive for West Antarctica (1.6 $\pm$ 1.37 Gt year^{-2}; p-value>0.05), which is consistent with RACMO2 outputs (-3.7 Gt year^{-2} for East Antarctica and 2.0 Gt year^{-2} for West Antarctica, both not significant).

Table 2.2: *SMB trends over grounded (i.e., excluding ice shelves) West Antarctica, East Antarctica and Antarctica as a whole from 1) our reconstruction based on data assimilation using iHadCM3 outputs and, SMB and $\delta^{18}O$ data in the data assimilation procedure; 2) Medley and Thomas [2019]; 3) RACMO2 outputs for various time intervals (in Gt year^{-2}). Stars stand for statistically significant trends at 5% level. Errors for our reconstructions correspond to the standard error of the linear trend obtained in the linear regression.*

	In this study			Medley and Thomas (2019)			RACMO2
	1801 – 2000	1957 – 2000	1979 – 2000	1801 – 2000	1957 – 2000	1979 – 2000	1979 – 2000
West Antarctica	0.07$\pm$0.04	0.82*$\pm$0.40	1.6$\pm$1.37	0.1	1.3	1.7	2.0
East Antarctica	0.19*$\pm$0.03	-0.13$\pm$0.33	-3.3*$\pm$0.87	0.3*	-0.4	-4.5*	-3.7
Antarctica	0.26*$\pm$0.05	0.70$\pm$0.45	-1.7$\pm$1.45	0.4*	1.0	-2.7	-1.7

2.5 Discussion and conclusions

This paper discusses the AIS SMB over the last two centuries and its links with surface air temperature in reconstructions and model simulations. The analysis of the relationship between SMB and surface air temperature in models and in ice core reconstructions highlighted the covariance between both variables that can potentially be used to reconstruct past changes. The relevance of SMB in the reconstruction of surface air temperature in Antarctica is based on a relatively simple concept: Antarctic precipitation originates mainly from lower latitudes, in the form of warm and wet air masses [Goodwin et al., 2016; Turner et al., 2016a; Clem et al., 2018]. Nevertheless, $\delta^{18}O$ also provides useful temperature-related information that can be used to complement the information provided by SMB, such as changes in moisture origin [e.g., Holloway et al., 2016a]. Our analyses pointed out

significant model-data discrepancies in the SMB-surface air temperature relationship. On the one hand, models show a strong correlation between δ^{18}O and SMB for many Antarctic regions and, on the other hand, the reconstructions based on ice cores display a weak relationship. Furthermore, unlike previous studies [e.g., Frieler et al., 2015] who suggest an increase of the SMB sensitivity to surface air temperature for the future in Antarctica ($\sim$ 40%), we show that the current sensitivity is not exceptionally high compared to the last 200 years, according to CMIP5 models.

These large discrepancies between model results and reconstructions can be explained by different factors. The GCMs may have biases in the simulated temperature changes. For example, as shown by Klein et al. [2019], GCMs display on average a homogeneous warming over Antarctica during the last decades while observations mainly show warming for West Antarctica with no significant change for East Antarctica. Additionally, climate model simulations generally display a warming starting in the 19th century in Antarctica while it begins much later in proxy-based reconstructions [Abram et al., 2016]. This suggests that reconstructions underestimate the response to anthropogenic forcing or that climate models overestimate it. In this latter case, this may contribute to an overestimation of the contribution of the simple thermodynamic link between temperature and precipitation and thus snow accumulation while it underestimates the role of changes in atmospheric circulation variability [Abram et al., 2016; Klein et al., 2019; PAGES 2k-PMIP3 group, 2015]. Nevertheless, by removing the linear trend of time series, we obtained similar results. Models may also neglect processes such as blowing snow that can reduce the correlation between temperature and SMB. On the other hand, RACMO2, which includes a simple representation of blowing snow and is nudged to observed temperature and large-scale circulation changes, displays similar correlations to that of the GCMs. Another hypothesis is that differences could rather arise from uncertainties in the reconstructions. To understand the potential origin of the disagreements between model results and reconstructions over the last millennium, Neukom et al. [2018] used pseudoproxy experiments. They found that uncertainties in the reconstructions and the data sampling could be an explanation for many observed discrepancies between models and reconstructions.

By analyzing isotope-enabled climate models, we showed that on average over the models, the relationship between SMB and surface air temperature is often higher (or at least equivalent) and more stable than the one between surface air temperature and δ^{18}O. This is true both on the continental and regional scale. Unlike SMB, δ^{18}O can be subject to large uncertainties linked to precipitation seasonality [Sime et al., 2008] or changes in moisture origins [Holloway et al., 2016a], which can explain the weaker correlations.

Our data assimilation experiments confirm the benefits of using both proxies – SMB and δ^{18}O – to reconstruct surface air temperature. When assimilating both δ^{18}O and SMB data, the resulting reconstruction shows a higher correlation with observed surface air temperature over the period 1958–2010 CE [i.e., Nicolas and Bromwich, 2014] for the entire Antarctic continent (r=0.73) than the one obtained with the reconstruction based on the statistical method of Stenni et al. (2017; r=0.57). The difference is larger for East Antarctica, where the reconstruction skill is enhanced by incorporating SMB data (r=0.61 for our reconstruction against 0.10 for the reconstruction of [Stenni et al., 2017]). For West Antarctica, our reconstruction is very similar to Stenni et al. [2017]'s statistical method. This improvement can be explained by the large uncertainties in δ^{18}O data for East Antarctica, probably because of the low amount of ice cores and low snow accumulation in those areas. In comparison to Stenni et al. [2017] and Klein et al. [2019], who obtain a higher surface air temperature trend over the last two centuries for East Antarctica (0.03 °C per decade and 0.018 °C per decade respectively, both significant) than for West Antarctica (0.011 °C per decade and 0.01 °C per decade respectively, both not significant), our data assimilation-based reconstruction reveals similar surface air temperature trends for both regions (0.02 °C per decade and 0.023 °C per decade respectively, both significant). However, over the entire continent, the trend is almost the same between the different datasets (0.022 °C per decade in this study (significant), 0.019 °C per decade for Stenni et al. [2017], significant, and 0.016 °C per decade for Klein et al. [2019], not significant). Over the last decades (1961–2010 CE), all the reconstructions are able to reproduce the observed contrast between West Antarctica (large warming) and East Antarctica (weak warming), but overall, they underestimate it (see Tab. A.4 for details). Our reconstruction displays smaller variance in time than the reconstruction from Stenni et al. [2017], which is a standard characteristic of estimates based on data assimilation using only a few uncertain data [e.g., Goosse et al., 2010].

Regarding changes in SMB over the last two centuries, our reconstruction shows large regional differences in SMB trends, both in magnitude and in signs, in accordance with Medley and Thomas (2019; Fig. A.4) who used the same ice core dataset but a different method. While they obtain a statistically significant SMB increase of 0.4 Gt year^{-2} over the grounded AIS for the 1801–2000 CE period, our result suggests a weaker increase (0.26 $\pm$ 0.05 Gt year^{-2}; p-value<0.001; see Tab. 2.2 for details). A similar underestimation is noticed for the 1957–2000 CE period, (1.0 Gt year^{-2} for Medley and Thomas [2019], not significant, and 0.70 $\pm$ 0.45 Gt year^{-2} for our reconstruction, p-value=0.130). Over the last decades (1979–2000 CE), both Medley and Thomas [2019] and our results reveal that grounded West Antarctica gains mass at its surface (1.6 $\pm$ 1.37 Gt year^{-2} in this study and 1.7 Gt year^{-2} for Medley and Thomas [2019], both not significant) while grounded East Antarctica has experienced a very large SMB decrease (-3.3 $\pm$ 0.87 Gt year^{-2} and

-4.5 Gt year^{-2} respectively, both significant), which is consistent with the value obtained in the RACMO2 outputs (2.0 Gt year^{-2} for West Antarctica -3.7 Gt year^{-2} for East Antarctica, both not significant).

More generally, in contrast to statistical methods, data assimilation ensures that reconstructions are compatible with the physics of the system as represented in the models chosen. Although it is not possible to independently evaluate our SMB reconstruction, our good results regarding surface air temperatures and SMB reconstructions suggest that the strong simulated correlation between surface air temperatures and SMB in GCMs is not a model artefact. This is supported by a strong link between these two variables in observations when using snow accumulation data from Thomas et al. [2017] and surface air temperatures from Nicolas and Bromwich [2014], in particular for East Antarctica (r=0.82, statistically significant). Therefore, our study shows that SMB records seem to be a relevant proxy in reconstructing surface air temperature in complementary with δ^{18}O records. Since only a few records are available before the instrumental period over Antarctica, any relevant record to reconstruct the Antarctic climate and more specifically surface air temperature is welcome. Additionally, data assimilation appears particularly well adapted for reconstructing surface air temperatures as the covariance between variables is obtained directly from climate models that explicitly include physical processes while statistical approaches restrict the problem to empirical linear relationships. By using data assimilation, no assumption such as stationarity or long calibration periods is required to estimate the link between variables, assumptions whose validity can strongly vary in time and space [Klein et al., 2019]. However, to get a skillful data assimilation-based reconstruction, it is essential that the selected climate models have an adequate representation of climate variability and that good uncertainty estimates are available for the chosen datasets.

3

Reconstructing atmospheric circulation and sea-ice extent in the West Antarctic over the past 200 years using data assimilation

Abstract

The West Antarctic climate has witnessed large changes during the second half of the 20th century including a strong and widespread continental warming, important regional changes in sea-ice extent and snow accumulation, as well as a major mass loss from the melting of some ice shelves. However, the potential links between those observed changes are still unclear and instrumental data do not allow determining if they are part of a long-term evolution or specific to the recent decades. In this study, we analyze the climate variability of the past two centuries in the West Antarctic sector by reconstructing the key atmospheric variables (atmospheric circulation, near-surface air temperature and snow accumulation) as well as the sea-ice extent at the annual timescale using a data assimilation approach. To this end, information from Antarctic ice core records (snow accumulation and δ^{18}O) and tree-ring width records situated in the mid-latitudes of the Southern Hemisphere are combined with the physics of climate models using a data assimilation method. This ultimately provides a complete spatial reconstruction over the West Antarctic region. Our reconstruction reproduces well the main characteristics of the observed changes over the instrumental period. We show that the observed sea-ice reduction in the Bellingshausen-Amundsen Sea sector over the satellite era is part of a long-term trend, starting at around 1850 CE, while the sea-ice expansion in the Ross Sea sector has only started around 1950 CE. Furthermore, according to our reconstruction, the Amundsen Sea Low pressure

This chapter is based on: Dalaiden, Q., Goosse, H., Rezsohazy, J. and Thomas, E.R. (2021). Reconstructing atmospheric circulation and sea-ice extent in the West Antarctic over the past 200 years using data assimilation, In review in *Climate Dynamics*. Supplementary materials are in Appendix B.

(ASL) displays no significant linear trend in its strength or position over 1850–1950 CE but becomes stronger and shifts eastward afterwards. The year-to-year sea-ice variations in the Ross Sea sector are strongly related to the ASL variability over the past two centuries, including the recent trends. By contrast, the link between ASL and sea-ice in the Bellingshausen-Amundsen Sea sector changes with time, being stronger in recent decades than before. Our reconstruction also suggests that the continental response to the variability of the ASL may not be stationary over time, being significantly affected by modification of the mean circulation. Finally, we show that the widespread warming since 1958 CE in West Antarctica is unusual in the context of past 200 years and is explained by both the deeper ASL and the positive phase of the Southern Annular Mode.

3.1 Introduction

The Antarctic Ice Sheet is the biggest reservoir of fresh water on Earth that would potentially rise the global sea-level of 58 m if the entire ice sheet melted [Shepherd et al., 2018a]. Despite the remote location, the Antarctic and the Southern Ocean have experienced major climate changes over the past decades [e.g., Jones et al., 2019; Bromwich et al., 2013; Medley and Thomas, 2019; Pritchard et al., 2012], demonstrating large variability and their vulnerability to the global climate change.

The largest changes have been found over the Antarctic Peninsula and the West Antarctic Ice Sheet (hereafter WAIS) [e.g., Jones et al., 2019], together forming West Antarctica. A major warming has been observed since the International Geophysical Year (i.e., 1958 CE), far exceeding the global warming during the same period [Vaughan et al., 2003; Turner et al., 2005a; Nicolas and Bromwich, 2014]. Although the warming is particularly pronounced over the Peninsula, the warming over the central WAIS since the 1950s is one of the fastest recorded on Earth [Steig et al., 2009; Bromwich et al., 2013]. Moreover, in the last decades, glaciers from West Antarctica (especially the Thwaites and Pine Island glaciers) have been losing mass at the ocean-ice shelf (i.e., the floating part of the glacier) interface at an accelerated rate [Pritchard et al., 2012; Rignot et al., 2019]. This ice shelf melting positively contributes to the global sea-level rise, by directly enhancing the ice flow to the Southern Ocean. In contrast with these spatially homogeneous changes, snow accumulation integrated over West Antarctica has increased at an increased pace over the 20th century, but with strong regional differences [Medley and Thomas, 2019; Wang et al., 2019]. While the Antarctic Peninsula and the Eastern WAIS have gained mass at the surface through snow accumulation, the Western WAIS has displayed a snow accumulation decrease [Medley and Thomas, 2019]. Additionally, a large reduction of the sea-ice extent has been noticed in the Bellingshausen/Amundsen Sea sector that contrasts with an expansion

in the Ross Sea sector over the satellite era (starting from 1979 CE) [Parkinson, 2019].

The observed changes in West Antarctica are not independent of each other, and have been widely attributed to changes in atmospheric circulation [e.g., Bromwich et al., 2013; Thomas et al., 2013; Steig et al., 2013], characterized by an increase in the intensity and a poleward shift of the westerly winds (Westerlies) [Marshall, 2003]. This has been observed as a deepening in the Amundsen Sea Low (ASL), a quasi-stationary low-pressure system located off the Amundsen coast (hereafter ASL) [e.g., Raphael et al., 2016]. Due to its location, variations in both the strength and position of the ASL strongly modulate the West Antarctic climate [e.g., Hosking et al., 2013]. For instance, a stronger ASL enhances the northerly flow (onshore winds) to the continent, which warms the Antarctic Peninsula and the eastern WAIS [e.g., Hosking et al., 2013] and increases snow accumulation [Turner et al., 2005b; Thomas et al., 2008]. At the same time a stronger ASL enhances the southerly flow (offshore winds) of cold dry air masses over the western WAIS leading to lower temperatures and reduced snow accumulation. In addition to continental changes, a stronger ASL is also associated with reduced sea-ice cover in the Bellingshausen/Amundsen Sea sector and a sea-ice cover expansion in the Ross Sea sector [e.g., Raphael and Hobbs, 2014]. A deeper ASL also drives oceanic changes, enhancing warm ocean water upwelling towards ice shelves, inducing basal melting [e.g., Mankoff et al., 2012; Dotto et al., 2020].

The ASL is thus a major feature of the atmospheric circulation in the Southern Hemisphere, which displays one of the greatest year-to-year variations on Earth [e.g., Turner et al., 2019a]. The ASL is strongly modulated by the atmospheric circulation of the high latitudes of the Southern Hemisphere. Particularly, the Southern Annular Mode (hereafter SAM) describes the latitudinal movement of the Westerlies as well as their strength [e.g., Fogt and Marshall, 2020]. When the SAM is in its positive phase, the Westerlies are stronger and located further south than in the negative phase, which in turn deepens the ASL [e.g., Raphael et al., 2016]. The ASL is thus strongly related to the SAM. Wind changes in the West Antarctic are also closely linked to the climate variability in tropical oceanic basins. Several studies [e.g., Ding et al., 2011; Steig et al., 2013; Thomas et al., 2013; Meehl et al., 2016; Holland et al., 2019] have suggested the important tropical teleconnections that exist between the mid-latitudes/tropics and the West Antarctic. More specifically, positive anomalies in sea surface temperature in the tropical Pacific Ocean induce a convective heat event that further propagates to the West Antarctic region via the formation of Rossby wave train.

Despite the large changes observed recently, the impact of the ASL variability on West Antarctic climate changes has not been fully studied because *in-situ* observations are lacking [Turner et al., 2004]. Over the satellite era (from 1979 CE), atmospheric reanalyses seem to be reliable for studying the ASL variability

and its impacts on the West Antarctic climate [Bracegirdle, 2013]. However, because of the high internal variability in the Amundsen region [e.g., Raphael et al., 2016], longer time-series are needed to understand the processes controlling the variability in the region.

In this study, we aim to better understand the West Antarctic climate variability on decadal to centennial timescales by analyzing the relationships between the main atmospheric variables with surface conditions and sea-ice cover. Furthermore, by making use of those potential links between variables, we provide historical estimations over the past two centuries that could not be directly observed. Special attention is given to the ASL, because of its major importance in the ongoing observed changes in West Antarctica. We investigate to which extent the ASL variability explains the West Antarctic climate change over the past two centuries, and if the role of the ASL has changed over time. The sea-ice extent (in particular the Bellingshausen/Amundsen Sea and Ross Sea sector) is also examined due to its key role in modulating West Antarctic climate [e.g., Lefebvre and Goosse, 2008; Thomas et al., 2013; Turner et al., 2017]. Up to now, no spatial estimate of wind fields or sea-ice extent has been specifically validated for this region before the instrumental era and thus we aim to fill this gap. In addition to improving the general long-term changes in the West Antarctic climate, we assess the representativeness of the climate changes occurring during the second half of the 20^{th} century on a longer time perspective. Finally, a complementary goal is to highlight the mechanisms that explain the warming over West Antarctica as a whole and the strong regional asymmetry in sea-ice extent trends over the past decades.

To this end, we provide a spatially complete and multi-variate reconstruction of the West Antarctic climate changes over the past two centuries (the period for which most paleoclimate proxies are available; see below) by optimally combining paleoclimate records and a climate model using a data assimilation approach. Over last years, data assimilation has been increasingly applied in paleoclimatology for estimating past climate changes [e.g., Goosse et al., 2009; Hakim et al., 2016; Steiger et al., 2017; Goosse et al., 2010]. Compared to simpler statistical methods [e.g., Stenni et al., 2017; Emile-Geay et al., 2017], data assimilation does not assume a stationary relationship between the proxy and the climate. Data assimilation ensures that the resulting climate reconstruction is dynamically coherent. Such a method is also particularly relevant for regions like the West Antarctic where a strong coupling exists between the observed changes from various variables [Jones et al., 2016; Fan et al., 2014; Goosse et al., 2009]. Here, the model is constrained by δ^{18}O and snow accumulation records from Antarctic ice cores. Over the Antarctic, ice core is the most widespread climate archive for assessing historical climate changes at high temporal resolution (i.e., annual scale). Compared to the instrumental network, the ice core network is well de-

veloped over West Antarctica thanks to a number of international drilling efforts. In addition to the ice cores, we also make use of the tree-ring width records from the mid-latitudes that capture changes in past climate variability [e.g., Emile-Geay et al., 2017]. The inclusion of non-specific-Antarctic proxies guarantees a large-scale coherence. This avoids forcing a local agreement with the Antarctic data that would not be based on processes compatible with larger-scale changes.

This study is organized as follows. Section 3.2 includes a description of the data assimilation method, the paleoclimate proxies and the model used for the reconstruction. We discuss the performance of our reconstruction in section 3.3 by comparing it with instrumental observations and other climate reconstructions, and discuss our main results, before concluding.

3.2 Data assimilation method

Data assimilation (DA) optimally combines the information from observations and the climate physics as included in climate models. In practice, the data assimilation process updates the initial state of the climate given by the model (i.e., the prior) according to the available observations to provide the best estimate of the climate state (i.e., the posterior), while also considering the errors associated with both the data and model. The prior includes all the variables to be reconstructed. For instance, the 500-hPa geopotential height can be reconstructed only by assimilating near-surface air temperature. In that situation, the reconstructed 500-hPa geopotential height relies on the covariance relationships between the 500-hPa geopotential height and near-surface air temperature in the model. If there is no covariance between the variable of interest and the assimilated variable, the reconstruction skill of the variable of interest will be null.

The DA method employed in this study is an offline approach (also called a no-cycling method). This method uses existing climate model simulations to draw the prior. In contrast to the standard online data assimilation approach, the prior is estimated by selecting different years of a climate model simulation. Therefore, no information is propagated in time. This approach is totally appropriate when the predictability time-scale of the system is much smaller than the data assimilation time step (here, one year). This is particularly true when assimilating atmospheric variables because of the small correlation time in the atmosphere. In such cases, no additional relevant information is gained when using an online approach, as shown by Matsikaris et al. [2015].

3.2.1 Particle filter

The DA method used here is based on a particle filter following the implementation of Dubinkina et al. [2011] (see this reference for more details). This method

has been recently applied to reconstruct successfully large-scale near-surface air temperature and snow accumulation over Antarctica during the last two millennia and the past two centuries [Klein et al., 2019; Dalaiden et al., 2020a]. We thus describe briefly the method here.

For each time step of the data assimilation process (here one year), all the model states, called here particles (i.e., the prior) are evaluated against the available observations. Those model states are given by all the years (annual mean) of the iCESM1 ensemble (3 simulations) spanning the 850–1850 CE period (see section 3.2.5 for the model evaluation). The prior includes 3003 particles, that are fixed throughout the data assimilation process, for all time steps. During the data assimilation process, the likelihood of each particle is computed by taking into account the data uncertainties (see section 3.2.6 for the error associated with the data). A weight is then given to each particle, based on its likelihood. For each time step, the climate variables are then reconstructed as the weighted mean of the particles. The range of the reconstruction (also called ensemble reconstruction) is estimated by computing the weighted standard deviation of the particles. The prior is estimated by taking all the years (annual mean) of the iCESM1 ensemble (3 simulations) spanning the 850–1850 CE period (see section 3.2.5 for the model evaluation). The prior includes 3003 particles, that are fixed throughout the data assimilation process, for all time steps. For more details on the implementation of the particle filter, see Dubinkina et al. [2011].

3.2.2 Evaluation metrics

In order to quantify the performance of our reconstruction, we use three different metrics that compare the results with observations or other reconstructions. The first one is the Pearson correlation coefficient (r), which determines the strength of the linear relationship between two time-series:

$$r = \frac{1}{n} \sum_{i=1}^{n} \left(\frac{(y_i - \overline{y})(x_i - \overline{x})}{\sigma_y \sigma_x} \right) \tag{3.1}$$

where n is the number of samples, y stands for the predicted vector while x is the true vector. Overbars indicate the mean over the time. σ_y and σ_x are the standard deviations of y and x, respectively. Although a high value of r indicates that the predicted values follow the direction of the true values, it does not ensure that the variations of the amplitude are well reproduced. Therefore, the second metric is the coefficient of efficiency [Nash and Sutcliffe, 1970], which depends on the amplitude of the signal:

$$\mathrm{CE} = 1 - \sum_{i=1}^{n} \frac{(x_i - y_i)^2}{(x_i - \overline{x})^2} \tag{3.2}$$

A high value for CE thus indicates that both the timing and the amplitude are right. Finally, we need to verify if the ensemble reconstruction is similar to the reconstruction error relative to observations. For this purpose, we compute the ensemble calibration ratio (ECR) defined here as:

$$\text{ECR} = \text{median}\left[\frac{(x_i - y_i)^2}{\sigma^2_{x,i}}\right] \tag{3.3}$$

where i varies from 0 to n and $\sigma^2_{x,i}$ is the variance of the reconstruction ensemble. An ECR of 1 means that the reconstruction is well calibrated (i.e., the reconstruction error equals the uncertainty of the reconstruction). When ECR<1, the ensemble has too much variance compared to the reconstruction error (i.e., underdispersive ensemble). On the contrary, when ECR>1, the ensemble is overdispersive, which means that the reconstruction ensemble does not include enough variance compared to the reconstruction error.

3.2.3 Proxy data

From the 79 ice core snow accumulation records included in the database of Thomas et al. [2017], we only keep the annually-resolved records (48 out of 79) as in Medley and Thomas [2019]. Medley and Thomas [2019] provide a spatially complete annual Antarctic snow accumulation over the past two centuries using this ice core snow accumulation database (Fig. 3.1). This excludes a majority of snow accumulation records in the continental Dronning Maud Land region. As in Medley and Thomas [2019], we also add the B40 ice core record of snow accumulation [Medley et al., 2018], which was published after the compilation of Thomas et al. [2017]. Additionally, we also employ the information from the ratio of stable isotopes oxygen in the ice core (δ^{18}O). Stenni et al. [2017] provide a compilation of the Antarctic precipitation-weighted δ^{18}O records (n=112) covering the last two millennia. We only keep the 29 annually-resolved δ^{18}O records. It is worth noting that the majority of the ice cores (both snow accumulation and δ^{18}O records) are located in West Antarctica (WAIS; Fig. 3.1).

In addition to the Antarctic proxies, we also utilize the continental annually-resolved proxies situated in the Southern Hemisphere from the global database of the PAGES2k working group that includes all the proxy records suitable for reconstructing the global temperature over the last two millennia [PAGES2k Consortium et al., 2013; Emile-Geay et al., 2017]. Among all the continental proxies included in the global database for the Southern Hemisphere, only the tree-ring width (hereafter TRW) are annually-resolved (in addition to some Antarctic ice cores already included in our study). A total of 18 sites presenting TRW time-series over past centuries are located in the Southern Hemisphere : three in New Zealand, three

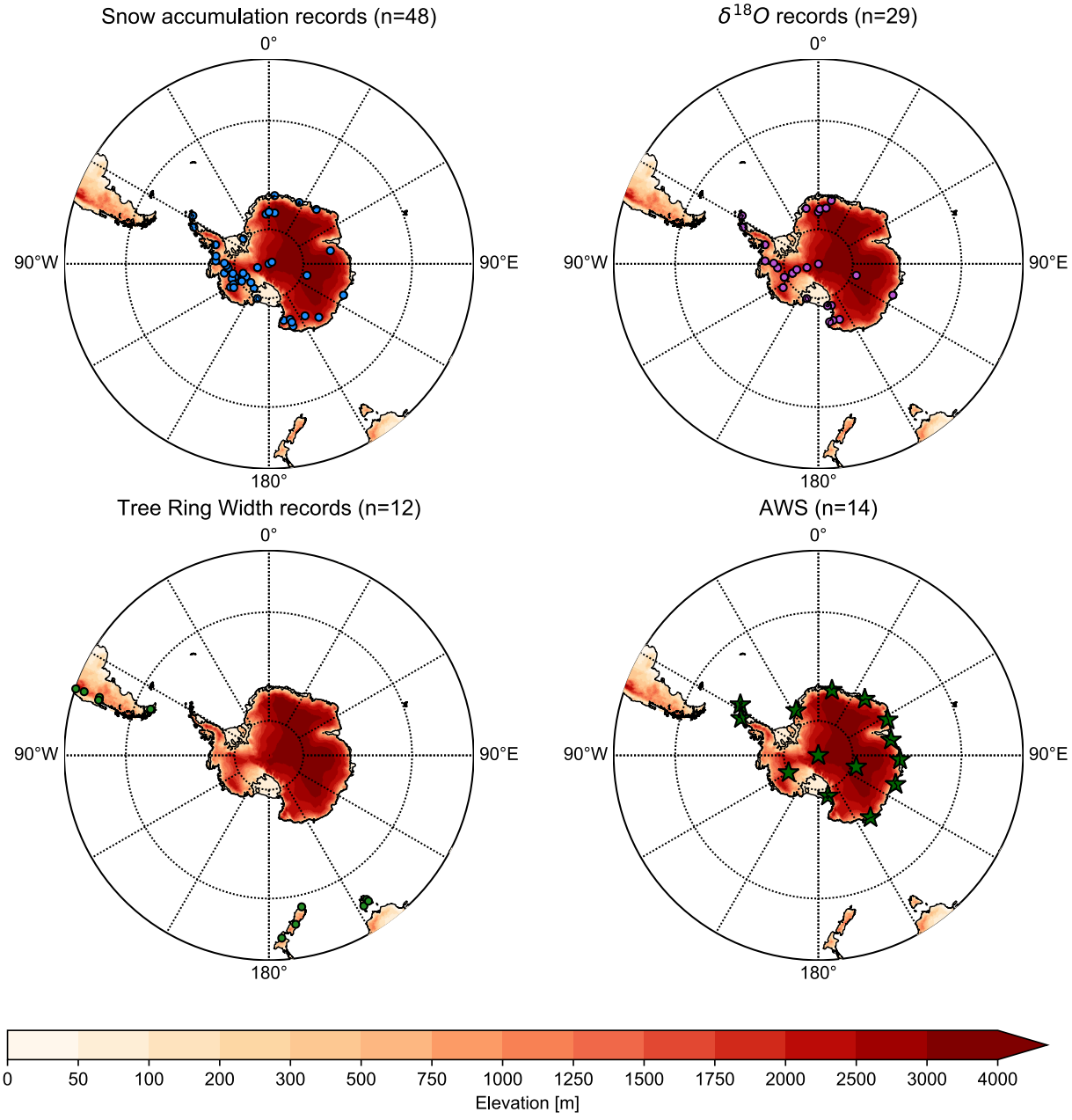


Figure 3.1: *Annually-resolved climate/proxy records used in this study: snow accumulation records (blue dots), $\delta^{18}O$ records (purple squares), Automatic Weather Stations (AWSs; green stars) and tree-ring width records (green dots). The map background represents the surface elevation (m).*

in Tasmania and 12 in South America. Among the 12 South American sites, only six are positively correlated with climate (either near-surface air temperature or precipitation) according to our dataset (see section 3.2.4) over the 1941–1990 CE period, and thus included. The geographical distribution of the selected sites is presented in Fig. 3.1.

In order to reduce the non-climatic noise and provide equal weighting in each region (i.e not bias a particular region with multiple records), a 500 km grid (square cells of 500 km side) was established and records from the same grid were averaged together. For snow accumulation records, they are all normalized over the 1941–1990 CE period (mean zero and unit standard deviation) and the records situated in the same cell are averaged. The mean of normalized snow accumulation records for each grid cell produces the normalized composites. For each composite, the variance is then scaled to the variance of the spatial snow accumulation reconstruction from Medley and Thomas [2019], linearly interpolated on the 500 km grid over the 1941–1990 CE period. Compared to snow accumulation, the δ^{18}O records display a weaker spatial variability as they are less dependent on the topography and do not need normalization. Instead, δ^{18}O composites for each grid cell are obtained by averaging the anomalies of δ^{18}O records over the 1941–1990 CE. Finally, we apply the same methodology as for the snow accumulation records to TRW time-series, but without correcting the variance (z-scored composites) since TRW data is originally normalized.

3.2.4 Proxy System Models

Snow accumulation records are directly compared to the precipitation minus sublimation/evaporation ($P - E$) from the climate model simulation. Snow accumulation recorded in ice cores is the sum of both precipitation and post depositional changes (wind erosion, sublimation and melt). Several studies have shown that precipitation dominates and that snow accumulation can be directly compared with the precipitation minus sublimation/evaporation ($P - E$) from the climate model simulation [Lenaerts et al., 2017; Souverijns et al., 2018; van Wessem et al., 2018; Agosta et al., 2019]. This is particularly true when working at a large spatial scale – as in our study (500 km grid) – and over the grounded ice sheet (i.e., the Antarctic Ice Sheet without ice shelves) [Agosta et al., 2019]. Additionally, since iCESM1 explicitly simulates the ratios of water isotopes in all the climate components, the δ^{18}O records are also directly compared to the δ^{18}O simulated by the model.

A Proxy System Model (PSM) specifically designed for the TRW is required in order to compare the model results to the proxy. To this end, a TRW PSM is built for each TRW time-series. Instead of a mechanistic model, which simulates tree-ring growth by explicitly including the biological processes that drives the relationship between climate and tree growth [e.g., Guiot et al., 2014; Misson, 2004;

Dufrêne et al., 2005; Rezsöhazy et al., 2020], we use a simple statistical model. It has the advantage of being easily implemented but the relationship between climate and tree growth is estimated empirically, without taking into account any biological processes. This method is similar to the one used in the Last Millennium Reanalysis [Tardif et al., 2018].

In this study, we consider that trees are sensitive to the temperature or precipitation, or to both. Therefore, we introduce two types of models:

$$y_i = \beta_0 + \beta_1 X_{1i} + \epsilon_i \tag{3.4}$$

$$y_i = \beta_0 + \beta_1 X_{1i} + \beta_2 X_{2i} + \epsilon_i \tag{3.5}$$

where y_i corresponds to the observed z-scored TRW time-series (i.e., the independent variable) for site *i*; β_{1i} and β_{2i} are the slopes associated with the X_{1i} and X_{2i} of the i time-series, which are the explanatory variables; ϵ_i are the errors, assumed to be normally (Gaussian) distributed with a zero mean and a unitary variance (0, σ^2). Parameters of the Eqs. (3.4) and (3.5) are estimated using the ordinary least squares method.

Similarly to the Last Millennium Reanalysis [Tardif et al., 2018], we use the near-surface air temperature and precipitation as explanatory variables (X_1 and X_2). In addition to the annual mean of near-surface air temperature and precipitation, the climate variables are also averaged over different months during the calendar year (January to December), in order to take into account the seasonal response of trees: JJA and OND. All the possible combinations are tested. The calibration of the PSM is performed over the 1941–1990 CE period using the Global Meteorological Forcing Dataset for land surface modeling (v2; http://hydrology.princeton.edu/data.php, last access: 22 June 2020; hereafter GMF) [Sheffield et al., 2006] interpolated on the 500 km grid excluding the oceanic grid cells. The sensitivity to the climate data has been assessed by also performing the calibration with the surface temperature from the NASA Goddard Institute for Space Studies Surface Temperature Analysis [Hansen et al., 2010] and precipitation from the Global Precipitation Climatology Centre [Schneider et al., 2014]. Results display no major difference (not shown).

To select the best PSM for each TRW composite, we rely on the Bayesian information criterion (BIC) [Schwarz, 1978] value defined as :

$$\text{BIC} = -2 * LL + log(n) * k \tag{3.6}$$

where LL is the natural logarithm of the likelihood for the model – estimated as the mean squared error of the linear regression model [Watkins and Mardia, 1992] – and k corresponds to the number of parameters in the regression model (i.e., 2 and 3 for the uni and bi-variate models, respectively). The BIC is a particularly

relevant metric to select the best model among uni and bi-variate models as the most complex models are penalized. Accordingly, the PSM displaying the lowest BIC is selected.

3.2.5 Climate model simulation

The initial estimate of the state of the climate system (i.e., the prior) is derived from an ensemble of three simulations performed with the Community Earth System Model (CESM) spanning the 850–1850 CE time period. We use the version of CESM including the simulation of water stable isotopes, iCESM1-CAM5 (hereafter iCESM1) [Brady et al., 2019; Stevenson et al., 2019]. iCESM1 is a coupled atmosphere-ocean model including a sea-ice component. The atmosphere is resolved at approximately 2° and the ocean at 1°. The iCESM1 simulations include the orbital changes, the solar variability, the volcanic forcing through changes in stratospheric aerosols and greenhouse gases, the land use changes and finally the human-induced greenhouse gases [Stevenson et al., 2019].

Although numerous studies have shown that CESM is well-suitable for studying the Antarctic climate over the past, present and future [Lenaerts et al., 2016; Fyke et al., 2017; England et al., 2016; Lenaerts et al., 2018; Dalaiden et al., 2020b], this version has not yet been evaluated over the Antarctic continent. Therefore, we briefly evaluate the Antarctic climate as simulated by iCESM1 by comparing it to the latest ECMWF's atmospheric reanalysis, ERA5 [Hersbach et al., 2020]. It is considered as one of the best reanalyses in simulating the Antarctic climate over the satellite-era [Gossart et al., 2019a; Tetzner et al., 2019]. Since the paleoclimate proxies used in this study are annually-resolved, the evaluation is carried out on annual averages.

Over the 1979–2005 CE period, the geopotential height at 500-hPa is well simulated in iCESM1 (Fig. B.1; below south of 45°S, R^2=97%; relative bias=-0.2% computed as the mean relative difference between the 500-hPa geopotential height from iCESM1 and ERA5 south of 45°S) and includes the three main low-pressure systems in Amundsen Sea, Dronning Maud Land and Wilkes Land. Regarding the near-surface air temperature, iCESM1 simulates the temperature gradient with the highest temperatures along the coasts and the lowest temperatures in the interior of the ice sheet (over the Antarctic continent, R^2=76%; relative bias=-2.0%). Like temperature, snow accumulation is highly dependent on the topography. iCESM1 reproduces the Antarctic snow accumulation pattern well from ERA5 (R^2=85% – based on log values as the snow accumulation distribution is log-normal [Agosta et al., 2019]–; relative bias=-6.9%). However, iCESM1 is not able to reproduce the high spatial variability of snow accumulation at local scale, because of its coarse horizontal spatial resolution. Besides, iCESM1 displays a total Antarctic sea-ice extent of 11.7 10^6 km^2 against 11.9 10^6 km^2 for observa-

tions from the National Snow and Ice Data Center (NSIDC; data available here: `https://nsidc.org/data/NSIDC-0051/versions/1`, last access: 5 September 2018). This suggests that iCESM1 is able to simulate relatively well the mean state of Antarctic sea-ice extent at present. Finally, although a quantitative evaluation of the simulated precipitation-weighted δ^{18}O is not possible because of the insufficient amount of Antarctic observations (3 records in the Global Network of Isotopes in Precipitation), the precipitation-weighted δ^{18}O pattern over Antarctica captures the gradient between the coasts (with the highest values, less negative) and the Plateau (with the lowest values, more negative) due to isotopic fractionations (Fig. B.2). Based on the skill of iCESM1 in simulating present-day Antarctic climate, we deem this model suitable for building the prior of the data assimilation experiment. As proxy data are averaged over a 500 km regular grid (see section 3.2.3), the prior has been linearly interpolated on this 500 km regular grid, as well.

3.2.6 Observation error

Data assimilation requires an error of the assimilated data. Three types of observation errors are usually mentioned [e.g., Badgeley et al., 2020]. The first type of observation error directly comes from the accuracy of the measurement, i.e., the instrumental error. The second type of observation error is related to the processes in observations that are unresolved at the spatial scale of the model because of its coarse resolution , the so-called representativeness observation error [e.g., Oke and Sakov, 2008; Janjić et al., 2018]. Finally, the last type of observation error arises from the performance of the PSM in simulating the relationship between the proxy and the climate variable(s). Overall, the instrumental error is much weaker than the two other observation errors [e.g., Oke and Sakov, 2008], especially in paleoclimatology [Tardif et al., 2018; Steiger et al., 2018; Badgeley et al., 2020]. This observation error is thus ignored in our study. Finally, regarding the snow accumulation and δ^{18}O records, we assume that the observation error related to the PSM is non-existent, since the model simulates both variables. The representativeness error is thus considered as the largest contributor to the observation error.

To estimate the representativeness error of the snow accumulation composite associated with the ice core records, we use an Antarctic simulation performed with the latest version of the Regional Atmospheric Climate MOdel (RACMO2.3p2, hereafter RACMO) at 27 km horizontal resolution) [van Wessem et al., 2018]. RACMO is a polar-oriented regional climate model that specifically resolves near-surface processes over Antarctica. For each snow accumulation composite, we proceed as follows. We retrieve the annual time-series of snow accumulation from RACMO at all the ice core snow accumulation records included in the composite, over the 1979–2016 CE period. In order to remove the dependence on the ele-

vation, the calculation is performed on time-series anomalies. All RACMO-time series are then averaged in time. Next, we compute the difference between this averaged snow accumulation time-series and the snow accumulation time-series from RACMO interpolated on the 500 km grid (i.e., the resolution of snow accumulation composites; see section 3.2.3). Eventually, the observation error is defined as the standard deviation of the time-series difference. Note that the error is calculated for each year of the composite (1800–2000 CE), based on the snow accumulation RACMO data (1979-2016 CE). As the number of ice cores in the composite decreases when going further in time, the observation error tends to increase. Finally, since RACMO does not simulate the δ^{18}O, we use the iCESM1 linearly interpolated on the RACMO grid over the 1950–2005 CE period to estimate the δ^{18}O observation error with the same methodology.

However, several studies [van Wessem et al., 2018; Lenaerts et al., 2016; Cavitte et al., 2020] have shown that the spatial variability of snow accumulation and δ^{18}O is underestimated in models (i.e., RACMO and iCESM1) compared to ice core observations. Therefore, using these models to estimate the observation error in our study probably also underestimates the errors. In order to provide more realistic errors we take into account the missing processes occurring between the scale represented in the models and the local scale of ice cores. This is achieved by performing a side-by-side comparison between adjacent snow accumulation records as in Fisher et al. [1985]. More specifically, we compute the standard deviation of the difference between each pair of annual time-series of snow accumulation records (in anomalies) within the same grid cell of the 500 km grid over the 1941–1990 CE. The calculation is made for all the possible combinations within the grid cell. According to the grid cell containing more than 5 ice cores (n=2; both situated in West Antarctica), the initial observation errors are underestimated on average by a 3.18 factor compared to the side-by-side comparison. Hence, the initial observation errors estimated from models at high resolution are increased by a spatially homogeneous factor of 3. The same exercise for δ^{18}O has been carried out and shows similar results (not shown).

Regarding the TRW composites, the error is estimated by taking the standard deviation of the residuals resulting from the linear regression (see Eqs. (3.4) and (3.5)) as in the Last Millennium Reanalysis (LMR) [Hakim et al., 2016; Tardif et al., 2018]. The error thus encompasses the representativeness error and the error related to the PSM since the PSM has been calibrated using the climate data interpolated on the 500 km grid and not using the local data.

3.2.7 Instrumental data assimilation-based reconstruction

Before using the paleo records to reconstruct the Antarctic climate over the past centuries (hereafter referred to as the paleo-reconstruction), we first reconstruct

the Antarctic climate over the 1958–2000 CE period using data assimilation with near-surface air temperature records and snow accumulation records from ice cores. Applying a methodology that is as close as possible to the one selected for the longer timescales allows us to validate the approach, in particular the data assimilation method and the estimations of the errors using observations with lower uncertainties than the paleo records. This reconstruction based on instrumental and snow accumulation records thus provides an upper bound for the skill we could expect with the paleoclimate network. To this end, we assimilate the near-surface air temperatures from the Automatic Weather Stations (AWSs) over the Antarctic continent [Turner et al., 2004] (n=14) starting from 1958 CE (see Fig. 3.1 for their geographical localization). The model is also constrained by the snow accumulation records from ice cores, which are the best estimate of long-term snow accumulation, since AWSs do not record this variable. Additionally, TRW records are replaced by the near-surface air temperatures from the dataset used for the calibration of the TRW PSM (i.e., GMF; only where TRW sites are available). This reconstruction is referred to as the instrumental reconstruction.

Such as for the paleo records, an error associated with the assimilated data is computed. The error on the near-surface air temperature from AWSs is calculated similarly to the snow accumulation error (see section 3.2.6) but using near-surface air temperatures from RACMO. The resulting error must be corrected to take into account the missing processes occurring between the local scale (i.e., the AWS scale) and the scale of RACMO (i.e., 27-km resolution). Because of the weaker spatial variability of near-surface air temperature compared to snow accumulation [e.g., Agosta et al., 2019; van Wessem et al., 2018], the error of near-surface air temperature is multiplied by a factor 2 and not 3 as used for snow accumulation (see section 3.2.6). Finally, similarly to Brennan et al. [2020], we take a constant error of 0.5 °C for the near-surface air temperature from GMF.

3.3 Results and discussion

3.3.1 Validation of the instrumental paleo reconstructions over the last decades

Before analyzing the long-term changes using the paleo-reconstruction over the past centuries, we first need to ensure that our data assimilation method works. We establish this by testing the skill of the instrumental and paleo reconstructions at reproducing interannual climate variability and trends over the last decades, in particular the atmospheric circulation, near-surface continental climate (temperature and snow accumulation) and sea-ice cover. To this end, Figure 3.2 presents the spatial correlation coefficients between our instrumental and paleo reconstructions and the latest ECMWF atmospheric reanalysis ERA5 [Hersbach et al., 2020]

over the 1979–2000 CE period for the 500-hPa geopotential height, near-surface air temperature and snow accumulation, as well as sea-ice concentration using the dataset from the National Snow and Ice Data Center (NSIDC) [Parkinson, 2019]. Although the period is short (22 years), this evaluation gives a first indication of the performance of our reconstruction when compared to independent data.

3.3.1.1 Near-surface air temperature

For continental near-surface air temperature, our spatial instrumental reconstruction is highly correlated with ERA5 over West Antarctica (Fig. 3.2). Our instrumental reconstruction is also close to the reconstruction of Nicolas and Bromwich [2014] – which is based on the same near-surface air temperature observations as in our reconstruction but using a kriging interpolation over 1958–2000 CE –, when averaging over the two main regions of the West Antarctic continent, i.e., the West Antarctic Ice Sheet (WAIS; 60-180°E and south of 72°S; r=0.88 (p-value<0.05), CE=0.71, ECR=0.27) and the Antarctic Peninsula (AP; west longitude north of 72°S; r=0.78 (p-value<0.05), CE=0.56, ECR=0.60; Fig. 3.3 a,b). The high CE and r values mean that both the interannual variability and the amplitude of changes are similar between the two reconstructions. ECR values are largely inferior to 1, which suggests that our reconstruction ensemble has too much variance compared to the mean squared error. However, this result is not surprising since both our instrumental reconstruction and Nicolas and Bromwich [2014] used the same near-surface air temperature dataset for the assimilation. Although the skill metrics are lower for the AP compared to the WAIS, our reconstruction correctly displays the largest warming in AP (0.38 °C per decade) as in Nicolas and Bromwich [2014] (0.46 °C per decade).

Comparing our paleo-reconstruction to the instrumental reconstruction shows that using paleo records instead of actual observations degrades the skill of the overall reconstruction, which is expected (Figs. 3.2 and 3.3a,b). However, near-surface air temperatures in the paleo-reconstruction still remain highly correlated with ERA5. This is in line with the good agreement with the near-surface air temperature reconstruction from Nicolas and Bromwich [2014] for the AP (r=0.62 (p-value<0.05), CE=0.21, ECR=0.95) and WAIS (r=0.53 (p-value<0.05), CE=0.28, ECR=0.37). For the linear trends over the 1958–2000 CE period, similarly to Nicolas and Bromwich [2014], our paleo-reconstruction displays warming of 0.42 °C per decade and 0.15 °C per decade for AP and WAIS respectively, which is closer than for our instrumental reconstruction (Fig. 3.3a,b). Our paleo-reconstruction therefore captures the trend better than the instrumental reconstruction, which could be related to the denser paleo network, but not the spatial variability, nor the interannual variability.

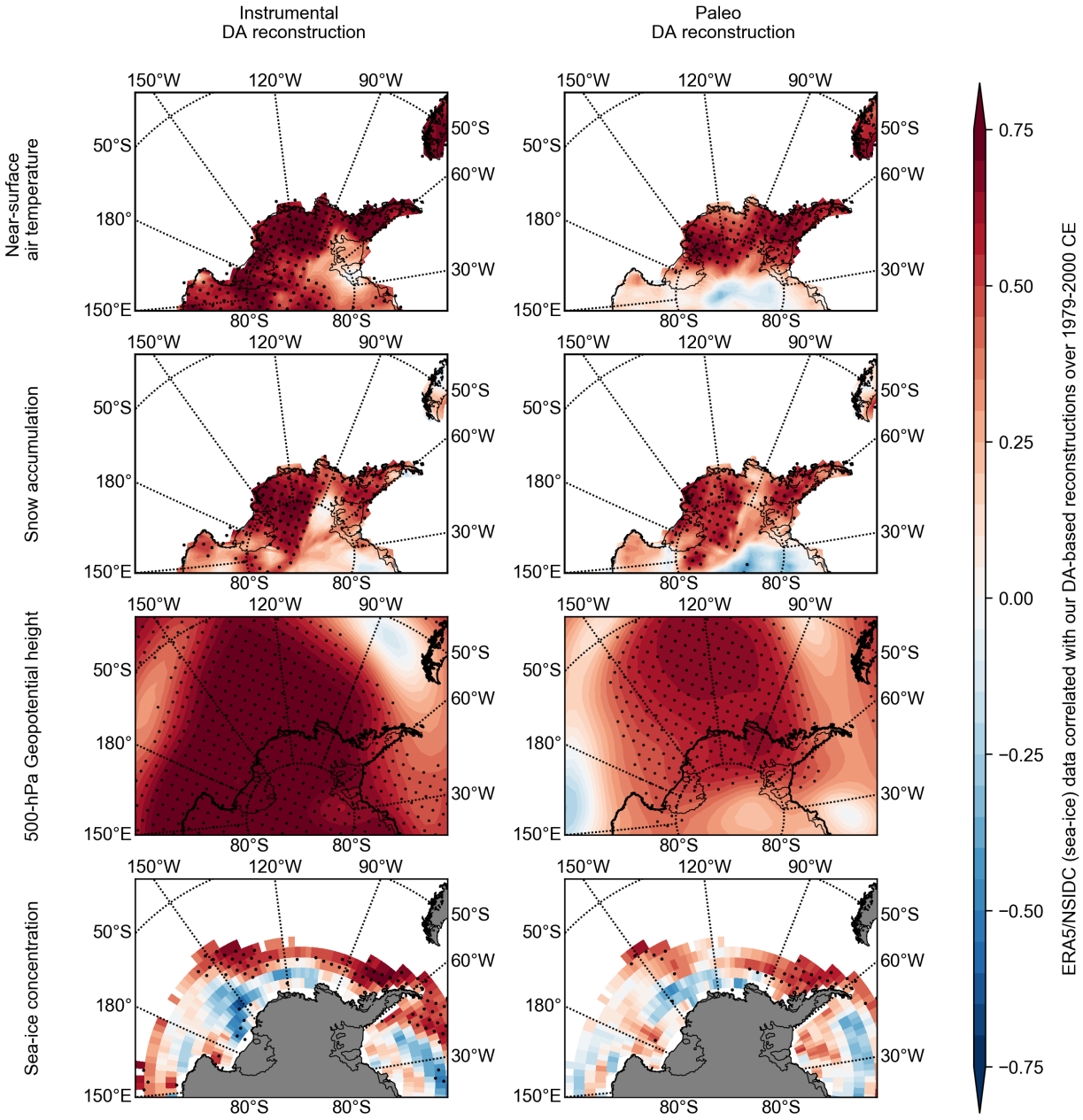


Figure 3.2: *Spatial correlation coefficients (r) between our instrumental (left) and paleo (right) reconstructions and the ERA5 reanalysis for the near-surface air temperature, snow accumulation, 500-hPa geopotential height and the sea-ice concentration from the National Snow and Ice Data Center (NSIDC) over the 1979–2000 CE period. Stippling indicates statistically significant correlations (95% confidence level).*

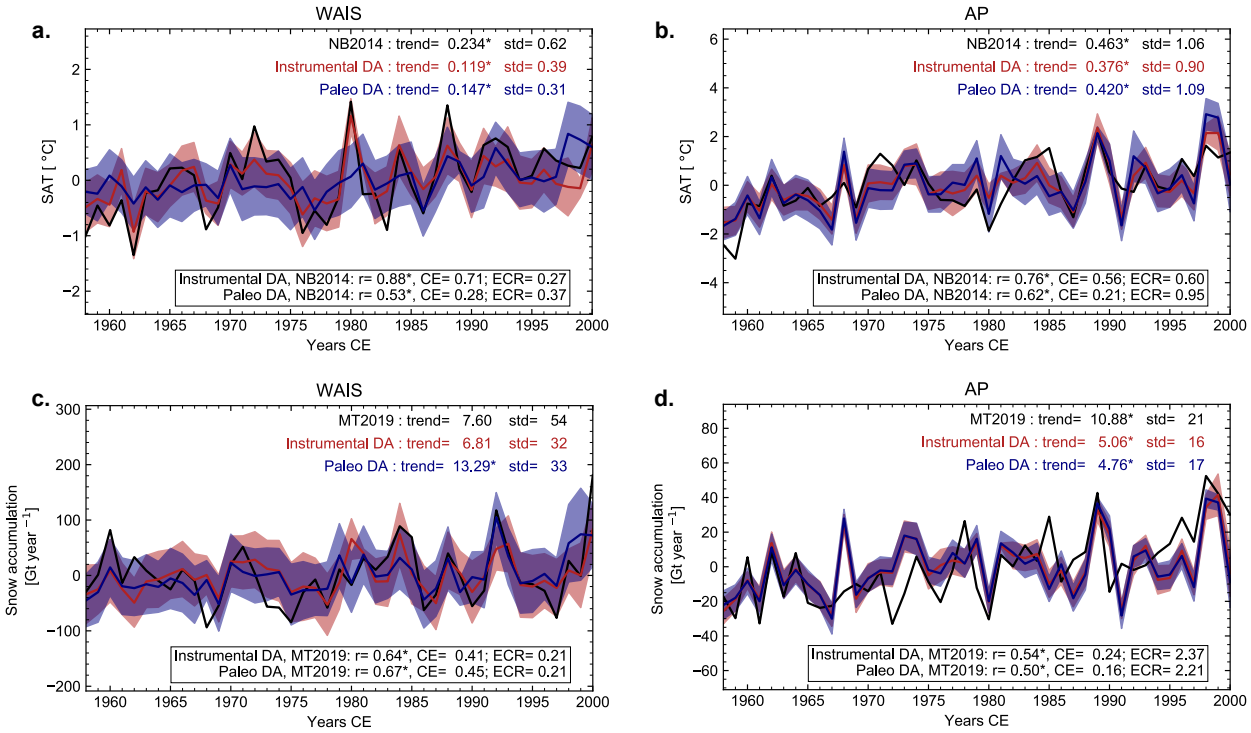


Figure 3.3: *(**a**-**b**) Comparison between our instrumental (red) and paleo (blue) near-surface air temperature (SAT; °C) anomalies and the reconstruction of Nicolas and Bromwich (2014; NB2014; in black) for the West Antarctic Ice Sheet (WAIS; 60-180° E and south of 72° S) and the Antarctic Peninsula (AP; west longitude north of 72° S) and over the 1958–2000 CE period. Regional definitions are identical as in Steig et al. [2009]. (**c**-**d**) Comparison between our instrumental (red) and paleo (blue) snow accumulation (Gt year^{-1}; in red) anomalies and the reconstruction of Medley and Thomas (2019; MT2019; in black) for the West Antarctic Ice Sheet (WAIS) and the Antarctic Peninsula (AP) and over the 1958–2000 CE period. Anomalies are computed over the 1958–2000 CE period. Linear trends of near-surface air temperature trends and snow accumulation are displayed (expressed in °C decade^{-1} and Gt year^{-1} decade^{-1}, respectively) and the standard deviation (std) of the time-series (expressed in °C and Gt year^{-1}, respectively) over the 1958–2000 CE period for each region. Asterisks indicate statistically significant trends at the 95% confidence level. Additionally, the correlation coefficient (r), coefficient of efficiency (CE) and ensemble calibration ratio (ECR) are computed over the 1958–2000 CE period. Uncertainty of the reconstruction estimated as the weighted standard deviation of the particles in the data assimilation process.*

3.3.1.2 Snow accumulation

The snow accumulation from our instrumental reconstruction is less spatially correlated with ERA5 than the near-surface air temperature (Fig. 3.2). This could be partially explained by the much higher spatial variability of snow accumulation over the Antarctic continent, compared to near-surface air temperature [van Wessem et al., 2018; Agosta et al., 2019]. Additionally, as all atmospheric reanalyses, ERA5 suffers from larger biases in snow accumulation than in near-surface air temperature [Gossart et al., 2019a]. At first order, the spatial variability of both near-surface air temperature and snow accumulation follows the topography (high temperature and snow accumulation on coastal areas, slowly decreasing towards the interior of the ice sheet), but snow accumulation is more affected by local processes, for example related to the wind (snow erosion/deposition and blowing snow) [Agosta et al., 2019]. As a consequence, some snow accumulation records may be poorly correlated with snow accumulation derived from atmospheric reanalyses [Medley and Thomas, 2019]. This is particularly prevalent for regions in East Antarctica [Medley and Thomas, 2019]. Since these snow accumulation records are used in our data assimilation, it is not surprising to obtain lower correlation coefficients for those areas.

When evaluating our snow accumulation reconstruction compared to the snow accumulation reconstruction from Medley and Thomas [2019], the skill metrics show that our instrumental reconstruction displays good and similar performance for the WAIS (r=0.64 (p-value<=0.05), CE=0.40 and ECR=0.21) and AP (r=0.54 (p-value<=0.05), CE=0.24 and ECR=2.37; Fig. 3.3c,d). Moreover, both our instrumental reconstruction and the Medley and Thomas [2019]'s reconstruction show a positive linear trend in West Antarctic-wide snow accumulation (i.e., the sum of the WAIS and AP regions) over the 1958–2000 CE period: 18.48 Gt year^{-1} per decade and 11.46 Gt year^{-1} per decade, respectively (both statistically significant; p-value<0.05). However, it is worth noting that our instrumental reconstruction for AP displays a smaller linear trend than in the Medley and Thomas [2019]'s reconstruction (5.06 Gt year^{-1} per decade against 16.88 Gt year^{-1} per decade, respectively). Additionally, the ECR for the AP reaches 2.37, which means that the uncertainty in our reconstruction is underestimated.

Finally, the performance of our paleo-reconstruction for snow accumulation is close to the instrumental reconstruction (Fig. 3.3c,d). The degradation of the performance between the instrumental and paleo reconstructions is very limited for snow accumulation compared to near-surface air temperature, which is expected as we use the same observational dataset in the two reconstructions of snow accumulation. Moreover, our paleo-reconstruction displays a 18.04 Gt year^{-1} per decade linear trend for the West Antarctic-wide snow accumulation over 1958-

2000 CE, which is very close to Medley and Thomas [2019] (18.48 Gt year^{-1} per decade over the same period).

3.3.1.3 Atmospheric circulation

Unlike near-surface air temperature and snow accumulation, no pressure data is used in the data assimilation process for both the instrumental and paleo reconstructions. The skill of the reconstruction of the non-assimilated variables is thus expected to be lower than for the assimilated variables. Spatial correlation coefficients between our instrumental reconstruction and the ERA5 reanalysis for the 500-hPa geopotential height during the 1979–2000 CE period show that interannual changes in the atmospheric circulation are well reconstructed over the West Antarctic and in the mid-high latitudes of the Pacific Sector of the Southern Hemisphere (Fig. 3.2). Furthermore, for the paleo-reconstruction, the stronger correlations over the ocean, compared to the continent, reflect the fact that changes in this region are driving the variability recorded in ice cores. This confirms that marine intrusions predominantly govern the near-surface climate variability in West Antarctica [Nicolas and Bromwich, 2011a]. This also gives confidence in the use of ice core records for reconstructing the atmospheric circulation in that sector.

We also analyze the Amundsen Sea Low pressure (ASL), which can be characterized by several indexes [e.g., Hosking et al., 2013], for example related to the change in the ASL position (latitudinal and longitudinal positions) or to the intensity of the minimum pressure in the ASL region. Here, the ASL index is defined as the annual average of the 500-hPa geopotential height from 75°S to 60°S and from 170°E to 70°W [Fogt et al., 2012; Turner et al., 2013; Hosking et al., 2013]. Note that geographical definitions can differ between studies but the resulting indexes are relatively similar. This index is then normalized (zero mean and unity standard deviation) over the 1941–1990 CE period. Following this definition, a negative (positive) ASL index corresponds to a deeper/stronger (weaker) ASL. Because no reconstruction of the ASL index exists, we use the ASL index derived from the ERA5 reanalysis as the reference ASL index for the evaluation.

Over the 1979–2000 CE period, the ASL index from both the instrumental and paleo reconstructions displays a high correlation coefficient with ERA5 (0.87 (p-value<0.05) and 0.65 (p-value<0.05), respectively), as well as CE values (0.74 and 0.30, respectively; Fig. 3.4a). Although no estimation of the ASL index change exists over the last decades, Fogt et al. [2019] have recently provided a complete spatially reconstruction of Antarctic pressure back to 1905 CE at seasonal scale based on available pressure data from the Antarctic and the mid-latitudes of the Southern Hemisphere. It is worth noting that the goal of Fogt et al. [2019] was not to reconstruct the ASL variability over the past decades. Furthermore, Fogt et al. [2019] mention that their reconstruction has a poor skill in the Amundsen region

mainly because of the sparse observational network in West Antarctica. In particular, prior to 1958 CE, this reconstruction only relies on pressure observations situated in the mid-latitudes, and thus only depends on the mid latitudes-Antarctic connections. However, the comparison with Fogt et al. [2019] is still valuable since this is the only Antarctic pressure dataset based on instrumental observations available before 1979 CE. The ASL index derived from Fogt et al. [2019] displays a correlation coefficient of 0.75 (p-value<0.05) with ERA5 over 1979–2000 CE.

Both our instrumental and paleo reconstructions are well correlated with the ASL index derived from Fogt et al. [2019] over 1979–2000 CE (r=0.74 (p-value<0.05) and 0.65 (p-value<0.05), respectively), but correlation coefficients drop to 0.55 (p-value<0.05) and 0.44 (p-value<0.05) over 1958–2000 CE. This decrease is probably related to the smaller number of data (associated with a weaker quality) used in Fogt et al. [2019] during the 1958–1978 CE period since our observational network remains unchanged over 1958–2000 CE. Over the 1958–2000 CE period, the ASL index derived from Fogt et al. [2019] displays a linear trend of -0.12 std per decade (p-value>0.1) while the trends from the instrumental and paleo reconstructions are -0.001 std per decade (p-value>0.1) and -0.17 std per decade (p-value>0.1), respectively. Our paleo-reconstruction is thus closer to Fogt et al. [2019] than our instrumental reconstruction. However, trends of the ASL index from Fogt et al. [2019] and our instrumental reconstruction are highly sensitive to the analyzed period, reflecting the high internal variability prevailing in this region [e.g., Raphael et al., 2016].

In addition to the ASL, we also analyze the main atmospheric mode of variability in the Southern Hemisphere, i.e., the Southern Annular Mode (SAM). SAM represents the intensity and position of the westerly winds. The SAM index (defined as the normalized difference in mean sea-level pressure between the 40° and 65° South longitude bands) derived from our instrumental reconstruction is correlated at 52% (p-value<0.05) with the Marshall index [Marshall, 2003] that is only based on atmospheric pressure observations (Fig. 3.4b). However, our instrumental reconstruction does not display the observed linear trend over 1958–2000 CE as in observations. On the contrary, our paleo-reconstruction is able to reconstruct the linear trend (albeit statistically insignificant) but the correlation coefficient drops to 31% (p-value<0.05). The SAM being an annular mode, a high number of geographically evenly distributed observations is required to correctly reproduce this mode. This partly explains the limited skill of our SAM index since the observational network is unequally distributed geographically. Consequently, we mainly focus our analysis on the ASL and not on the SAM.

The best performance of our reconstructions for simulating the ASL compared to the SAM could be explained by two factors. The ASL is a more local atmospheric feature in comparison with the SAM. The observational network (instrumental and paleo observations) used in our reconstructions is limited to the Antarctic conti-

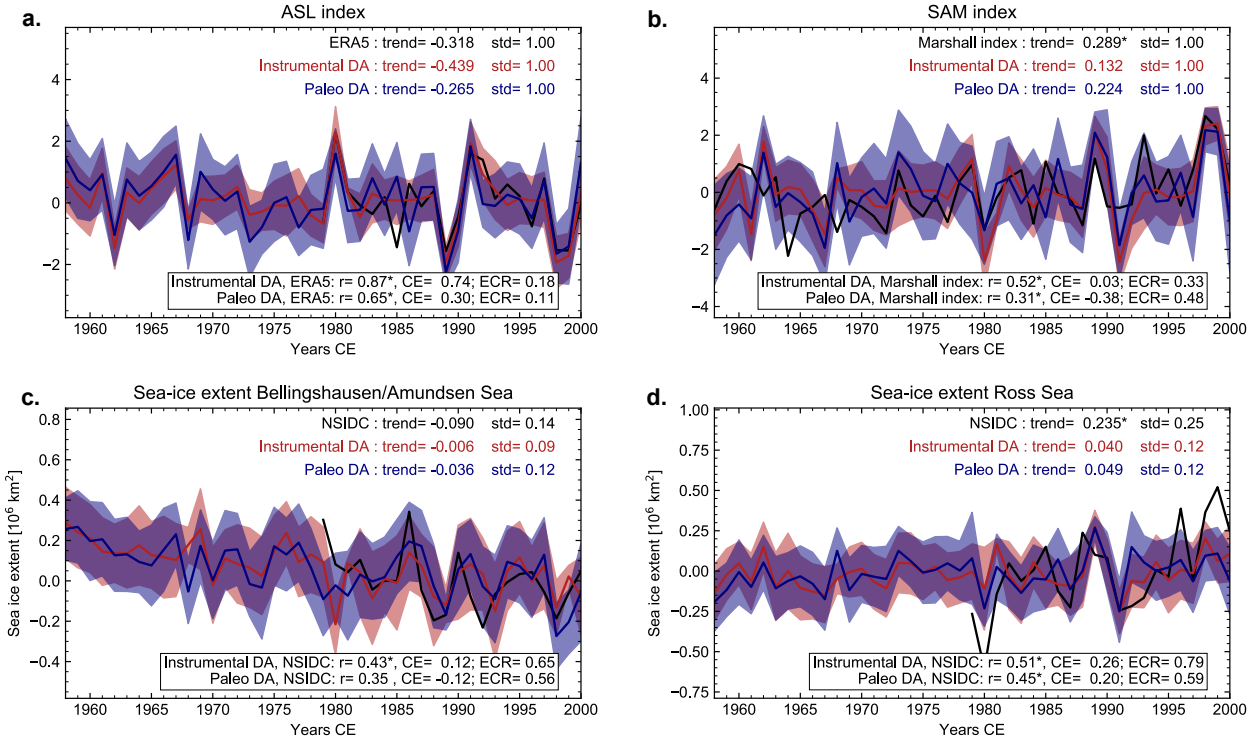


Figure 3.4: *(**a**) The Amundsen Sea Low (ASL) and (**b**) Southern Annular Mode (SAM; **b**) indexes derived from our instrumental (red) and paleo (blue) reconstructions correlated with ERA5 data (in black) for the ASL over 1979–2000 CE and the Marshall Index [Marshall, 2003] (in black) for the SAM over 1958–2000 CE. For all the datasets plotted, the linear trends are displayed (expressed in decade $^{-1}$) and the standard deviation (std) of the time-series (unitless) over the 1979–2000 CE and 1958–2000 CE periods for the ASL and SAM, respectively. (**c**-**d**) Comparison between our instrumental (red) and paleo (blue) sea-ice extent (10^6 km^2) reconstructions (in anomalies) and the observed sea-ice extent from the National Snow and Ice Data Center (NSIDC; in black; only available from 1979 CE) for the Bellingshausen/Amundsen Sea (130° W-60° E) and Ross Sea (160° E-130° W) sectors over the 1958–2000 CE period. Regional definitions are identical as in Parkinson [2019]. Anomalies are computed over the 1979–2000 CE period. The linear sea-ice extent trends are displayed (expressed in 10^6 km^2 decade $^{-1}$) and the standard deviation (std) of the time-series (expressed in 10^6 km^2) over the 1979–2000 CE period for each region. Additionally, the correlation coefficient (r), coefficient of efficiency (CE) and ensemble calibration ratio (ECR) are computed over the respective periods depending on the observations. Uncertainty of the reconstruction estimated as the weighted standard deviation of the particles in the data assimilation process. Our SAM index is computed as the normalized difference in mean sea-level pressure between the 40° S and 65° S longitude bands. Note that by construction, the standard deviation of all the SAM and ASL time-series are equal to 1.*

nent, with few records in East Antarctica, plus Tasmania, New Zealand and South America, which makes difficult to reconstruct the SAM. In contrast, our observational network includes a large number of records in West Antarctica, which is the region where the ASL has the largest influence. Additionally, the correlation coefficient between the SAM and ASL index in our paleo-reconstruction over the 1800–2000 CE period reaches -97% (p-value<0.001; non-sensitive to the analyzed period), meaning our reconstructed SAM variability mainly captures the ASL-related variability. Although our reconstruction seems to overestimate the ASL-SAM relationship, several studies have demonstrated that the ASL is highly correlated with the SAM in observations [Turner et al., 2013; Hosking et al., 2013; Raphael et al., 2016; Fogt and Marshall, 2020].

3.3.1.4 Sea-ice cover

As the atmospheric circulation, the sea-ice cover reconstructions rely totally on the relationships between the assimilated variables and sea-ice cover as represented by the model since this variable is not assimilated. Figure 3.2 shows that the sea-ice concentration from our instrumental reconstruction is well correlated with the observed sea-ice concentration from the National Snow and Ice Data Center (NSIDC) over the 1979–2000 CE period. This is especially true at the winter sea-ice edge where the interannual variability is the highest. In order to quantify the sea-ice extent (i.e., oceanic surface covered by at least 15% of ice) at the regional scale, we divide the West Antarctic sector into two sectors following the geographical definitions of Parkinson [2019]: the Bellingshausen/Amundsen Sea sector (130°W-60°E) and Ross Sea sector (160°E-130°W). It is important to stress that the overlapped period of 22 years between the NSIDC dataset and our reconstructions is short to evaluate in detail our sea-ice extent reconstruction. Therefore, this limits our ability to assess the quality of our reconstruction in terms of trends over the past decades.

Our instrumental reconstruction is correlated at 43% (p-value<0.05) and 51% (p-value<0.05) with the NSIDC dataset over the 1979–2000 CE period for the Bellingshausen/Amundsen Sea and Ross Sea sectors, respectively (Fig. 3.4c,d). Regarding our paleo-reconstruction, we observe an overall reduction of the local skill compared to our instrumental reconstruction (Fig. 3.2). However, our paleo-reconstruction still displays high correlation coefficients for both the Ross Sea and Bellingshausen/Amundsen Sea sectors when compared to the NSIDC dataset (r=0.45 (p-value<0.05) and r=0.35 (p-value>0.05), respectively; Fig. 3.4c,d). Additionally, the sea-ice extent for these two regions are highly correlated between the two reconstructions over the 1958–2000 CE period (r=0.67 (p-value<0.05) and r=0.56 (p-value<0.05), respectively; Fig. B.3). Finally, both the instrumental and paleo reconstructions show a decrease in sea-ice extent for the Belling-

shausen/Amundsen Sea sector over the 1958–2000 CE period (both -0.057 10^6 km^2 per decade; p-value<0.05), and an increase for the Ross Sea sector (0.018 10^6 km^2 per decade (p-value>0.05) and 0.026 10^6 km^2 per decade (p-value<0.05), respectively for the instrumental and paleo-reconstruction). These changes over 1958–2000 CE are consistent with observations over the 1979–2000 CE period [Parkinson, 2019].

3.3.2 Reconstruction of the ASL and sea-ice in the West Antarctic sector over the last 200 years

Now that we have evaluated the skill of our reconstructions during the recent period, we can extend the reconstruction back in time. According to our annual paleo-reconstruction of the ASL index (Fig. 3.5), the ASL displays three main phases over the last two centuries. From 1800 CE to around 1840 CE, we observe a positive linear trend (trend=0.34 std per decade; p-value<0.001) following by a period of about one century (until around 1940 CE) with virtually no trend (trend=0.05 std per decade; p-value>0.05). From around 1940 CE, the ASL displays a strong negative linear trend (trend=-0.30 std per decade; p-value<0.001). This strong negative linear trend is consistent with the observed positive linear trend in the Southern Annular Mode, which deepens the ASL [e.g., Raphael et al., 2016]. In addition to being stronger since 1940 CE, our results show that the ASL has also moved eastwards at the same time (Fig. B.4; in our paleo-reconstruction, the longitudinal position of the ASL is anti-correlated at 88% (p-value<0.001) with the ASL index over the 1800–2000 CE period) but no change in latitudinal position is noticed (not shown).

Along with the ASL changes over the past two centuries, we analyze annual sea-ice extent changes in the West Antarctic sector, in particular in the Bellingshausen/Amundsen Sea sector (130°W-60°E) and in the Ross Sea sector (160°E-130°W; Fig. 3.6a,b). These two regions are anti-correlated at the annual scale in observations over 1979–2000 CE (r=-0.26 (p-value>0.1). In our paleo-reconstruction, this correlation coefficient reaches -0.50 (p-value<0.05) over the same period. However, our paleo-reconstruction indicates that this correlation coefficient varies over the past two centuries. In the Bellingshausen/Amundsen Sea sector, the sea-ice has grown from 1800 CE to around 1860 CE (trend=0.037 10^6 km^2 per decade; p-value<0.001) before starting a long-term reduction until present (trend=-0.021 10^6 km^2 per decade; p-value<0.001). On the contrary, the Ross Sea sector displays a different picture during the past two centuries. Over the first forty years of the 19^{th} century, our reconstruction indicates a reduction of the sea-ice extent in the Ross Sea sector (trend=-0.017 10^6 km^2 per decade; p-value>0.1), which is followed afterwards by a slight long-term reduction of sea-ice extent until around 1940 CE (trend=-0.009 10^6 km^2 per decade; p-value<0.01). Finally, a positive lin-

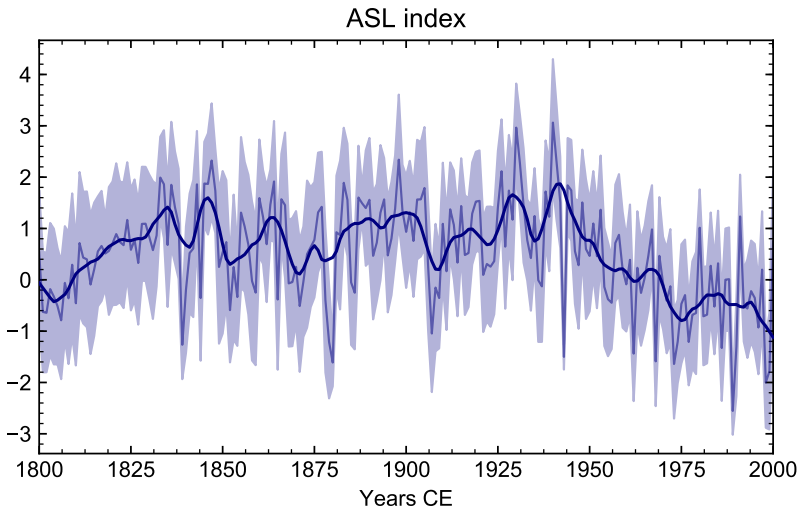


Figure 3.5: *ASL index derived from our paleo-reconstruction over 1800–2000 CE. Thin line corresponds to the annual index while the thick line is the decadal mean (10-year lowess smoothing). Uncertainty of the reconstruction estimated as the weighted standard deviation of the particles in the data assimilation process.*

ear trend is observed over the last sixty years (trend=-0.021 10^6 km^2 per decade; p-value<0.05).

3.3.2.1 Comparison with independent sea-ice reconstructions

Our paleo sea-ice reconstructions can be compared to two independent reconstructions, which are based on phytoplankton productivity emissions from marine algae at the sea-ice edge (Methane Sulphonic Acid; hereafter MSA; Thomas et al., 2019). First, Thomas and Abram [2016b] have reconstructed the position of the winter sea-ice edge at 146°W in the Amundsen-Ross sector since 1702 CE using an ice core MSA record situated in West Antarctica. Over the 1800–2000 CE, the sea-ice edge at 146°W derived from our paleo-reconstruction is correlated at 22% (p-value<0.05) with the MSA-based reconstruction from Thomas and Abram [2016b] and 34% (p-value<0.05) over the 1900–2000 CE period (Fig. 3.6d). Over the 20^{th} century, our reconstruction displays a sea-ice extent northward expansion of 0.13° per decade, which is very similar to Thomas and Abram [2016b] (0.12 $\pm$ 0.02° per decade). Therefore, although the interannual correlation is relatively low between both reconstructions, the long-term changes are consistent with each other. We also notice that our paleo-reconstruction is not able to reconstruct the exceptional sea-ice expansion for the 1997–1999 CE period [Hanna, 2001] in contrast with the MSA-based reconstruction from Thomas and Abram [2016b].

The weaker agreement between two reconstructions at the interannual timescale is something to expect when comparing two very different paleo proxies.

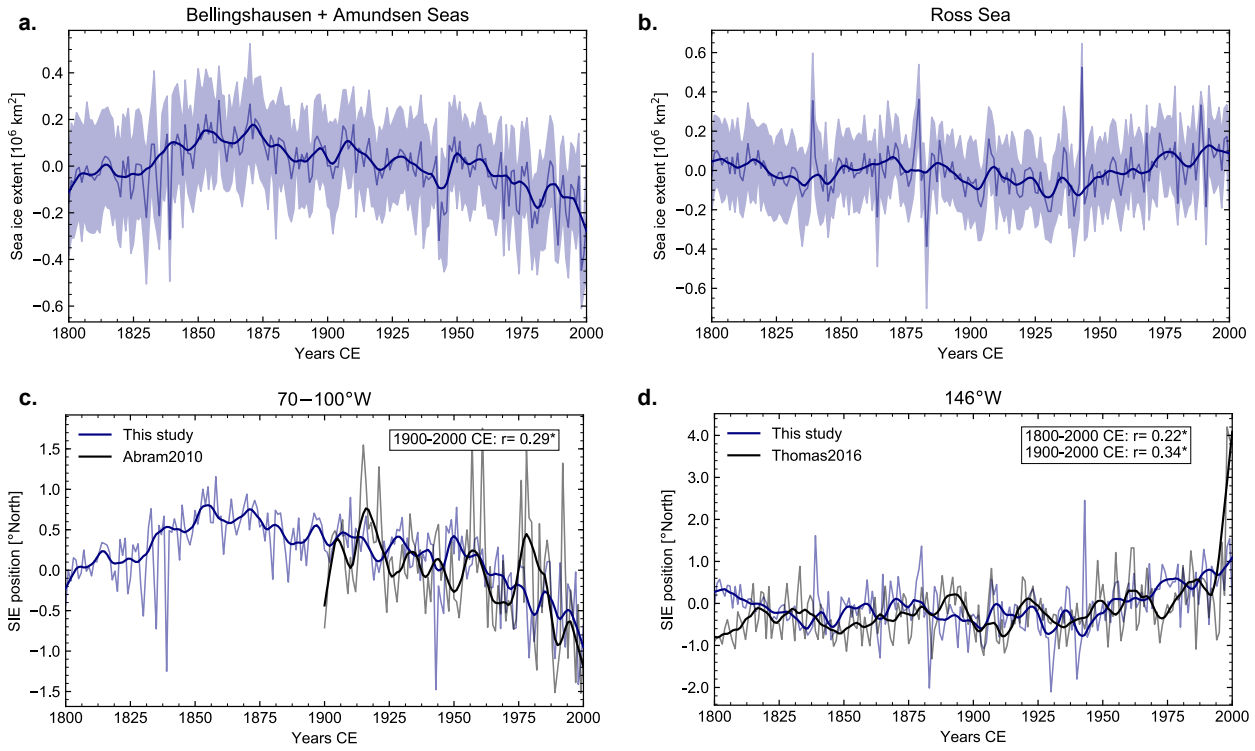


Figure 3.6: *Sea-ice extent for Bellingshausen/Amundsen Sea (**a**) and Ross Sea (**b**) sectors (10^6 km^2) derived from our paleo-reconstruction over 1800–2000 CE. Uncertainty of the reconstruction estimated as the weighted standard deviation of the particles in the data assimilation process. (**c**) Latitudinal position of the annual sea-ice extent edge averaged over 70–100° W in our paleo-reconstruction (in blue) and the MSA-based reconstruction of Abram et al. [2010] (in black) over 1800–2000 CE. (**d**) Latitudinal position of the annual sea-ice extent edge at 146° W in our paleo-reconstruction (in blue) and the MSA-based reconstruction of Thomas and Abram [2016b] (in black) over 1800–2000 CE. Thin lines correspond to the annual reconstructions while thick lines are the decadal means (10-year lowess smoothing). For (**c**) and (**d**), correlation coefficients (r) between the paleo and MSA-based reconstructions are computed over 1900–2000 CE (star indicates statistically significant correlation at the 95% confidence level).*

The MSA emissions arise from the algal blooms that occur in the spring, during the period of sea-ice break-up. Thus, this record is indicative of seasonal changes, closely linked to winter sea-ice extent, rather than annual sea-ice changes. The differences between the reconstructions can also partly be explained by the fact that the MSA record is influenced by conditions at the source as well as the transport pathways and potentially includes a non-climatic signal. In contrast, our data assimilation approach is unable to capture these small-scale local processes and, by construction, our method tends to minimize the non-climatic signal.

Second, using a similar methodology as Thomas and Abram [2016b], Abram et al. [2010] have estimated a -0.08 $\pm$ 0.02° per decade southward retreat in the Bellingshausen/Amundsen Sea sector (70°W–100°W) over the 1901–1990 CE

period, while our reconstruction suggests a slightly greater retreat (-0.10 ° per decade; p-value<0.05). Over the 20th century, the correlation coefficient between the two reconstructions is 0.29 (p-value<0.05). Thus, despite the differences on the seasonal and inter-annual scale, our reconstruction independently confirms the long-term changes in sea-ice extent over the 20th century as suggested by Thomas and Abram [2016b], including the persistent dipole between the Bellingshausen/Amundsen Sea and Ross Sea sectors (r=-0.70 (p-value<0.001) in our reconstruction over 1900–1999 CE). However, our reconstruction indicates that the sea-ice extent retreat in the Bellingshausen/Amundsen Sea sector started around one century before the sea-ice extent expansion in the Ross Sea sector (Fig. 3.6a,b).

The evolution of the sea-ice extent in the Ross Sea sector over the past two centuries coincides with the evolution of the ASL, with a correlation coefficient of -0.82 (p-value<0.001) in our paleo-reconstruction. This confirms the dominant role of the ASL in modulating annual sea-ice variations in this sector, as highlighted by several studies [e.g., Hosking et al., 2013; Raphael and Hobbs, 2014; Raphael et al., 2019]. The ASL has deepened (negative ASL index) over the past few decades, associated with enhanced cold southerly winds coming from the Ross Ice Shelf, resulting in sea-ice expansion in the Ross Sea sector [e.g., Lefebvre and Goosse, 2008]. On the opposite, when the ASL is deeper, this atmospheric situation tends to bring more warm air into the Bellingshausen/Amundsen Sea sector in concert with the horizontal movement of the sea-ice to the coast (i.e., ice compaction), which leads to a reduction of sea-ice cover.

However, the sea-ice variability in the Bellingshausen/Amundsen Sea sector is less correlated with the ASL index than for the Ross Sea sector in our reconstruction over the same period (r=0.37; p-value<0.001). Additionally, unlike the Ross Sea sector, the correlation between the sea-ice extent and the ASL depends on the analyzed time period. For instance, this correlation coefficient drops to -0.16 (p-value>0.1) over 1851-1950 CE (against 0.37 over 1800–2000 CE (p-value<0.001)). During this period, the sea-ice extent for the Bellingshausen/Amundsen Sea sector is decreasing while the ASL index does not present a linear trend. This suggests that the ASL is not the unique driver controlling the variability of sea-ice extent in the Bellingshausen/Amundsen Sea sector. In particular, the analysis of the spatial correlation coefficients between the sea-ice extent in the Bellingshausen/Amundsen Sea sector and the 500-hPa geopotential height based on our paleo-reconstruction (Fig. 3.7a) indicates that the circulation changes along the Drake Passage (between Cape Horn and the South Shetland Islands) and in the Weddell Sea are correlated with the sea-ice extent in this region. This is confirmed by performing the same analysis with observations (NSIDC and ERA5) over 1979–2000 CE but the amplitude of the correlation coefficients is lower but still statistically significant (Fig. 3.7b). These lower correlation coef-

ficients compared with our reconstruction probably come from the fact that our reconstruction provides a dynamical consistency between the reconstructed variables As the NSIDC dataset and the ERA5 renalysis are more independant, lower correlations coefficients may be expected. Nevertheless, the correlation coefficient between the sea-ice extent in the Bellingshausen/Amundsen Sea sector and the ASL over the 1951–2000 CE period reaches 0.66 (p-value<0.001; against -0.16 over 1851–1950 CE (p-value>0.1)), pointing out the strong role of the ASL in the reduction of the sea-ice extent in this region over the last decades.

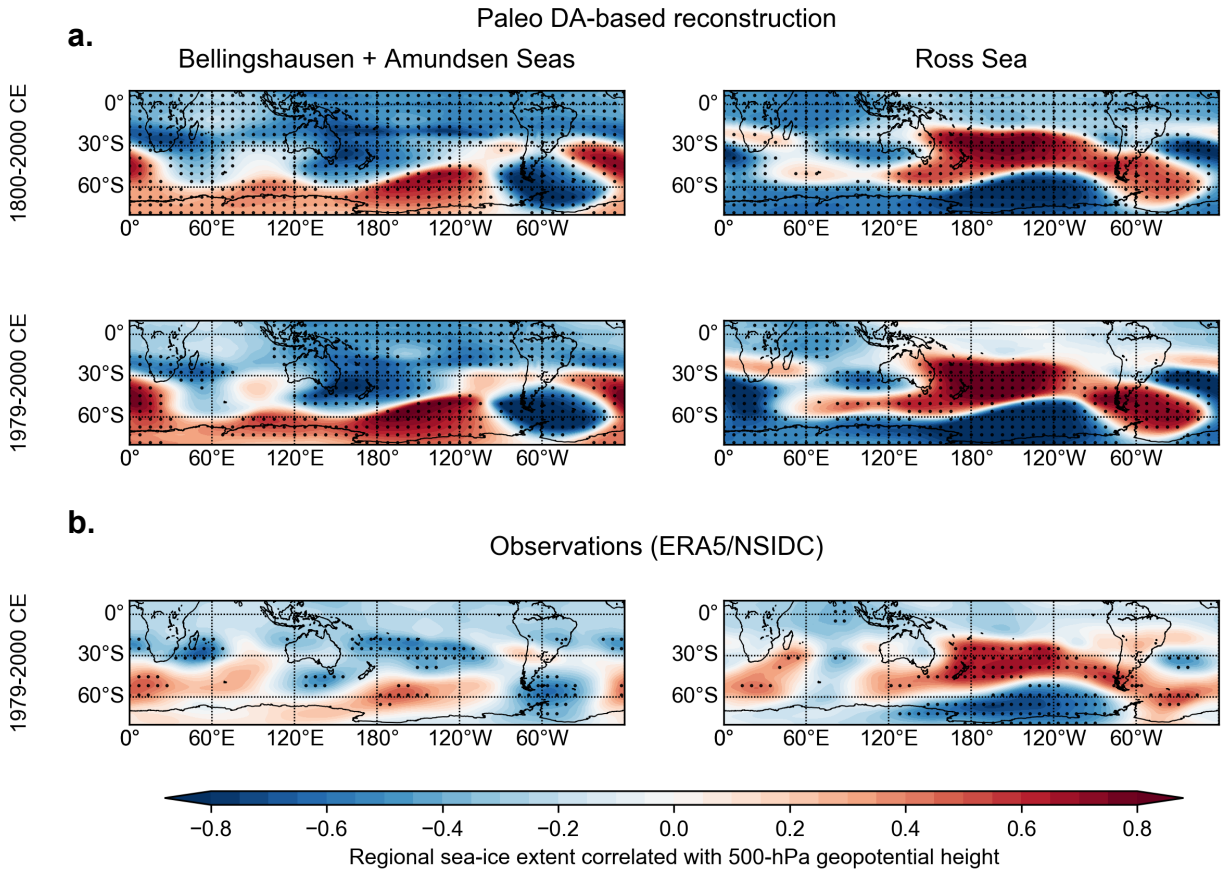


Figure 3.7: *(**a**) Annual sea-ice extent averaged over the Bellingshausen/Amundsen Sea and Ross Sea sectors correlated with the 500-hPa geopotential height in our paleo-reconstruction for the 1800–2000 CE and 1979–2000 CE periods. (**b**) As (**a**) but based on observations (ERA5 and NSIDC) over the 1979–2000 CE. Stippling indicates statistically significant correlations at the 95% and 90% confidence levels for the 1800–2000 CE and 1979–2000 CE periods, respectively.*

3.3.3 Is the current widespread warming over West Antarctica representative of changes in the past 200 years?

Numerous studies have pointed out a strong west-east asymmetry in the surface warming since 1958 CE as West Antarctica has undergone a large widespread warming, unlike East Antarctica [e.g., Steig et al., 2009; Nicolas and Bromwich, 2014; Schneider et al., 2012; Jun et al., 2020]. As a result, West Antarctica is often seen as a region that behaves homogeneously in terms of climate change and variability. However, it is still unknown if this observed widespread warming in West Antarctica over the past decades is representative of the behavior of the region on longer timescales. Our paleo-reconstruction allows examination of this representativeness by analyzing the near-surface air temperature changes over the past 200 years along with changes in other key variables such as snow accumulation, sea-ice extent and atmospheric circulation.

Figure 3.8 displays the linear trends for the 500-hPa geopotential height, 700-hPa air temperature, near-surface air temperature, snow accumulation and sea-ice concentration over 50-year periods between 1801 and 2000 CE. Over 1801–1850 CE, we observe a clear continental dipole in the trends of near-surface air temperature and snow accumulation between the Peninsula and a part of eastern WAIS compared to the western WAIS. The 500-hPa geopotential height field shows that the ASL weakened during 1801–1850 CE (trend=0.30 std per decade; p-value<0.01), which is consistent with the time-series of the ASL index over the last two centuries (Fig. 3.5). These atmospheric conditions are associated with weaker northerly winds in the Peninsula that result in a cooling, while the opposite occurs in the western WAIS (i.e., the west of the WAIS Divide where the ice flow is null, which separates the WAIS into two regions). It has been shown that a strong positive correlation exists between temperature and snow accumulation over the Antarctic Ice Sheet [Frieler et al., 2015; Dalaiden et al., 2020a; Cavitte et al., 2020]. Higher temperature induces an increase of the saturation vapor pressure that potentially leads to more continental precipitations (i.e., the Clausius-Clapeyron relationship). This is consistent with the cooling in the Peninsula (which corresponds to a snow accumulation decrease) and the warming in the western WAIS (which corresponds to a snow accumulation increase). In addition to the atmospheric circulation changes, continental changes are highly influenced by oceanic conditions [Kittel et al., 2018; Krinner et al., 2008]. Particularly, when the ocean is ice-free, the air potentially contains more humidity because of the enhanced evaporation above the ocean. This eventually leads to a warming and an increase in snow accumulation over the continent when the airflow hits the coastline. Accordingly, we observe an increase in sea-ice concentration in the Bellingshausen/Amundsen Sea sector in contrast with a decrease in the Ross Sea sector.

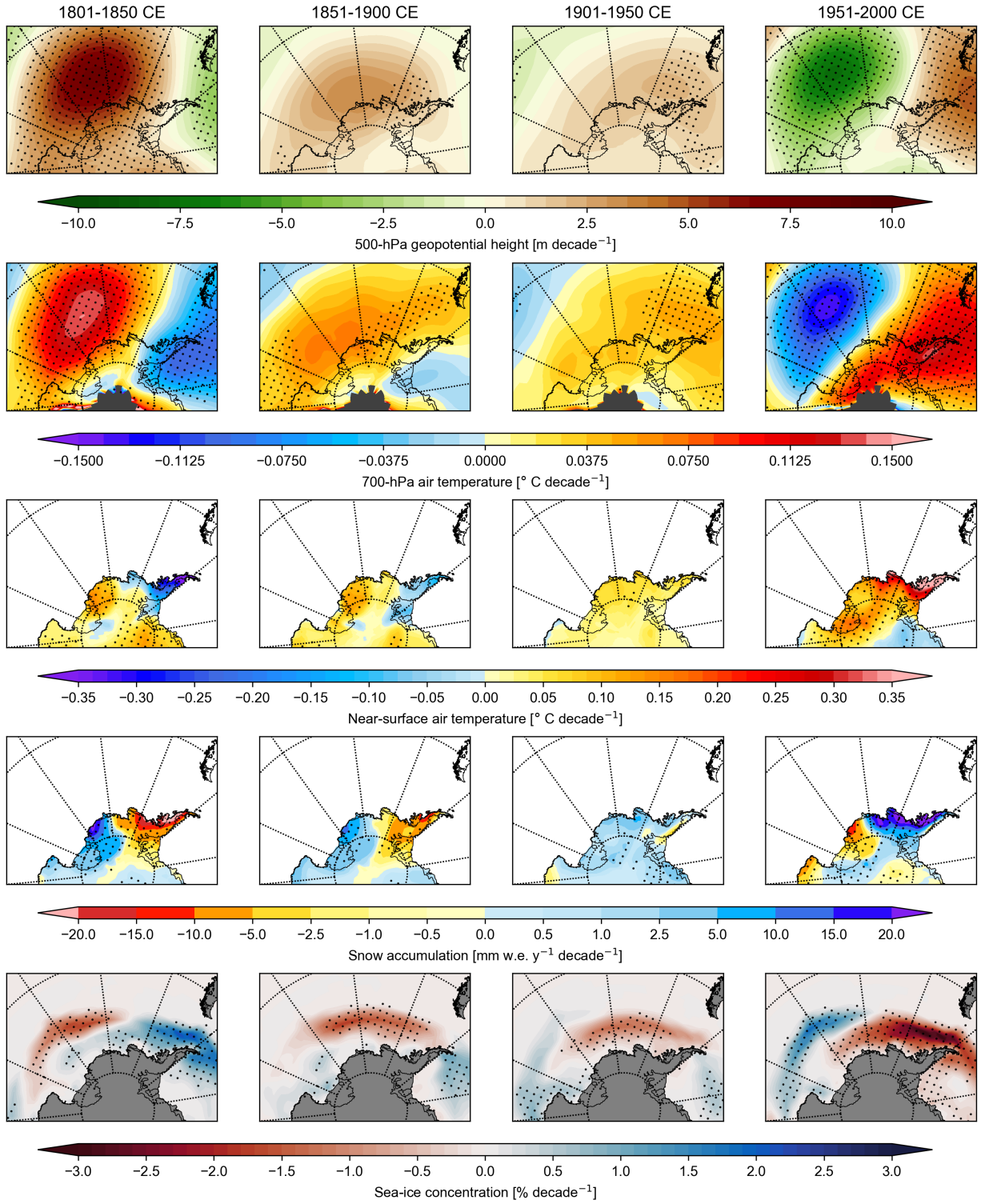


Figure 3.8: *Linear trends in 500-hPa geopotential height (m per decade), 700-hPa air temperature (°C per decade), near-surface air temperature (°C per decade), snow accumulation (mm w.e. eq. year^{-1} par decade) and sea-ice cover (% per decade) over the last 200 years separated by 50-year intervals. Stippling indicates statistically significant correlations (95% confidence level).*

During the second interval (i.e., 1851–1900 CE period), the continental and atmospheric circulation patterns are relatively similar to the one over the 1801–1850 CE period. However, the amplitude of the surface changes is weaker and the ASL seems slightly shifted eastwards (Fig. 3.8). This induces an eastward shift of the warming pattern over the continent compared to the period 1801–1850 CE. Moreover, the typical dipole in sea-ice is no longer observed since a general reduction of the sea-ice extent is noticed in the West Antarctic sector. The 1901–1950 CE period is characterized by small and insignificant changes, except that a widespread sea-ice cover reduction is noticed as during the 1851–1900 CE period. Over the last fifty years of the 20^{th} century, the atmospheric circulation corresponds almost to the opposite 1801–1850 CE pattern (Fig. 3.8). With an increasing ASL (trend=-0.22 std per decade; p-value<0.01), warmer and moister air is brought in the Peninsula resulting in a decrease of sea-ice cover in the Bellingshausen/Amundsen Sea sector, as well as a warming associated with an increase in snow accumulation in the Peninsula. As expected from the deeper ASL, the Ross Sea sector gained sea-ice during the same period while the western WAIS displays a decrease in snow accumulation. However, in contrast to the 1801–1850 CE period, the temperature change has the same sign over the whole West Antarctic region, in agreement with previous studies [e.g., Steig et al., 2009; Nicolas and Bromwich, 2014]. The boundary between regions showing a warming and those displaying a cooling at 700-hPa is shifted offshore over the ocean while it was located close to the WAIS Divide for the period 1801–1850 (Fig. 3.8). The dipole is still present but the entire continent is experiencing a warming. The trends of 700-hPa air temperature over 1951–2000 CE on both sides of the Amundsen coasts are thus opposite.

Since the change in the atmospheric circulation during this period roughly corresponds to the opposite pattern of the 1801–1850 CE period, the homogeneous warming over the continent could either indicate a change in the role of the ASL on the West Antarctic climate or a relationship between the ASL and the West Antarctic climate that may have changed over time. Figure 3.9 displays spatial correlation coefficients between the ASL index and near-surface air temperature, snow accumulation and 700-hPa air temperature over the 1801–1850 CE and 1951–2000 CE periods. Over the 1801–1850 CE period, the spatial patterns of correlation coefficients between the ASL index and the three variables are very similar to the spatial pattern of trends for the same variables and over the same period. This indicates that over that period, the ASL is the major contributor to those changes.

In contrast to the ASL-snow accumulation relationship, the relationship between the ASL and near-surface air temperature has changed between the two periods (Fig. 3.9). Correlation coefficients between the ASL index and near-surface air temperature over 1951–2000 CE still exhibit a dipole like for the 1801–1850 CE period, but this dipole is shifted eastward. Additionally, the strength of the corre-

lation over the western WAIS is weaker compared to the 1801–1850 CE period. This change in the link between the ASL and near-surface air temperature could be related to a change in the mean state of the atmospheric circulation. According to our reconstruction and in agreement with previous studies, the atmospheric conditions prevailing in the Antarctic over 1951–2000 CE correspond to a positive phase of SAM in regards to the 1801–1850 CE period (Fig. 3.10). Based on the SAM index derived from our reconstruction and normalized over the 1800–2000 CE period, the SAM index averaged over 1801–1850 CE is -0.11 against 0.87 over 1951–2000 CE.

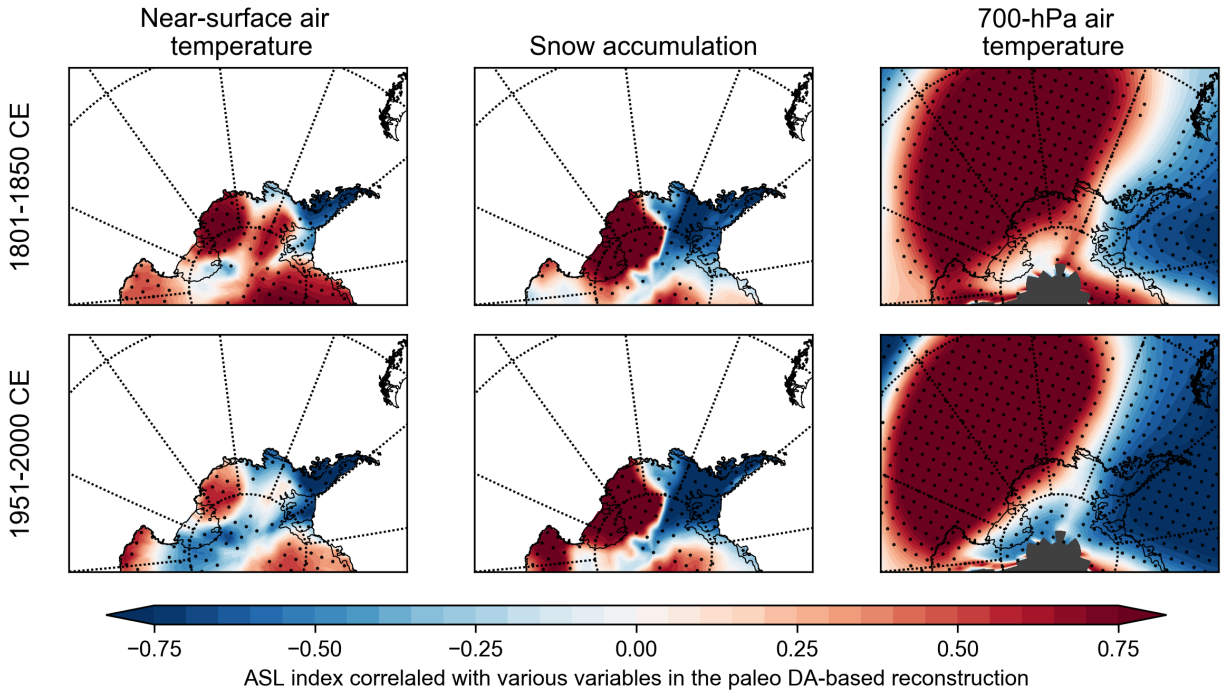


Figure 3.9: *Annual ASL index linearly correlated with near-surface air temperature, snow accumulation and 700-hPa air temperature in our paleo-reconstruction for the 1801–1850 CE and 1951–2000 CE periods. Stippling indicates statistically significant correlations (95% confidence level).*

To examine the role of the SAM in the relationship between the ASL and the near-surface air temperature and snow accumulation independently of our reconstruction, we analyze the relationships between the ASL and these two variables in the ERA5 reanalysis over 1979–2019 CE. More specifically, we perform the correlation of climate variables with the ASL index over negative SAM (SAM-) years compared with positive SAM (SAM+) years (Fig. 3.11). The analysis confirms that depending on the large-scale atmospheric background (i.e., the sign of the SAM index), the impact of the ASL on the near-surface air temperature and snow accumulation is different. During the SAM- years, the fingerprint of the ASL on the continent displays a clear dipole in both near-surface air temperature and snow

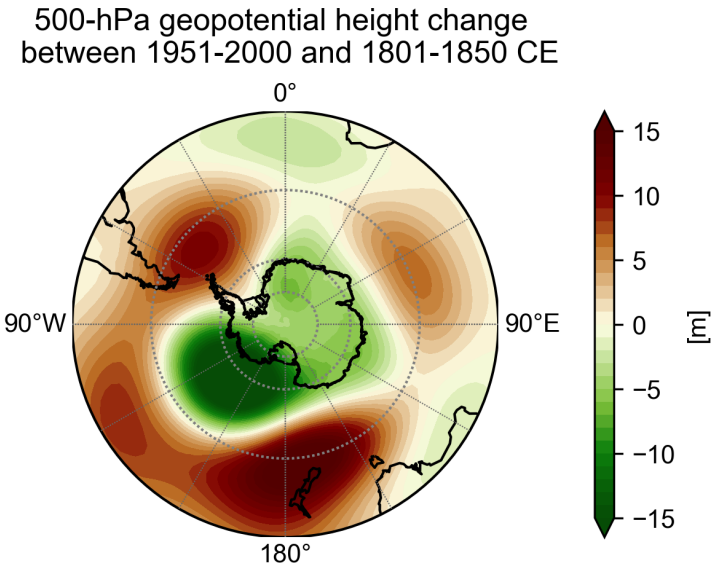


Figure 3.10: *Change in the 500-hPa geopotential height (m) between the 1951–2000 CE and 1801–1850 CE periods in our paleo-reconstruction.*

accumulation. During the SAM+ years, the dipole in near-surface air temperature over the continent is much less clear with weaker correlation coefficients between the ASL and the near-surface air temperature in the western WAIS. This potentially indicates that snow accumulation is a better proxy for reconstructing the ASL than the near-surface air temperature as shown in Thomas and Bracegirdle [2015].

As a consequence of the general warming in West Antarctica over the last 50 years, the western part of the region warms but has lower snow accumulation. This is opposite to the classical link between the two variables due to Clausius-Clapeyron relationship. Cavitte et al. [2020] have shown that some areas over the Antarctic continent in fact display a negative relationship between snow accumulation and near-surface air temperature because of winds-topography interactions. This is for instance observed over the Peninsula. We argue that the same phenomenon at larger spatial scale has occurred in WAIS during the 1951–2000 CE period because of the presence of the WAIS Divide. When warm moist air driven by the ASL is brought in the eastern WAIS towards the WAIS Divide, the air moisture is released as snowfall during the uplift towards the Divide. At that point, the air masses start to descend towards the Ross Ice Shelf on the leeside. This results in an adiabatic warming, which is not associated with an increase in snow accumulation. However, this feature is mainly observed over the 1951–2000 CE period due to the position of the winds at that time.

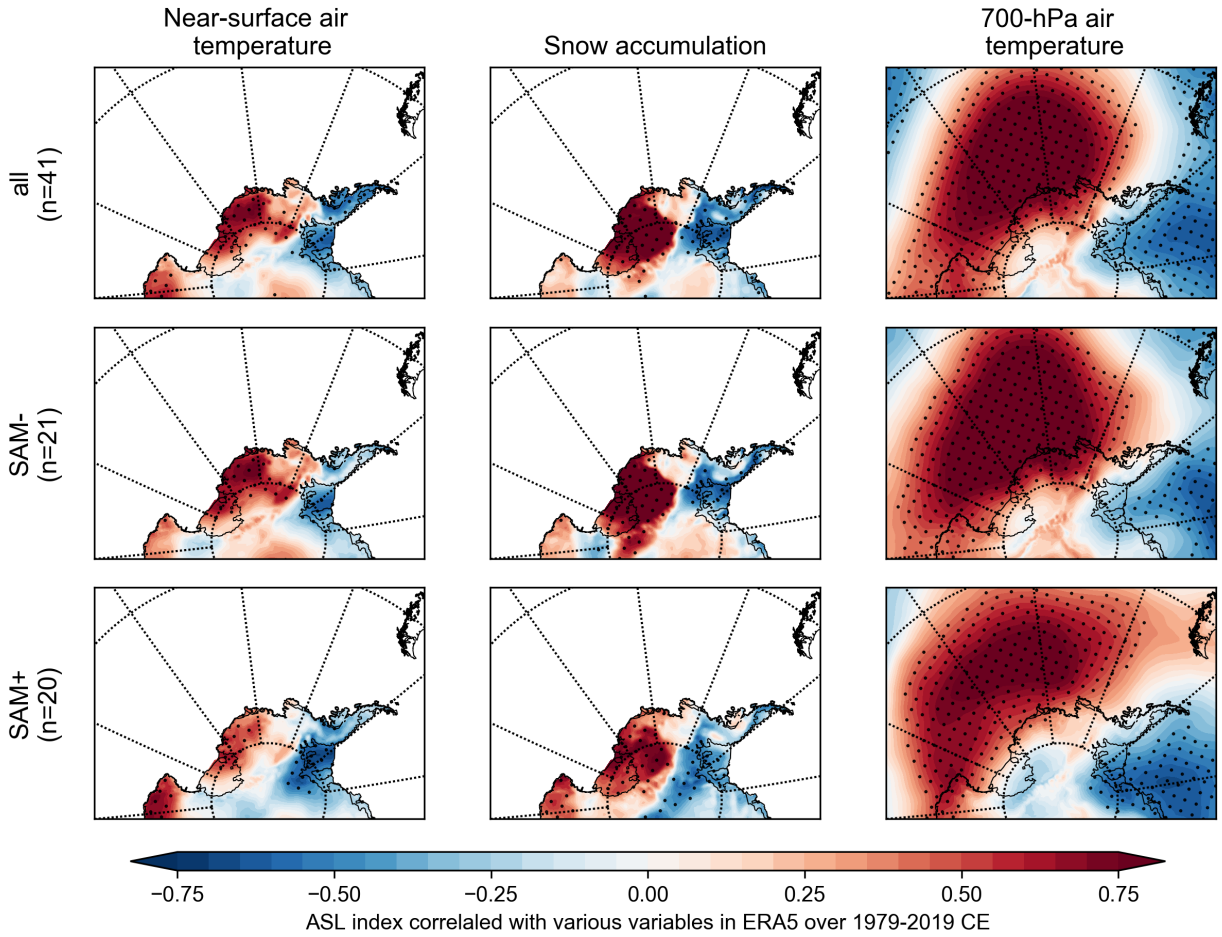


Figure 3.11: *Annual ASL index linearly correlated with near-surface air temperature, snow accumulation and 700-hPa air temperature in the ERA5 reanalysis over 1979–2019 CE. Correlations have been computed on all (All), SAM+ (SAM+) or SAM- (SAM-) years with n corresponding to the sample length. Stippling indicates statistically significant correlations (90% confidence level).*

3.4 Conclusions

In this paper, we have investigated the West Antarctic climate variability over the past two centuries by providing a complete reconstruction for the main atmospheric variables, as well as the sea-ice concentration. This is achieved by using a data assimilation approach that combines optimally the information brought by paleoclimate proxies and the climate physics from climate models. The reconstruction is based on all the annually-resolved snow accumulation and δ^{18}O records from the Antarctic ice cores, as well as tree-ring width records situated in the mid-latitudes from the Southern Hemisphere. The use of the isotope-enable climate model iCESM1 in the data assimilation allows to avoid strong assumptions on the relationship between the δ^{18}O in ice cores and climate variables.

We have evaluated our reconstruction using various independent data over the instrumental era and shown that our reconstruction is able to reproduce well the climate variability over West Antarctica (near-surface air temperature and snow accumulation), the atmospheric circulation in the West Antarctic sector (in particular, the ASL), and the sea-ice cover. Snow accumulation and δ^{18}O records from ice core, as well as tree-ring width, are thus providing valuable information to reconstruct the West Antarctic climate over the past 200 years at least. This is further confirmed by comparing our sea-ice extent reconstructions with two independent sea-ice reconstructions based on MSA records from ice cores, which leads to similar results as our reconstruction at the decadal scale.

According to our reconstruction, the overall observed reduction of sea-ice extent in the Bellingshausen/Amundsen Sea sector over the instrumental era [e.g., Parkinson, 2019] is part of a long-term linear trend starting at the beginning of the industrial period. In contrast, the increase of sea-ice extent in the Ross Sea sector has started one century later, around 1950 CE and is preceded by a small sea-ice reduction between 1850 and 1950 CE. Our results show that the deeper ASL over the second half of the 20th century generally explains these long-term changes by modulating winds in the West Antarctic sector. However, we observe that the strength of the relationship between the sea-ice extent in the Bellingshausen-Amundsen Sea sector and the ASL strongly varies over the past two centuries.

We have also shown that the observed general warming since 1958 CE in West Antarctica is not representative of changes over the past 200 years, which usually present a dipole on the continent due to the ASL. Our reconstruction suggests that this widespread warming is explained by both the stronger ASL and the positive phase of SAM. Therefore, this could not be simply related to the fingerprint of the ASL impact on the continent or ocean surface, but also the SAM. The continental response to a change in the atmospheric circulation may not be stationary. Care must be thus taken when inferring changes at the West Antarctica-scale from local proxies. Care should also be taken when relying on the short instrumental period to infer changes in Antarctic climate variability and its drivers. Future climate scenarios are often reliant on our understanding of climate variability during the instrumental period. But our study demonstrates that this time period may not be the most representative of the climate variability over multi-decadal to centennial timescales.

Additionally, those time-dependent relationships, as well as the potential complex response of the climate in West Antarctica to the atmospheric circulation, raise concerns about simple statistical methods that assume, by construction, constant relationships between the proxy and the reconstructed climate variable. Using a more sophisticated method like data assimilation is a clear advantage because it directly relies on the covariance between the reconstructed variables and

the observations as described by the model. Data assimilation-based reconstruction thus ensures that all reconstructed variables are dynamically consistent.

This present work is focused on the ongoing West Antarctic climate by analyzing local changes. Our study demonstrates that the recent period appears unusual in the longer context but further work is needed to understand the drivers and the underlying mechanisms of those changes. Atmospheric circulation changes in the high latitudes of the Southern Hemisphere over the past decades have been attributed to various factors [Thompson et al., 2011b], most notably the atmospheric ozone depleting and the increase of the atmospheric greenhouse gases [e.g., Fogt et al., 2009; Polvani et al., 2011]. Additionally, an increasing number of studies [e.g., Ding et al., 2011; Steig et al., 2013; Clem et al., 2016; Holland et al., 2019] have shown that changes in the West Antarctic climate are closely linked to the climate variability in the tropical Pacific and other basins through tropical-Antarctic teleconnections. These teleconnections influence the West Antarctic climate by modifying the atmospheric circulation around Antarctica. Therefore, quantifying the contribution of these teleconnections on the West Antarctic climate is a next step to improve the knowledge of the climate changes in West Antarctica over the past centuries.

4

Future Antarctic snow accumulation trend is dominated by atmospheric synoptic-scale events

Abstract

Over the last century, the increase in snow accumulation over Antarctica has partly mitigated the total dynamic Antarctic Ice Sheet mass loss. However, the mechanisms behind this increase are poorly understood. Here we analyze the Antarctic Ice Sheet atmospheric moisture budget based on a climate reanalysis and model simulations to reveal that the interannual variability of regional snow accumulation is controlled by both the large-scale atmospheric circulation and short-lived synoptic-scale events. Yet, when considering the entire continent at the multi-decadal scale, only the synoptic-scale events (i.e. storm systems) can explain the recent and expected future snow accumulation increase. In a warmer climate, these synoptic-scale events transport air that can contain more humidity due to the increasing temperatures. This leads to more precipitation on the Antarctic Ice Sheet, therefore mitigating the sea-level rise contribution of the Antarctic continent. Changes in the atmospheric westerlies over the Antarctic have an important role in controlling interannual and regional variations in snow accumulation, but a marginal role on longer timescales and at the ice sheet scale. Our findings highlight that the multi-decadal and interannual snow accumulation variability is governed by different processes, and that we thus cannot rely directly on the mechanisms driving interannual variations in snow accumulation to predict long-term changes in snow accumulation in the future.

This chapter is based on: Dalaiden, Q., Goosse, H., Lenaerts, J.T.M., Cavitte, M.G.P. and Henderson, N. (2020). Future Antarctic snow accumulation trend is dominated by atmospheric synoptic-scale events. *Communications Earth & Environment*, **1**(62), https://doi.org/10.1038/s43247-020-00062-x. Supplementary materials are in Appendix C.

4.1 Introduction

The Antarctic Ice Sheet (AIS) is currently losing mass at an accelerated pace at its margins of the West Antarctic Ice Sheet, driven by oceanic warming that induces ice shelf melting, subsequent grounding line retreat and enhanced ice discharge [Shepherd et al., 2018b; Pattyn and Morlighem, 2020; Smith et al., 2020]. Partly opposing this mass loss, snowfall has increased over much of the AIS since the early 19th century, as shown in a recent AIS-wide reconstruction based on ice core compilation [Medley and Thomas, 2019]. This positive trend in snow accumulation, i.e. the difference between total precipitation and losses from the evaporation/sublimation, wind snow redistribution and meltwater runoff, is estimated to have led to the mitigation of sea-level rise [Medley and Thomas, 2019]. Both ice core records and climate models suggest an increase in snow accumulation over the last century, in concert with and driven by the warming of the AIS near-surface atmosphere [Medley and Thomas, 2019; Dalaiden et al., 2020a]. Accordingly, climate model projections predict that the Antarctic snow accumulation will continue to increase and partially offset dynamic AIS mass loss by the end of the 21st century [Ligtenberg et al., 2013; Lenaerts et al., 2016; Kittel et al., 2021].

However, the regional variations in the trends suggest that the processes driving this snow accumulation increase are more subtle than a simple temperature-snow accumulation relationship. Additionally, ice cores reveal that the snow accumulation over the Holocene period might not be systematically related to changes in air temperature [Fudge et al., 2016; Frieler et al., 2015]. In this regard, some areas over the West Antarctic Ice Sheet have witnessed warming over 1950-2010 CE without a snow accumulation increase [Wang et al., 2017; Nicolas and Bromwich, 2014], pointing out the role of the interaction between orography and atmospheric circulation in the temperature-accumulation relationship [Fyke et al., 2017].

Our limited understanding of those processes governing the snow accumulation variations has two important consequences. First, it restrains our ability to assess future Antarctic contribution to global sea-level rise [Lenaerts et al., 2019]. Second, it introduces uncertainties in the information inferred from interpretation of ice core records such as snow accumulation or the isotopic ratio of oxygen, that are notably used to reconstruct past near-surface air temperature, sea ice extent and atmospheric circulation [Sime et al., 2009; Thomas and Abram, 2016b]. Nevertheless, without a thorough understanding of the atmospheric processes that control AIS snow accumulation, inferring the past climate beyond the instrumental period from these records may be hazardous.

Snow accumulation variability is mainly controlled by three mechanisms: thermodynamic processes, large-scale dynamics, and synoptic-scale dynamics [Grieger et al., 2016; Fyke et al., 2017; Medley and Thomas, 2019; Thomas et al.,

2017; Lenaerts et al., 2019]. Thermodynamic processes refer to snow accumulation changes attributed to a change in air temperature. Following the Clausius-Clapeyron relation, the maximum atmospheric moisture content increases with increasing air temperature, and potentially leads to more AIS continental snow accumulation in a warming climate [Frieler et al., 2015; Palerme et al., 2017b; Dalaiden et al., 2020a; Medley and Thomas, 2019]. In contrast to thermodynamic processes that have a pervasive impact on snow accumulation changes, large-scale atmospheric dynamics, which bring moisture from lower latitudes, lead to more regional variability as topography largely controls precipitation changes in response to modification in atmospheric circulation [Fyke et al., 2017]. Finally, recent studies [Gorodetskaya et al., 2014; Turner et al., 2019b] have pointed out the large contribution of short-lived synoptic-scale events, such as atmospheric rivers, to the interannual variability of snow accumulation. Some Antarctic regions receive more than 50% of their annual snowfall in just a few days, such as the Amery Ice Shelf [Turner et al., 2019b], but the net contribution of these short-lived synoptic-scale events in the long-term snow accumulation changes for Antarctica as a whole is unknown. It is worth noting that these three mechanisms are difficult to disentangle because they are not mutually exclusive.

To better understand the individual contributions of these three mechanisms on past, present, and future AIS snow accumulation, we calculate a moisture budget for the AIS atmosphere, analogous to that of previous studies [Bromwich et al., 1995; Seager et al., 2010] (Methods). From this budget, we can separate the contributions of the moisture transported by large-scale atmospheric dynamics from the moisture transported by synoptic-scale events (Methods). The proposed methodology makes the distinction between the two by assuming that synoptic-scale events mainly influence day-to-day variations, while the influence of large-scale circulation is obtained as the result when monthly means are used. Separating these two mechanisms across temporal scales also corresponds to a separation in the spatial scales, as synoptic-scale events are typically 100-2000 km scale systems embedded within the large-scale flow characterized by scales larger than 2000 km. The analysis uses the European Centre for Medium-Range Weather Forecasts Interim reanalysis, the latter which is ERA-Interim, the best reanalysis to study the Antarctic climate over the last few decades [Bromwich et al., 2011; Nicolas and Bromwich, 2011b], and Global Climate Model (GCM) simulations covering the 20^{th} and 21^{st} centuries, including ozone depletion experiments. The goal is to investigate all the known mechanisms that explain the snow accumulation variability from the interannual to multi-decadal scale, at both regional and continental scales, in a common framework.

Although it is not possible to estimate the errors introduced by the moisture budget calculation on each term of the budget, it is worth noting that the moisture budget calculation underestimates the Antarctic snow accumulation, which

most likely originates from an underestimation of the contribution of the moisture brought by the synoptic-scale transport (around 18% when integrating over the entire continent over 1985-2014 CE). However, both the spatial and temporal variability of the snow accumulation are well reproduced (see section C.4 for the discussion of the errors related to the moisture budget calculations).

4.2 Methods

4.2.1 Moisture budget calculation

The moisture budget calculation is fully described in Seager and Henderson [2013]. Therefore, only a short description is given here. The column-integrated moisture budget in pressure coordinates can be expressed as:

$$P - E = -\frac{1}{g\,\rho_w} \nabla \cdot \int_0^{p_s} \mathbf{u}\, q\, dp \tag{4.1}$$

where P stands for total precipitation, E for total evaporation (including sublimation), $\mathbf{u}$ for the horizontal wind, q for the specific humidity, ρ_w for the water density, g for the gravitational acceleration and p_s for the surface pressure. Over the Antarctic Ice Sheet, snow accumulation is estimated by calculating the precipitation-minus-evaporation/sublimation ($P - E$) [Lenaerts et al., 2019]. This definition of the snow accumulation does not include the runoff coming from the melt, mass change due to wind (snow deposition/erosion) and the sublimation of the snow particles induced by the drifting snow. At the continental scale, the contribution of this later term to the total Antarctic snow accumulation is about 15-20% [Palm et al., 2017; Agosta et al., 2019]. In contrast, the runoff under present-day conditions represents less than 0.1% of the total Antarctic snow accumulation [van Wessem et al., 2018; Agosta et al., 2019]. Although the melt is expected to increase in the current century with climate warming, a large part of the melt will refreeze in the firn [Lenaerts et al., 2019], which implies this increase in the melt will not be thus necessarily converted into a runoff contribution. Consequently, the use of snow accumulation resulting from the difference between precipitation and evaporation/sublimation is adequate since $P - E$ is the largest component of snow accumulation [Agosta et al., 2019; van Wessem et al., 2018].

Considering monthly means, we can rewrite Eq. (4.1):

$$\overline{P} - \overline{E} = -\frac{1}{g\,\rho_w} \nabla \cdot \int_0^{p_s} \overline{\mathbf{u}\, q}\, dp - \frac{1}{g\,\rho_w} \nabla \cdot \int_0^{p_s} \overline{\mathbf{u}'\, q'}\, dp \tag{4.2}$$

where the first term represents the monthly mean moisture convergence and the second term represents the sub-monthly transient eddy moisture convergence.

To facilitate the reading, we use “large-scale transport” when referring to the moisture convergence due to the mean atmospheric circulation and we use “synoptic-scale transport” to refer to the moisture convergence due to the transient eddies. The overbar indicates a monthly mean while the prime indicates a departure from the monthly mean (i.e., $\mathbf{u}' = \mathbf{u} - \overline{\mathbf{u}}$). The change in large-scale transport (the first term of the right hand side of Eq. (4.2)) between two periods p2 and p1 can be further separated into humidity- and circulation-induced change components as follows:

$$\begin{aligned}\delta\left(\frac{1}{g\,\rho_w}\nabla\cdot\int_0^{p_s}\overline{\mathbf{u}\,q}\,dp\right)_{\text{p2-p1}} &\simeq \frac{1}{g\,\rho_w}\overline{\nabla\cdot\int_0^{p_s}\overline{\delta\mathbf{u}_{\text{p2-p1}}}\;\overline{q_{\text{p1}}}\,dp} + \\ &\quad \frac{1}{g\,\rho_w}\overline{\nabla\cdot\int_0^{p_s}\overline{\mathbf{u}_{\text{p1}}}\;\overline{\delta q_{\text{p2-p1}}}\,dp} \\ &= \delta\overline{\text{DYN}} + \delta\overline{\text{TH}} \end{aligned} \tag{4.3}$$

where $\delta\overline{\mathbf{u}_{\text{p2-p1}}} = \overline{\mathbf{u}_{\text{p2}}} - \overline{\mathbf{u}_{\text{p1}}}$ and $\delta\overline{q_{\text{p2-p1}}} = \overline{q_{\text{p2}}} - \overline{q_{\text{p1}}}$ represent the changes in horizontal wind and humidity, respectively, between the periods p2 and p1. This breakdown allows us to gain insight into the origin of the changes in $P - E$. However, the part of the $P - E$ change resulting from a change in specific humidity combined to a change in winds (given by $\nabla\cdot\int_0^{p_s}\overline{\delta\mathbf{u}_{\text{p2-p1}}}\,dp$), the so-called quadratic term is neglected in Eq. (4.3). See section C.4 for the evaluation of the moisture budget calculation.

4.2.2 Atmospheric reanalysis and climate model simulations

We have selected the ERA-Interim reanalysis from the ECMWF [Dee et al., 2011] as input for the moisture budget calculation over the last decades (1985–2014 CE period). ERA-Interim, which has a spatial resolution of 0.75° [Dee et al., 2011], is considered as one of the best reanalysis products in reproducing the present-day Antarctic climate and, more specifically in the present framework, to analyze Antarctic snow accumulation [Bromwich et al., 2011; Nicolas and Bromwich, 2011b; Gossart et al., 2019b]. Nonetheless, ERA-Interim suffers from some biases such as a large underestimation of the snow accumulation over the Antarctic Plateau where the snow accumulation values are lower than 10 mm w.e. eq. year^{-1} [Bromwich et al., 2011; Nicolas and Bromwich, 2011b]. Biases in ERA-Interim mainly come from the weak observational network and because of processes that are not included in ERA-Interim such as drifting snow and diamond dust [Bromwich et al., 2011; Nicolas and Bromwich, 2011b], which are the main contributors to the mass gain over the dry Antarctic Plateau [Ricaud et al., 2017]. We also use the ERA-Interim results to assess the climate models’ simulated moisture budgets.

Since ERA-Interim displays a strong dry bias over the Antarctic Plateau, the model evaluation based on ERA-Interim has to be taken with caution for this region.

For the historical period (1850–2014 CE period) and for the end of the 21st century, we calculate the moisture budget from simulations performed by the National Centre For Atmospheric Research (NCAR) with the Community Earth System Model (CESM). CESM is a fully coupled global climate model simulating the interactions between the atmosphere, ocean and land at a horizontal spatial resolution of approximately 1°. Numerous studies have shown the good performance of CESM in simulating the Antarctic climate [Agosta et al., 2015; Lenaerts et al., 2016, 2018; Fyke et al., 2017]. In particular, CESM1 provides a reasonable representation of the climatology and interannual variability of the Antarctic snow accumulation when comparing to observations and regional climate models [Lenaerts et al., 2016; Fyke et al., 2017]. Albeit the evaluation of the latest version of CESM (CESM2.1, hereafter CESM2) is as detailed for CESM1, this new version seems to simulate more accurately the Antarctic climate [Danabasoglu et al., 2020]. First, we calculate the moisture budget using this latest version of CESM (i.e. CESM2) that participates in the Coupled Model Intercomparison Project (CMIP) phase 6 (CMIP6). We analyze the historical simulation (1850–2014 CE period) and the future projection simulation (2015–2100 CE period) under the Societal Development Pathway (SSP) 5-85 (hereafter SSP5-85; high energy imbalance), which is at the upper end of available scenarios and is the nearest equivalent to the RCP8.5 applied in CMIP phase 5 (CMIP5)). We use 6-hourly data on atmospheric model levels (33 atmospheric levels expressed in hybrid coordinates) for the computation of the moisture budget [Seager and Henderson, 2013]. Unfortunately, data at this temporal and spatial resolution is only available for one simulation. In addition to the CESM2 simulation, we also calculate the moisture budget using the Large Ensemble (LE) of the CESM version 1 (CESM1-CAM5; hereafter CESM1-LE) spanning 1920–2100 CE [Kay et al., 2015]. After 2005 CE, the representative concentration pathway 8.5 (RCP8.5) is used as a forcing in CESM1-LE. This large ensemble, which includes 35 members, allows us to quantify the role played by the internal variability on the moisture budget, something that cannot be done with the other CMIP5 models or with CESM2. The high temporal resolution requirements are only met for the 1990–2005 CE, 2031–2040 CE and 2071–2080 CE periods, but for all CESM1-LE members.

In addition to the CESM simulations, we also use two other climate models from the CMIP5 database to support our results (Figs. C.7–C.18). Among all the climate models which can provide the required data for the moisture budget available for the historical and future (under the RCP8.5 scenario) simulations, the selection of the CMIP5 models is based on data availability and a model evaluation [Agosta et al., 2015] which ranked CMIP5 models in the aim of using them for regional climate modeling over the Antarctic Ice Sheet. We selected the models

that are the best ranked in the evaluation of Agosta et al. [2019]. This evaluation is adequate in the present framework as it analyses the performance of models in representing the atmospheric mechanisms behind snow accumulation changes, although it does assess model behavior in simulating Antarctic climate itself. Therefore, according to this evaluation, we selected ACCESS1-3 and NorESM1-M. However, given that the CMIP5 model simulations are only available from 1950 CE, we mainly use CESM2 to describe the mechanisms involved in the snow accumulation.

4.2.3 Clausius-Clapeyron approximation

To determine to what extent the near-surface air temperature change can explain the $P - E$ change, we estimate the snow accumulation changes that can be related to a change in near-surface air temperature – the so-called Clausius-Clapeyron (hereafter CC) approximation as in Held and Soden [2006]:

$$\delta\left[(P-E)_{CC}\right]_{\text{p2-p1}} = \alpha \delta T_{\text{p2-p1}}\ (P-E)_{\text{p1}} \tag{4.4}$$

where T is the near-surface air temperature and α is the sensitivity of the saturation vapor pressure to temperature ($dlne_s\ dT^{-1}$), equal to 0.07 K^{-1} for typical temperatures in the lower troposphere [Held and Soden, 2006; Frieler et al., 2015]. This means that for each degree of warming, the saturation vapor pressure is 7% higher. This value is consistent with the snow accumulation sensitivity to air temperature found in multi-GCM-based estimations of 6.1 $\pm$ 2.6 % K^{-1} for Antarctica [Frieler et al., 2015].

4.2.4 SAM-congruent change

To establish the SAM-congruent snow accumulation changes, we first need to calculate the SAM index. It is defined as the annual mean of the normalized zonal-average of the difference between 40°S and 65°S geopotential heights at 500 hPa [Gong and Wang, 1999]. Then, we compute the snow accumulation sensitivity to deviations in the SAM index by performing a linear regression between the two variables for each grid cell after removing linear trends over the 1850–2014 period for CESM2 and over the 1920–2005 period for CESM1. We then multiply the snow accumulation sensitivities obtained from this regression (in mm w.e. eq. $year^{-1}$) by the change in the SAM index between the two time periods (or between the evolving and fixed ozone member ensembles for the ozone case) to obtain the SAM-congruent snow accumulation changes between those two periods. The methodology applied here is identical as in Medley and Thomas [2019].

4.2.5 Antarctic regions

The Antarctic continent is divided into seven regions, which are further grouped into two bigger regions: East Antarctica and West Antarctica, as defined in Thomas et al. [2017]. The five regions that form East Antarctica are: the Plateau where the altitude is higher than 2000 m and four coastal regions, namely Wilkes Land Coast (70–150°E), Weddell Sea Coast (60–15°W), Victoria Land and Ross Sea (150–170°E), and Dronning Maud Land (DML) Coast (15°W–70°E). West Antarctica is split into two regions with a division at 88°W: the West Antarctic Ice Sheet (WAIS) and the Antarctic Peninsula.

4.3 Results

Despite those uncertainties in the moisture budget calculation, the main contributor to the mean Antarctic snow accumulation averaged over the 1985–2014 CE period for each of the seven geographical regions defined here (Methods) is the synoptic-scale transport, with an average contribution slightly exceeding 100% (105 $\pm$ 4% for Antarctica as a whole; Fig. 4.1). This is consistent with previous studies [Bromwich et al., 1995; Cullather et al., 1998]. While the synoptic-scale transport positively contributes to the mean snow accumulation for each of the seven regions, the contribution of the large-scale transport is only positive for the Antarctic Peninsula and the West Antarctic Ice Sheet (WAIS) (18 $\pm$ 9% and 32 $\pm$ 6%, respectively). For East Antarctica, the contribution of the large-scale transport is negative (-34 $\pm$ 7%), which implies that the mean atmospheric circulation tends to transport the moisture brought by the synoptic-scale transport away from the region. This finally adds up to a quasi-null contribution of large-scale transport for the continent as a whole (-5 $\pm$ 4%). The net contribution of the mean atmospheric circulation to the Antarctic snow accumulation averaged over the 1985–2014 CE period is therefore a net atmospheric moisture transport, and associated snowfall, from West to East Antarctica.

Although the contribution of the large-scale transport to the mean snow accumulation integrated over the entire AIS is small compared to the synoptic-scale transport, it provides a large contribution to the interannual variability of the snow accumulation on the regional scale. Except for the Antarctic Plateau, the role of the large-scale transport in the interannual variability is larger than 29% and is similar to or higher than the role of the synoptic-scale transport (Fig. 4.1). For instance, for the Antarctic Peninsula, year-to-year variations in the large-scale transport explain almost 80% of interannual variability in snow accumulation, while it only contributes to 18% of the long-term mean. However, the synoptic-scale transport still dominates the interannual variability of snow accumulation at the continental scale (Fig. 4.1, Antarctica as whole).

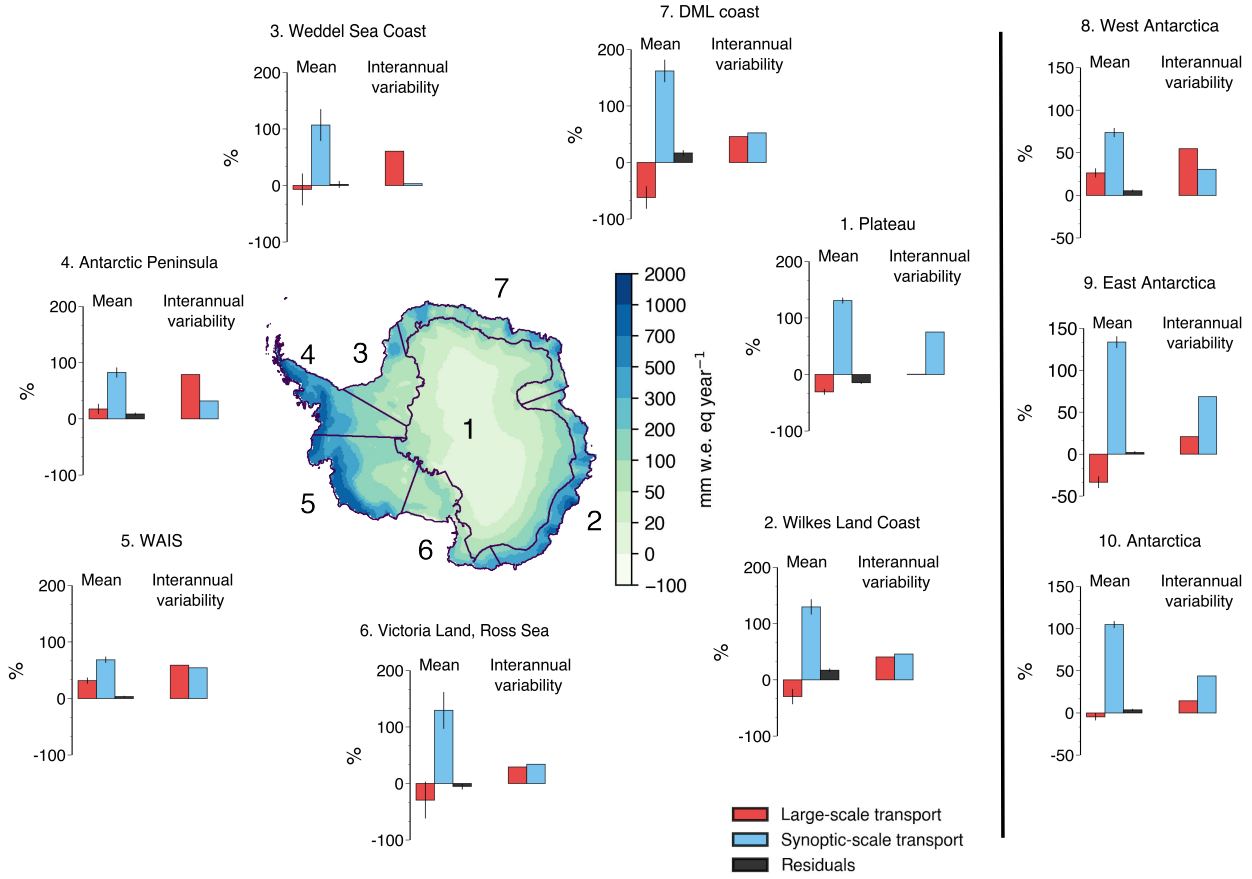


Figure 4.1: ***Relative contributions of the large-scale and synoptic-scale transports to Antarctic snow accumulation.*** *The bar plots show the contributions of the large-scale transport (red) and synoptic-scale transport (blue) to the mean and interannual variability of snow accumulation for the seven Antarctic regions based on ERA-Interim over the 1985–2014 CE period. The residuals (black; i.e. the error related to the moisture budget calculation) are defined as the difference between the mean snow accumulation from model outputs and the one from the moisture budget (see Methods for more details). In the center, the Antarctic snow accumulation climatology over the 1985–2014 CE period (in mm w.e. year^{-1}) with the regional boundaries defined. The error bars are calculated as the standard deviation of the annual contribution to the snow accumulation mean. Antarctic regions are defined as in Thomas et al. [2017]: the Plateau where the altitude is higher than 2000 m, Wilkes Land Coast (70–150° E), Weddell Sea Coast (60–15° W), Victoria Land and Ross Sea (150–170° E), and Dronning Maud Land (DML) Coast (15° W–70° E). All these regions together is considered as East Antarctica. West Antarctica is divided into two regions with a division at 88° W: the Antarctic Peninsula and the West Antarctic Ice Sheet (WAIS).*

4.3.1 Contributions of large-scale and synoptic-scale transports in multi-decadal trends

To analyze snow accumulation changes over longer timescales including the last century, we calculate the moisture budget for the AIS using Earth System Model (ESM) outputs over the 1850–2014 CE period. For this purpose, we use the most recent version of the Community Earth System Model, CESM2 [Danabasoglu et al., 2020]. The use of CESM2 is justified by large similarities between the calculated CESM2 moisture budget and the one from ERA-Interim for the 1985–2014 CE period (Fig. C.1 and Tab. C.1). Both ERA-Interim and CESM2 indicate the synoptic-scale transport as the main contributor to the mean of snow accumulation for all the regions, with for instance a total contribution of 100% for Antarctica as a whole for CESM2 against 105% for ERA-Interim. Additionally, in accordance with ERA-Interim, CESM2 highlights the role of the large-scale circulation on the interannual variability of the regional snow accumulation (on average over the seven regions without the Plateau, this contribution reaches 58% against 53% for ERA-Interim), but the interannual variability at the continental scale is dominated by the synoptic-scale transport (63% for CESM2 against 44% for ERA-Interim).

On the continental scale, we obtain a modeled snow accumulation increase of 211 Gt year^{-1} (relative increase: +8%) between the 1850–1879 CE and 1985–2014 CE periods, with the largest relative increase for Dronning Maud Land (+17%: +62 Gt year^{-1}; Fig. 4.2). This large increase over recent years over Dronning Maud Land is consistent with several other data and model studies [Lenaerts et al., 2013; Philippe et al., 2016; Medley et al., 2018]. CESM2 shows a positive snow accumulation change for all seven regions. Analogously, CESM2 under the SSP5-85 scenario (Methods) predicts that Antarctic snow accumulation over the 2071–2100 CE period will be 1200 Gt year^{-1} higher compared to the 1985–2014 CE period (relative increase of 42%; Fig. C.2). CESM2 shows an increase for all seven regions, with the Weddell region displaying the highest relative increase (+54%), closely followed by the Dronning Maud Land region (+52%; Fig. C.2).

According to our results, it turns out that the snow accumulation increase for the 1985–2014 CE period at the continental scale is mainly explained by an increase in the synoptic-scale transport (+95%) as the change in the large-scale transport leads to almost no change in snow accumulation (+5%; Fig. 4.2). However, on the regional scale, changes in the large-scale transport do contribute to snow accumulation changes for WAIS (13%) and Dronning Maud Land (30%). Separating the contribution of the large-scale transport into dynamic and thermodynamic components (i.e., due to changes in the winds or humidity, respectively; Methods) indicates that for the Wilkes Land Coast and Dronning Maud Land regions, the snow accumulation increase is driven by an atmospheric circulation change and not a specific humidity change (Fig. C.3). Similarly to these changes

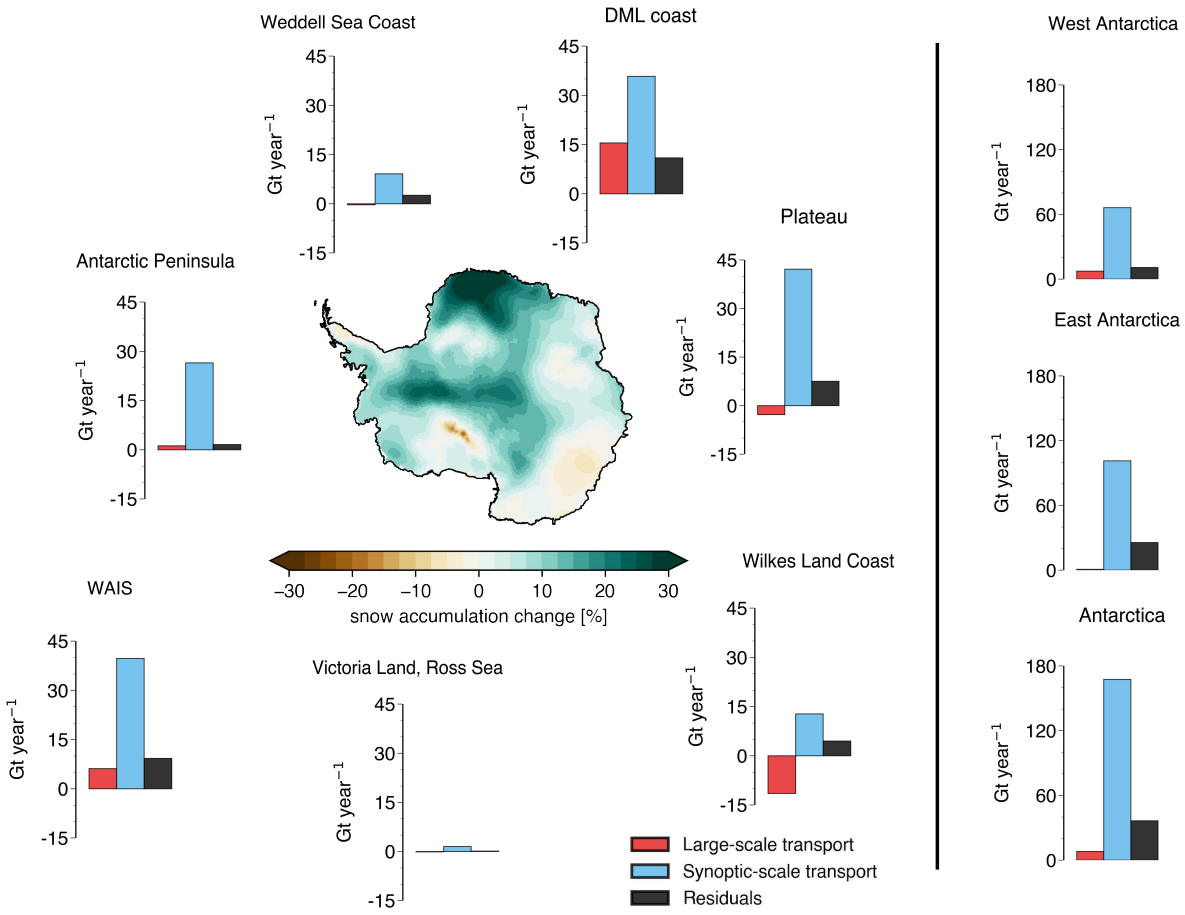


Figure 4.2: ***Snow accumulation changes in the CESM2 simulation between the 1985–2014 CE and 1850–1879 CE periods.*** *The bar plots represent the absolute contributions of the large-scale transport (red) and synoptic-scale transport (blue) to the snow accumulation change per region (in Gt year^{-1}). The change in the residuals (black; i.e. the error related to the moisture budget calculation) is defined as the change in the difference between the snow accumulation from model outputs and the one from the moisture budget (in Gt year^{-1}; see Methods for more details). Regional boundaries are as in Fig. 4.1.*

described over the past decades, future snow accumulation increases at the continental scale are dominated by an increase in the contribution of the synoptic-scale transport (96%; Fig. C.2). The change in the large-scale transport leads to no change in snow accumulation at this continental scale (4%), but at the regional scale, changes in the large-scale transport are important for almost all regions with its highest relative positive contribution for Victoria Land (+89%) followed by WAIS (+55%) and the Antarctic Peninsula (+41%).

4.3.2 Physical mechanisms behind snow accumulation changes

The ESM-based results allow us to also assess the mechanisms (i.e., thermodynamic processes, large-scale and synoptic-scale dynamics) behind recent and fu-

ture AIS snow accumulation changes. At first, given that the water vapor pressure of the air depends directly on the air temperature following the Clausius-Clapeyron relation (i.e. the concentration of water in the atmosphere is potentially higher in a warmer atmosphere), we assume that snow accumulation changes are proportional to air temperature changes (i.e., the CC approximation; Methods). If applying the CC approximation shows a good match of the changes observed in air temperatures and snow accumulation rates, thermodynamic changes can explain the modeled snow accumulation changes. On the other hand, a non-matching CC approximation potentially indicates that the origin of snow accumulation changes arise from a dynamic change (changing atmospheric circulation, bringing more or less humidity) rather than a thermodynamic change (change in air temperature).

The CC approximation largely underestimates the modeled snow accumulation interannual variability at the regional scale over the 1985–2014 CE period (Fig. C.4). It better explains the long-term changes in snow accumulation between the 1985–2014 CE and 1850–1879 CE periods, obtaining a relative underestimation of 16% of the total AIS snow accumulation change (Fig. 4.3a), with large regional disparities. This suggests that the interannual changes are more directly influenced by local changes such as a change in the winds (i.e., atmospheric dynamics), while long-term changes are well approximated by large-scale temperature changes. This result confirms that the large-scale circulation largely explains the interannual variability of regional snow accumulation. Similarly, the CC approximation overestimates the total future AIS change by 1% (i.e., between the 2071–2100 CE and 1985–2014 CE periods), albeit with less regional differences than for recent changes (Fig. 4.3b).

The trend in AIS snow accumulation not explained by the thermodynamic effect but rather attributed to changes in atmospheric dynamics might be linked to the Southern Annular Mode (hereafter SAM), the main mode of atmospheric variability in the Southern Hemisphere [Marshall, 2003]. The SAM is related to changes in the strength and position of Westerlies around the Antarctic. A recent study [Medley and Thomas, 2019] has shown that the SAM is the dominant contributor for the interannual variations of snow accumulation at the regional scale, explaining more than 80% of the spatial snow accumulation variability in trends over the 1957–2000 CE period. The increase in SAM index between the 1985–2014 CE and 1850–1879 CE periods (+0.32 standard deviation of the SAM index in the model) induces a contraction and poleward shift of the Westerlies over the Southern Ocean, which leads to less snowfall around the Ross Ice Shelf and more over the Peninsula [Turner et al., 2013]. Comparing the modeled snow accumulation changes with the SAM-congruent changes over the 1985–2014 CE period, we notice that the strongest regional impact of the SAM is observed for Victoria Land (Fig. 4.4; -2.31 Gt year^{-1} against 1.45 Gt year^{-1} for the modeled change; Methods). When integrating the SAM-congruent AIS-wide snow accumulation change

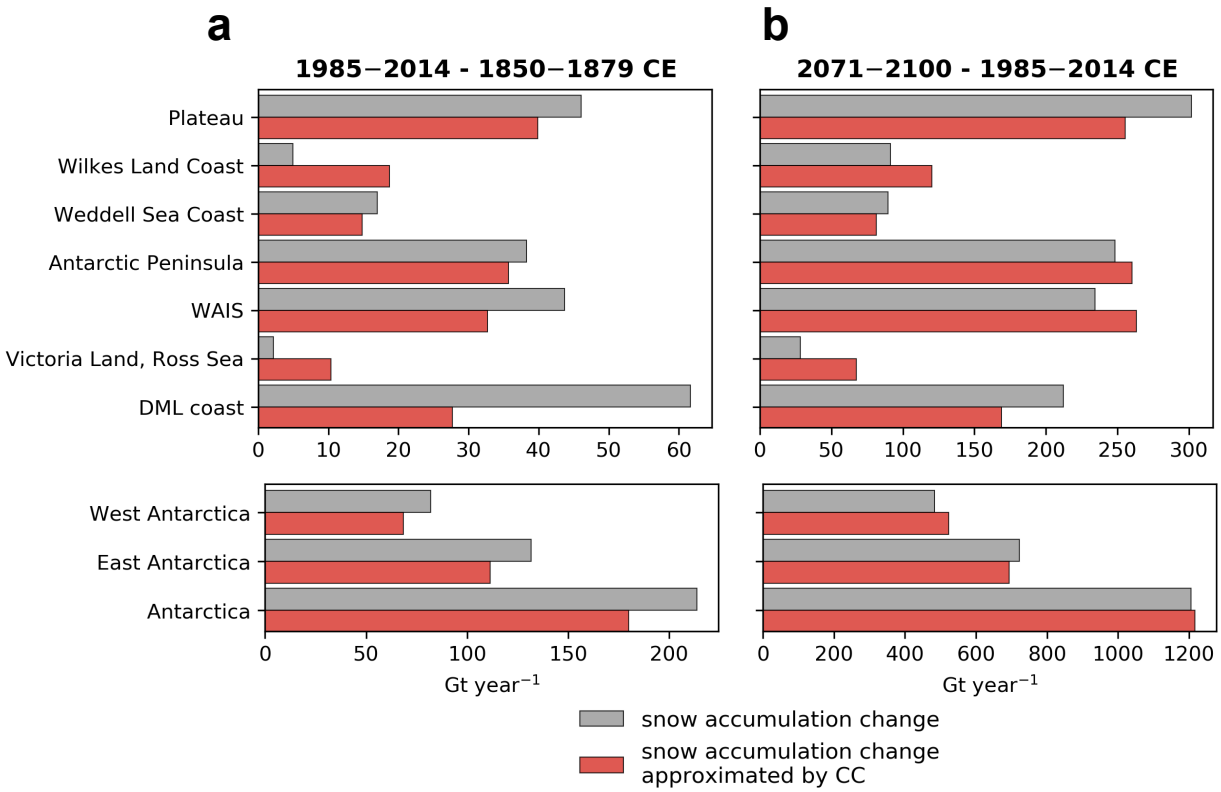


Figure 4.3: ***Snow accumulation changes approximated by the Clausius-Clapeyron relation.*** *Regional snow accumulation changes (grey) with their estimations by the Clausius-Clapeyron approximation (red) for the CESM2 simulations between the 1985–2014 CE and 1850–1879 CE periods (**a**) and between the 2071–2100 CE and 1985–2014 CE periods (**b**; in Gt year^{-1}). Regional boundaries are as in Fig. 4.1. Note that for readability, limits of the x-axis are different for the two plots.*

over the 1985–2014 CE period relative to the 1850–1879 CE period, the SAM has only caused a 6 Gt year^{-1} total AIS snow accumulation decrease (equivalent to less than 3%). This implies that the SAM is not the driver of the AIS-wide snow accumulation increase over the recent decades in the simulations analyzed here, in agreement with other studies [Medley and Thomas, 2019; van den Broeke and van Lipzig, 2004]. Additionally, the Antarctic climate is also influenced by tropical large-scale modes of variability [Ding et al., 2011]. In this regard, the Interdecadal Pacific Oscillation (IPO) displays a negative trend over the last decades and may partially explain the recent Antarctic snow accumulation increase [Clem et al., 2020]. However, similar to the SAM, the IPO only contributes to 4% of the Antarctic snow accumulation increase over the 1985-2014 CE period according to CESM2 (see section C.1).

Along with the SAM and IPO variations, stratospheric ozone depletion over the last decades might have played a role in the snow accumulation changes at both regional and continental scales [Lenaerts et al., 2018]. In addition to constituting

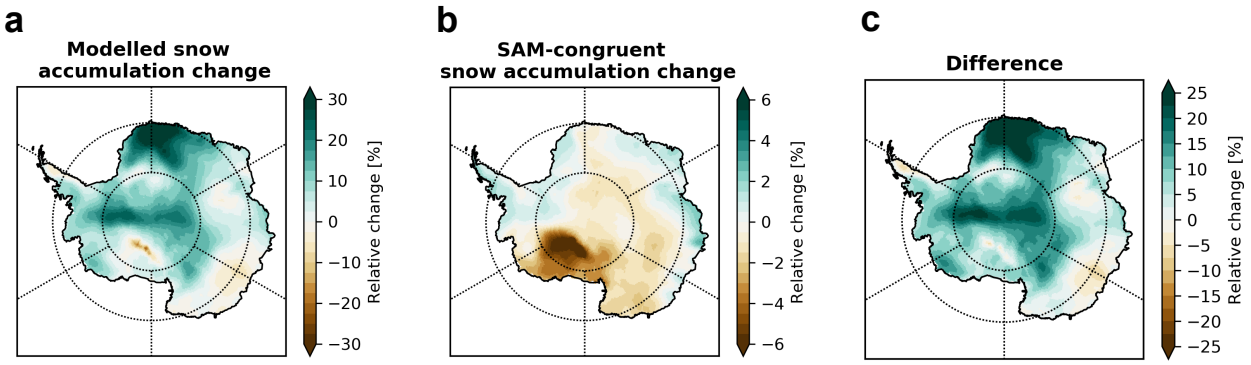


Figure 4.4: ***Snow accumulation changes and their relationship with the Southern Annular Mode (SAM).*** ***a****, Relative snow accumulation changes in the CESM2 simulation between the 1985–2014 CE and 1850–1879 CE periods.* ***b****, relative SAM-congruent snow accumulation changes in the CESM2 simulation between the 1985–2014 CE and 1850–1879 CE periods.* ***c****, the difference between* ***a*** *and* ***b*** *(****a****-****b****).*

one of the likely drivers of the SAM increase over the last decades [Thompson et al., 2011b], based on sensitivity experiments, the ozone depletion accounts for 31 $\pm$ 19% of the AIS snow accumulation increase over the 1986–2005 CE period in model simulations (see section C.2 and Lenaerts et al. [2018]). As ozone depletion leads to increased snow accumulation without a near-surface air temperature increase (Fig. C.5b), its contribution is considered here as a dynamic input. Since the CC approximation explains 58% of the AIS snow accumulation increase over the 1985–2005 CE period, the total AIS snow accumulation change is predominantly explained by thermodynamic processes, and, to a lesser degree, by dynamic processes, likely largely driven by stratospheric ozone depletion.

In addition to the thermodynamic effect and impact of large-scale atmospheric variations, other mechanisms might explain why the synoptic-scale events lead to more Antarctic snow accumulation over the past decades and in the future. In particular, changes in the intensity or frequency of cyclones that bring snowfall to the AIS coastal areas could have contributed to this snow accumulation increase. In order to characterize the cyclone activity associated with high-precipitation events, we calculate the difference in contribution of the Extreme Precipitations Events (EPEs) [Turner et al., 2019b] to total snowfall between the 1985–2014 CE and 1850–1879 CE periods. We assume that if this contribution has not changed between the two periods, the frequency or/and relative intensity of the cyclones is unchanged as well. In such a case, only an air temperature change can explain a snow accumulation increase from these synoptic-scale events. In many regions, the EPE contribution has changed between the two periods (Fig. 4.5a). On the continental scale, however, the EPE contribution to AIS precipitation has not significantly changed between the two periods (57.2% and 57.3%; respectively for the 1985–2014 CE and 1850–1879 CE periods). Similar results are obtained for

future changes (Fig. 4.5b) with a contribution of EPEs slightly lower for the 2071–2100 CE period (55.8%; statistically significant). Consequently, as their relative influence of EPEs is nearly unchanged, the Antarctic-wide snow accumulation increase linked to the synoptic-scale events is likely related to a thermodynamic effect.

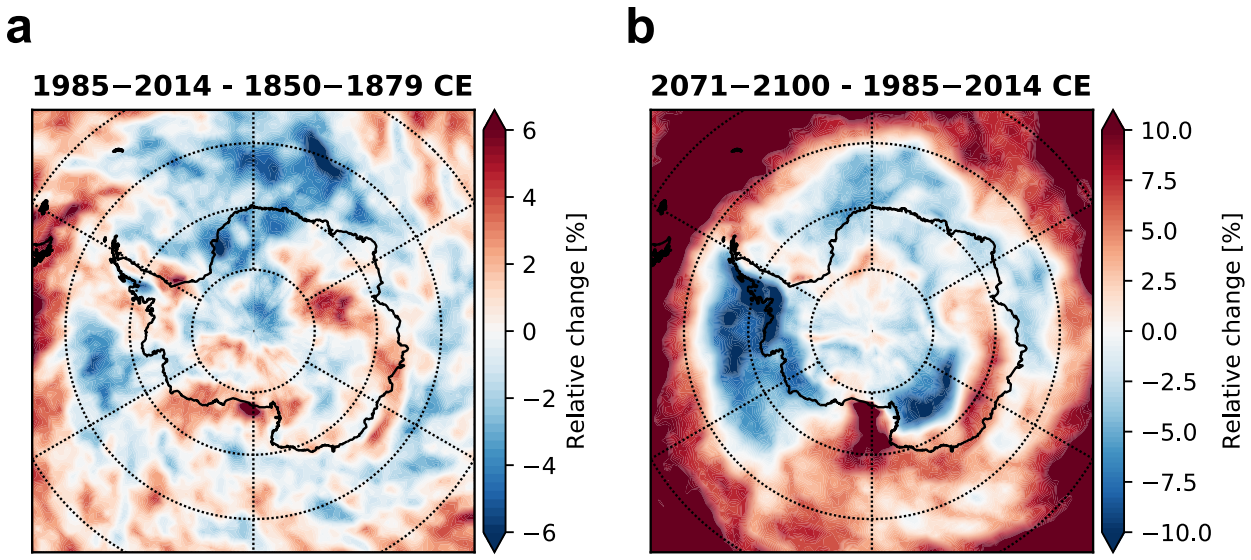


Figure 4.5: ***Changes in the contributions of Extreme Precipitations Events.*** *Relative differences in the contribution of Extreme Precipitation Events (EPEs) to the total precipitation in CESM2 between the 1985–2014 CE and 1850–1879 CE periods (**a**), and between the 2071–2100 CE and 1985–2014 CE periods (**b**). Here, EPEs follow the definition of Turner et al. [2019b]: they correspond to the events for which the total daily precipitation is higher than the 90th percentile of the entire time series. The computation of the contribution of EPEs is done by calculating the 90th percentiles for each of the three periods (i.e., 1850–1879 CE, 1985–2014 CE and 2071–2100 CE periods) and used to determine the contribution of the EPEs to the total precipitation. See Fig. C.6 for the same diagnostic using the 95th percentile as threshold.*

4.4 Discussion

Although CESM2 is an Earth System Model (ESM) from the latest generation (i.e. the Climate Model Intercomparison Project Phase 6, CMIP6) and displays a good performance at simulating the Antarctic Climate (see Lenaerts et al. [2016] for the evaluation of the previous version of the model and section C.3), a comparison of the results derived from the CESM2 with the ones from other climate models allows for more robust conclusions. For this, two CMIP5 models, among the ones that simulate best the atmospheric dynamics above the Antarctic (ACCESS1-3 and NorESM1-M) [Agosta et al., 2015], and the large ensemble of CESM1

(CESM1-LE) are analyzed (see their evaluations in section C.3). Under present-day conditions, as for ERA-Interim and CESM2, all these models show that the synoptic-scale transport is the main contributor to the mean of the snow accumulation at the continental scale (100% on average) while the contribution of the large-scale transport to Antarctic snow accumulation on average is close to zero (Figs. C.7–C.9). When analyzing the interannual variability of the snow accumulation, the large-scale transport plays a large role since it explains on average 49% over all regions except the Plateau. Additionally, the three models show a negative contribution (-2%) of the SAM to the Antarctic snow accumulation increase over the last decades. This confirms that the SAM is not responsible for the observed increase at the continental scale even though it contributes to regional changes, in particular over the Peninsula with a contribution of 51% on average for the three models (Figs. C.10–C.12). For the snow accumulation changes expected for the end of the century, the absolute AIS-integrated snow accumulation increase is different between all the models but, all indicate that the synoptic-transport remains the main driver of the snow accumulation increase for Antarctica as a whole (104%; Figs. C.13–C.15). The large-scale transport explains some snow accumulation increase such the Antarctic Peninsula with a relative contribution of 47% on average over the three models but, as highlighted by CESM2, this corresponds mainly to a snow redistribution between the regions. Finally, the additional models show that using the classical Clausius-Clapeyron relationship and the near-surface air temperature increase over the 21st century provides a good approximation of the future snow accumulation increase at the continental scale with an underestimation of 1% for the two CMIP5 models (Figs. C.16 and C.17) and an overestimation of 2% for CESM1-LE (Fig. C.18). This implies that all the major conclusions derived from CESM2 results are confirmed by the analysis of outputs of several other, independent climate models.

4.4.1 Implication for the future AIS contribution to sea-level rise

Our study shows that the mechanisms behind AIS snow accumulation change as a function of the spatial and temporal scales. According to our results, the SAM, i.e., the main Antarctic mode of atmospheric circulation variability, plays a minor role in the AIS-wide snow accumulation changes over long periods compared to changes in short-lived synoptic-scale events. We argue that the recent and expected (i.e., for the 21st century) snow accumulation increase arise from global air warming that leads to more continental snowfall, carried by these synoptic-scale events. As a direct implication, the drivers of the observed year-to-year changes in snow accumulation cannot be directly used to infer future snow accumulation changes, and therefore predict the future contribution of the AIS to global sea-level rise.

5

Conclusions and perspectives

5.1 Main achievements

The future Antarctic snow accumulation may partly offset the contribution of the dynamic loss (ice shelf melting and ice discharge by icebergs) of the AIS to the future sea-level rise. However, the current snow accumulation variability is poorly known. It is even more true for the multi-decadal variability. Yet, without a clear understanding of the processes governing the Antarctic snow accumulation variability, our confidence in the contribution of the AIS to the future sea-level rise is limited. Therefore, the work presented in this thesis was devoted to improve our understanding of the snow accumulation over Antarctica from the interannual to multi-decadal timescales. The main objective of this thesis is to highlight the physical mechanisms behind snow accumulation variability by investigating the links between snow accumulation and other variables characterizing the surface climate at high southern latitudes. As the observational network is particularly limited in the Antarctic, the present work has been based on various types of data – instrumental observations, paleoclimate records and climate model simulations –, focused on different time periods – from the last millennium to the 21st century – and used diverse methodologies. The overarching question asked in the introduction of the thesis was : "*How is the Antarctic snow accumulation over the past centuries related to changes in atmospheric temperature, winds and sea-ice extent and how those links can help us to better reconstruct past changes in accumulation and their drivers?*". This has been answered through the development of three sub-questions, each of them representing a chapter of the thesis. The main findings are summarized below.

5.1.1 Examining the relationship between Antarctic snow accumulation and surface air temperature over past centuries in ice core-based reconstructions and climate models

Several studies [e.g., Palerme et al., 2017b; Frieler et al., 2015; Ligtenberg et al., 2013] have suggested that the Antarctic snow accumulation will increase over the 21st century in concert with the surface air warming. However, an analysis of the relationship between snow accumulation and surface air temperature over the past centuries is needed to better constrain the future snow accumulation changes. This relationship has been assessed in climate models and regional ice core-based reconstructions over the past centuries. The analysis has shown an important data-model discrepancy at the regional scale with a much stronger relationship between the two variables in models than in regional ice core-based reconstructions. This discrepancy may arise from biases in the models (i.e., overestimation of the thermodynamic response, through the Clausius-Clapeyron relationship, or missing processes as well as the coarse spatial resolution), a too weak signal to noise ratio in ice-core based reconstructions, or a combination of both [e.g., Neukom et al., 2018]. Additionally, the surface air temperature reconstruction used in this study is derived from ice core δ^{18}O records. Yet, the relationship between surface air temperature and δ^{18}O varies in space and time [e.g., Klein et al., 2019]. Therefore, the weak relationship between snow accumulation in ice core-based reconstructions may also be related to the surface air temperature estimation from δ^{18}O records. In order to decrease the uncertainties of the ice core-based reconstruction, we have taken advantage of the relationship between the regional reconstruction of snow accumulation and δ^{18}O to provide a new reconstruction of snow accumulation and surface air temperature at the regional scale. This has been achieved through a data assimilation method that fuses these two regional reconstructions with the dynamic constrain given by an isotope-enabled climate model. Although an independent evaluation is difficult as the instrumental observations cover a short period, the resulting reconstructions for snow accumulation and surface air temperature covering the past two centuries are improved compared to the latest ice core-based reconstructions at the sub-continental scale (West Antarctica, East Antarctica and Antarctica as a whole), in particular for surface air temperature. Our results have thus suggested that the past snow accumulation is closely related to surface air temperature at the sub-continental scale. Additionally, we have demonstrated the benefit of using multi proxies-based reconstruction in Antarctica, especially in a data assimilation framework.

5.1.2 Investigating the interest of using information from ice core data for better reconstructing and understanding surface climate changes in the Antarctic over the last 200 years

Chapter 2 focused exclusively on the relationship between snow accumulation and surface air temperature at the regional scale. This framework did not allow a detailed analysis of the spatial structure of surface climate changes and the processes responsible for these changes. Therefore, in Chapter 3, we have analyzed the surface climate changes in the West Antarctic sector, which has been undergoing major surface climate changes since the second half of the 20^{th} century. To this end, we have provided a spatially complete reconstruction for the main surface variables in that region based on a data assimilation approach. In contrast with Chapter 2, ice core records have been assimilated at the local scale, and paleoclimate records located in the mid-latitudes (i.e., tree-ring width records) have been added. Records tend to reconstruct the local atmospheric circulation. The inclusion of the non-Antarctic records thus ensures a coherence in the large-scale atmospheric circulation by increasing the spatial coverage of observations. Including those records thus allows a better reconstruction of the large-scale atmospheric circulation. Similarly to Chapter 2, we have relied on the co-variance between the assimilated records and the reconstructed variables, as given by the climate model used in the data assimilation procedure.

Our results have demonstrated that ice core records (snow accumulation and $\delta^{18}O$), as well as tree-ring width records in the mid-latitudes, combined with the physics from iCESM1 allow to skillfully reconstruct surface climate changes over the past centuries. We have thus provided estimations of the past variability of some variables such as the atmospheric circulation or sea-ice extent that cannot be directly deduced from available records. Based on our multi-variate reconstruction, we have shown that the ASL has deepened from around 1950 CE. Additionally, our results suggest that observed sea-ice extent reduction over the satellite era (1979 CE onwards) in the Amundsen/Bellinghausen Sea sector is part of a longer negative trend starting around 1850 CE, while the observed sea-ice extent expansion in the Ross Sea sector over the same period has started one century later, around 1950 CE, in concert with the deepening of the ASL. Furthermore, we highlighted possible non-stationarity over time in the relationship between the sea-ice extent in Amundsen/Bellinghausen Sea sector and the ASL. Finally, we have shown that small changes in the strength and position of the ASL, which are related to the SAM conditions, can lead to large changes on the continent.

5.1.3 Determining the physical mechanisms that are responsible for the Antarctic snow accumulation increase observed over the 20th century and projected for the end of the 21st century

The last part of the thesis (Chapter 4) has focused on the physical processes behind the relationship between snow accumulation and surface air temperature. Therefore, we have assessed the relative contributions of the thermodynamic and dynamic processes to the total snow accumulation changes at the interannual and multi-decadal timescales for the 20th century and the end of 21st century. Unlike Chapter 2 and 3, the analysis has been carried out only on reanalysis data and climate models. The moisture budget performed for the atmosphere over the Antarctic has shown that the Antarctic-wide snow accumulation increase during the 20th century and projected for the end of the 21st century is mainly governed by short-lived synoptic-scale events and are not related to the large-scale modes such as the SAM or IPO. In a warmer climate, the air potentially contains more humidity (because of enhanced saturation vapor pressure), and thus increases the moisture transport by storms towards Antarctica. This ultimately leads to more snowfall on the Antarctic continent. In contrast to the multi-decadal changes, the year-to-year snow accumulation variability is influenced by both the large-scale and synoptic transports. Consequently, we have shown that the mechanisms governing the snow accumulation variability depend on the analyzed timescale. Therefore, the mechanisms explaining the interannual variability of Antarctic snow accumulation cannot be used to predict the future increase in Antarctic-wide snow accumulation.

5.2 General conclusions

This thesis has confirmed that the Antarctic snow accumulation changes are strongly correlated to atmospheric temperature changes (Chapters 2-4), and therefore that the Clausius-Clapeyron relationship explains relatively well the snow accumulation changes. This is generally valid for regional (Chapters 2 and 3) and multi-decadal (Chapter 4) changes. However, the link between snow accumulation and atmospheric temperature can be strongly reduced in some cases and accounting for it is important to describe adequately the processes ruling snow accumulation (Chapters 3 and 4). The dynamic component, i.e., the interactions between the atmospheric circulation and the topography as well as the large-scale modes of variability such as the SAM, plays a significant role in the year-to-year variations, in particular at the local scale (Chapter 3). However, when averaging over Antarctica as a whole, the contribution of the dynamic component is null (Chapter 4) as a snow accumulation increase induced by a change in the atmospheric circulation is counteracted by a snow accumulation decrease elsewhere.

The major issue that we have had to deal with in this thesis is the limited observational network that is available in Antarctica. However, this present work has shown that, when using an integrated approach relying on various types of data (instrumental observations, paleoclimate records and climate model simulations), it is possible to assess the Antarctic snow accumulation at the interannual and multi-decadal timescale and to determine the mechanisms responsible for the changes. Therefore, for analyzing the past snow accumulation variability, it is crucial to incorporate as many different types of records as possible, as well as information brought by climate models. Indeed, as shown by previous studies [e.g., Jones et al., 2016], the Antarctic surface climate changes in multiple variables are strongly coupled. This means that not only ice core snow accumulation records are useful for assessing the past Antarctic snow accumulation variability but also other records, as long as the variables are correlated. In particular, we have shown in Chapters 2 and 3 that ice core δ^{18}O records, and even tree-ring width records from the mid-latitudes, provide relevant information for snow accumulation. Through Chapters 2 and 3, data assimilation has been demonstrated to be particularly appropriate for reconstructing the surface climate changes in the Antarctic over the past centuries as the observational network is sparse and includes various types of records. Furthermore, data assimilation has the advantage not to be dependent on a stationary relationship between the assimilated and reconstructed variables. This feature is valuable for reconstructing the Antarctic surface climate since we have shown that the relationship between the sea-ice extent and the atmospheric circulation may have changed over time. Furthermore, the impact of the ASL on the West Antarctic surface climate depends on the SAM conditions (Chapter 3). This kind of time-dependent relationship along with the complex response of the West Antarctic surface climate to the ASL raise concerns about the use of simple statistical methods, as these methods often struggle to account for such non-stationarities. In addition, Chapter 4 has highlighted important timescale-dependent processes since the mechanisms governing the interannual variability of snow accumulation differ from the mechanisms responsible for the multi-decadal variability. Therefore, year-to-year snow accumulation changes cannot be used for estimating the long-term snow accumulation changes.

Additionally, we know that climate models struggle at simulating climate changes in the Antarctic. For instance, they are not able on average to reproduce the recent general sea-ice expansion [e.g., Roach et al., 2020], or the west-east asymmetry in the continental warming [e.g., Jun et al., 2020]. However, the thesis has demonstrated that, albeit those inherent biases, climate models are useful tools for understanding physical processes driving the Antarctic snow accumulation variability as some of them display realistic snow accumulation pattern (Chapters 2 and 4). In Chapter 4, which is only based on reanalysis and model results, the moisture budget for the atmosphere over the Antarctic with an atmospheric re-

analysis and climate model simulations has allowed to highlight the mechanisms that are responsible for the 20th century and future (21st century) snow accumulation increase at different timescales.

5.3 Perspectives

As emphasized throughout the manuscript, the paleoclimate observational network is sparse in Antarctica and its surrounding areas. The scientific community studying the past snow accumulation variability stresses the need for increasing the amount of ice core snow accumulation records. However, fieldwork campaigns along with ice core drilling is very expensive. Alternatively, other available records (apart from ice core snow accumulation and δ^{18}O records and tree-ring width records, used in this thesis) could be utilized to reconstruct the past variability of snow accumulation, as we have shown that climate reconstruction benefits from incorporating different types of records (Chapters 2 and 3). For instance, the chemical composition from ice cores, in particular sea salts (e.g., Na^+ and SO_4^{2-}), has been used for reconstructing the past atmospheric circulation [e.g., Legrand and Mayewski, 1997; Mayewski et al., 2017] and sea-ice cover [e.g., Abram et al., 2013]. Yet, both the sea-ice cover and the atmospheric circulation largely govern the snow accumulation variability. Therefore, those proxies are also promising for reconstructing the snow accumulation. Recently, the Antarctic 2k group has opened a community data call to gather all the available Antarctic ice core chemical records. This new database will complement the two existing Antarctic databases of snow accumulation and δ^{18}O records [i.e., Thomas et al., 2017; Stenni et al., 2017]. Incorporating these new records in the data assimilation would be thus highly relevant for better reconstructing the snow accumulation, and more generally the Antarctic climate.

A PSM is required to simulate the signal recorded in the natural archive (i.e., sea salt concentration) from climatic variables. However, setting a PSM for ice core chemical records may be difficult as many processes are involved [e.g., Rhodes et al., 2018; Thomas et al., 2019; Abram et al., 2013]. A simple statistical PSM based on a linear regression may be an interesting first step but may be found insufficient to simulate the proxy records adequately. Therefore, similarly to the isotope-enable climate models that explicitly simulate water isotopes in the hydrological cycle [e.g., Brady et al., 2019; Steiger et al., 2017; Sjolte et al., 2018], some process-based models simulate the sea salt transport [e.g., Levine et al., 2014; Rhodes et al., 2017]. Performing a data assimilation reconstruction by using the ice core chemical records combined with such a process-based model would be very informative. Furthermore, implementing a model that simulates the sea salt transport from the ocean to its deposition in isotope-enable climate models would

allow to directly assimilate the ice core $\delta^{18}O$ along with chemical records without using an explicit PSM a posteriori.

Additionally, the paleo climate community would benefit from additional ensembles of isotope-enabled climate model simulations, in particular spanning the last millennium. Indeed, in Chapter 3, we were not able to test the sensitivity of our results to the selected climate model for the data assimilation – albeit iCESM1 relatively well simulates the Antarctic climate (Chapter 3) –, as only iCESM1 provides a last millennium ensemble with water isotopes. Additionally, a more general perspective would be to reduce the biases present in climate model simulations, in particular on how the variables within the climate model co-vary. The co-variance among the variables in the climate models is key in data assimilation for reconstructing variables that are not directly assimilated, since data assimilation relies on this co-variance to spread the local information from the assimilated variable to other variables. To obtain a skillful reconstruction, it is thus important to ensure that the co-variance between the assimilated and reconstructed variables are well represented in the model used for data assimilation. In this regard, the second version of CESM (CESM2) [Danabasoglu et al., 2020] better represents the large-scale teleconnections, such as the Antarctic-tropical teleconnections. Furthermore, additional ensembles of isotope-enabled climate model simulations would allow for building multi-model prior in data assimilation, which could ultimately reduce the errors related to the use of a single model, by assuming that the biases of each model cancel each other out [e.g., Amrhein et al., 2020].

In Chapter 3, we have highlighted that the surface climate in the West Antarctic sector has experienced major changes over the past centuries. Albeit we have shown that both the continental surface changes and the sea-ice extent in this sector are closely related to the atmospheric circulation changes, in particular the deepening of the ASL, the origin of these changes are still missing. For instance, we did not provide an explanation on why the ASL has deepened over the second half of the 20^{th} century. A follow-up of Chapter 3 would thus be to understand what the drivers of those changes are, especially the deepening of the ASL. Analyzing large ensemble of climate model simulations (e.g., CESM1-LE) [Kay et al., 2015] would be useful in order to disentangle the forced response (especially the response related to the ozone depletion and atmospheric greenhouse gazes) from the natural variability.

Finally, an increasing number of studies have suggested that the tropical variability exerts an important impact on the West Antarctic climate through teleconnections. For instance, Ding et al. [2011] have suggested that the widespread continental warming in West Antarctica in winter over the second half of the 20^{th} century can to a large extent be explained by the tropical Pacific variability. However, the impact of the tropical variability on the West Antarctic surface climate changes over the past two centuries has not been investigated in a comprehen-

sive way. For handling this, two complementary methods are possible. Firstly, the marine corals located in the tropics are excellent natural archives for reconstructing the past variability of sea surface temperature. Like the ice cores chemical records, the tropical marine corals could improve our knowledge of the past climate variability in the Antarctic by exploiting the existing teleconnections between the tropics and Antarctic. Incorporating coral records in the data assimilation approach proposed in Chapter 3 and analyzing the impact of their added value on the Antarctic climate reconstruction would be thus useful to better understand the role of the tropical variability on Antarctic climate changes. This method relies on the co-variance between the tropical and Antarctic variability, and thereby does not ensure that the two regions are dynamically linked. On the contrary, the second method allows to investigate explicitly the dynamical role of the tropics on the Antarctic climate with sensitivity numerical simulations. The method relies on two sets of climate model simulation ensembles. The first ensemble consists of several simulations constrained by both the natural variability and the anthropogenic forcing, while the second ensemble is also constrained by the observed sea surface temperature in the tropics (the so-called pacemaker simulations). By making the difference between the two ensembles, the impact of tropical variability can be assessed. This method has been utilized for example by Holland et al. [2019] for estimating the impact of the tropical Pacific variability on the mass loss of West Antarctic ice shelves over the past century. Applying a similar method to the main surface variables in the West Antarctic sector would be interesting to quantify the exact contribution of the tropical variability on the West Antarctic climate.

A

Supplement to Chapter 2

A.1 Statistical surface temperature reconstructions from Stenni et al. [2017]

Using the δ^{18}O composites, Stenni et al. [2017] reconstructed regional surface temperature over the last two millennia based on the statistical relationship between δ^{18}O and surface temperature. Three methods have been used to scale the δ^{18}O composites. In the first approach, the regional slopes between δ^{18}O and temperatures were computed from the outputs of the ECHAM5-wiso model forced by ERA-Interim atmospheric reanalysis [Goursaud et al., 2018] over the 1979–2013 CE period. In the second method, the reconstruction obtained from the first method for the WAIS region is corrected using an independent temperature record: the borehole temperature reconstruction at WAIS divide [Orsi et al., 2012]. This allows to match the cooling trend over the 1000–1600 period [Stenni et al., 2017]. This method provides a different reconstruction for the WAIS region – implying thus also the West Antarctic and the whole Antarctic reconstructions –, but not for the regions in East Antarctica. Finally, in the third method, the regional normalized δ^{18}O composites have been scaled to the variance of the surface temperature observations [i.e., Nicolas and Bromwich, 2014] over the 1960–1990 CE period. The second reconstruction is used throughout this study for two reasons: 1) the third method is based on the surface temperature observations, which are used here to estimate the skill of the reconstructions which could lead to a bias; 2) the correction introduced in the second method is expected to improve the reconstruction compared to the previous method. The temporal resolution of these surface temperature reconstruction is the same as the δ^{18}O composites: 10 years for 0–1800 period and 5 years for 1800–2010 CE period.

A.2 Defining uncertainties associated with proxy data used during data assimilation process

Data assimilation requires estimates of the uncertainty associated with the proxy data used. Unfortunately, uncertainty estimations are not provided with published reconstructions used here and the instrumental time series are too short to reliably derive the uncertainty. If we apply the same error for all the Antarctic regions, the assimilation will tend to give more weight to the time series that have more variance (i.e., the high-accumulation regions). On the other hand, if we apply an error proportional to the standard deviation of the time series, each region will tend to have the same weight. The uncertainly could also be related to the amount of ice cores included in each regional composite, but the link between this number and the quality of the composite is not straightforward [Stenni et al., 2017]. Several experiments have been performed to test the impact of different estimates of the data uncertainties on the data assimilation results. The results are qualitatively similar to standard choices of the uncertainty [Klein et al., 2019]. The experiments shown here assume a signal to noise ratio of 1 for each regional composite. This is probably an optimistic estimate but this has the advantage of providing a strong data constraint and the comparison of the reconstruction using data assimilation with instrumental data indicates a good skill of the methods using this value.

A.3 Present-day AIS SMB simulated by GCMs

Overall, the AIS SMB simulated by GCMs is in good agreement with the SMB simulated by the regional climate model RACMO2 over the last decades (1979–2005 CE, R^2 = 0.63; Figs. A.5, A.6, A.7 and A.8). As expected, both display high values of SMB along the coast (>300 mm w.e. year^{-1}) – especially for West Antarctica and the Antarctic Peninsula – and lower values at high elevations (e.g., the Plateau: <100 mm w.e. year^{-1}). The mean of the SMB over the entire AIS simulated by the selected models (including isotope-enable models) is 6.4 mm w.e. year^{-1} lower than the SMB simulated by RACMO2 over the 1979–2005 CE period (relative bias: -3.4%; Fig. A.8 for the correlation plots for each model and Fig. A.9 for the integrated SMB over the entire AIS for each model).

However, Figure A.5 shows that the GCMs, compared to RACMO2, underestimate SMB in areas below 1500 m (mean bias of -55 mm w.e. year^{-1}; relative bias: -15%) over 1979–2005 CE. For the areas above 1500 m, the mean bias of the simulated SMB by GCMs compared to RACMO2 is 11 mm w.e. year^{-1} (relative bias: 11%). These results are in agreement with previous studies [e.g., Palerme et al., 2017b; Genthon et al., 2009; Krinner et al., 2008] who have shown that due to the lower spatial resolution of GCMs in comparison to the regional model, SMB is underestimated at the coasts while an overestimation occurs in the interior of

the ice sheet. The bias in the difference between the coastal and higher elevation regions are smaller for the models that have a higher spatial resolution, such as CCSM4 (Fig. A.10), confirming that the spatial resolution has a crucial impact on the simulated SMB. However, models with similar resolutions may also have very different results, in particular in coastal regions (relative SMB biases of +47% and +100% for CCSM4 and MRI-CGCM3 respectively compared to RACMO for DML coast over the 1979–2005 CE period), suggesting a critical role of model physics in some of the GCM biases.

A.4 Supplementary figures

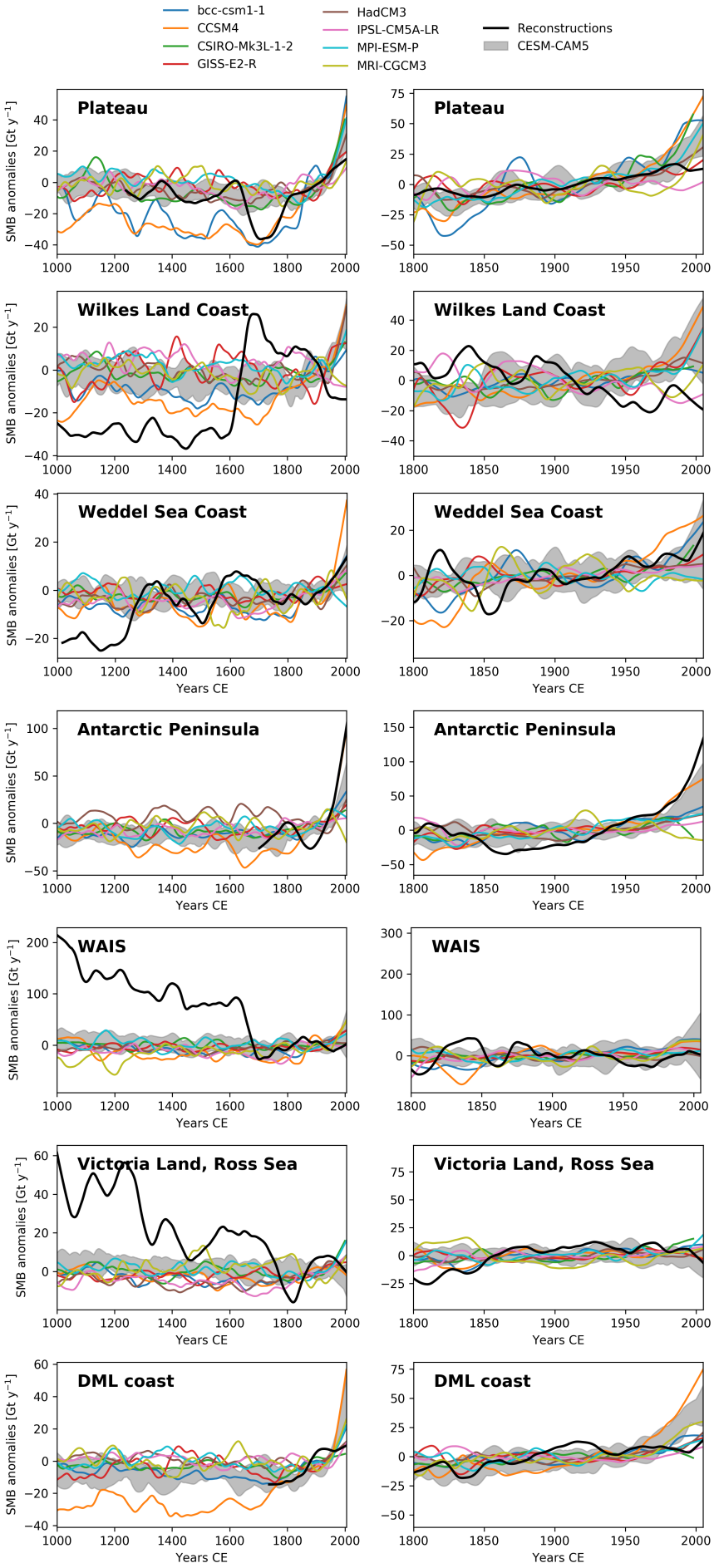

bcc-csm1-1
CCSM4
CSIRO-Mk3L-1-2
GISS-E2-R
HadCM3
IPSL-CM5A-LR
MPI-ESM-P
MRI-CGCM3
Reconstructions
CESM-CAM5
Plateau
Wilkes Land Coast
Weddel Sea Coast
Antarctic Peninsula
WAIS
Victoria Land, Ross Sea
DML coast
SMB anomalies [Gt y^{-1}]
Years CE

Figure A.1: *Surface mass balance anomalies [Gt y^{-1}] simulated by the GCMs (the average of all the available simulations has been represented; Tab. A.1) and snow accumulation reconstructions [Thomas et al., 2017] for 1000–2005 CE and for 1800–2005 CE periods for all the Antarctic subregions. Anomalies are computed for the 1800–2000 CE period. The shaded area corresponds to the range of the CESM1-CAM5 simulations. For visibility, data has been smoothed with a 100-year moving average for the last millennium and a 30 years moving average for the last 200 years.*

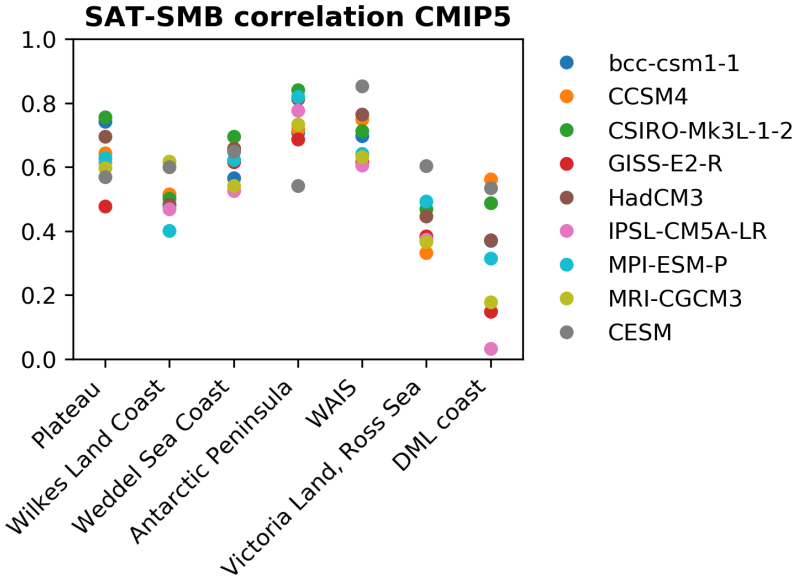


Figure A.2: *Annual correlations (r) between surface mass balance and surface temperature for all seven Antarctic regions (see Fig. 2.1 for geographical definitions) for all the GCMs over the 1850–2005 CE period.*

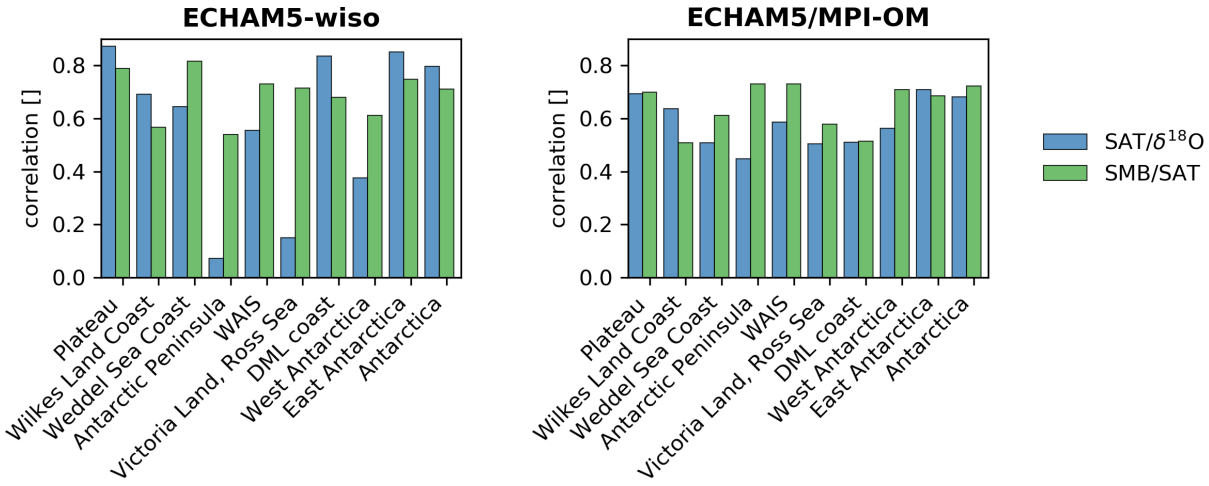


Figure A.3: *5-year mean correlations between surface temperature and $\delta^{18}O$ (blue) and between SMB and surface temperature (green) for the seven Antarctic regions for the entire period simulation (1871–2010 CE for ECHAM5-wiso and 801–2000 CE for ECHAM5/MPI-OM).*

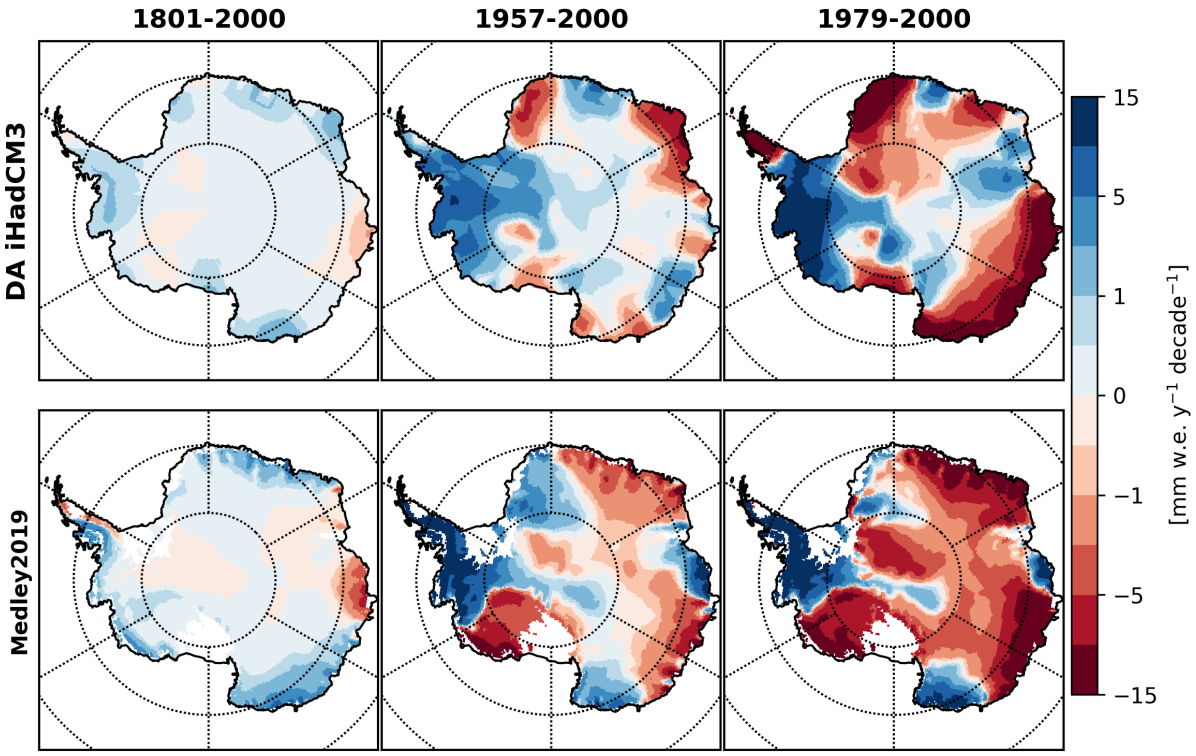


Figure A.4: *Spatial Antarctic surface mass balance trends (mm w.e. y^{-1} $decade^{-1}$) over the 1801–2000 CE, 1957–2000 CE and 1979–2000 CE periods from 1) our data assimilation-based reconstruction using the iHadCM3 outputs constrained by both $\delta^{18}O$ and SMB (first row) and from 2) Medley and Thomas [2019] (second row).*

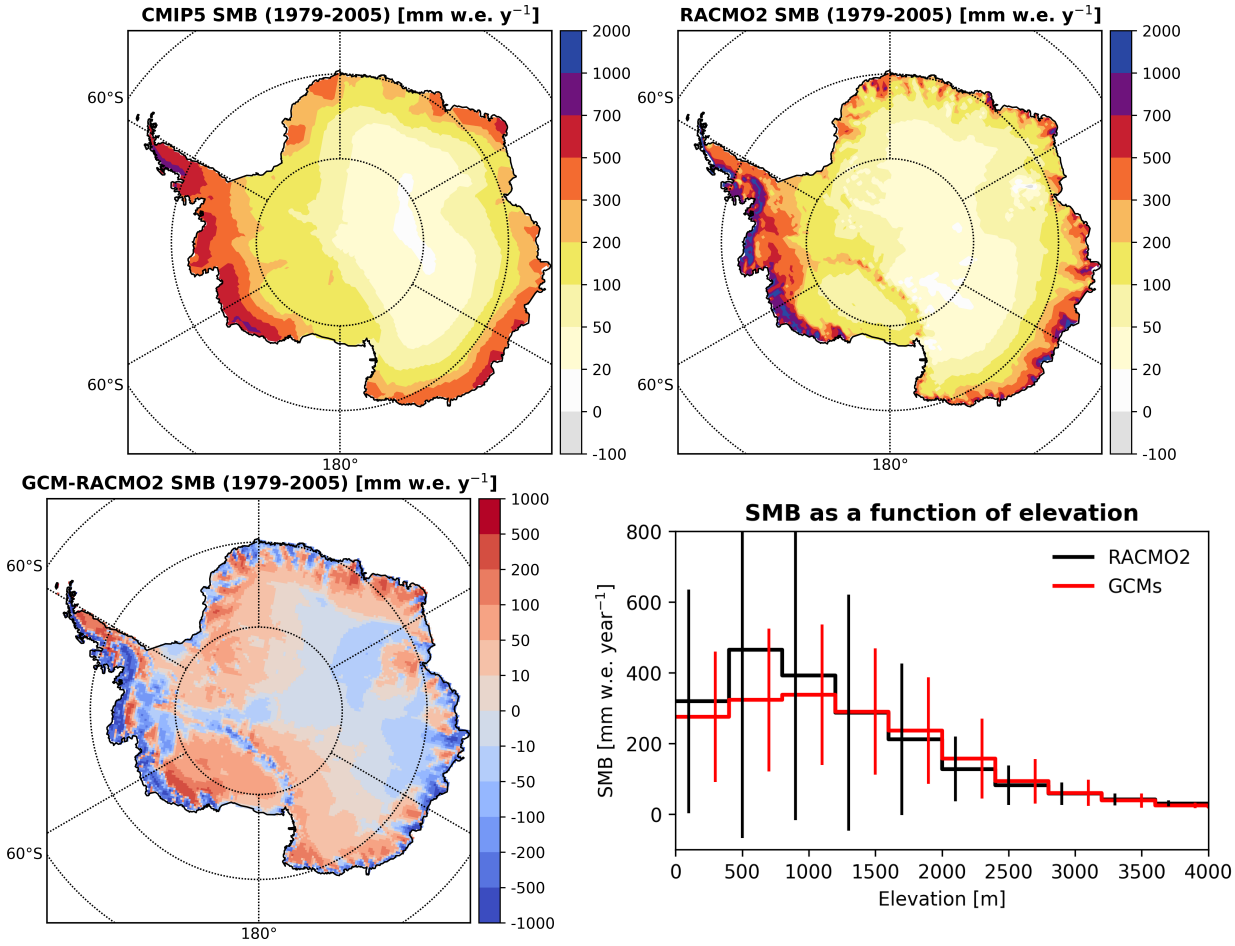


Figure A.5: *Antarctic Ice Sheet Surface Mass Balance [mm w.e. y^{-1}] over 1979–2005 CE averaged over all the GCMs simulations (see Tab. A.1 for the list) (top left), for RACMO2 [van Wessem et al., 2018] (top right), the difference between them (bottom left) and the distribution of the SMB simulated by RACMO2 and the GCMs as a function of elevation, binned in 400m elevation intervals (bottom right). The bars represent one standard deviation of the cell grids within each elevation bin. The equivalent of the latter panel for each model is provided on Fig. A.10.*

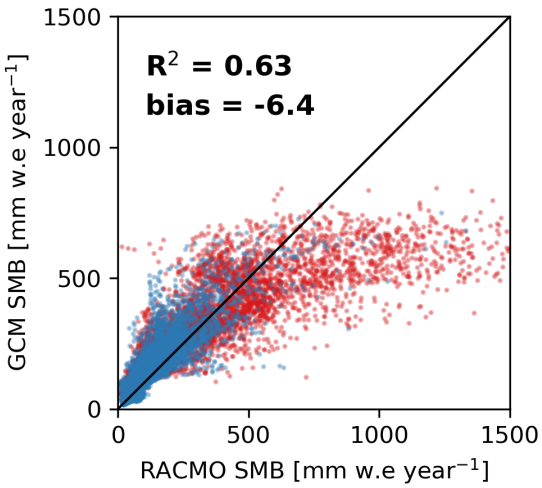


Figure A.6: *Correlation plot of SMB climatology from GCM mean (average over all the GCMs including isotope-enabled models) as a function of RACMO SMB over the 1979–2005 CE period. R^2 is the determination coefficient and bias the average of the difference between GCM mean and RACMO (in mm w.e. year^{-1}). Red (blue) dots are for places where the altitude is lower (higher) than 1500m. See Fig. A.8 for each model.*

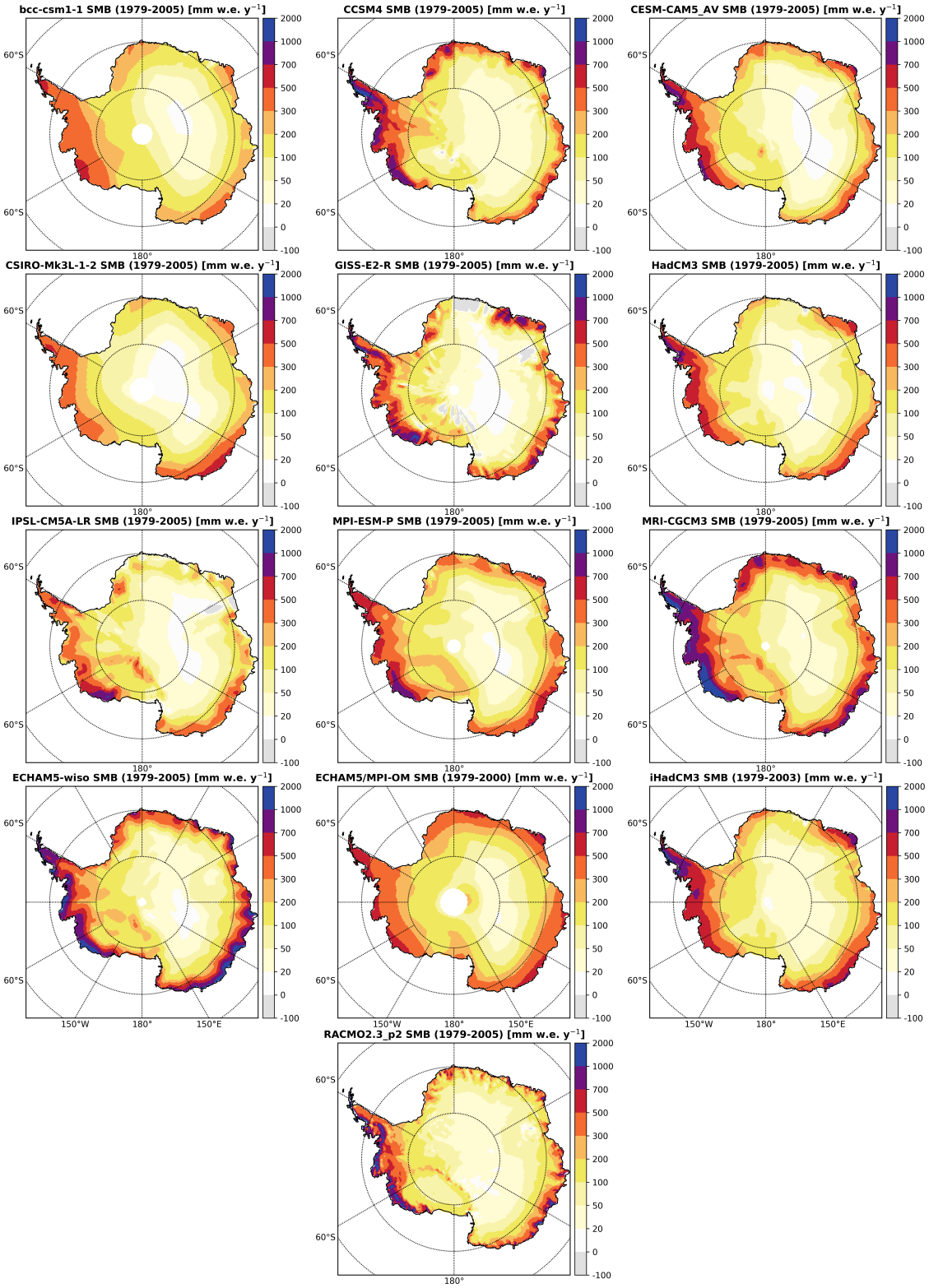


Figure A.7: *Antarctic Ice Sheet surface mass balance [mm w.e. y^{-1}] for all the models used in this study over the 1979–2005 CE period.*

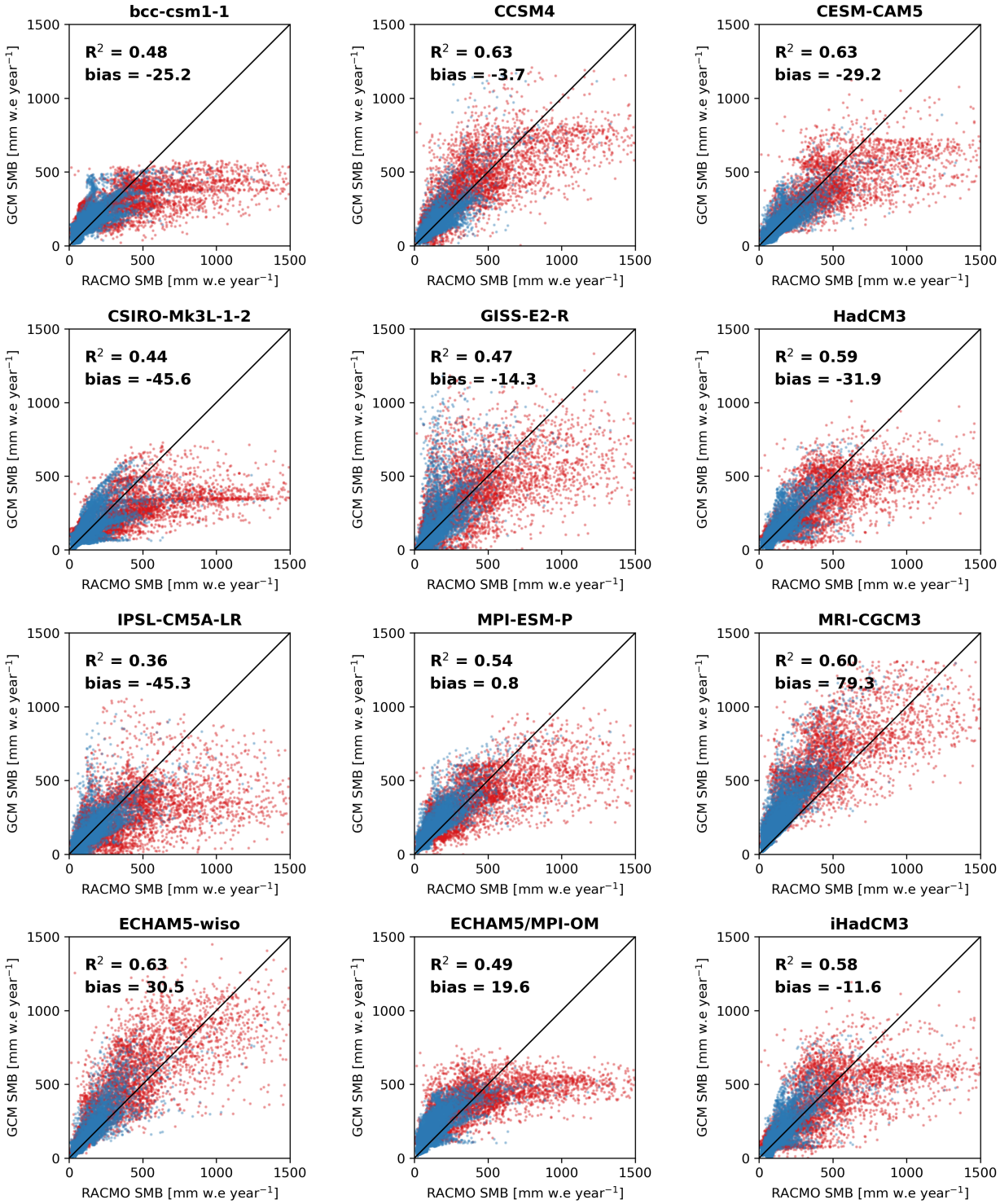


Figure A.8: *As in Fig. A.6 but for all GCMs.*

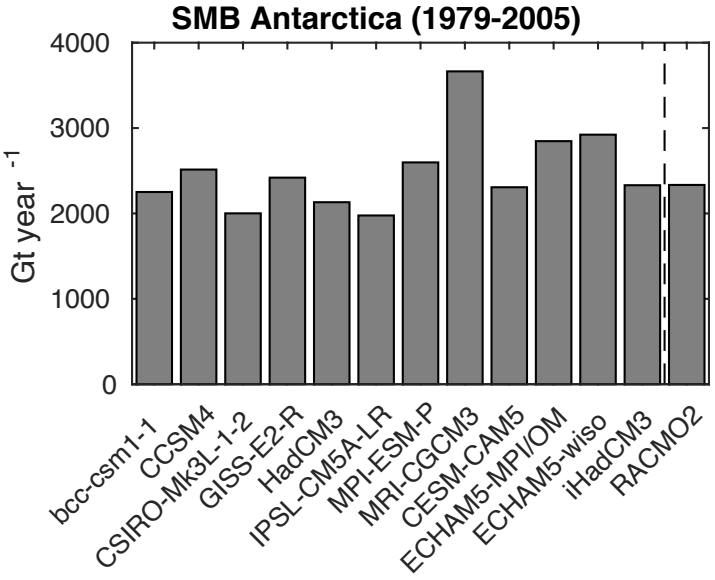


Figure A.9: *Mean Antarctic Ice Sheet surface mass balance (Gt year^{-1}) simulated by all the models used in this study.*

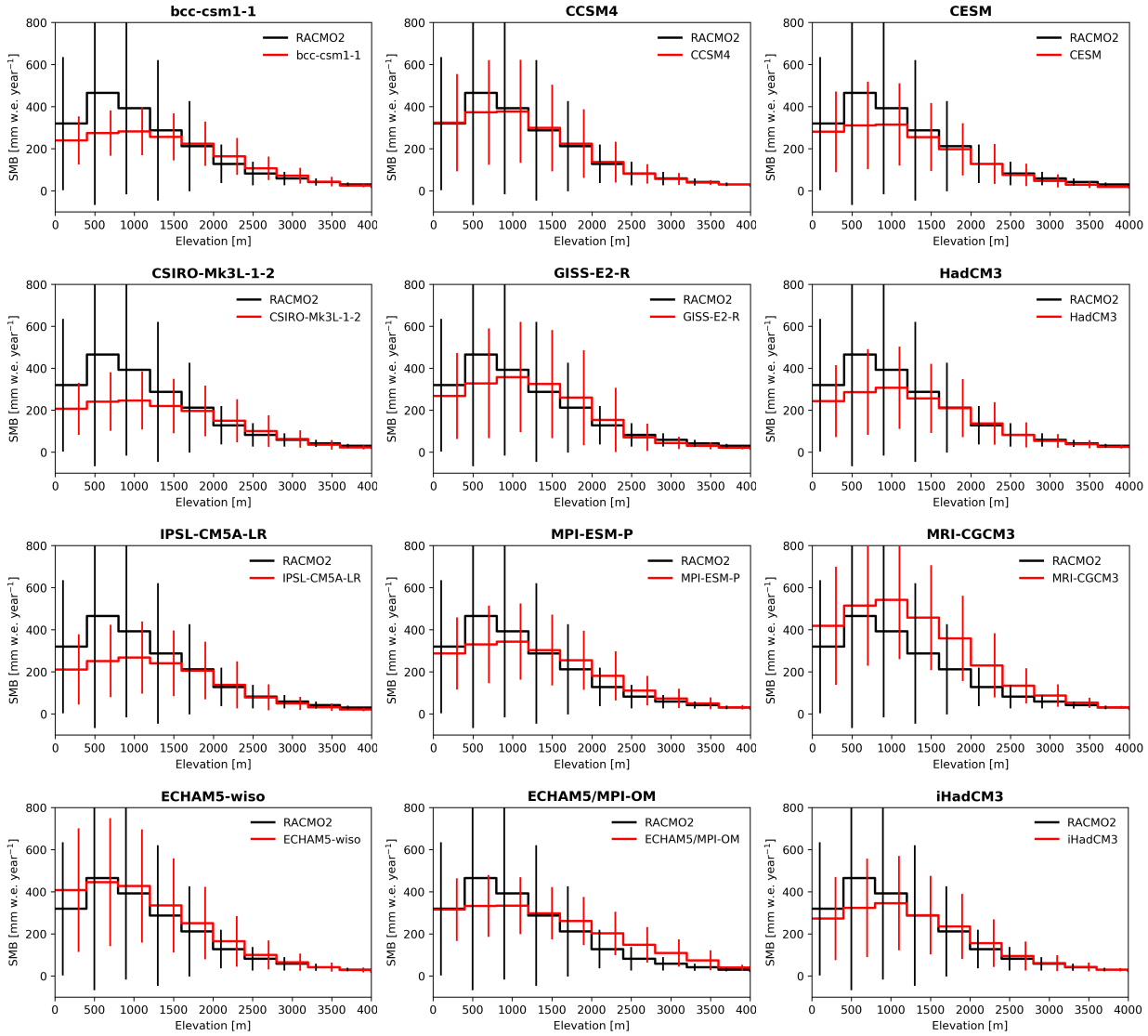


Figure A.10: *Distribution of the surface mass balance simulated by all climate models used in this study as a function of elevation, binned in 400m elevation intervals. The bars represent one standard deviation of the cell grids within each elevation bin.*

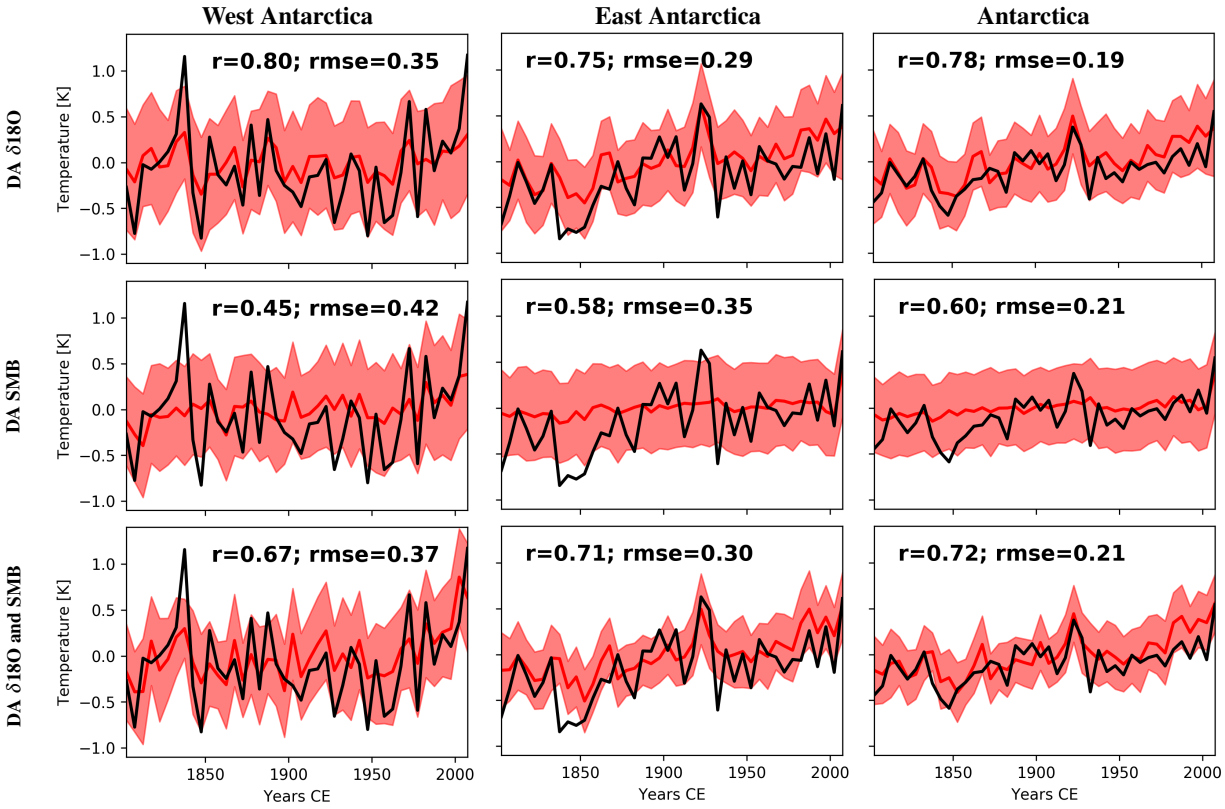


Figure A.11: *Reconstructed surface temperatures (5-year mean) for West Antarctica, East Antarctica and Antarctica as a whole from our data assimilation experiment using the ECHAM5-wiso outputs and, $\delta^{18}0$ [Stenni et al., 2017] and SMB reconstruction [Thomas et al., 2017] as data. The period is 1800–2010 CE. DA $\delta^{18}O$ is the data assimilation experiment using only the $\delta^{18}O$ data to constrain the model while DA SMB uses only the SMB reconstruction and DA $\delta^{18}O$ and SMB uses both. For each experiment and each region, the correlation (r) between the reconstruction based on ice cores and that based on data assimilation is computed. The shaded areas represent $\pm$ 1 standard deviation of the model particles.*

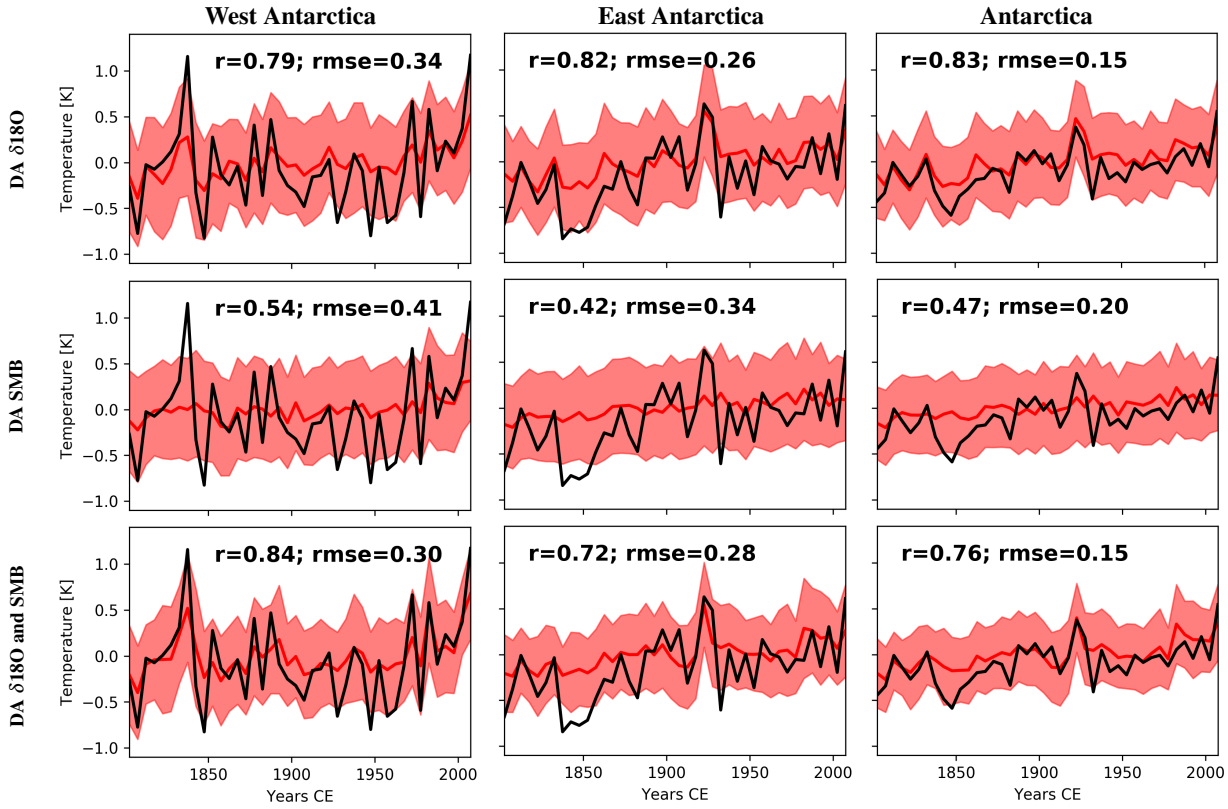


Figure A.12: *Reconstructed surface temperatures (5-year mean) for West Antarctica, East Antarctica and Antarctica as a whole from data assimilation experiment using the ECHAM5-MPI/OM outputs and, $\delta^{18}O$ [Stenni et al., 2017] and SMB reconstruction [Thomas et al., 2017] as data. The period is 1800–2010 CE. DA $\delta^{18}O$ is the data assimilation experiment using only the $\delta^{18}O$ data to constrain the model while DA SMB uses only the SMB reconstruction and DA $\delta^{18}O$ and SMB uses both. For each experiment and each region, the correlation (r) between the reconstruction based on ice cores and that based on data assimilation is computed. The shaded areas represent $\pm$ 1 standard deviation of the model particles.*

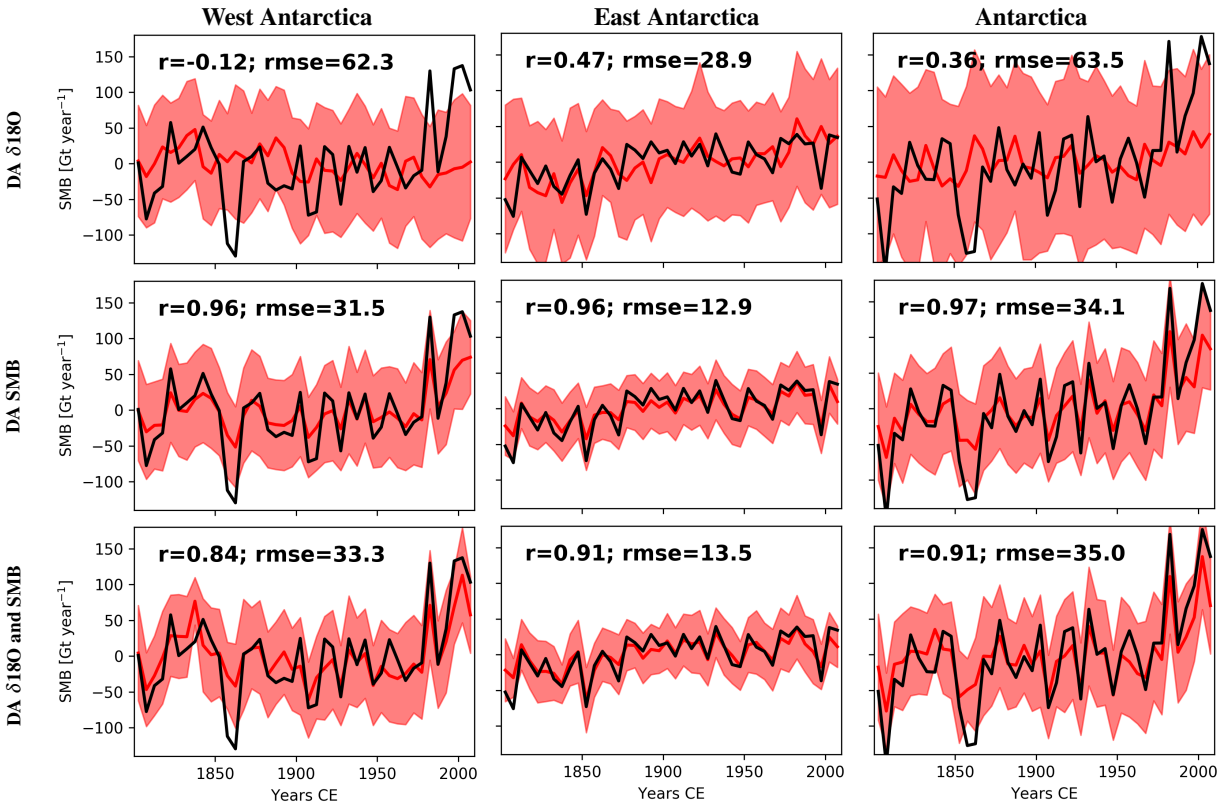


Figure A.13: *Reconstructed SMB (5-year mean) for West Antarctica, East Antarctica and Antarctica as a whole from data assimilation experiment using the ECHAM5-wiso outputs and, $\delta^{18}O$ [Stenni et al., 2017] and SMB reconstruction [Thomas et al., 2017] as data. The period is 1800–2010 CE. DA $\delta^{18}O$ is the data assimilation experiment using only the $\delta^{18}O$ data to constrain the model while DA SMB uses only the SMB reconstruction and DA $\delta^{18}O$ and SMB uses both. For each experiment and each region, the correlation (r) between the reconstruction based on ice cores and that based on data assimilation is computed. The shaded areas represent $\pm$ 1 standard deviation of the model particles.*

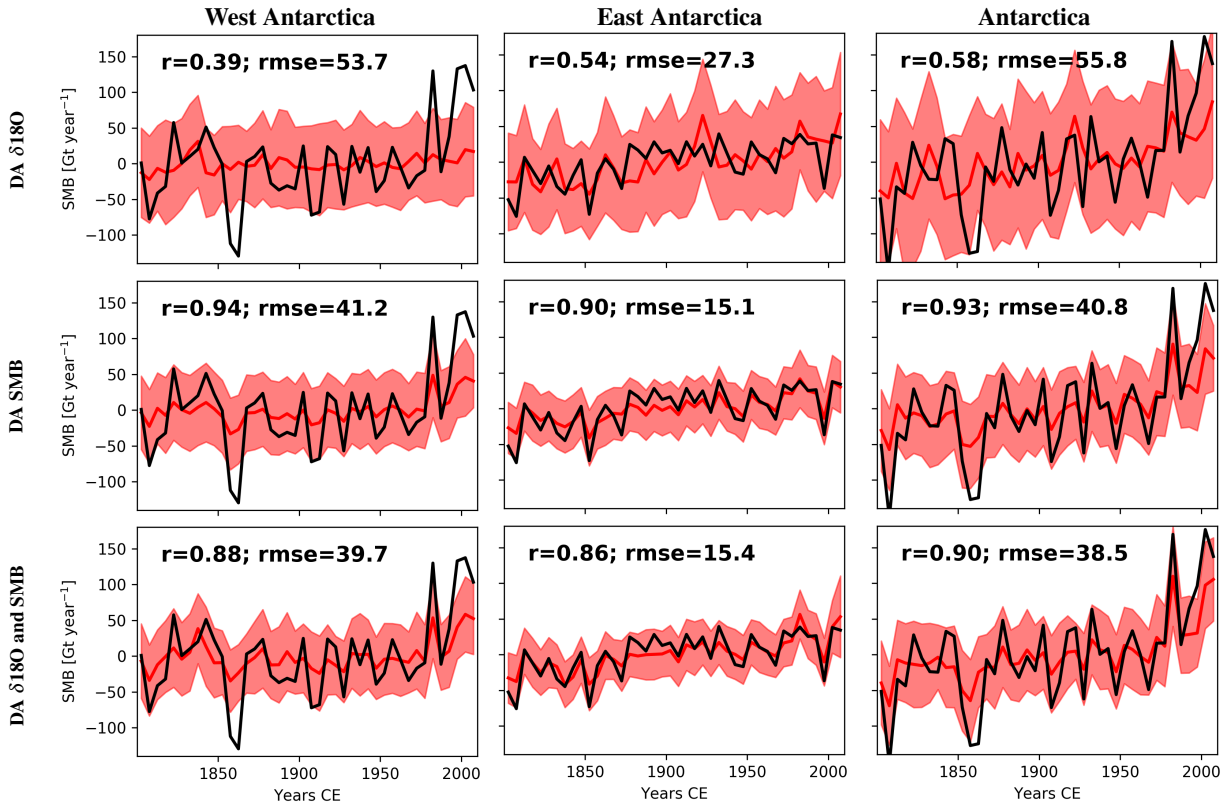


Figure A.14: *Reconstructed SMB (5-year mean) for West Antarctica, East Antarctica and Antarctica as a whole from data assimilation experiment using the ECHAM5-MPI/OM outputs and, $\delta^{18}O$ [Stenni et al., 2017] and SMB reconstruction [Thomas et al., 2017] as data. The period is 1800–2010 CE. DA $\delta^{18}O$ is the data assimilation experiment using only the $\delta^{18}O$ data to constrain the model while DA SMB uses only the SMB reconstruction and DA $\delta^{18}O$ and SMB uses both. For each experiment and each region, the correlation (r) between the reconstruction based on ice cores and that based on data assimilation is computed. The shaded areas represent $\pm$ 1 standard deviation of the model particles.*

A.5 Supplementary tables

Table A.1: *PMIP3/CMIP5 GCMs characteristics and references.*

Model name	Atmospheric model resolution (lat × lon)	Number of simulations for 850–1850 CE period	Number of simulations for 1850–2005 CE period	Reference
BCC-CSM1-1	64 × 128	1	3	Wu et al. [2014]
CCSM4	192 × 288	1	6	Gent et al. [2011]
CESM1-CAM5	96 × 144	12	12	Otto-Bliesner et al. [2015]
CSIRO-Mk3L-1-2	56 × 64	1	1	Rotstayn et al. [2010]
GISS-E2-R	90 × 144	1	6	Schmidt et al. [2014]
HadCM3	73 × 96	1	10	Turner et al. [2006]
IPSL-CM5A-LR	96 × 96	1	6	Dufresne et al. [2013]
MPI-ESM-P	96 × 192	1	2	Stevens et al. [2013]
MRI-CGCM3	160 × 320	1	3	Yukimoto et al. [2012]

Table A.2: *Surface mass balance trends (in Gt 100y^{-2}) for West Antarctica, East Antarctica and Antarctica as a whole in GCMs, in isotopic climate models (ECHAM5-wiso, ECHAM5/MPIOM and HadCM3) and in reconstructions based on ice cores [Thomas et al., 2017] over 1950–2000 CE. The number in brackets is the number of simulations. The trend computation is based on yearly data.*

	West Antarctica			East Antarctica			Antarctica		
	min	max	mean	min	max	mean	min	max	mean
bcc-csm1-1 (3)	-29.46	152.47	77.62	-63.11	381.09	200.39	-92.57	533.56	278.01
CCSM4 (6)	148.02	390.50	234.13	274.32	455.65	368.19	469.24	846.15	602.32
CSIRO-Mk3L-1-2 (1)			3.14			135.86			139.00
GISS-E2-R (6)	25.69	183.66	107.27	-71.92	250.18	140.43	-46.23	416.21	247.71
HadCM3 (10)	4.79	150.27	70.75	-68.85	242.18	89.39	-34.18	303.11	160.14
IPSL-CM5A-LR (6)	57.07	123.78	99.07	-104.18	66.82	-10.06	-47.11	174.30	89.01
MPI-ESM-P (2)	-33.85	-28.74	-31.30	54.75	231.84	143.29	26.01	197.99	112.00
MRI-CGCM3 (3)	28.62	178.64	86.45	-59.28	242.24	125.66	-7.19	420.89	212.11
CESM1-CAM5 (12)	30.90	349.67	153.07	55.72	340.24	162.27	161.99	592.43	315.34
iHadCM3 (6)	76.23	232.69	162.29	15.52	350.87	213.61	115.85	542.61	375.90
ECHAM5-wiso (1)			-8.79			195.22			186.43
ECHAM5/MPIOM (1)			41.44			35.43			76.87
Reconstructions (1)			256.74			-35.80			220.95

Table A.3: *5-year mean correlations between the three surface temperature reconstructions from data assimilation experiments using the iHadCM3 outputs and the statistical reconstruction of Stenni et al. [2017], with the surface temperature reconstructions from Nicolas and Bromwich [2014] over the 1958–2010 CE period for East Antarctica, West Antartica and Antarctica as a whole. All the correlations are performed on detrended time series. Stars represent statistically significant correlations (p-value<0.10).*

	West Antarctica	East Antarctica	Antarctica
DA δ^{18}O	-0.02	-0.16	-0.25
DA SMB	-0.19	0.51	0.31
DA δ^{18}O and SMB	0	0.60*	0.44
Stenni et al. [2017]	0.45*	-0.20	0.12*

Table A.4: *Slopes ($^{\circ}$C 100yr^{-1}) of each surface temperature reconstruction (Stenni et al., 2017; Klein et al., 2019; Nicolas and Bromwich, 2014; in this study) over the 1961–2010 CE period for West Antarctica, East Antarctica and the Antarctica. Statistically significant (p-value < 0.05) trends are represented by a star.*

Dataset	West Antarctica	East Antarctica	Antarctica
Stenni et al. (2017)			
Stat ECHAMvariance	1.69*	0.75*	1.27
Stat borehole	2.07*	0.75*	0.77*
Klein et al. (2018)			
DA ECHAM5-wiso	1.15	0.94	0.98
DA ECHAM5/MPI-OM	1.0	0.48	0.59
Nicolas and Bromwich (2014)			
	2.22*	0.53	0.90*
In this study			
DA δ^{18}O and SMB iHadCM3	0.99*	0.60*	0.69*

B

Supplement to Chapter 3

B.1 Supplementary figures

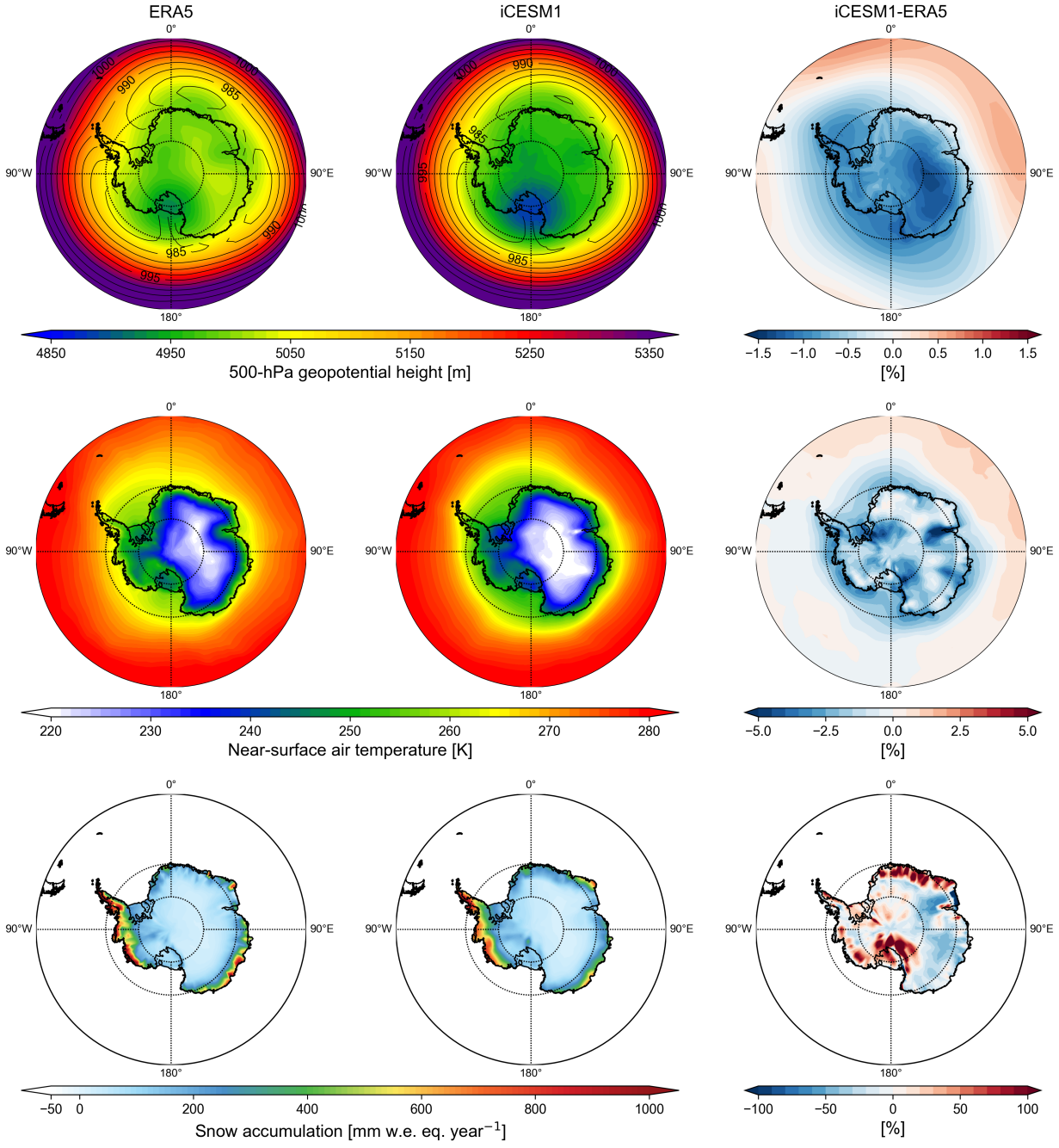


Figure B.1: *Mean of 500-hPa geopotential height (m), near-surface air temperature (K) and snow accumulation (mm w.e. eq. year^{-1}) from ERA5, and iCESM1, and the difference between iCESM1 and ERA5 (%) over the 1979–2005 CE period. For the 500-hPa geopotential height maps, contours represent the sea-level pressure (hPa).*

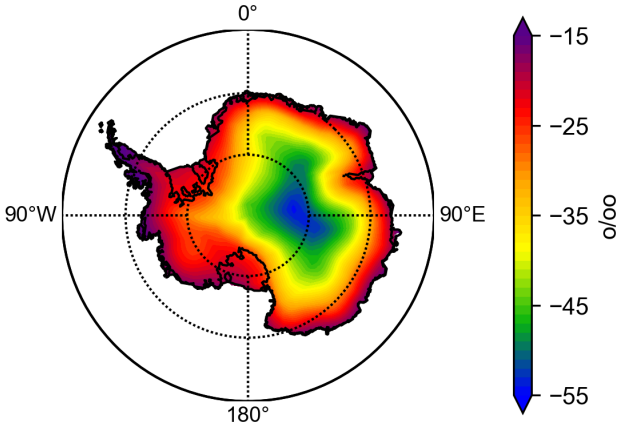


Figure B.2: *Mean of precipitation-weighted $\delta^{18}O$ (‰) from iCESM1 over the 1979–2005 CE period*

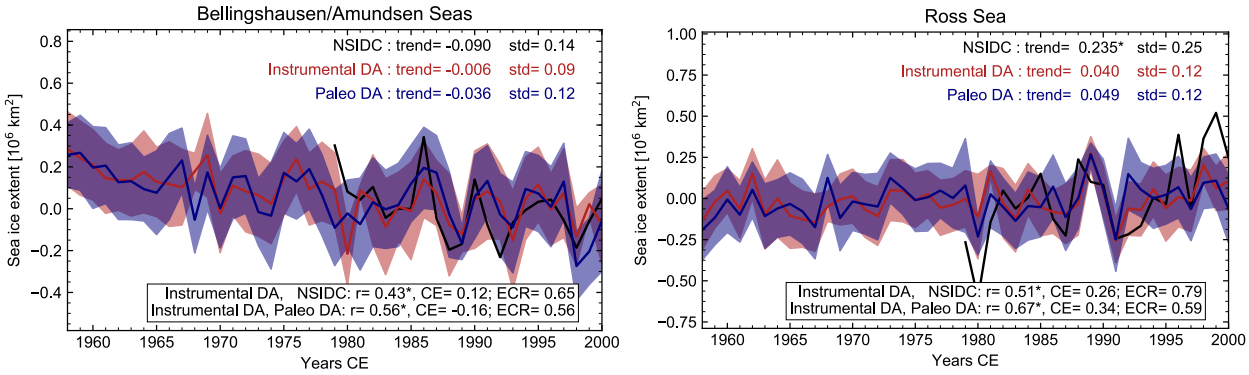


Figure B.3: *Regional sea-ice extent (10^6 km^2) anomalies from our instrumental (red) and paleo (blue) reconstructions and from the National Snow and Ice Data Center (NSIDC; in black; only available from 1979 CE) for the Bellingshausen and Amundsen Sea (130° W-60° E) and Ross Sea (160° E-130° W)over the 1958–2000 CE period. Regional definitions are identical as in Parkinson [2019]. Anomalies are computed over the 1979–2000 CE period. The linear sea-ice extent trends are displayed (expressed in 10^6 km^2 $decade^{-1}$) and the standard deviation (std) of the time-series (expressed in 10^6 km^2) over the 1979–2000 CE period for each region. Asterisks indicate statistically significant trends at the 95% confidence level. Additionally, the correlation coefficient (r), coefficient of efficiency (CE) and the ensemble calibration ratio (ECR) between our instrumental reconstruction and NSIDC are computed over the 1979–2000 CE period, as well as between the instrumental and paleo reconstructions over the 1958–2000 CE period. ECR values are computed for our the instrumental and paleo reconstructions with the NSIDC dataset. Uncertainty of the reconstruction estimated as the weighted standard deviation of the particles in the data assimilation process.*

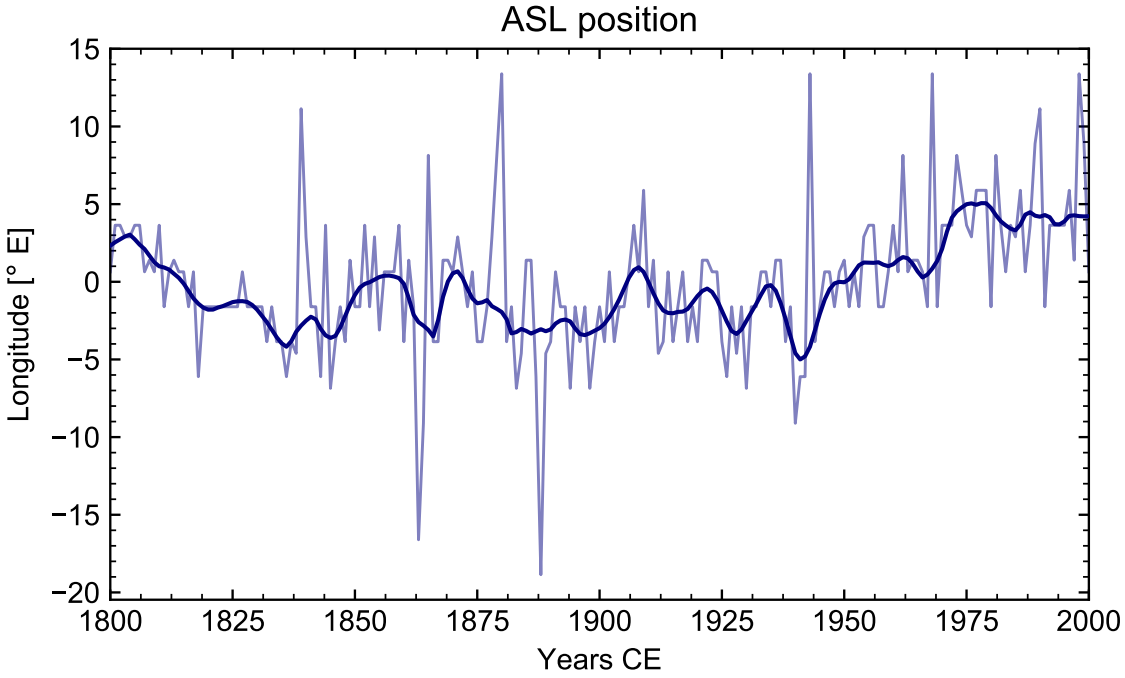


Figure B.4: *Anomalies of the longitudinal position (° E) of the pressure minimum within the ASL region (60° S–80° S; 170° E–298° E) in our paleo-reconstruction over 1800–2000 CE. Thin line corresponds to the annual index while the thick line is the decadal mean (10-year lowess smoothing).*

C

Supplement to Chapter 4

C.1 Role of tropical climate modes of variability on snow accumulation changes

Other modes displaying clear multi-decadal changes like the Interdecadal Pacific Oscillation (IPO) do also have an impact on the Antarctic climate [Clem et al., 2020] and may explain part of the recent trend in surface mass balance. Based on the extended reconstructed sea surface temperature dataset of the National Oceanic and Atmospheric Administration (ERSST.v5; Huang et al. [2017]), the observed IPO trend reaches -0.081 standard deviation over the 1985-2014 CE period against -0.093 standard deviation for CESM2 over the same period. Therefore, we have performed the same analysis as we did for the SAM in order to quantify how the IPO may explain the snow accumulation increase over the 1985-2014 CE period. We have followed the same methodology as in Clem et al. [2020] to calculate the IPO index: the IPO index is calculated as the difference in integrated Sea Surface Temperature (SST) between three regions: central equatorial pacific (170°E–90°W; 10°S–10°N), the South Pacific (150°E–160°W; 50°S–15°S) and extratropical North (140°E–145°W; 25°N–45°N). Since the IPO index is highly correlated with the El-Niño index, we have removed their co-variability by subtracting the linear regression between the two indexes as in Clem et al. [2020]. Although the IPO positively contributes to the snow accumulation increase over the 1985–2014 CE period with the higher contribution observed in Dronning Maud Land (10%), the IPO only contributes 4% of the snow accumulation at the continental scale over the 1985–2014 CE period. Consequently, like the SAM, the IPO cannot be responsible for the snow accumulation increase over the last century.

C.2 Impact of ozone depletion on Antarctic snow accumulation changes over the last decades

We analyze two ensembles of eight simulations performed with CESM1 [Landrum et al., 2017] to establish the impact of the ozone depletion on Antarctic snow accumulation changes over the recent past (1955–2005 CE period). In the first ensemble, the ozone concentration in the atmosphere increases with time as observed (Fig. 1b from Lenaerts et al. [2018]) while in the second ensemble, the ozone concentration is prescribed at the year 1955 CE levels. The eight simulations of each ensemble have been initialized imposing a slight perturbation at year 1920 CE to represent the internal variability of the climate. By calculating the difference between the two ensemble means, we obtain the response to the ozone depletion. This set of simulations has been already used in several studies [Lenaerts et al., 2018; Landrum et al., 2017; England et al., 2016] to constrain the role of ozone depletion on the Antarctic precipitation, sea ice extent and Amundsen Sea Low changes. Complementary to these studies, we examine the impact of ozone depletion on snow accumulation changes by looking at the relation with SAM and temperature changes over the last decades. The analysis of the attribution of the ozone depletion on recent Antarctic snow accumulation changes is performed on the 1986–2005 CE period because its impact is only significantly statistically detectable from the mid-1980s [Lenaerts et al., 2018].

Regional recent snow accumulation changes can be partially explained by the ozone depletion. In agreement with Lenaerts et al. [2018], we observe that the ozone depletion contributes to a large snow accumulation increase over the past decades: 52 $\pm$ 30 Gt year^{-1} for the response to ozone depletion over the 1986–2005 CE period at the continental scale against 170 $\pm$ 28 Gt year^{-1} for the response to all forcing between the 1986–2005 CE and 1920–1949 CE periods. At the same time, the effect of depletion on surface temperature is very small (-0.06 $\pm$ 0.12 °C for Antarctica as a whole). Besides, while the ozone depletion is usually pointed at as the main cause for the recent increase in the SAM index [Thompson et al., 2011b], the SAM-congruent snow accumulation changes due to the response to ozone depletion are significantly weaker than the total snow accumulation response (Fig. C.19a-b), indicating that the ozone's effect on snow accumulation changes is not primarily related to the SAM.

C.3 Evaluation of the Antarctic snow accumulation as simulated by selected ESM/GCMs

The snow accumulation from all these models have been compared to the snow accumulation from the regional climate model RACMO2.3 (hereafter RACMO2),

which is specifically designed for Antarctic surface process modeling [van Wessem et al., 2018] over the 1979–2005 CE period. Although the model evaluation is only based on one model, Agosta et al. [2019] have demonstrated that the Model Atmospheric Regional (MAR), which has been extensively used to study the processes related to the Antarctic surface processes, and RACMO2 do not display significant differences in simulating snow accumulation at the regional scale (as defined in this study).

The snow accumulation from all these models have been compared to the snow accumulation from the regional climate model RACMO2.3 (hereafter RACMO2), which is specifically designed for Antarctic surface process modeling [van Wessem et al., 2018] over the 1979–2005 CE period. ACCESS1-3 and CESM1-LE are the models showing the best spatial agreement with RACMO2 (R^2 = 87%; Fig. C.20) with a negative relative bias (-10.8% and -9.2% for ACCESS1-3 and CESM1-LE, respectively). The latest version of CESM, CESM2 displays a R^2 of 85% and a relative bias of 9.7%. Finally, NorESM1-M is also in good agreement with RACMO2 (R^2 =76%; bias = -1.2%). According to Bracegirdle et al. [2020b], across all the available CMIP6 GCMs for this study (15), the relative Antarctic precipitation changes between the 2081–2100 CE and 1995–2014 CE periods under the SSP5-8.5 scenario used by CESM2 is 31 $\pm$ 12% (mean $\pm$ standard deviation), which places CESM2 in the upper range (46%). CESM2 is also in the upper range for the warming between these two periods, with a surface temperature increase of 6.8 °C compared to 4.8 $\pm$ 1.2 °C for the multi-model ensemble [Bracegirdle et al., 2020b]. This large warming simulated by CESM2 mainly arises from the improvement of the cloud microphysics directly affecting the aerosol feedbacks [Danabasoglu et al., 2020; Gettelman et al., 2019].

C.4 Evaluation of the *P–E* from the moisture budget

The accuracy of the method can be evaluated by comparing the $P - E$ pattern calculated by the moisture budget to the $P - E$ pattern given directly by the model itself. Both should be similar but differences between the two can occur because of two main reasons: 1) the time step used in the moisture budget differs from the model time step; 2) the numerical method applied in the discretization in the offline evaluation of the moisture budget is not the same as used in the model. Seager and Henderson [2013] explains all the details regarding the errors induced by the moisture budget calculation. The moisture budget equation can be schematically expressed as:

$$(P - E) = MC + TE + R \tag{C.1}$$

where P stands for precipitation, E for evaporation and sublimation. MC corresponds to the moisture brought by the large-scale circulation and TE the moisture due to the synoptic-scale transport. R are the residuals as the sum of MC and TE is not strictly equal to $(P - E)$ because of the approximations made in our diagnostic evaluation of the moisture budget. The value of R, which can be simply calculated from Eq. (C.1), thus provides a quantitative estimate of the error of the moisture budget. Fig. C.22 shows the 4 terms of the moisture budget (Eq. (C.1)) in CESM2 over the 1985–2014 CE period for all the Antarctic regions. The residuals (R) are positive for all regions (i.e. the diagnostic moisture budget underestimates the direct estimation of $P - E$). The contribution of the residuals to the $P - E$ from model outputs lies between 12% and 26%. Therefore, the residuals are always of the same sign as the synoptic-scale transport contribution. One of the main causes of uncertainties in the budget calculation is the use of 6-hourly data instead of the model time-step. When using 6-hourly data, we underestimate the $P - E$ AIS-integrated by 18% compared to the model outputs (Fig. C.21 for the imbalance for each region), while the underestimation reaches 30% when degrading the time resolution to the daily timescale (Fig. C.21). It is thus reasonable to consider that the residuals account to a large extent for an underestimation of the contribution of the synoptic-scale transport in our calculation of the budget. However, because of the data assimilation in ERA-Interim, the precipitation, evaporation and humidity fields are influenced, which adds an error in the $P - E$ from the moisture budget [Seager and Henderson, 2013; Trenberth et al., 2011] and leads to regional residuals displaying a different sign than the synoptic-scale transport for the Plateau and Victoria Land regions. It must be noted that the residuals in the difference between two periods is much smaller than the residuals in each period (Figs. C.2 and C.22), which indicates that the error is constant to the first order between the periods and that the error is reduced when comparing two periods.

In addition to the use of 6-hourly data, in order to reduce as much as possible the imbalance between $P - E$ from the model output itself and the one calculated a-posteriori from the moisture budget, we only work with climate fields available on model atmospheric levels [Seager and Henderson, 2013]. Because of the limitations of the model outputs, it is not possible to reduce further the errors. The pattern of $P - E$ calculated by the moisture budget is similar to the one from the model outputs (Fig. C.23; correlation of 92%). Furthermore, the time series of the $P - E$ from the moisture budget and the ones from the model output itself are nearly identical (correlation of 99% to 100%). Consequently, even though an underestimation is noticed, the interannual variations of snow accumulation are well reproduced.

It is important to note that the goal of the moisture budget is not to obtain an accurate reconstruction of snow accumulation and the values can differ from other

methods used to estimate the surface mass balance. Firstly, the moisture budget underestimates the snow accumulation, which mainly comes from the use of 6-hourly data instead of the model time-step (typically a few minutes). Secondly, our definition of the snow accumulation excludes some terms such as the runoff and the sublimation of snow particles by the wind (the so-called drifting snow sublimation).

C.5 Antarctic moisture budget using climate model simulations

As an evaluation of the Antarctic moisture budget in the climate model simulations, the same analysis as for ERA-Interim was carried out with the ESM/GCM outputs (Figs. C.1–C.9). Results from the three climate models are similar to the results from ERA-Interim: the synoptic-scale transport mainly explains the regional snow accumulation mean under present-day conditions, but both the large-scale transport and synoptic-scale transport matter for the snow accumulation interannual variability. This indicates that the selected models are suitable for our study purpose.

C.6 Supplementary figures

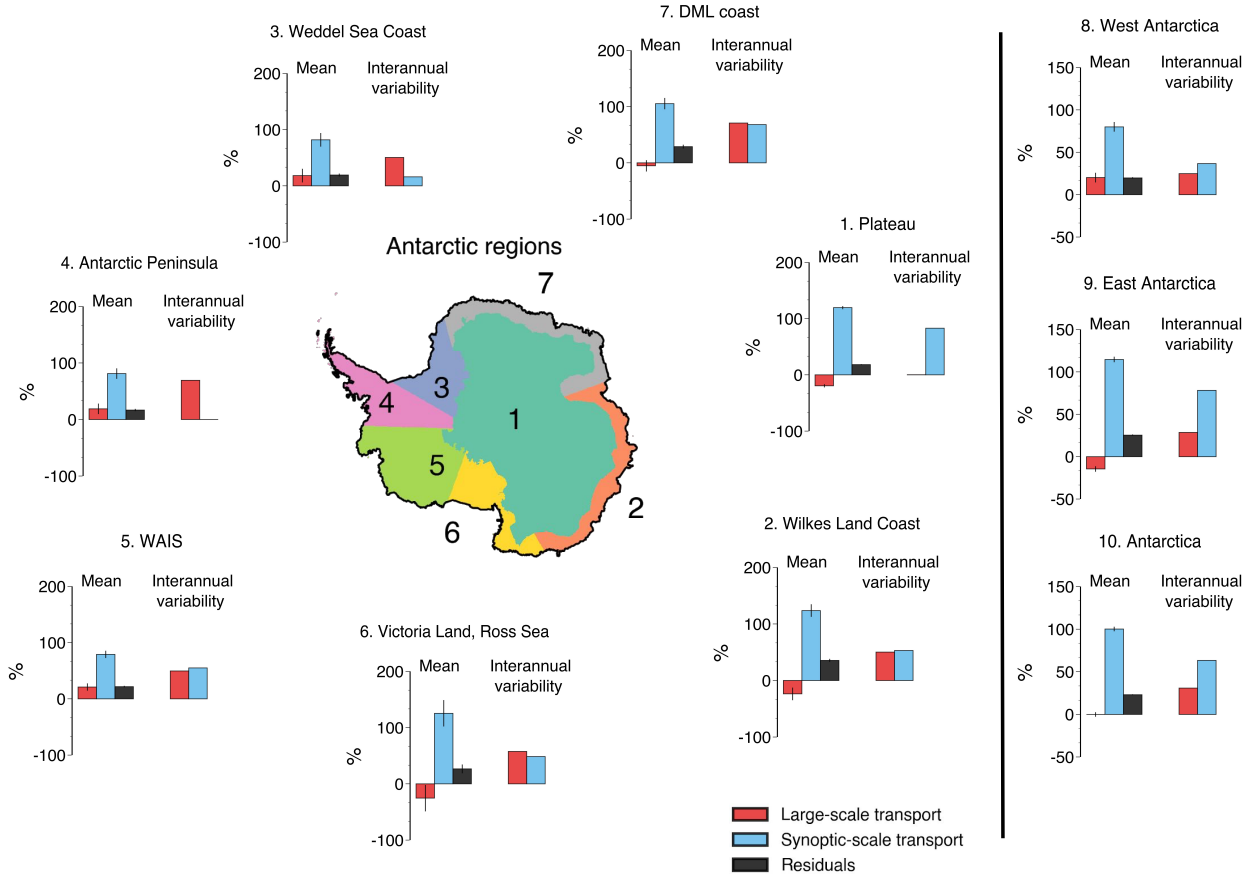


Figure C.1: ***Relative contributions of the large-scale and synoptic-scale transports to AIS snow accumulation in CESM2.*** *The bar plots show the contributions of the large-scale transport (red) and synoptic-scale transport (blue) to the mean and interannual variability of snow accumulation (variance) for the seven Antarctic regions based on CESM2 over the 1985–2014 CE period. The residuals (purple; i.e. the error related to the moisture budget calculation) are defined as the difference between the mean snow accumulation from model outputs and the one from the moisture budget (see Methods for more details). Antarctic regions are defined as in Thomas et al. [2017]: the Plateau where the altitude is higher than 2000 m, Wilkes Land Coast (70–150° E), Weddell Sea Coast (60–15° W), Victoria Land and Ross Sea (150–170° E), and Dronning Maud Land (DML) Coast (15° W–70° E). All these regions together is considered as East Antarctica. West Antarctica is divided in two regions with a division at 88° W: the Antarctic Peninsula and the West Antarctic Ice Sheet (WAIS).*

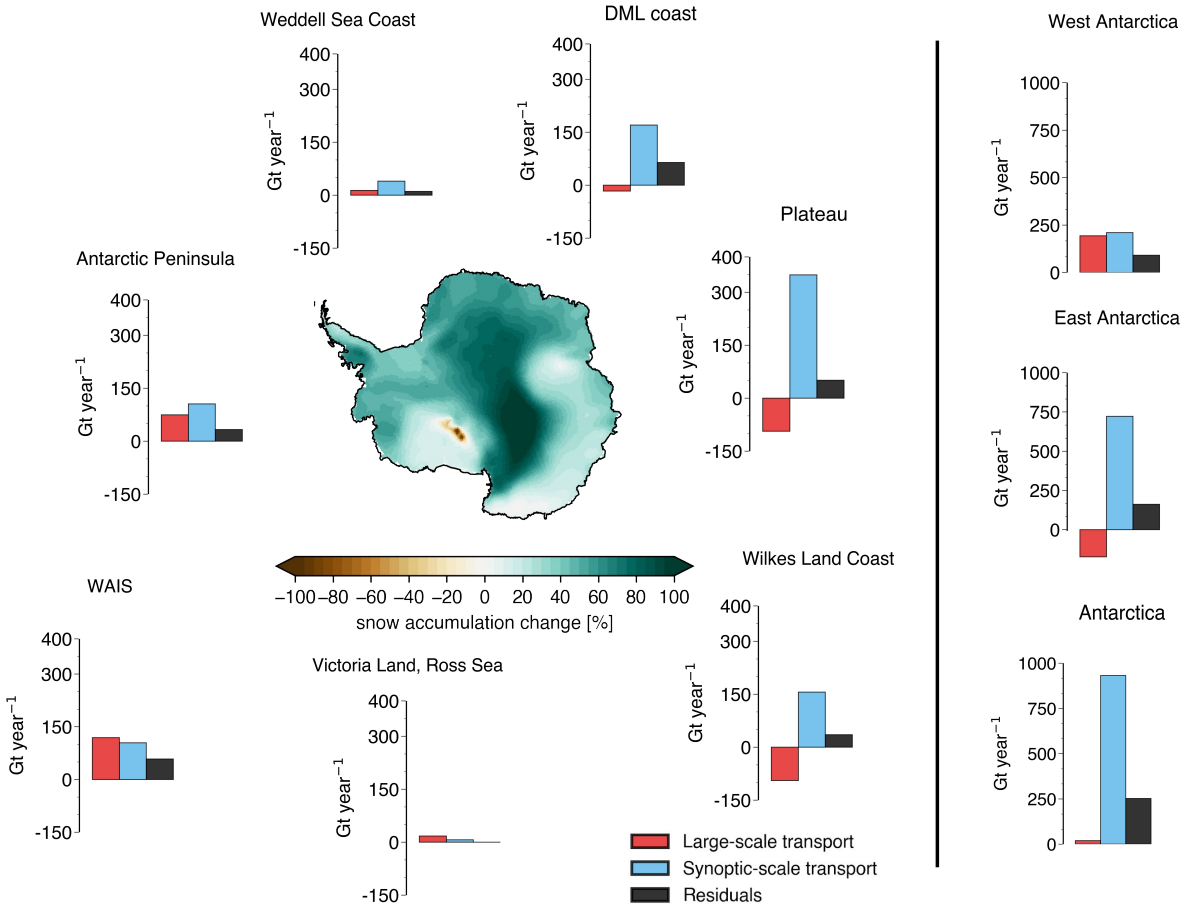


Figure C.2: ***Snow accumulation changes in the CESM2 simulation between the 2071–2100 CE and 1985–2014 CE periods.*** *The bar plots represent the absolute contributions of the large-scale transport (red) and synoptic-scale transport (blue) to the snow accumulation change per region (in Gt year^{-1}). The change in the residuals (purple; i.e. the error related to the moisture budget calculation) is defined as the change in the difference between the snow accumulation from model outputs and the one from the moisture budget (in Gt year^{-1}p; see Methods for more details). Regional boundaries are as in Fig. C.1.*

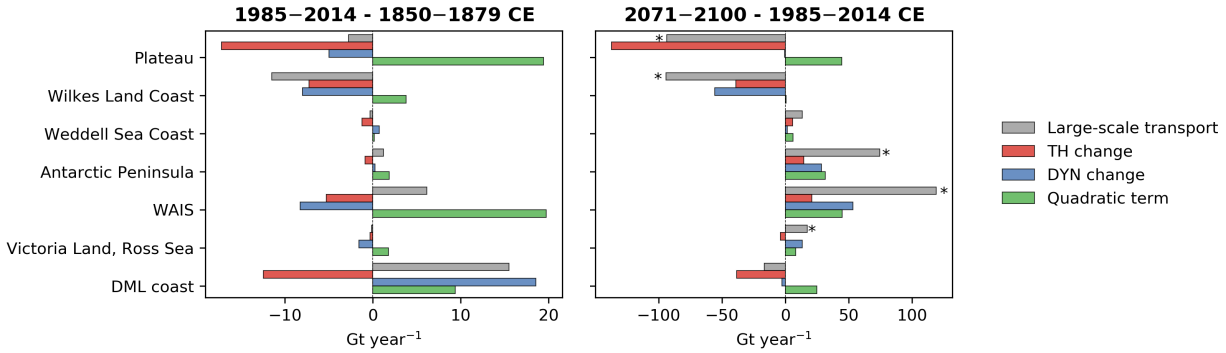


Figure C.3: ***Regional changes in the contribution of the large-scale transport to snow accumulation changes with their dynamic (DYN), thermodynamic (TH) and quadratic components in CESM2.*** *(left) between the 1985–2014 CE and 1850–1879 CE periods and (right) between the 2071–2100 CE and 1985–2014 CE periods (right; (in Gt year^{-1}). Asterisks correspond to absolute changes in the large-scale transport higher than the inter-annual variability estimated as one standard deviation of the annual large-scale transport over the 1850-1879 CE period for changes between the 1985-2014 CE and 1850-1879 CE periods and over the 1985-2014 CE period for changes between the 2071-2100 CE and 1985-2014 CE periods. Note that for readability, limits of the x-axis are different for the two plots.*

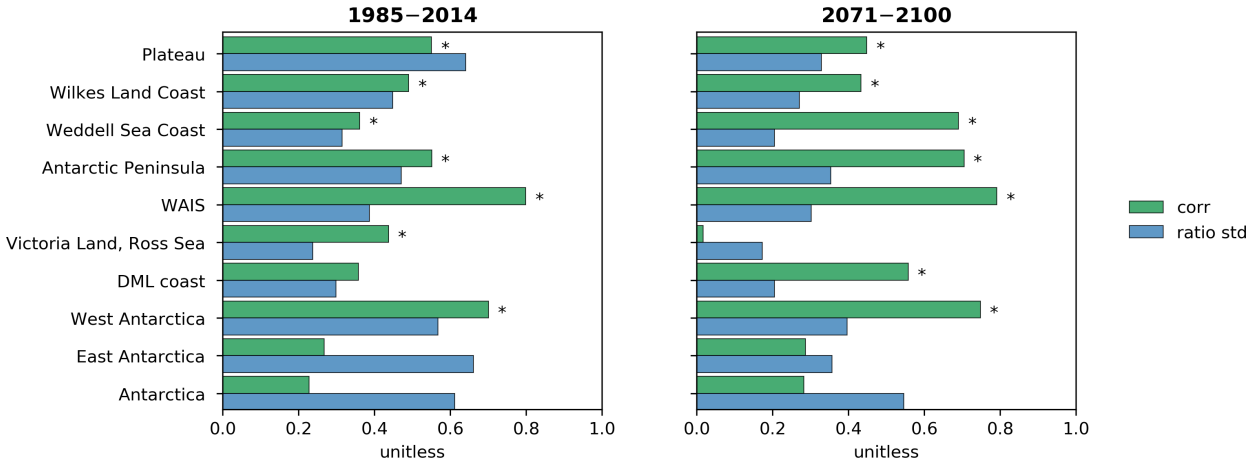


Figure C.4: ***Interannual snow accumulation changes approximated by the Clausius-Clapeyron relationship.*** *Regional correlations (green) between annual modeled snow accumulation and the Clausius-Clapeyron approximations of annual snow accumulation, and the ratio between the standard deviation of the approximation and the modeled annual snow accumulation over the 1985–2014 CE (left) and 2071–2100 CE (right) periods. Asterisks stand for statistically significant correlations (p-value < 0.05).*

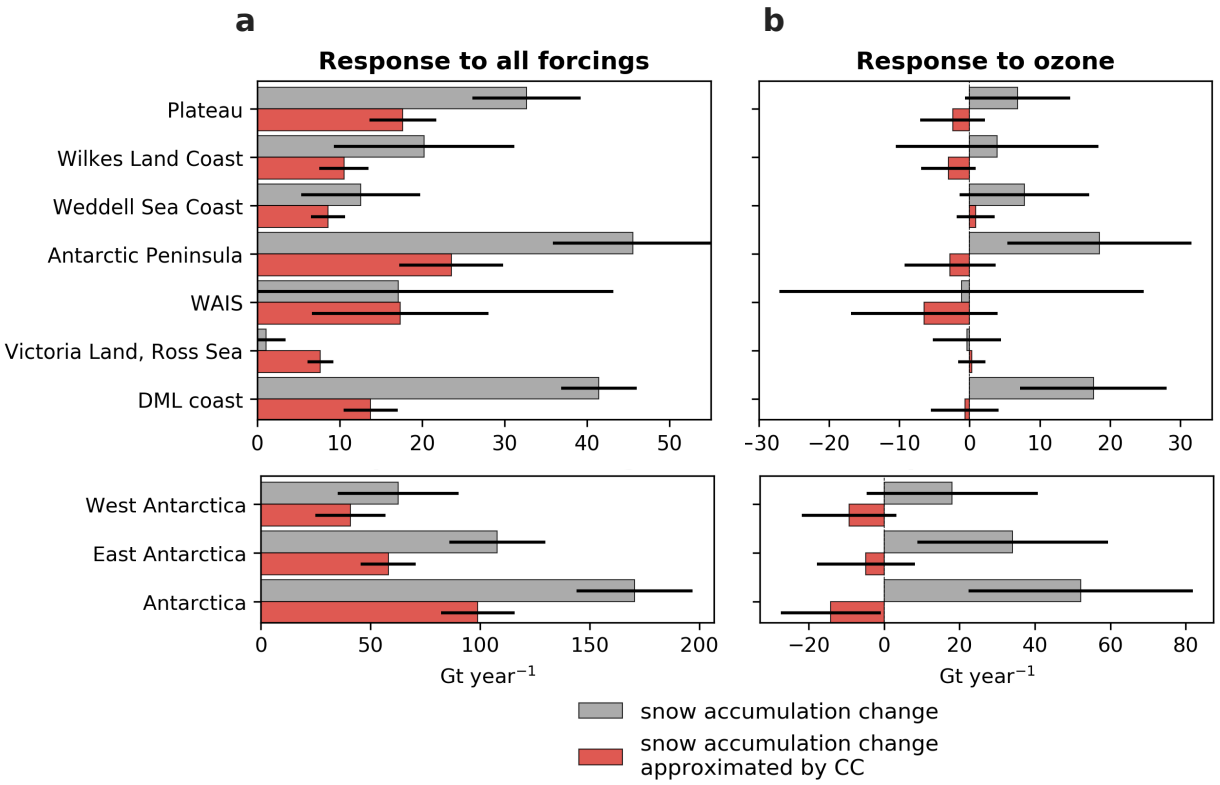


Figure C.5: ***Snow accumulation changes approximated by the Clausius-Clapeyron relationship in response to ozone depletion.*** *Regional snow accumulation changes (grey) with their estimations by the Clausius-Clapeyron approximation (red) between the 1986–2005 CE and 1920–1949 CE periods in CESM1-LE (**a**) and the regional snow accumulation changes (grey) with their estimations by the Clausius-Clapeyron approximation (red) attributed to ozone depletion over the 1986–2005 CE period (**b**; in Gt year^{-1}). Error bars correspond to one standard deviation of the ensemble members (8 simulations). Note that for readability, limits of the x-axis are different for the two plots.*

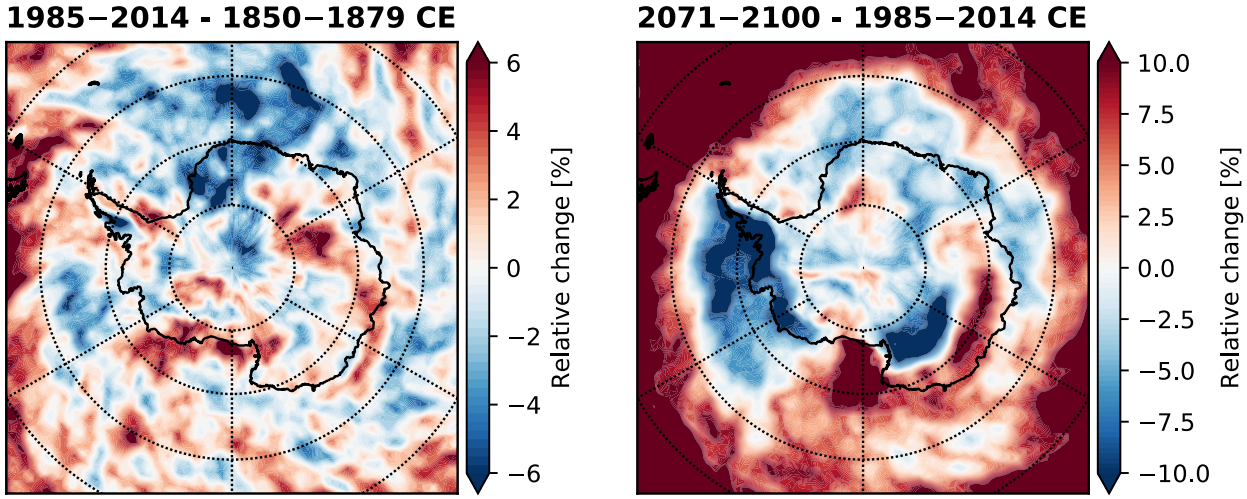


Figure C.6: ***Changes in the contributions of Extreme Precipitations Events.*** *Relative differences in the contribution of Extreme Precipitation Events (EPEs) to the total precipitation in CESM2 between the 1985–2014 CE and 1850–1879 CE periods (left), and between the 2071–2100 CE and 1985–2014 CE periods (right). EPEs follow the definition of Turner et al. [2019b]: they correspond to the events for which the total daily precipitation is higher than the 95th percentile of the entire time series. The contribution of EPEs is obtained by calculating the 95th percentiles for each of the three periods (i.e., 1850–1879 CE, 1985–2014 CE and 2071–2100 CE periods) and used to determine the contribution of the EPEs to the total precipitation.*

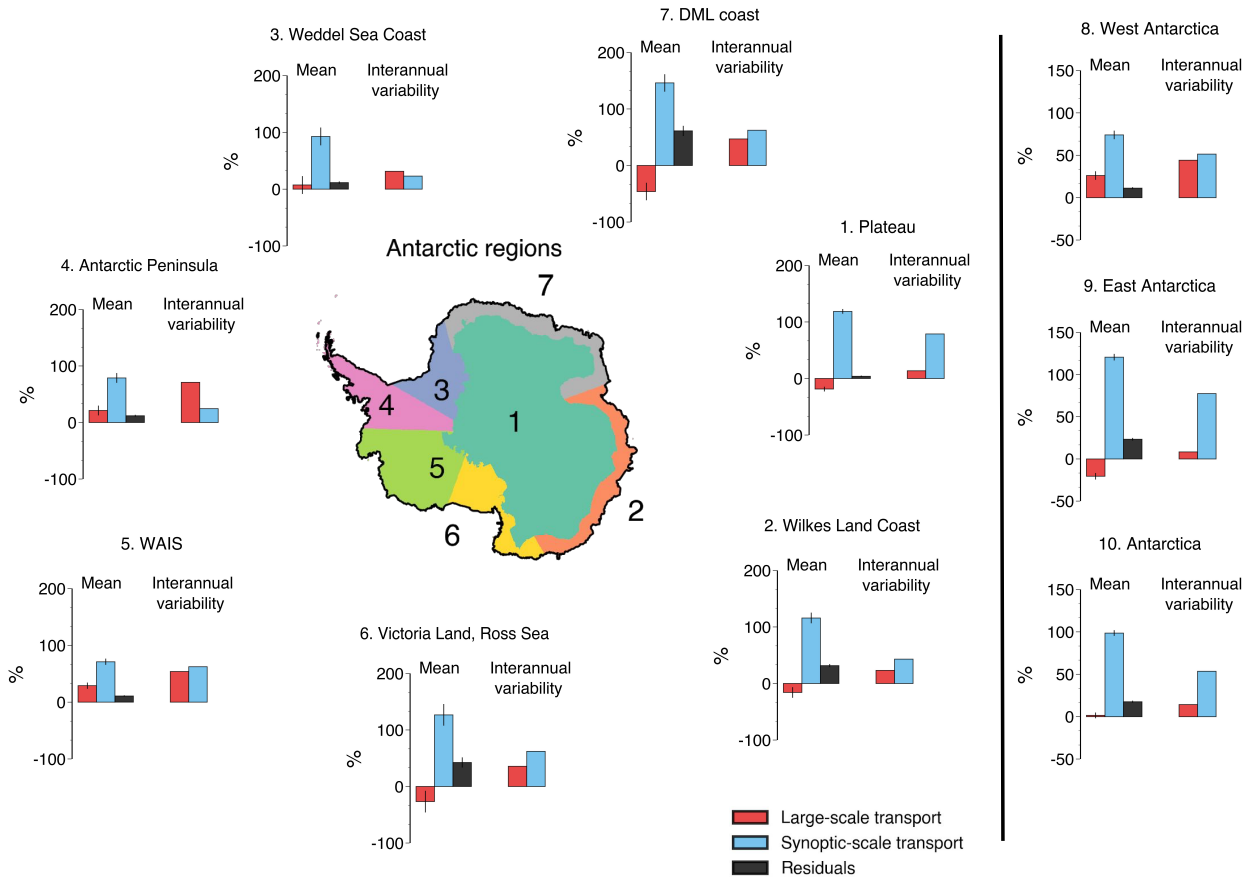


Figure C.7: ***Relative contributions of the large-scale and synoptic-scale transports to AIS snow accumulation in ACCESS1-3.*** *The bar plots show the contributions of the large-scale transport (red) and synoptic-scale transport (blue) to the mean and interannual variability of snow accumulation (variance) for the seven Antarctic regions based on ACCESS1-3 over the 1985–2014 CE period. The error bars are calculated as the standard deviation of the annual contribution to the snow accumulation mean. Antarctic regions are defined as in Thomas et al. [2017]: the Plateau where the altitude is higher than 2000 m, Wilkes Land Coast (70–150° E), Weddell Sea Coast (60–15° W), Victoria Land and Ross Sea (150–170° E), and Dronning Maud Land (DML) Coast (15° W–70° E). All these regions together is considered as East Antarctica. West Antarctica is divided in two regions with a division at 88° W: the Antarctic Peninsula and the West Antarctic Ice Sheet (WAIS).*

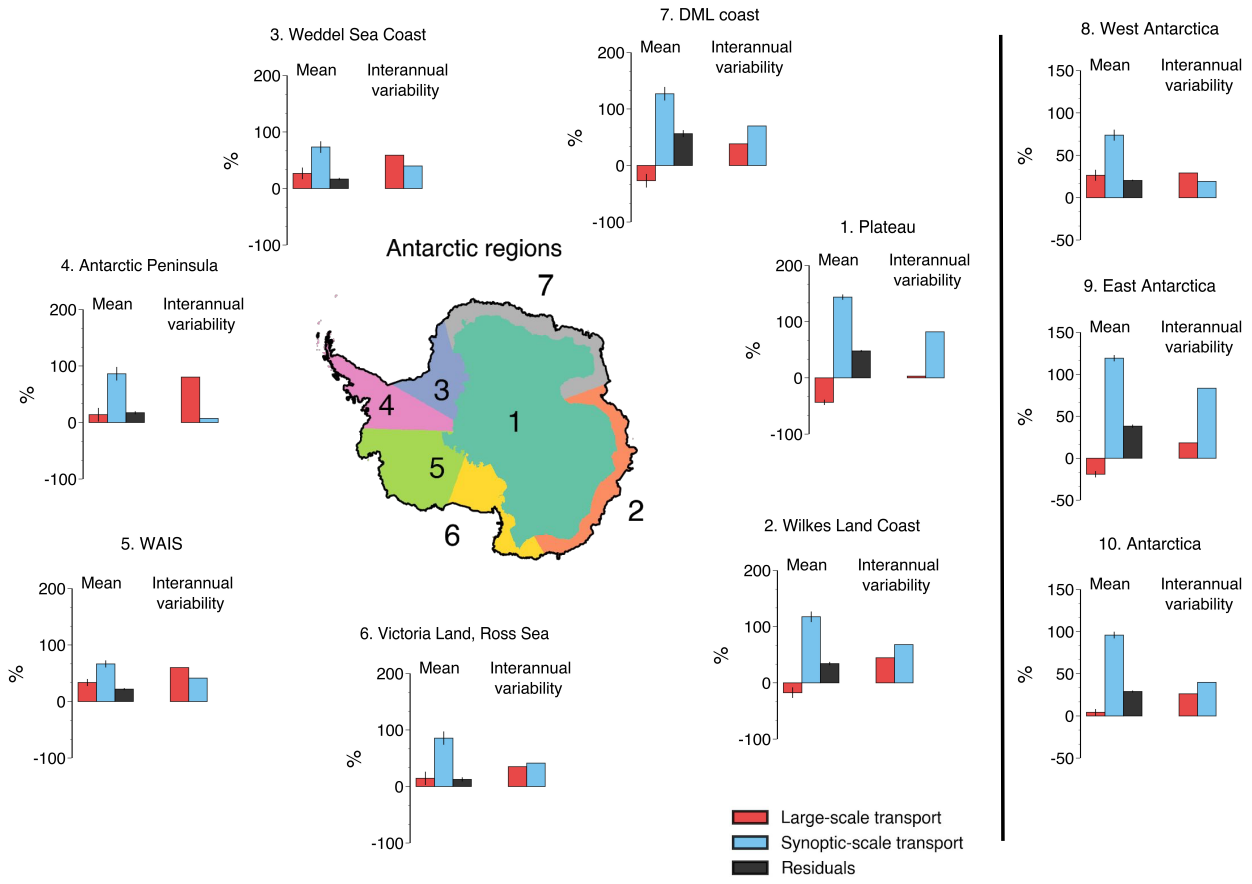


Figure C.8: ***Relative contributions of the large-scale and synoptic-scale transports to AIS snow accumulation in NorESM1-M.*** *The bar plots show the contributions of the large-scale transport (red) and synoptic-scale transport (blue) to the mean and interannual variability of snow accumulation (variance) for the seven Antarctic regions based on NorESM1-M over the 1985–2014 CE period. The error bars are calculated as the standard deviation of the annual contribution to the snow accumulation mean. Antarctic regions are defined as in Thomas et al. [2017]: the Plateau where the altitude is higher than 2000 m, Wilkes Land Coast (70–150° E), Weddell Sea Coast (60–15° W), Victoria Land and Ross Sea (150–170° E), and Dronning Maud Land (DML) Coast (15° W–70° E). All these regions together is considered as East Antarctica. West Antarctica is divided in two regions with a division at 88° W: the Antarctic Peninsula and the West Antarctic Ice Sheet (WAIS).*

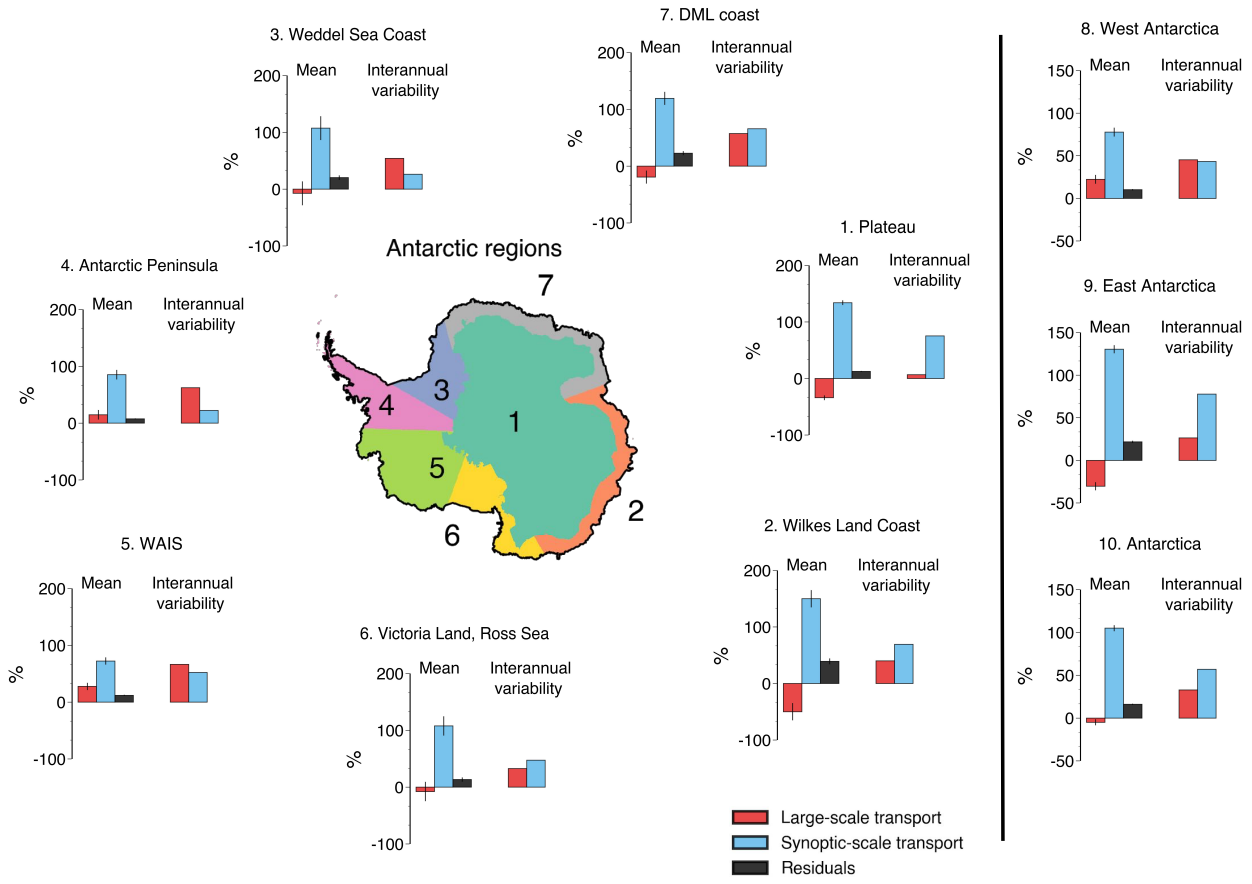


Figure C.9: ***Relative contributions of the large-scale and synoptic-scale transports to AIS snow accumulation in CESM1-LE.*** *The bar plots show the contributions of the large-scale transport (red) and synoptic-scale transport (blue) to the mean and interannual variability of snow accumulation (variance) for the seven Antarctic regions based on CESM1-LE (35 members) over the 1990–2005 CE period. The error bars are calculated as the standard deviation of the annual contribution to the snow accumulation mean. Antarctic regions are defined as in Thomas et al. [2017]: the Plateau where the altitude is higher than 2000 m, Wilkes Land Coast (70–150° E), Weddell Sea Coast (60–15° W), Victoria Land and Ross Sea (150–170° E), and Dronning Maud Land (DML) Coast (15° W–70° E). All these regions together is considered as East Antarctica. West Antarctica is divided in two regions with a division at 88° W: the Antarctic Peninsula and the West Antarctic Ice Sheet (WAIS).*

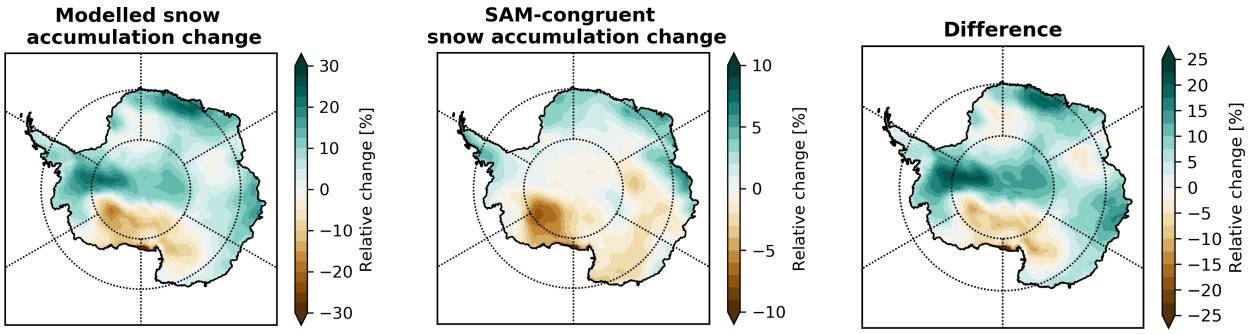


Figure C.10: ***Snow accumulation changes and their relationship with the SAM in ACCESS1-3.*** *Relative snow accumulation changes in the ACCESS1-3 simulation between the 1985–2014 CE and 1850–1879 CE periods (left), relative SAM-congruent snow accumulation changes in the ACCESS1-3 simulation between the 1985–2014 CE and 1850–1879 CE periods (center) and the difference between the two (right).*

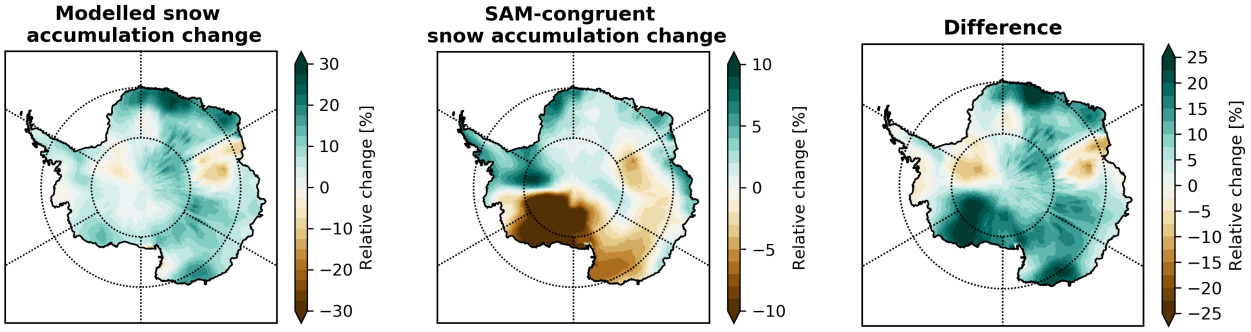


Figure C.11: ***Snow accumulation changes and their relationship with the SAM in NorESM1-M.*** *Relative snow accumulation changes in the NorESM1-M simulation between the 1985–2014 CE and 1850–1879 CE periods (left), relative SAM-congruent snow accumulation changes in the NorESM1-M simulation between the 1985–2014 CE and 1850–1879 CE periods (center) and the difference between the two (right).*

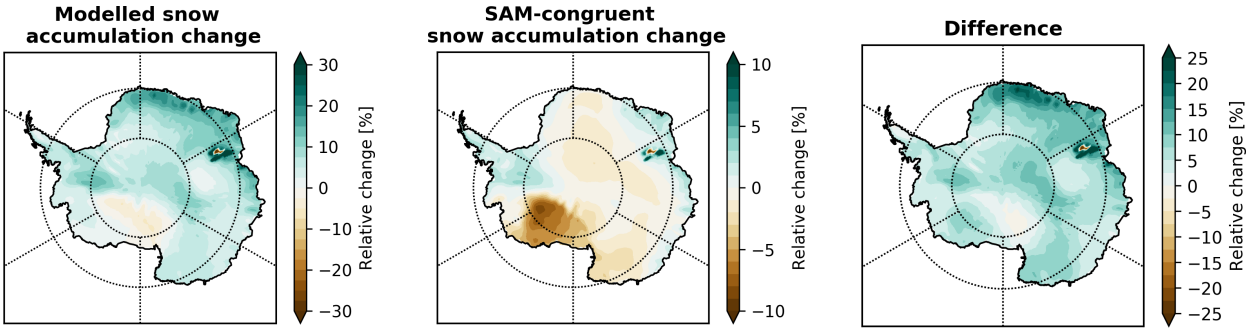


Figure C.12: ***Snow accumulation changes and their relationship with the SAM in CESM1-LE.*** *Relative snow accumulation changes in the CESM1-LE simulation between the 1976–2005 CE and 1920–1949 CE periods (left), relative SAM-congruent snow accumulation changes in the CESM1-LE simulation between the 1976–2005 CE and 1920–1949 CE periods (center) and the difference between the two (right).*

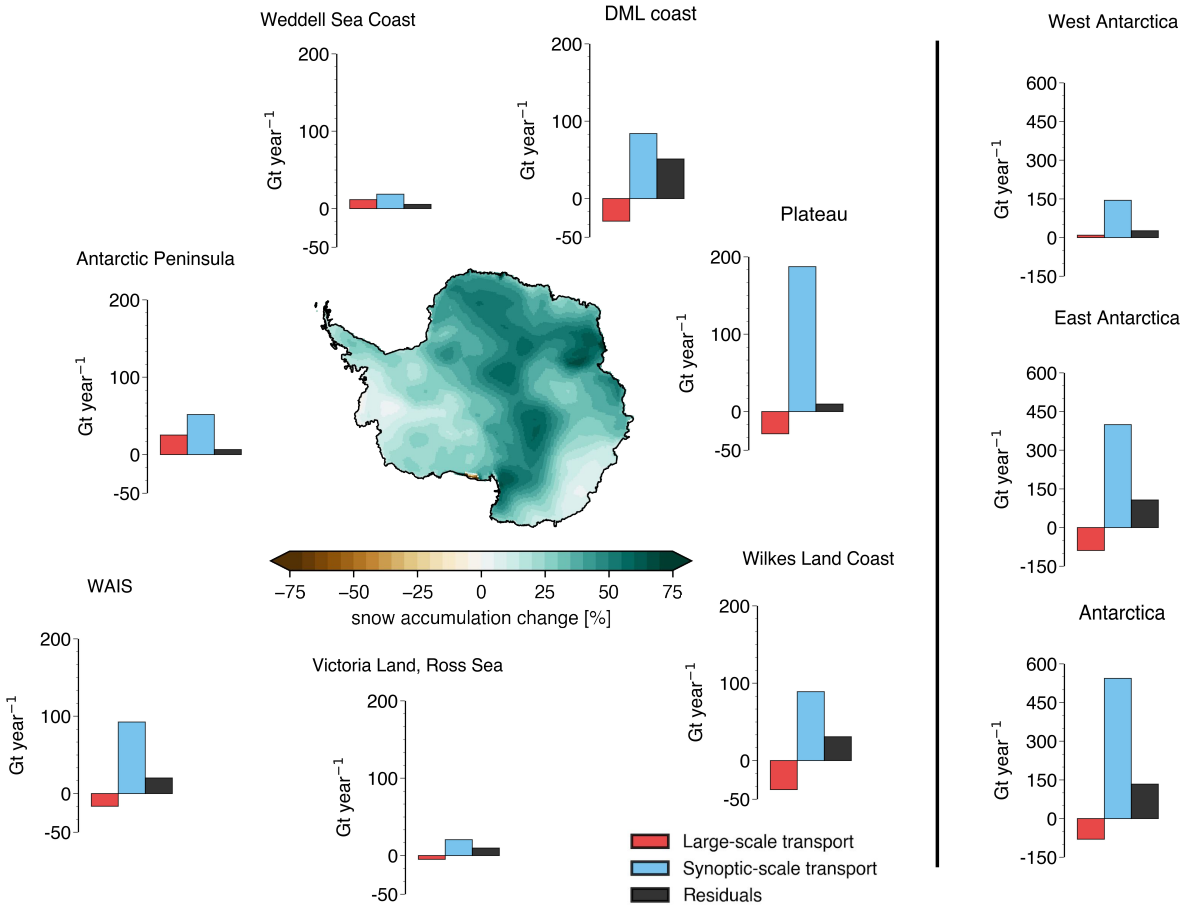


Figure C.13: ***Snow accumulation changes in the ACCESS1-3 simulation between the 2071–2100 CE and 1985–2014 CE periods.*** *The bar plots represent the absolute contributions of the large-scale transport (red) and synoptic-scale transport (blue) to the snow accumulation change per region (in Gt year^{-1}). The change in the residuals (purple; i.e. the error related to the moisture budget calculation) is defined as the change in the difference between the snow accumulation from model outputs and the one from the moisture budget (in Gt year^{-1}; see Methods for more details). Regional boundaries are as in Fig. C.7.*

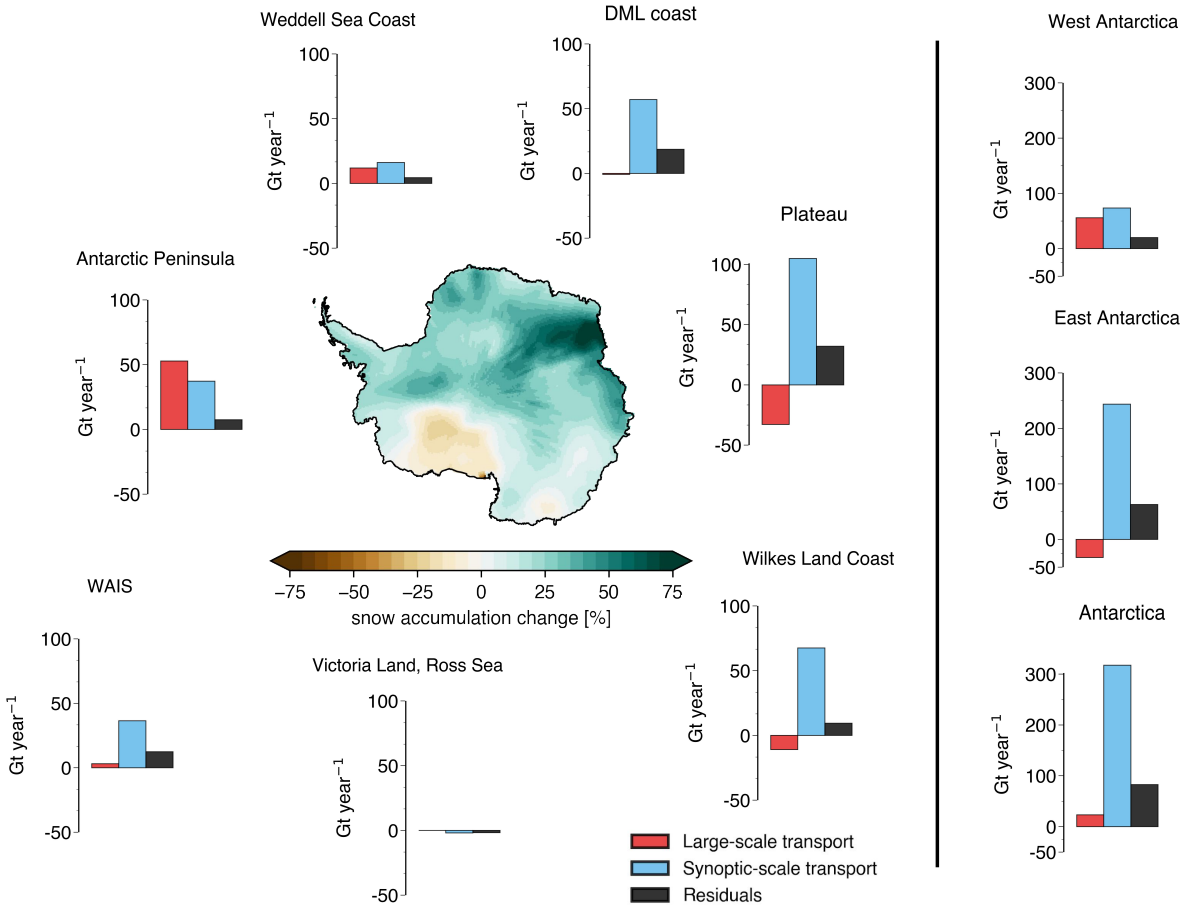


Figure C.14: ***Snow accumulation changes in the NorESM1-M simulation between the 2071–2100 CE and 1985–2014 CE periods.*** *The bar plots represent the absolute contributions of the large-scale transport (red) and synoptic-scale transport (blue) to the snow accumulation change per region (in Gt year^{-1}). The change in the residuals (purple; i.e. the error related to the moisture budget calculation) is defined as the change in the difference between the snow accumulation from model outputs and the one from the moisture budget (in Gt year^{-1}; see Methods for more details). Regional boundaries are as in Fig. C.8.*

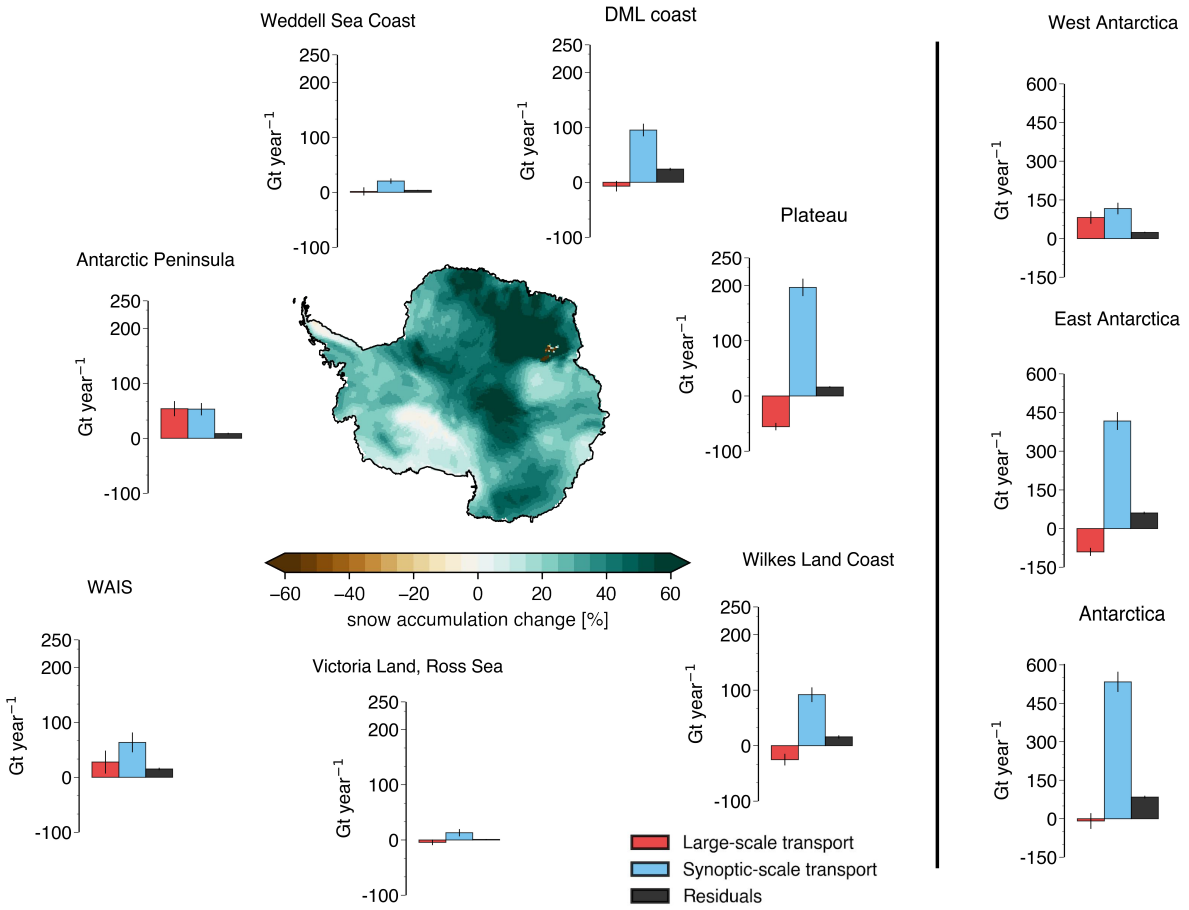


Figure C.15: ***Snow accumulation changes in CESM1-LE between the 2071–2080 CE and 1990–2005 CE periods.*** *The bar plots represent the absolute contributions of the large-scale transport (red) and synoptic-scale transport (blue) to the snow accumulation change per region (in Gt year^{-1}). The change in the residuals (purple; i.e. the error related to the moisture budget calculation) is defined as the change in the difference between the snow accumulation from model outputs and the one from the moisture budget (in Gt year^{-1}; see Methods for more details). The error bars are calculated as the standard deviation of the ensemble member. Regional boundaries are as in Fig. C.9.*

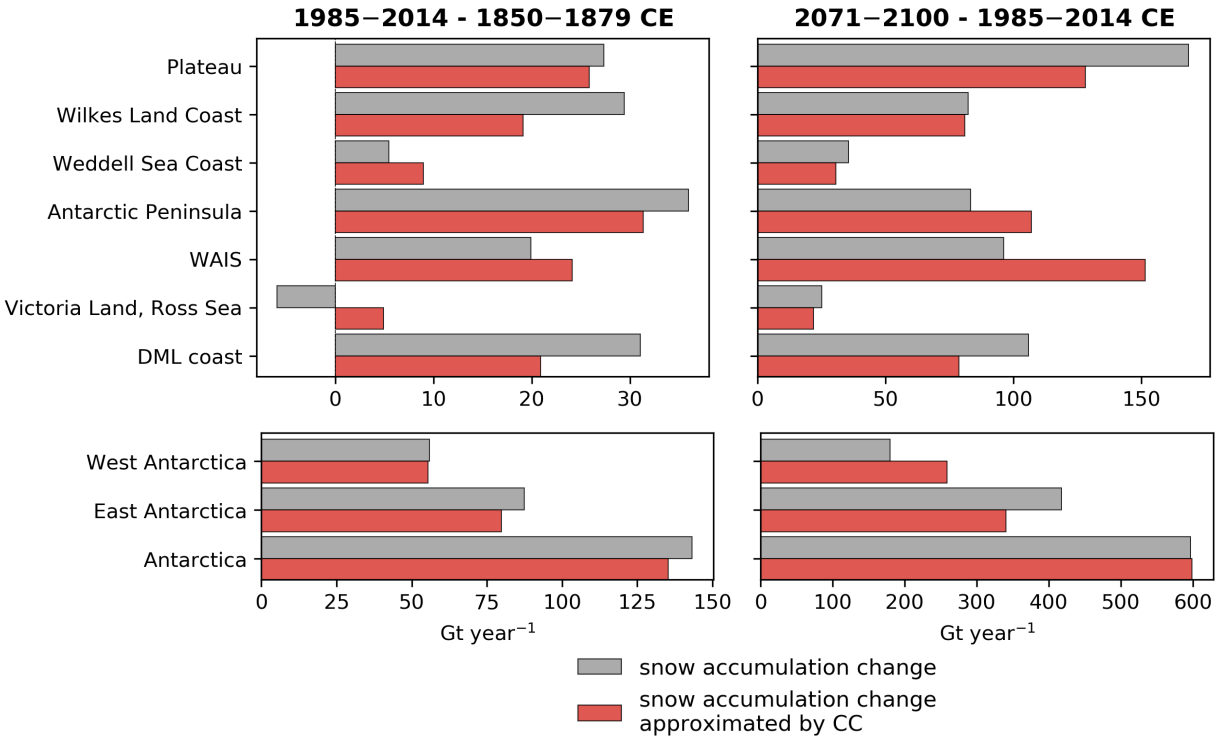


Figure C.16: ***Snow accumulation changes approximated by the Clausius-Clapeyron relation in ACCESS1-3.*** *Regional snow accumulation change (grey) with their estimations by the Clausius-Clapeyron approximation (red) between the 1985–2014 and 1850–1879 periods (left) and between the 2071–2100 and 1985–2014 periods (right) for the ACCESS1-3 simulation (in Gt year^{-1}). Note that for readability, limits of the x-axis are different for the two plots.*

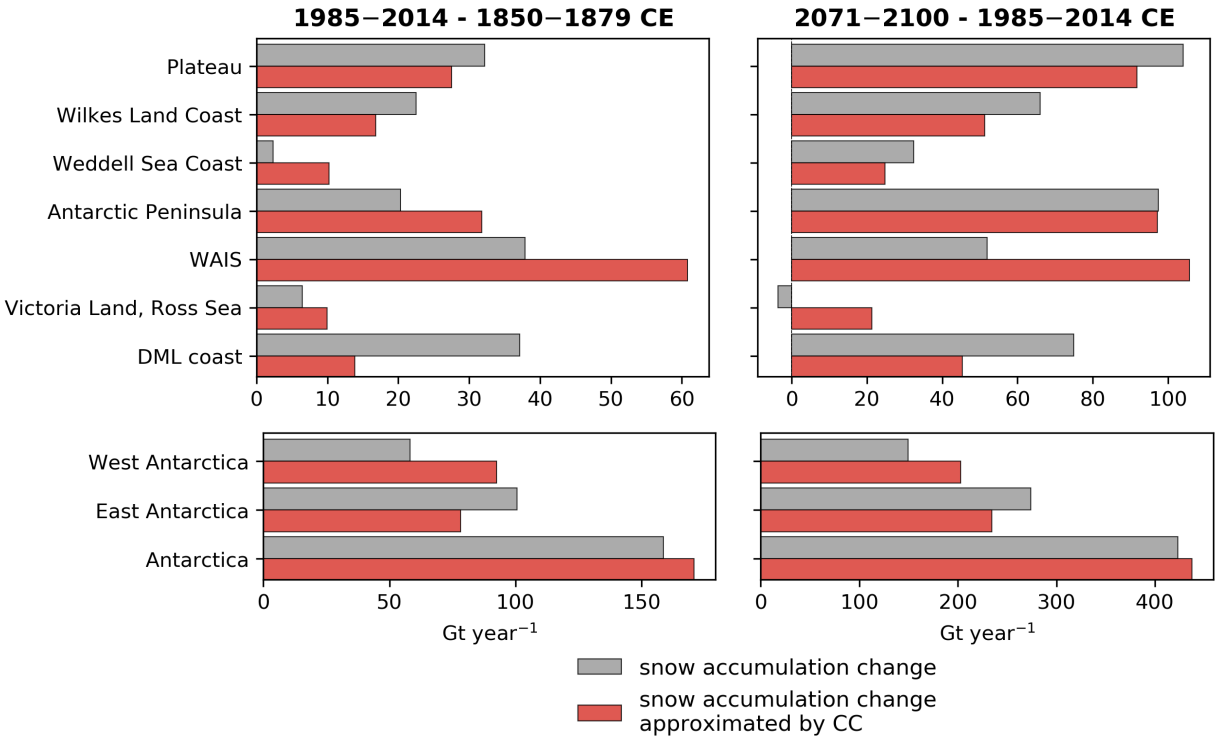


Figure C.17: ***Snow accumulation changes approximated by the Clausius-Clapeyron relation in NorESM1-M.*** *Regional snow accumulation changes (grey) with their estimations by the Clausius-Clapeyron approximation (red) between the 1985–2014 CE and 1850–1879 CE periods (left) and between the 2071–2100 CE and 1985–2014 CE periods (right) for the NorESM1-M simulation (in Gt year^{-1}). Note that for readability, limits of the x-axis are different for the two plots.*

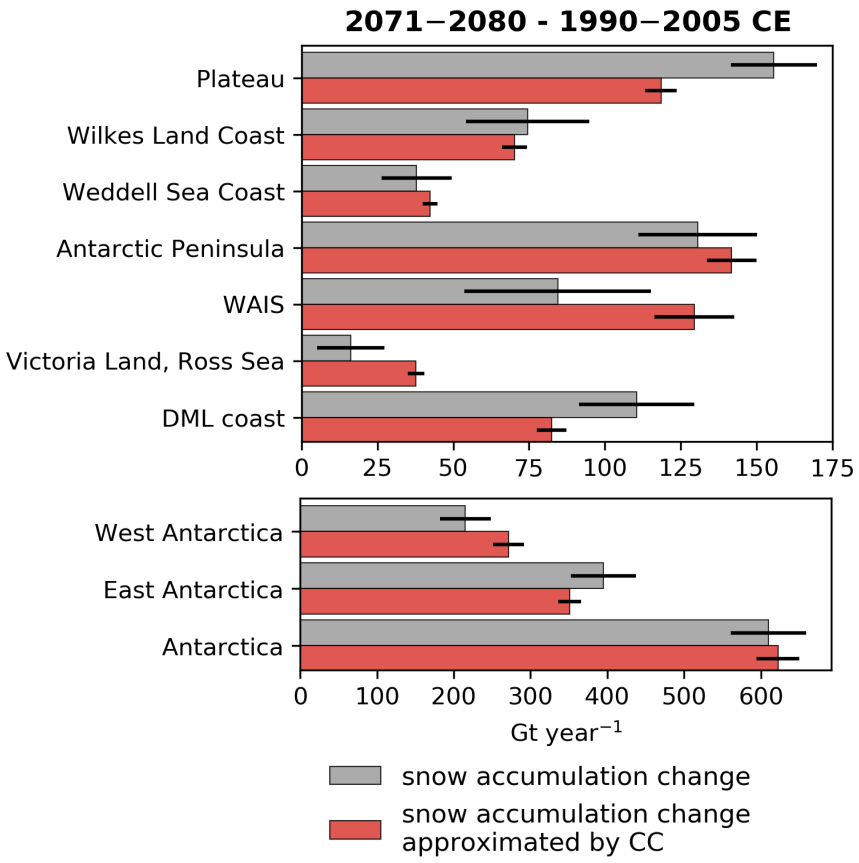


Figure C.18: ***Snow accumulation changes approximated by the Clausius-Clapeyron relation in CESM1-LE.*** *Regional snow accumulation changes (grey) with their estimations by the Clausius-Clapeyron approximation (red) between the 2071–2080 CE and 1990–2005 CE periods for CESM1-LE (in Gt year^{-1}). Error bars correspond to one standard deviation of the ensemble members (35 simulations)*

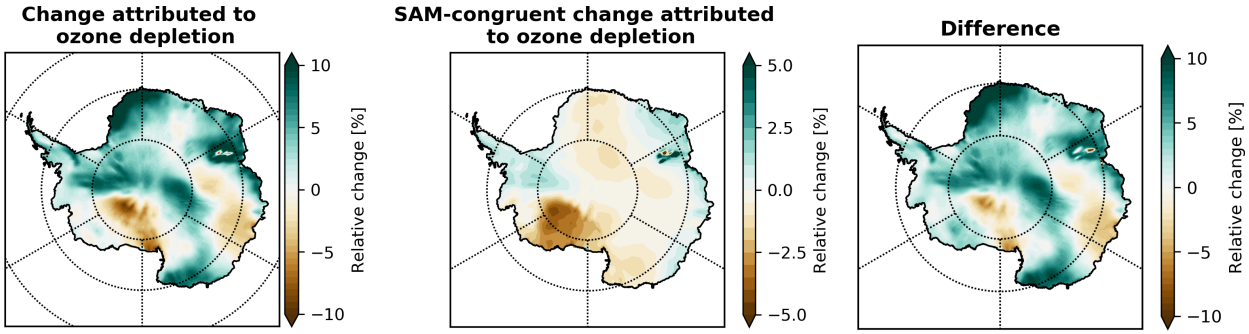


Figure C.19: ***Snow accumulation changes attributed to the ozone depletion.*** *Relative snow accumulation changes attributed to ozone depletion over the 1986–2005 CE period (based on CESM1; left), relative SAM-congruent snow accumulation changes in the attribution of ozone depletion to snow accumulation changes over the same period (center), the difference between the two (right).*

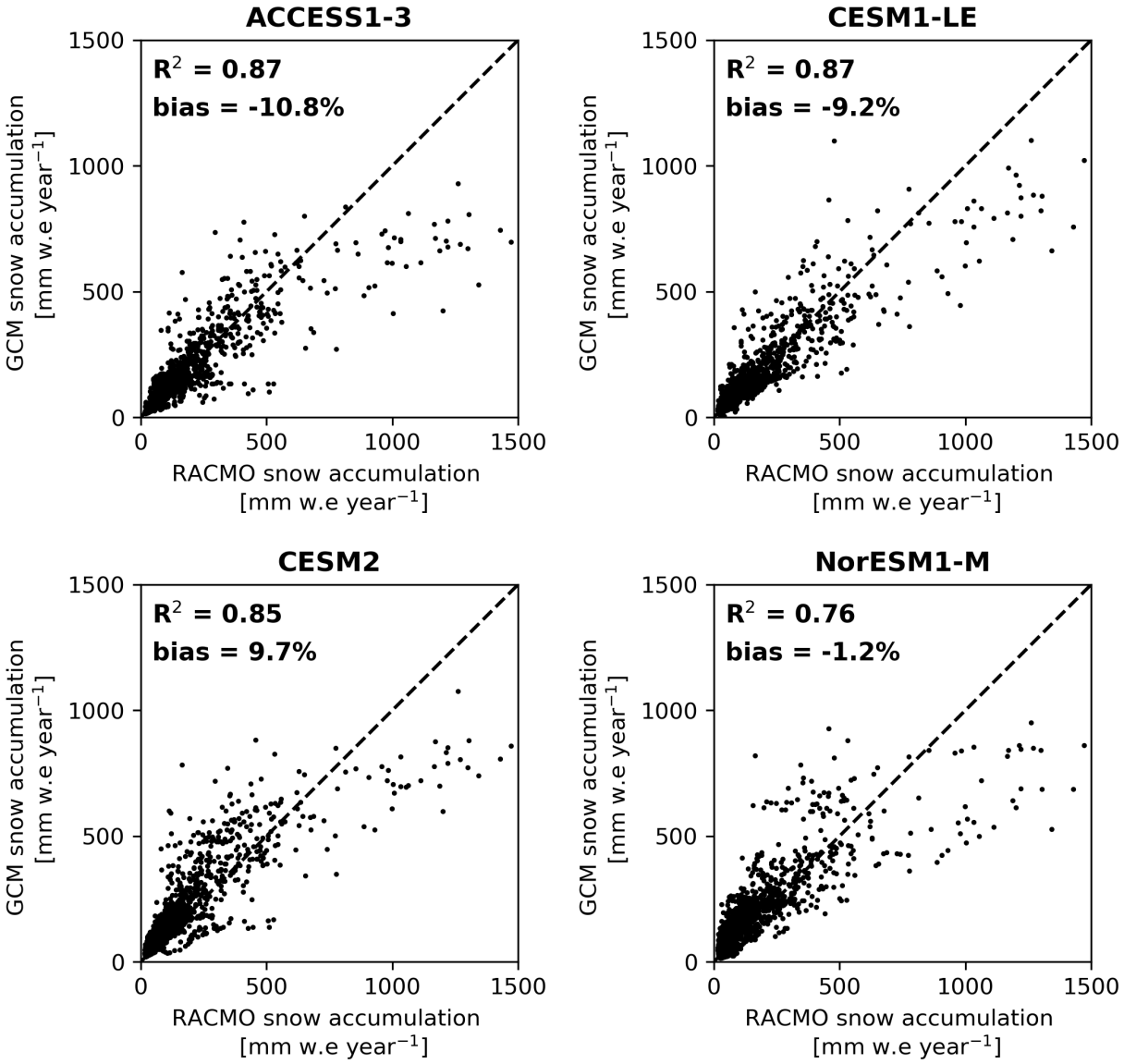


Figure C.20: ***Evaluation of Antarctic snow accumulation in models used in this study.*** *Antarctic snow accumulation climatology from ACCESS1-3 (above left), CESM1-LE (above right), CESM2 (below left) and NorESM1-M (below right) as a function of the snow accumulation climatology of the regional climate model RACMO2.3 (RACMO) over the 1979–2005 CE period (in mm w.e. year^{-1}). ESM/GCM and RACMO outputs have been linearly interpolated on a 1.5°×2° Gaussian grid. The R^2 is computed on logarithmic values as the distribution of snow accumulation distribution is log-normal. The bias is the relative difference in AIS-integrated snow accumulation between the ESM/GCM and RACMO2. Note that in contrast to the ESM/GCMs, RACMO includes the sublimation of snow particles transported by the snow (the so-called sublimation drifting snow; its contribution to the snow accumulation is lower than 5%) and the runoff (its contribution is lower than 0.1%) [van Wessem et al., 2018]. For the regional evaluation of the snow accumulation, see Tab. C.2.*

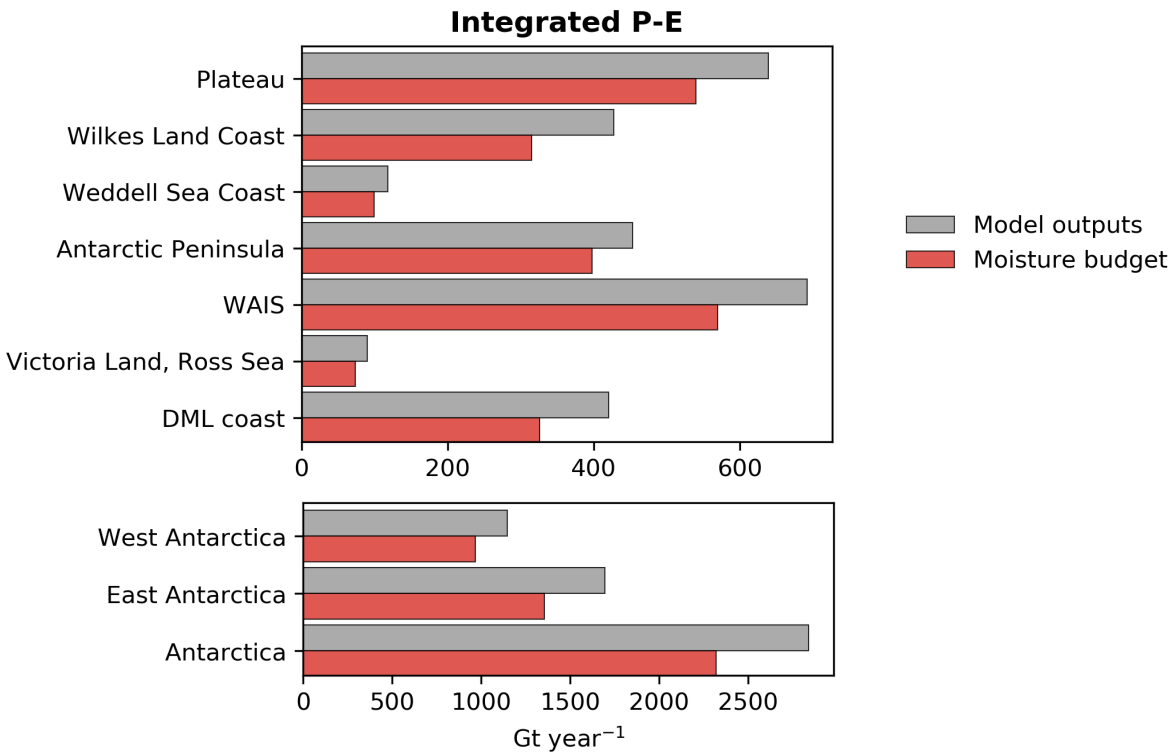


Figure C.21: ***Regional Antarctic snow accumulation from the moisture budget.*** *Region integrated $P - E$ from model outputs and from the moisture budget using CESM2 over the 1985–2014 CE period (in Gt year^{-1}). The $P - E$ computed from the moisture budget is based on 6-hourly data.*

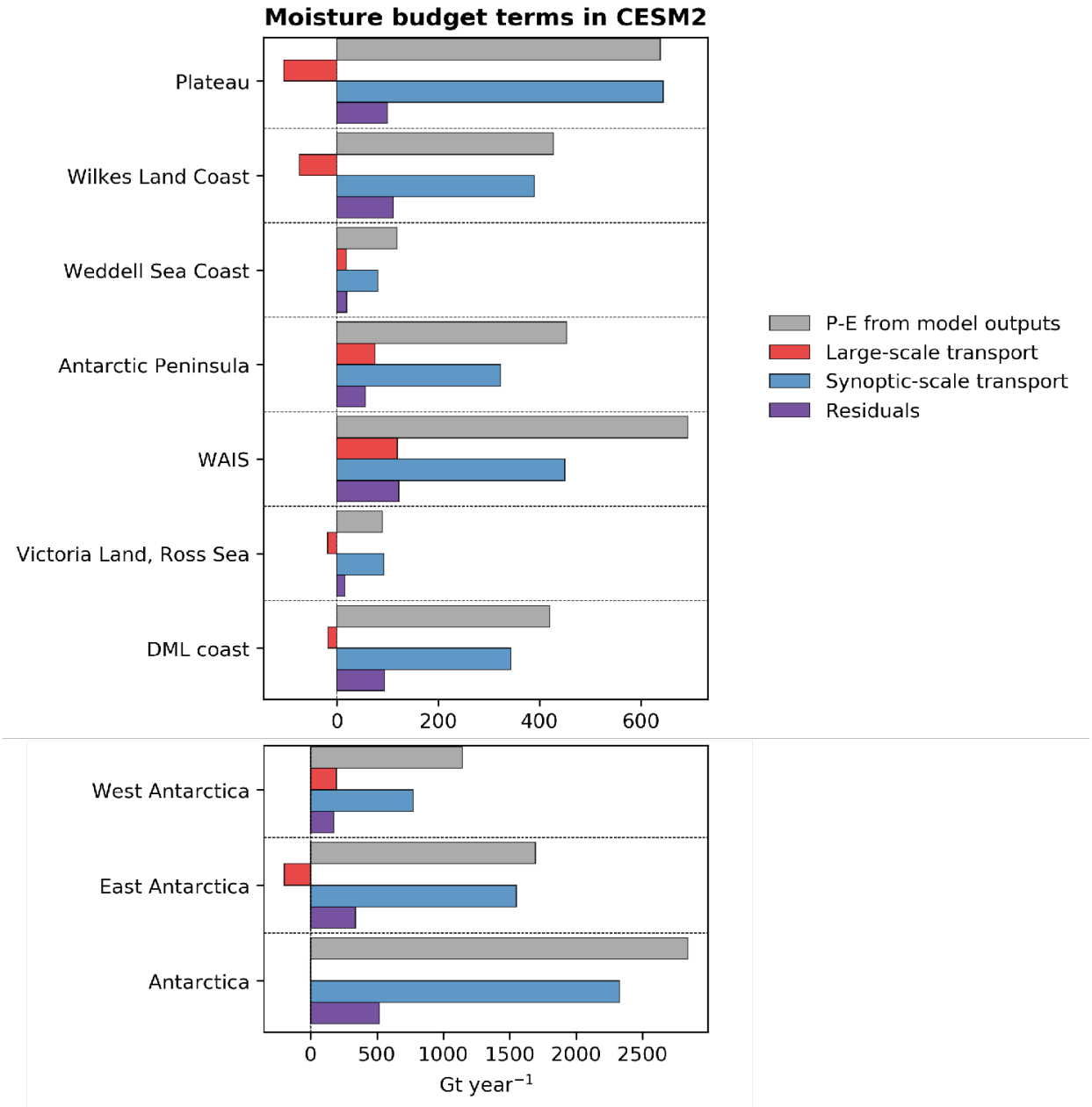


Figure C.22: ***Snow accumulation imbalance induced by the moisture budget calculation.*** *The four terms of the moisture budget, namely $P - E$ ($P - E$ from model outputs; grey), MC (Large-scale transport; red), TE (Synoptic-scale transport; blue) and R (Residuals; purple) in CESM2 over the 1985–2014 CE period for all the Antarctic regions. All the terms are expressed in Gt year^{-1}.*

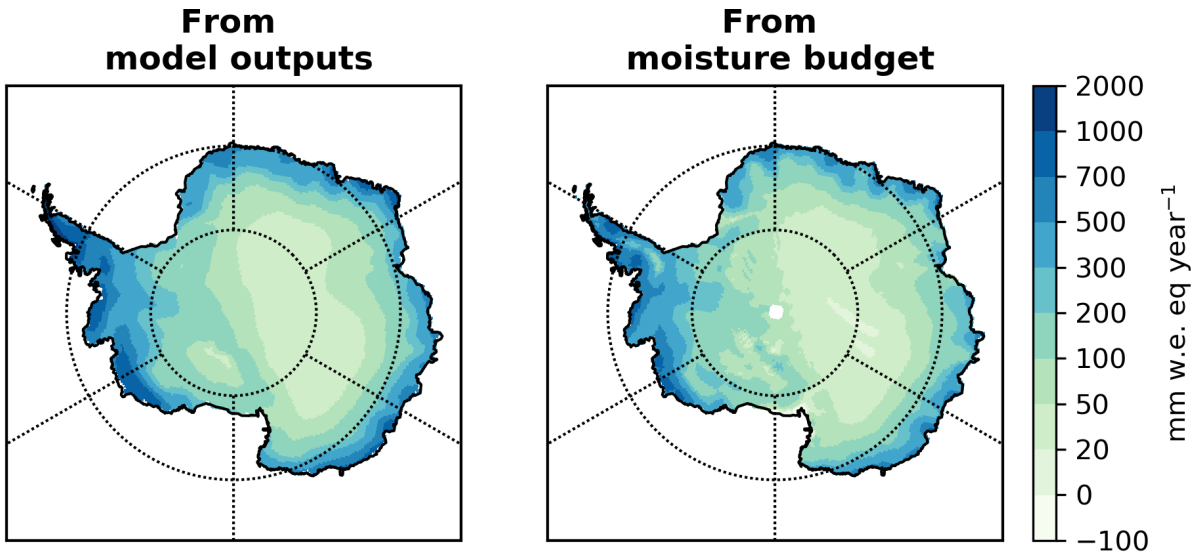


Figure C.23: ***Antarctic snow accumulation from the moisture budget.*** *$P - E$ from model outputs and from the moisture budget using CESM2 over the 1985–2014 CE period (in mm w.e. year^{-1}).*

C.7 Supplementary tables

Region	ERA-Interim				CESM2			
	Mean		Interannual variability		Mean		Interannual variability	
	Large-scale transport [%]	Synoptic-scale transport [%]	Large-scale transport [%]	Synoptic-scale transport [%]	Large-scale transport [%]	Synoptic-scale transport [%]	Large-scale transport [%]	Synoptic-scale transport [%]
Plateau	-31	131	0	75	-19	119	0	83
Wilkes Land	-30	130	41	46	-24	124	50	53
Weddell	-7	107	61	3	18	82	50	16
Peninsula	18	82	79	32	19	81	59	0
WAIS	32	68	59	54	21	79	50	55
Victoria Land	-29	129	29	34	-25	125	58	49
DML coast	-62	162	46	52	-5	105	71	68
West Antarctica	26	74	55	31	20	80	25	37
East Antarctica	-34	134	21	68	-15	115	29	78
Antarctica	-5	105	14	44	0	100	31	63

Table C.1: ***Contributions of the large-scale and synoptic-scale transports to regional snow accumulation changes.*** *Relative contributions (%) of the large-scale and synoptic-scale transport to the mean and interannual variability of the snow accumulation for all the Antarctic regions over 1985–2014 CE for ERA-Interim and CESM2.*

Region	ACCESS1-3		CESM1-LE		CESM2		NorESM1-M	
	R^2 [%]	Relative bias [%]	R^2 [%]	Relative bias [%]	R^2 [%]	Relative bias [%]	R^2 [%]	Relative bias [%]
Plateau	84	-8.3	79	-8.4	77	24.8	60	-6.3
Wilkes Land Coast	78	-15.0	85	-21.3	78	-0.2	72	-20.9
Weddell Sea Coast	51	12.8	58	1.7	69	26.9	54	38.5
Antarctic Peninsula	85	-18.2	89	-14.1	88	-7.4	80	-10.8
WAIS	87	-13.9	86	-11.8	82	-4.6	82	8.0
Victoria Land, Ross Sea	22	-15.3	48	-3.5	21	2.4	21	44.7
DML coast	58	8.8	62	21.3	57	68.4	53	3.5
West Antarctica	85	-15.7	86	-12.7	82	-5.7	81	0.5
East Antarctica	83	-6.4	82	-6.1	81	23.4	68	-2.8
Antarctica	87	-10.8	87	-9.2	85	9.7	76	-1.2

Table C.2: ***Evaluation of regional Antarctic snow accumulation in models used in this study.*** *Statistics of the snow accumulation climatology as simulated by ACCESS1-3, CESM1-LE, CESM2 and NorESM1-M over the 1979–2005 CE period compared to RACMO2.3 over the same period for all the Antarctic regions. Both the ESM/GCM and RACMO2.3 outputs have been linearly interpolated on a* $1.5^\circ \times 2^\circ$ *Gaussian grid to compute the* R^2 *(based on the log values) while the relative bias is computed on each model grid.*

D

List of publications related to the thesis

First author

- Dalaiden, Q., Goosse, H., Klein, F., Lenaerts, J.T.M., Holloway, M., Sime, L., and Thomas, E.R. (2020). How useful is snow accumulation in reconstructing surface air temperature in Antarctica? A study combining ice core records and climate models, *The Cryosphere*, **14**, 1187–1207, https://doi.org/10.5194/tc-14-1187-2020. (Chapter 2)
- Dalaiden, Q., Goosse, H., Rezsohazy, J. and Thomas, E.R. (2021). Reconstructing atmospheric circulation and sea-ice extent in the West Antarctic over the past 200 years using data assimilation, In review in *Climate Dynamics*. (Chapter 3)
- Dalaiden, Q., Goosse, H., Lenaerts, J.T.M., Cavitte, M.G.P. and Henderson, N. (2020). Future Antarctic snow accumulation trend is dominated by atmospheric synoptic-scale events. *Communications Earth & Environment*, **1**(62), https://doi.org/10.1038/s43247-020-00062-x. (Chapter 4)

Co-author

- Goosse, H., Barriat, P.-Y., Dalaiden, Q., Klein, F., Marzeion, B., Maussion, F., Pelucchi, P., and Vlug, A. (2018). Testing the consistency between changes in simulated climate and Alpine glacier length over the past millennium, *Climate of the Past*, **14**, 1119–1133, https://doi.org/10.5194/cp-14-1119-2018.
- Vannitsem, S., Dalaiden, Q. and Goosse, H. (2019). Testing for Dynamical Dependence: Application to the Surface Mass Balance Over Antarctica, *Geophysical Research Letters* ,**46**, 12125–12135.
- Cavitte, M., Dalaiden, Q., Goosse, H., Lenaerts, J.T.M and Thomas, E.R. (2020). Reconciling the surface temperature–surface mass balance rela-

tionship in models and ice cores in Antarctica over the last two centuries, *The Cryosphere*. **14**, 4083–4102.

- Goosse, H., Dalaiden, Q., Cavitte, M. G. P., and Zhang, L. (2021). Can we reconstruct the formation of large open-ocean polynyas in the Southern Ocean using ice core records?, *Climate of the Past*, **17**, 111–131, https://doi.org/10.5194/cp-17-111-20211.

- Crosta, X., Etourneau, J., Orme, L., Dalaiden, Q., Campagne, P., Swingedouw, D., Goosse, H., Massé, G., Miettinen, A., McKay, R., Dunbar, R., Escutia, C. and Ikehara, M. (2021). Multi-decadal trends in Antarctic sea-ice extent driven by ENSO-SAM over the last 2000 years. *Nature Geosciences*, **14**, 156-160, 10.1038/s41561-021-00697-1.

- Ghilain, N., Vannitsem, S., Dalaiden, Q., Goosse, H., De Cruz, L., and Wei, W. (2021). Reconstruction of daily snowfall accumulation at 5.5 km resolution over Dronning Maud Land, Antarctica, from 1850 to 2014 using an analog-based downscaling technique, In review in *Earth System Science Data*, https://doi.org/10.5194/essd-2021-12.

References

Abram, N. J., Henley, B. J., Sen Gupta, A., Lippmann, T. J. R., Clarke, H., Dowdy, A. J., Sharples, J. J., Nolan, R. H., Zhang, T., Wooster, M. J., Wurtzel, J. B., Meissner, K. J., Pitman, A. J., Ukkola, A. M., Murphy, B. P., Tapper, N. J., and Boer, M. M. (2021). Connections of climate change and variability to large and extreme forest fires in southeast Australia. *Communications Earth & Environment*, 2(1).

Abram, N. J., McGregor, H. V., Tierney, J. E., Evans, M. N., McKay, N. P., Kaufman, D. S., Thirumalai, K., Martrat, B., Goosse, H., Phipps, S. J., Steig, E. J., Kilbourne, K. H., Saenger, C. P., Zinke, J., Leduc, G., Addison, J. A., Mortyn, P. G., Seidenkrantz, M. S., Sicre, M. A., Selvaraj, K., Filipsson, H. L., Neukom, R., Gergis, J., Curran, M. A., and Von Gunten, L. (2016). Early onset of industrial-era warming across the oceans and continents. *Nature*, 536(7617):411–418.

Abram, N. J., Mulvaney, R., Vimeux, F., Phipps, S. J., Turner, J., and England, M. H. (2014). Evolution of the Southern Annular Mode during the past millennium. *Nature Climate Change*, 4(7):564–569.

Abram, N. J., Thomas, E. R., McConnell, J. R., Mulvaney, R., Bracegirdle, T. J., Sime, L. C., and Aristarain, A. J. (2010). Ice core evidence for a 20th century decline of sea ice in the Bellingshausen Sea, Antarctica. *Journal of Geophysical Research Atmospheres*, 115(23):1–9.

Abram, N. J., Wolff, E. W., and Curran, M. A. (2013). A review of sea ice proxy information from polar ice cores. *Quaternary Science Reviews*, 79:168–183.

Agosta, C., Amory, C., Kittel, C., Orsi, A., Favier, V., Gallée, H., Van Den Broeke, M. R., Lenaerts, J. T., Van Wessem, J. M., Van De Berg, W. J., and Fettweis, X. (2019). Estimation of the Antarctic surface mass balance using the regional climate model MAR (1979-2015) and identification of dominant processes. *Cryosphere*, 13(1):281–296.

Agosta, C., Fettweis, X., and Datta, R. (2015). Evaluation of the CMIP5 models in the aim of regional modelling of the Antarctic surface mass balance. *The cryosphere*, 9:2311–2032.

Altnau, S., Schlosser, E., Isaksson, E., and Divine, D. (2015). Climatic signals from 76 shallow firn cores in Dronning Maud Land, East Antarctica. *Cryosphere*, 9(3):925–944.

Amrhein, D. E., Hakim, G. J., and Parsons, L. A. (2020). Quantifying Structural Uncertainty in Paleoclimate Data Assimilation With an Application to the Last Millennium. *Geophysical Research Letters*, 47(22):1–22.

Badgeley, J. A., Steig, E. J., Hakim, G. J., and Fudge, T. J. (2020). Greenland temperature and precipitation over the last 20,000 years using data assimilation. *Climate of the Past*, 16:1335–1346.

Bamber, J. L. and Griggs, J. A. (2009). A new 1 km digital elevation model of the Antarctic derived from. pages 101–111.

Bamber, J. L., Westaway, R. M., Marzeion, B., and Wouters, B. (2018). The land ice contribution to sea level during the satellite era. *Environmental Research Letters*, 13(6).

Bentsen, M., Bethke, I., Debernard, J. B., Iversen, T., Kirkevåg, A., Seland, Ø., Drange, H., Roelandt, C., Seierstad, I. A., Hoose, C., and Kristjánsson, J. E. (2013). The norwegian earth system model, noresm1-m – part 1: Description and basic evaluation of the physical climate. *Geoscientific Model Development*, 6(3):687–720.

Bi, D., Dix, M., Marsland, S. J., O'Farrell, S., Rashid, H., Uotila, P., Hirst, A. C., Kowalczyk, E., Golebiewski, M., Sullivan, A., Yan, H., Hanna, N., Franklin, C., Sun, Z., Vohralik, P., Watterson, I., Zhou, X., Fiedler, R., Collier, M., Ma, Y., Noonan, J., Stevens, L., Uhe, P., Zhu, H., Griffies, S., Hill, R., Harris, C., and Puri, K. (2013). The ACCESS Coupled Model: Description, Control Climate and Preliminary Validation. *Australian Meteorological and Oceanographic Journal*, 63:63.

Bintanja, R. (1998). The interaction between drifting snow and atmospheric turbulence. *Annals of Glaciology*, 26:167–173.

Bintanja, R., van Oldenborgh, G. J., Drijfhout, S. S., Wouters, B., and Katsman, C. A. (2013). Important role for ocean warming and increased ice-shelf melt in Antarctic sea-ice expansion. *Nature Geoscience*, 6(5):376–379.

Bracegirdle, T. J. (2013). Climatology and recent increase of westerly winds over the Amundsen Sea derived from six reanalyses. *International Journal of Climatology*, 33(4):843–851.

Bracegirdle, T. J., Holmes, C. R., Hosking, J. S., Marshall, G. J., Osman, M., Patterson, M., and Rackow, T. (2020a). Improvements in Circumpolar Southern Hemisphere Extratropical Atmospheric Circulation in CMIP6 Compared to CMIP5. *Earth and Space Science*, pages 0–2.

Bracegirdle, T. J., Krinner, G., Tonelli, M., Haumann, F. A., Naughten, K. A., Rackow, T., Roach, L. A., and Wainer, I. (2020b). Twenty first century changes in Antarctic and Southern Ocean surface climate in CMIP6. *Atmospheric Science Letters*, (December 2019):1–14.

Brady, E., Stevenson, S., Bailey, D., Liu, Z., Noone, D., Nusbaumer, J., Otto-Bliesner, B. L., Tabor, C., Tomas, R., Wong, T., Zhang, J., and Zhu, J. (2019). The Connected Isotopic Water Cycle in the Community Earth System Model Version 1. *Journal of Advances in Modeling Earth Systems*, 11(8):2547–2566.

Brennan, M. K., Hakim, G. J., and Blanchard-Wrigglesworth, E. (2020). Arctic Sea-Ice Variability During the Instrumental Era. *Geophysical Research Letters*, 47(7):1–9.

Bromwich, D. H. (1988). Snowfall in high southern latitudes. *Reviews of Geophysics*, 26(1):149–168.

Bromwich, D. H., Guo, Z., Bai, L., and Chen, Q. S. (2004). Modeled Antarctic precipitation. Part I: Spatial and temporal variability. *Journal of Climate*, 17(3):427–447.

Bromwich, D. H., Nicolas, J. P., and Monaghan, A. J. (2011). An Assessment of precipitation changes over antarctica and the southern ocean since 1989 in contemporary global reanalyses. *Journal of Climate*, 24(16):4189–4209.

Bromwich, D. H., Nicolas, J. P., Monaghan, A. J., Lazzara, M. A., Keller, L. M., Weidner, G. A., and Wilson, A. B. (2013). Central West Antarctica among the most rapidly warming regions on Earth. *Nature Geoscience*, 6(2):139–145.

Bromwich, D. H., Robasky, F. M., Cullather, R. I., and Van Woert, M. L. (1995). The Atmospheric Hydrologic Cycle over the Southern Ocean and Antarctica from Operational Numerical Analyses. *Monthly Weather Review*, 123(12):3518–3538.

Brown, P. T., Ming, Y., Li, W., and Hill, S. A. (2017). Change in the magnitude and mechanisms of global temperature variability with warming. *Nature Climate Change*, 7(10):743–748.

Cavitte, M., Dalaiden, Q., Goosse, H., Lenaerts, J., and Thomas, E. (2020). Reconciling the surface temperature–surface mass balance relationship in models and ice cores in Antarctica over the last two centuries. *The Cryosphere*, 14:4083–4102.

Church, J., Clark, P., Cazenave, A., Gregory, J., Jevrejeva, S., Levermann, A., Merrifield, M., Milne, G., Nerem, R., Nunn, P., Payne, A., Pfeffer, W., Stammer, D., and A.S., U. (2013). The Physical Science Basis. Contribution of Working Group I to the Fifth Assessment Report of the Intergovernmental Panel on Climate Change [Stocker, T.F., D. Qin, G.-K. Plattner, M. Tignor, S.K. Allen, J. Boschung, A. Nauels, Y. Xia, V. Bex and P.M. Midg. Technical report, Cambridge University Press, Cambridge, United Kingdom and New York, NY, USA.

Clem, K. R., Fogt, R. L., Turner, J., Lintner, B. R., Marshall, G. J., Miller, J. R., and Renwick, J. A. (2020). Record warming at the South Pole during the past three decades. *Nature Climate Change*.

Clem, K. R., Renwick, J. A., and McGregor, J. (2018). Autumn Cooling of Western East Antarctica Linked to the Tropical Pacific. *Journal of Geophysical Research: Atmospheres*, 123(1):89–107.

Clem, K. R., Renwick, J. A., Mcgregor, J., and Fogt, R. L. (2016). The relative influence of ENSO and SAM on Antarctic Peninsula climate.

Comiso, J. C. (2012). Large decadal decline of the arctic multiyear ice cover. *Journal of Climate*, 25(4):1176 – 1193.

Craig, H. (1961). Isotopic variations in meteoric waters. *Science*, 133(3465):1702–1703.

Cullather, R. I., Bromwich, D. H., and Van Woert, M. L. (1998). Spatial and temporal variability of antarctic precipitation from atmospheric methods. *Journal of Climate*, 11(3):334–367.

Dalaiden, Q., Goosse, H., Klein, F., Lenaerts, J. T. M., Holloway, M., Sime, L., and Thomas, E. R. (2020a). How useful is snow accumulation in reconstructing surface air temperature in antarctica? a study combining ice core records and climate models. *The Cryosphere*, 14(4):1187–1207.

Dalaiden, Q., Goosse, H., Lenaerts, J. T., Cavitte, M. G., and Henderson, N. (2020b). Future Antarctic snow accumulation trend is dominated by atmospheric synoptic-scale events. *Nature Communications Earth & Environment*, 1:1–9.

Danabasoglu, G., Lamarque, J. F., Bacmeister, J., Bailey, D. A., DuVivier, A. K., Edwards, J., Emmons, L. K., Fasullo, J., Garcia, R., Gettelman, A., Hannay, C., Holland, M. M., Large, W. G., Lauritzen, P. H., Lawrence, D. M., Lenaerts, J. T., Lindsay, K., Lipscomb, W. H., Mills, M. J., Neale, R., Oleson, K. W., Otto-Bliesner, B., Phillips, A. S., Sacks, W., Tilmes, S., van Kampenhout, L., Vertenstein, M., Bertini, A., Dennis, J., Deser, C., Fischer, C., Fox-Kemper, B., Kay, J. E., Kinnison, D., Kushner, P. J., Larson, V. E., Long, M. C., Mickelson, S., Moore, J. K., Nienhouse, E., Polvani, L., Rasch, P. J., and Strand, W. G. (2020). The Community Earth System Model Version 2 (CESM2). *Journal of Advances in Modeling Earth Systems*, 12(2):1–35.

Danielson, J. and Gesch, D. (2011). Global Multi-resolution Terrain Elevation Data 2010(GMTED2010). *U.S. Geological Survey*, 2010:26.

Dansgaard, W. (1964). Stable isotopes in precipitation. *Tellus*, 16(4):436–468.

Dansgaard, W. and Johnsen, S. J. (1969). A Flow Model and a Time Scale for the Ice Core from Camp Century, Greenland. *Journal of Glaciology*, 8(53):215–223.

Deb, P., Orr, A., Bromwich, D. H., Nicolas, J. P., Turner, J., and Hosking, J. S. (2018). Summer Drivers of Atmospheric Variability Affecting Ice Shelf Thinning in the Amundsen Sea Embayment, West Antarctica. *Geophysical Research Letters*, 45(9):4124–4133.

Dee, D. P., Uppala, S., Simmons, A., Berrisford, P., Poli, P., Kobayashi, S., Andrae, U., Balmaseda, M. A., Balsamo, G., Bauer, P., Bechtold, P., Beljaars, A. C. M., van de Berg, L., Bidlot, J.-R., Bormann, N., Delsol, C., Dragani, R., Fuentes, M., Geer, A., Haimberger, L., Healy, S., Hersbach, H., Hólm, E. V., Isaksen, L., K\r allberg, P. W., Köhler, M., Matricardi, M., McNally, A., Monge-Sanz, B. M., Morcrette, J.-J., Peubey, C., Rosnay, P. D., Tavolato, C., Thepaut, J.-J., and Vitart, F. (2011). The ERA-Interim reanalysis: Configuration and performance of the data assimilation system. *Quarterly Journal of the Royal Meteorological Society*, 137:553–597.

Dee, S., Emile-Geay, J., Evans, M. N., Allam, A., Steig, E. J., and Thompson, D. (2015). Prysm: An open-source framework for proxy system modeling, with applications to oxygen-isotope systems. *Journal of Advances in Modeling Earth Systems*, 7(3):1220–1247.

Depoorter, M. A., Bamber, J. L., Griggs, J. A., Lenaerts, J. T. M., Ligtenberg, S. R. M., van den Broeke, M. R., and Moholdt, G. (2013). Calving fluxes and basal melt rates of Antarctic ice shelves. *Nature*, 502:89.

Déry, S. J. and Yau, M. K. (1999). A Bulk Blowing Snow Model. *Boundary-Layer Meteorology*, 93(2):237–251.

Ding, Q., Steig, E. J., Battisti, D. S., and Küttel, M. (2011). Winter warming in West Antarctica caused by central tropical Pacific warming. *Nature Geoscience*, 4(6):398–403.

Donat-Magnin, M., Jourdain, N. C., Spence, P., Le Sommer, J., Gallée, H., and Durand, G. (2017). Ice-Shelf Melt Response to Changing Winds and Glacier Dynamics in the Amundsen Sea Sector, Antarctica. *Journal of Geophysical Research: Oceans*, 122(12):10206–10224.

Dotto, T. S., Naveira Garabato, A. C., Wåhlin, A. K., Bacon, S., Holland, P. R., Kimura, S., Tsamados, M., Herraiz-Borreguero, L., Kalén, O., and Jenkins, A. (2020). Control of the Oceanic Heat Con-

tent of the Getz-Dotson Trough, Antarctica, by the Amundsen Sea Low. *Journal of Geophysical Research: Oceans*, 125(8).

Dubinkina, S., Goosse, H., Sallaz-Damaz, Y., Crespin, E., and Crucifix, M. (2011). Testing a Particle Filter To Reconstruct Climate Changes Over the Past Centuries. *International Journal of Bifurcation and Chaos*, 21(12):3611–3618.

Dufrêne, E., Davi, H., François, C., le Maire, G., Dantec, V. L., and Granier, A. (2005). Modelling carbon and water cycles in a beech forest: Part I: Model description and uncertainty analysis on modelled NEE. *Ecological Modelling*, 185(2):407–436.

Dufresne, J.-L., Foujols, M.-A., Denvil, S., Caubel, A., Marti, O., Aumont, O., Balkanski, Y., Bekki, S., Bellenger, H., Benshila, R., Bony, S., Bopp, L., Braconnot, P., Brockmann, P., Cadule, P., Cheruy, F., Codron, F., Cozic, A., Cugnet, D., de Noblet, N., Duvel, J.-P., Ethé, C., Fairhead, L., Fichefet, T., Flavoni, S., Friedlingstein, P., Grandpeix, J.-Y., Guez, L., Guilyardi, E., Hauglustaine, D., Hourdin, F., Idelkadi, A., Ghattas, J., Joussaume, S., Kageyama, M., Krinner, G., Labetoulle, S., Lahellec, A., Lefebvre, M.-P., Lefevre, F., Levy, C., Li, Z. X., Lloyd, J., Lott, F., Madec, G., Mancip, M., Marchand, M., Masson, S., Meurdesoif, Y., Mignot, J., Musat, I., Parouty, S., Polcher, J., Rio, C., Schulz, M., Swingedouw, D., Szopa, S., Talandier, C., Terray, P., Viovy, N., and Vuichard, N. (2013). Climate change projections using the IPSL-CM5 Earth System Model: from CMIP3 to CMIP5. *Climate Dynamics*, 40(9):2123–2165.

Dutrieux, P., Stewart, C., Jenkins, A., Nicholls, K. W., Corr, H. F., Rignot, E., and Steffen, K. (2014). Basal terraces on melting ice shelves. *Geophysical Research Letters*, 41(15):5506–5513.

ECMWF (2008). Part IV : Physical Processes (CY33R1). Technical report.

ECMWF (2021). Copernicus: 2020 warmest year on record for europe; globally, 2020 ties with 2016 for warmest year recorded. https://climate.copernicus.eu/copernicus-2020-warmest-year-record-europe-globally-2020-ties-2016-warmest-year-recorded.

Emile-Geay, J., McKay, N. P., Kaufman, D. S., von Gunten, L., Wang, J., Anchukaitis, K. J., Abram, N. J., Addison, J. A., Curran, M. A. J., Evans, M. N., Henley, B. J., Hao, Z., Martrat, B., McGregor, H. V., Neukom, R., Pederson, G. T., Stenni, B., Thirumalai, K., Werner, J. P., Xu, C., Divine, D. V., Dixon, B. C., Gergis, J., Mundo, I. A., Nakatsuka, T., Phipps, S. J., Routson, C. C., Steig, E. J., Tierney, J. E., Tyler, J. J., Allen, K. J., Bertler, N. A. N., Björklund, J., Chase, B. M., Chen, M.-T., Cook, E., de Jong, R., DeLong, K. L., Dixon, D. A., Ekaykin, A. A., Ersek, V., Filipsson, H. L., Francus, P., Freund, M. B., Frezzotti, M., Gaire, N. P., Gajewski, K., Ge, Q., Goosse, H., Gornostaeva, A., Grosjean, M., Horiuchi, K., Hormes, A., Husum, K., Isaksson, E., Kandasamy, S., Kawamura, K., Kilbourne, K. H., Koç, N., Leduc, G., Linderholm, H. W., Lorrey, A. M., Mikhalenko, V., Mortyn, P. G., Motoyama, H., Moy, A. D., Mulvaney, R., Munz, P. M., Nash, D. J., Oerter, H., Opel, T., Orsi, A. J., Ovchinnikov, D. V., Porter, T. J., Roop, H. A., Saenger, C., Sano, M., Sauchyn, D., Saunders, K. M., Seidenkrantz, M.-S., Severi, M., Shao, X., Sicre, M.-A., Sigl, M., Sinclair, K., St. George, S., St. Jacques, J.-M., Thamban, M., Kuwar Thapa, U., Thomas, E. R., Turney, C., Uemura, R., Viau, A. E., Vladimirova, D. O., Wahl, E. R., White, J. W. C., Yu, Z., and Zinke, J. (2017). A global multiproxy database for temperature reconstructions of the Common Era. *Scientific data*, 4(July):170088.

England, M. R., Polvani, L. M., Smith, K. L., Landrum, L., and Holland, M. M. (2016). Robust response of the Amundsen Sea Low to stratospheric ozone depletion. *Geophysical Research Letters*, 43(15):8207–8213.

Epstein, S., , and Mayeda, T. (1953). Variation of o18 content of waters from natural sources. *Geochimica et Cosmochimica Acta*, 4(5):213–224.

Ettema, J., van den Broeke, M. R., van Meijgaard, E., van den Berg, W. J., Box, J. E., and Steffen, K. (2010). Climate of the greenland ice sheet using a high - resolution climate model - part 1 : evaluation. *The cryosphere*, (4):511–527.

Evans, M. N., Tolwinski-Ward, S. E., Thompson, D. M., and Anchukaitis, K. J. (2013). Applications of proxy system modeling in high resolution paleoclimatology. *Quaternary Science Reviews*, 76:16–28.

Fan, T., Deser, C., and Schneider, D. (2014). Recent Antarctic sea ice trends in the context of Southern Ocean surface climate variations since 1950. *Geophysical Research Letters*, 41:2419–2426.

Favier, V., Agosta, C., Parouty, S., Durand, G., Delaygue, G., Gallée, H., Drouet, A. S., Trouvilliez, A., and Krinner, G. (2013). An updated and quality controlled surface mass balance dataset for Antarctica. *Cryosphere*, 7(2):583–597.

Fisher, D. A., Reeh, N., and Clausen, H. (1985). Stratigraphic Noise in Time Series Derived from Ice Cores. *Annals of Glaciology*, 7:76–83.

Fogt, R. L., Bromwich, D. H., and Hines, K. M. (2011). Understanding the SAM influence on the South Pacific ENSO teleconnection. *Climate Dynamics*, 36(7):1555–1576.

Fogt, R. L. and Marshall, G. J. (2020). The Southern Annular Mode: Variability, trends, and climate impacts across the Southern Hemisphere. *WIREs Climate Change*, n/a(n/a):e652.

Fogt, R. L., Perlwitz, J., Monaghan, A. J., Bromwich, D. H., Jones, J. M., and Marshall, G. J. (2009). Historical SAM variability. Part II: Twentieth-century variability and trends from reconstructions, Observations, and the IPCC AR4 models. *Journal of Climate*, 22(20):5346–5365.

Fogt, R. L., Schneider, D. P., Goergens, C. A., Jones, J. M., Clark, L. N., and Garberoglio, M. J. (2019). Seasonal Antarctic pressure variability during the twentieth century from spatially complete reconstructions and CAM5 simulations. *Climate Dynamics*, 53(3):1435–1452.

Fogt, R. L. and Wovrosh, A. J. (2015). The relative influence of tropical sea surface temperatures and radiative forcing on the Amundsen Sea Low. *Journal of Climate*, 28(21):8540–8555.

Fogt, R. L., Wovrosh, A. J., Langen, R. A., and Simmonds, I. (2012). The characteristic variability and connection to the underlying synoptic activity of the Amundsen-Bellingshausen Seas Low. *Journal of Geophysical Research Atmospheres*, 117(7):1–22.

Fretwell, P., Pritchard, H. D., Vaughan, D. G., Bamber, J. L., Barrand, N. E., Bell, R., Bianchi, C., Bingham, R. G., Blankenship, D. D., Casassa, G., Catania, G., Callens, D., Conway, H., Cook, A. J., Corr, H. F., Damaske, D., Damm, V., Ferraccioli, F., Forsberg, R., Fujita, S., Gim, Y., Gogineni, P., Griggs, J. A., Hindmarsh, R. C., Holmlund, P., Holt, J. W., Jacobel, R. W., Jenkins, A., Jokat, W., Jordan, T., King, E. C., Kohler, J., Krabill, W., Riger-Kusk, M., Langley, K. A., Leitchenkov, G., Leuschen, C., Luyendyk, B. P., Matsuoka, K., Mouginot, J., Nitsche, F. O., Nogi, Y., Nost, O. A., Popov, S. V., Rignot, E., Rippin, D. M., Rivera, A., Roberts, J., Ross, N., Siegert, M. J., Smith, A. M., Steinhage, D., Studinger, M., Sun, B., Tinto, B. K., Welch, B. C., Wilson, D., Young, D. A., Xiangbin, C., and Zirizzotti, A. (2013). Bedmap2: Improved ice bed, surface and thickness datasets for Antarctica. *Cryosphere*, 7(1):375–393.

Frezzotti, M., Scarchilli, C., Becagli, S., Proposito, M., and Urbini, S. (2013). A synthesis of the Antarctic surface mass balance during the last 800 yr. *Cryosphere*, 7(1):303–319.

Frezzotti, M., Urbini, S., Proposito, M., Scarchilli, C., and Gandolfi, S. (2007). Spatial and temporal variability of surface mass balance near Talos Dome, East Antarctica. *Journal of Geophysical Research: Earth Surface*, 112(2).

Frieler, K., Clark, P. U., He, F., Buizert, C., Reese, R., Ligtenberg, S. R., Van Den Broeke, M. R., Winkelmann, R., and Levermann, A. (2015). Consistent evidence of increasing Antarctic accumulation with warming. *Nature Climate Change*, 5(4):348–352.

Fudge, T. J., Markle1, B. R., Cuffey, K. M., Buizert, C., Taylor4, K. C., Steig, E. J., Waddington, E. D., Conway, H., and Koutnik, M. (2016). Variable relationship between accumulation and temperature in West Antarctica for the past 31,000 years. *Geophysical Research Letters*, 43:3795–3803.

Fyke, J., Lenaerts, J. T., and Wang, H. (2017). Basin-scale heterogeneity in Antarctic precipitation and its impact on surface mass variability. *Cryosphere*, 11(6):2595–2609.

Fyke, J., Sergienko, O., Löfverström, M., Price, S., and Lenaerts, J. T. (2018). An Overview of Interactions and Feedbacks Between Ice Sheets and the Earth System. *Reviews of Geophysics*, 56(2):361–408.

Galewsky, J., Steen-Larsen, H. C., Field, R. D., Worden, J., Risi, C., and Schneider, M. (2016). Stable isotopes in atmospheric water vapor and applications to the hydrologic cycle. *Reviews of Geophysics*, 54(4):809–865.

Gallée, H. and Schayes, G. (1994). Development of a Three-Dimensional Meso-γ Primitive Equation Model: Katabatic Winds Simulation in the Area of Terra Nova Bay, Antarctica. *Monthly Weather Review*, 122(4):671–685.

Gent, P. R., Danabasoglu, G., Donner, L. J., Holland, M. M., Hunke, E. C., Jayne, S. R., Lawrence, D. M., Neale, R. B., Rasch, P. J., Vertenstein, M., Worley, P. H., Yang, Z. L., and Zhang, M. (2011). The community climate system model version 4. *Journal of Climate*, 24(19):4973–4991.

Genthon, C., Krinner, G., and Castebrunet, H. (2009). Antarctic precipitation and climate-change predictions: horizontal resolution and margin vs plateau issues. *Annals of Glaciology*, 50(50):55–60.

Gettelman, A., Hannay, C., Bacmeister, J. T., Neale, R. B., Pendergrass, A. G., Danabasoglu, G., Lamarque, J.-F., Fasullo, J. T., Bailey, D. A., Lawrence, D. M., and Mills, M. J. (2019). High climate sensitivity in the community earth system model version 2 (cesm2). *Geophysical Research Letters*, 46(14):8329–8337.

Gong, D. and Wang, S. (1999). Definition of Antarctic oscillation index. *Geophysical Research Letters*, 26(4):459–462.

Goodwin, B. P., Mosley-Thompson, E., Wilson, A. B., Porter, S. E., and Roxana Sierra-Hernandez, M. (2015). Accumulation variability in the Antarctic Peninsula: The role of large-scale atmospheric oscillations and their interactions*. *Journal of Climate*, 29(7):2579–2596.

Goodwin, B. P., Mosley-Thompson, E., Wilson, A. B., Porter, S. E., and Roxana Sierra-Hernandez, M. (2016). Accumulation variability in the Antarctic Peninsula: The role of large-scale atmospheric oscillations and their interactions*. *Journal of Climate*, 29(7):2579–2596.

Goosse, H. (2015). *Climate System Dynamics and Modelling*. Cambridge University Press.

Goosse, H. (2017). Reconstructed and simulated temperature asymmetry between continents in both hemispheres over the last centuries. *Climate Dynamics*, 48(5-6):1483–1501.

Goosse, H., Braida, M., Crosta, X., Mairesse, A., Masson-Delmotte, V., Mathiot, P., Neukom, R., Oerter, H., Philippon, G., Renssen, H., Stenni, B., van Ommen, T., and Verleyen, E. (2012). Antarctic temperature changes during the last millennium: evaluation of simulations and reconstructions. *Quaternary Science Reviews*, 55:75–90.

Goosse, H., Crespin, E., de Montety, A., Mann, M. E., Renssen, H., and Timmermann, A. (2010). Reconstructing surface temperature changes over the past 600 years using climate model simulations with data assimilation. *Journal of Geophysical Research*, 115(D9):D09108.

Goosse, H., Dalaiden, Q., Cavitte, M., and Zhang, L. (2021). Can we reconstruct the formation of large open ocean polynyas in the Southern Ocean using ice core records? *Climate of the Past*, 17:111–131.

Goosse, H., Kay, J. E., Armour, K. C., Bodas-Salcedo, A., Chepfer, H., Docquier, D., Jonko, A., Kushner, P. J., Lecomte, O., Massonnet, F., Park, H. S., Pithan, F., Svensson, G., and Vancoppenolle, M. (2018). Quantifying climate feedbacks in polar regions. *Nature Communications*, 9(1).

Goosse, H., Lefebvre, W., de Montety, A., Crespin, E., and Orsi, A. H. (2009). Consistent past half-century trends in the atmosphere, the sea ice and the ocean at high southern latitudes. *Climate Dynamics*, 33(7-8):999–1016.

Gorodetskaya, I. V., Tsukernik, M., Claes, K., Ralph, M. F., Neff, W. D., and Van Lipzig, N. P. M. (2014). The role of atmospheric rivers in anomalous snow accumulation in East Antarctica. *Geophysical Research Letters*, 41(17):6199–6206.

Gossart, A., Helsen, S., Lenaerts, J. T., Vanden Broucke, S., van Lipzig, N. P., and Souverijns, N. (2019a). An evaluation of surface climatology in state-of-the-art reanalyses over the Antarctic Ice Sheet. *Journal of Climate*, 32(20):6899–6915.

Gossart, A., Helsen, S., Lenaerts, J. T. M., Broucke, S. V., van Lipzig, N. P. M., and Souverijns, N. (2019b). An Evaluation of Surface Climatology in State-of-the-Art Reanalyses over the Antarctic Ice Sheet. *Journal of Climate*, 32(20):6899–6915.

Goursaud, S., Masson-Delmotte, V., Favier, V., Orsi, A., and Werner, M. (2018). Water stable isotopes spatio-temporal variability in Antarctica in 1960–2013: observations and simulations

from the ECHAM5-wiso atmospheric general circulation model. *Climate of the Past Discussions*, 14:923–946.

Goursaud, S., Masson-Delmotte, V., Favier, V., Preunkert, S., Legrand, M., Minster, B., and Werner, M. (2019). Challenges associated with the climatic interpretation of water stable isotope records from a highly resolved firn core from Adélie Land, coastal Antarctica. *The Cryosphere*, 13:1297–1324.

Greuell, W. and Thomas, K. (1994). Numerical modelling of the energy balance and the englacial temperature of the Greenland Ice Sheet. Calculations for the ETH-Camp location (West Greenland, 1155 m a.s.l.). *Global and Planetary Change*, 9(1):91–114.

Grieger, J., Leckebusch, G. C., and Ulbrich, U. (2016). Net precipitation of Antarctica: Thermodynamical and dynamical parts of the climate change signal. *Journal of Climate*, 29(3):907–924.

Guiot, J., Boucher, E., and Gea-Izquierdo, G. (2014). Process models and model-data fusion in dendroecology. *Frontiers in Ecology and Evolution*, 2:52.

Hakim, G. J., Emile-Geay, J., Steig, E. J., Noone, D., Anderson, D. M., Tardif, R., Steiger, N., and Perkins, W. A. (2016). The last millennium climate reanalysis project: Framework and first results. *Journal of Geophysical Research*, 121(12):6745–6764.

Hanna, E. (2001). Anomalous peak in antarctic sea-ice area, winter 1998, coincident with enso. *Geophysical Research Letters*, 28(8):1595–1598.

Hansen, J., Ruedy, M., Sato, M., and Lo, K. (2010). Global surface temperature change. *Reviews of Geophysics*, 48:1–29.

Held, I. M. and Soden, B. J. (2006). Robust Responses of the Hydrological Cycle to Global Warming. *J. Clim.*, 19(21):5686.

Herron, M. M. (1982). Impurity sources Of F-, Cl-, NO3- and SO4 2- in Greenland and Antarctic precipitation. *Journal of Geophysical Research: Oceans*, 87(C4):3052–3060.

Hersbach, H., Bell, B., Berrisford, P., Hirahara, S., Horányi, A., Muñoz-Sabater, J., Nicolas, J., Peubey, C., Radu, R., Schepers, D., Simmons, A., Soci, C., Abdalla, S., Abellan, X., Balsamo, G., Bechtold, P., Biavati, G., Bidlot, J., Bonavita, M., De Chiara, G., Dahlgren, P., Dee, D., Diamantakis, M., Dragani, R., Flemming, J., Forbes, R., Fuentes, M., Geer, A., Haimberger, L., Healy, S., Hogan, R. J., Hólm, E., Janisková, M., Keeley, S., Laloyaux, P., Lopez, P., Lupu, C., Radnoti, G., de Rosnay, P., Rozum, I., Vamborg, F., Villaume, S., and Thépaut, J. N. (2020). The ERA5 global reanalysis. *Quarterly Journal of the Royal Meteorological Society*, 146(730):1999–2049.

Holland, P. R., Bracegirdle, T. J., Dutrieux, P., Jenkins, A., and Steig, E. J. (2019). West Antarctic ice loss influenced by internal climate variability and anthropogenic forcing. *Nature Geoscience*.

Holloway, M. D., Sime, L. C., Singarayer, J. S., Tindall, J. C., Bunch, P., and Valdes, P. J. (2016a). Antarctic last interglacial isotope peak in response to sea ice retreat not ice-sheet collapse. *Nature Communications*, 7:1–9.

Holloway, M. D., Sime, L. C., Singarayer, J. S., Tindall, J. C., and Valdes, P. J. (2016b). Reconstructing paleosalinity from δ18O: Coupled model simulations of the Last Glacial Maximum, Last Interglacial and Late Holocene. *Quaternary Science Reviews*, 131:350–364.

Hooke, R. L. (2005). *Principles of Glacier Mechanics*. Cambridge University Press, 2 edition.

Hosking, J. S., Orr, A., Marshall, G. J., Turner, J., and Phillips, T. (2013). The influence of the amundsen-bellingshausen seas low on the climate of West Antarctica and its representation in coupled climate model simulations. *Journal of Climate*, 26(17):6633–6648.

Huang, B., Thorne, P. W., Banzon, V. F., Boyer, T., Chepurin, G., Lawrimore, J. H., Menne, M. J., Smith, T. M., Vose, R. S., and Zhang, H.-M. (2017). Extended Reconstructed Sea Surface Temperature, Version 5 (ERSSTv5): Upgrades, Validations, and Intercomparisons. *Journal of Climate*, 30(20):8179–8205.

Huybrechts, P., Gregory, J., Janssens, I., and Wild, M. (2004). Modelling Antarctic and Greenland volume changes during the 20th and 21st centuries forced by GCM time slice integrations. *Global and Planetary Change*, 42(1-4):83–105.

IPCC (2019). IPCC Special Report on the Ocean and Cryosphere in a Changing Climate [H.-O. Pörtner, D.C. Roberts, V. Masson-Delmotte, P. Zhai, M. Tignor, E. Poloczanska, K. Mintenbeck, A. Alegría, M. Nicolai, A. Okem, J. Petzold, B. Rama, N.M. Weyer (eds.)]. *In press*.

Jacobs, S. S., Jenkins, A., Giulivi, C. F., and Dutrieux, P. (2011). Stronger ocean circulation and increased melting under Pine Island Glacier ice shelf. *Nature Geoscience*, 4(8):519–523.

Janjić, T., Bormann, N., Bocquet, M., Carton, J. A., Cohn, S. E., Dance, S. L., Losa, S. N., Nichols, N. K., Potthast, R., Waller, J. A., and Weston, P. (2018). On the representation error in data assimilation. *Quarterly Journal of the Royal Meteorological Society*, 144(713):1257–1278.

Jones, J. M., Gille, S. T., Goosse, H., Abram, N. J., Canziani, P. O., Charman, D. J., Clem, K. R., Crosta, X., De Lavergne, C., Eisenman, I., England, M. H., Fogt, R. L., Frankcombe, L. M., Marshall, G. J., Masson-Delmotte, V., Morrison, A. K., Orsi, A. J., Raphael, M. N., Renwick, J. A., Schneider, D. P., Simpkins, G. R., Steig, E. J., Stenni, B., Swingedouw, D., and Vance, T. R. (2016). Assessing recent trends in high-latitude Southern Hemisphere surface climate. *Nature Climate Change*, 6(10):917–926.

Jones, M. E., Bromwich, D. H., Nicolas, J. P., Carrasco, J., Plavcová, E., Zou, X., and Wang, S.-H. (2019). Sixty Years of Widespread Warming in the Southern Mid- and High-Latitudes (1957-2016). *Journal of Climate*, pages 6875–6898.

Jouzel, J. (2003). Magnitude of isotope/temperature scaling for interpretation of central Antarctic ice cores. *Journal of Geophysical Research*, 108(D12):4361.

Jouzel, J., Alley, R. B., Cuffey, K. M., Dansgaard, W., Grootes, P., Hoffmann, G., Johnsen, S. J., Koster, R. D., Peel, D., Shuman, C. A., Stievenard, M., Stuiver, M., and White, J. (1997). Validity of the temperature reconstruction from ice cores. *Journal of Geophysical Research*, 102(C12):26471–26487.

Jun, S. Y., Kim, J. H., Choi, J., Kim, S. J., Kim, B. M., and An, S. I. (2020). The internal origin of the west-east asymmetry of Antarctic climate change. *Science Advances*, 6(24):1–9.

Kay, J. E., Deser, C., Phillips, A., Mai, A., Hannay, C., Strand, G., Arblaster, J. M., Bates, S. C., Danabasoglu, G., Edwards, J., Holland, M., Kushner, P., Lamarque, J. F., Lawrence, D., Lindsay, K., Middleton, A., Munoz, E., Neale, R., Oleson, K., Polvani, L., and Vertenstein, M. (2015). The community earth system model (CESM) large ensemble project : A community resource for studying climate change in the presence of internal climate variability. *Bulletin of the American Meteorological Society*, 96(8):1333–1349.

King, M. A. and Watson, C. S. (2020). Antarctic surface mass balance: Natural variability, noise, and detecting new trends. *Geophysical Research Letters*, 47(12):e2020GL087493. e2020GL087493 2020GL087493.

Kittel, C., Amory, C., Agosta, C., Delhasse, A., Doutreloup, S., Huot, P. V., Wyard, C., Fichefet, T., and Fettweis, X. (2018). Sensitivity of the current Antarctic surface mass balance to sea surface conditions using MAR. *Cryosphere*, 12(12):3827–3839.

Kittel, C., Amory, C., Agosta, C., Jourdain, N. C., Hofer, S., Delhasse, A., Doutreloup, S., Huot, P.-V., Lang, C., Fichefet, T., and Fettweis, X. (2021). Diverging future surface mass balance between the antarctic ice shelves and grounded ice sheet. *The Cryosphere*, 15(3):1215–1236.

Klein, F., Abram, N. J., Curran, M. A. J., Goosse, H., Goursaud, S., Masson-Delmotte, V., Moy, A., Neukom, R., Orsi, A., Sjolte, J., Steiger, N., Stenni, B., and Werner, M. (2019). Assessing the robustness of Antarctic temperature reconstructions over the past two millennia using pseudoproxy and data assimilation experiments. *Climate of the Past*, 15:661–684.

Klein, F. and Goosse, H. (2018). Reconstructing East African rainfall and Indian Ocean sea surface temperatures over the last centuries using data assimilation. *Climate Dynamics*, 50(11-12):3909–3929.

Krinner, G., Guicherd, B., Ox, K., Genthon, C., and Magand, O. (01 Mar. 2008). Influence of oceanic boundary conditions in simulations of antarctic climate and surface mass balance change during the coming century. *Journal of Climate*, 21(5):938 – 962.

Krinner, G., Largeron, C., Ménégoz, M., Agosta, C., and Brutel-Vuilmet, C. (2014). Oceanic forcing of Antarctic climate change: A study using a stretched-grid atmospheric general circulation model. *Journal of Climate*, 27(15):5786–5800.

Krinner, G., Magand, O., Simmonds, I., Genthon, C., Dufresne, J.-l., Krinner, G., Magand, O., Simmonds, I., Genthon, C., and Simulated, J.-l. D. (2007). Simulated antarctic precipitation and surface mass balance of the end of the 20th and 21st centuries To cite this version : HAL Id : hal-00184741 Simulated Antarctic precipitation and surface mass balance at. *Climate Dynamics*, 28:215–230.

Kuipers Munneke, P., Picard, G., Van Den Broeke, M. R., Lenaerts, J. T., and Van Meijgaard, E. (2012). Insignificant change in Antarctic snowmelt volume since 1979. *Geophysical Research Letters*, 39(1):6–10.

Lachlan-Cope, T. A., Connolley, W. M., and Turner, J. (2001). The Role of the Non-Axisymmetric Antarctic Orography in forcing the Observed Pattern of Variability of the Antarctic Climate. *Geophysical Research Letters*, 28(21):4111–4114.

Laepple, T., Münch, T., Casado, M., Hoerhold, M., Landais, A., and Kipfstuhl, S. (2018). On the similarity and apparent cycles of isotopic variations in East Antarctic snow pits. *Cryosphere*, 12(1):169–187.

Landrum, L. L., Holland, M. M., Raphael, M. N., and Polvani, L. M. (2017). Stratospheric Ozone Depletion: An Unlikely Driver of the Regional Trends in Antarctic Sea Ice in Austral Fall in the Late Twentieth Century. *Geophysical Research Letters*, 44(21):11,062–11,070.

Lefebvre, W. and Goosse, H. (2008). An analysis of the atmospheric processes driving the large-scale winter sea ice variability in the Southern Ocean. *Journal of Geophysical Research: Oceans*, 113(2):1–15.

Legrand, M. and Mayewski, P. (1997). Glaciochemistry of polar ice cores: A review. *Reviews of Geophysics*, 35(3):219–243.

Lenaerts, J. T., Brown, J., Van Den Broeke, M. R., Matsuoka, K., Drews, R., Callens, D., Philippe, M., Gorodetskaya, I., Van Meijgaard, E., Reijmer, C. H., Pattyn, F., and Van Lipzig, N. P. (2014). High variability of climate and surface mass balance induced by Antarctic ice rises. *Journal of Glaciology*, 60(224):1101–1110.

Lenaerts, J. T., Fyke, J. G., and Medley, B. (2018). The signature of ozone depletion in recent Antarctic precipitation change: a study with the Community Earth System Model. *Geophys. Res. Lett.*, 45:12931—-12939.

Lenaerts, J. T., Medley, B., Broeke, M. R., and Wouters, B. (2019). Observing and Modeling Ice-Sheet Surface Mass Balance. *Reviews of Geophysics*, pages 1–45.

Lenaerts, J. T., Van Meijgaard, E., Van Den Broeke, M. R., Ligtenberg, S. R., Horwath, M., and Isaksson, E. (2013). Recent snowfall anomalies in Dronning Maud Land, East Antarctica, in a historical and future climate perspective. *Geophysical Research Letters*, 40(11):2684–2688.

Lenaerts, J. T., Vizcaino, M., Fyke, J., van Kampenhout, L., and van den Broeke, M. R. (2016). Present-day and future Antarctic ice sheet climate and surface mass balance in the Community Earth System Model. *Climate Dynamics*, 47(5-6):1367–1381.

Lenaerts, J. T. M., Ligtenberg, S. R. M., Medley, B., Van de Berg, W. J., Konrad, H., Nicolas, J. P., Van Wessem, J. M., Trusel, L. D., Mulvaney, R., Tuckwell, R. J., Hogg, A. E., and Thomas, E. R. (2017). Climate and surface mass balance of coastal West Antarctica resolved by regional climate modelling. *Annals of Glaciology*, pages 1–13.

Lenaerts, J. T. M., van den Broeke, M. R., Déry, S. J., König-Langlo, G., Ettema, J., and Munneke, P. K. (2010). Modelling snowdrift sublimation on an Antarctic ice shelf. *The Cryosphere*, 4(2):179–190.

Lenaerts, J. T. M., Van Den Broeke, M. R., Van De Berg, W. J., Van Meijgaard, E., and Kuipers Munneke, P. (2012). A new, high-resolution surface mass balance map of Antarctica (1979-2010) based on regional atmospheric climate modeling. *Geophysical Research Letters*, 39(4):1–5.

Levine, J. G., Yang, X., Jones, A. E., and Wolff, E. W. (2014). Sea salt as an ice core proxy for past sea ice extent: A process-based model study. *Journal of Geophysical Research: Atmospheres*, 119(9):5737–5756.

Ligtenberg, S. R. M., van de Berg, W. J., van den Broeke, M. R., Rae, J. G. L., and van Meijgaard, E. (2013). Future surface mass balance of the Antarctic ice sheet and its influence on sea level change, simulated by a regional atmospheric climate model. *Climate Dynamics*, 41(3-4):867–884.

Magand, O., Picard, G., Brucker, L., Fily, M., and Genthon, C. (2008). Snow melting bias in microwave mapping of Antarctic snow accumulation. *The Cryosphere*, pages 109–115.

Mankoff, K. D., Jacobs, S. S., Tulaczyk, S. M., and Stammerjohn, S. E. (2012). The role of pine island glacier ice shelf basal channels in deep-water upwelling, polynyas and ocean circulation in pine island bay, antarctica. *Annals of Glaciology*, 53(60):123–128.

Marshall, G. J. (2003). Trends in the Southern Annular Mode from Observations and Reanalyses. *Journal of Climate*, 16(1999):4134–4143.

Marshall, G. J. and Thompson, D. W. (2016). The signatures of large-scale patterns of atmospheric variability in Antarctic surface temperatures. *Journal of Geophysical Research*, 121(7):3276–3289.

Marshall, G. J., Thompson, D. W., and van den Broeke, M. R. (2017). The Signature of Southern Hemisphere Atmospheric Circulation Patterns in Antarctic Precipitation. *Geophysical Research Letters*, 44(22):11,580–11,589.

Marshall, J. and Plumb, A. (2007). *Atmosphere, Ocean and Climate Dynamics. International Geophysics*. Academic Press.

Marzeion, B., Cogley, J. G., Richter, K., and Parkes, D. (2014). Attribution of global glacier mass loss to anthropogenic and natural causes. *Science*, 345(6199):919–921.

Masson-Delmotte, V., Hou, S., Ekaykin, A., Jouzel, J., Aristarain, A., Bernardo, R. T., Bromwich, D., Cattani, O., Delmotte, M. M., Falourd, S., Frezzotti, M., Gallée, H., Genoni, L., Isaksson, E., Landais, A., Helsen, M. M., Hoffmann, G., Lopez, J., Morgan, V., Motoyama, H., Noone, D., Oerter, H., Petit, J. R., Royer, A., Uemura, R., Schmidt, G. A., Schlosser, E., Simões, J. C., Steig, E. J., Stenni, B., Stievenard, M., Van Den Broeke, M. R., Van De Wal, R. S., Van De Berg, W. J., Vimeux, F., and White, J. W. (2008). A review of antarctic surface snow isotopic composition: Observations, atmospheric circulation, and isotopic modeling. *Journal of Climate*, 21(13):3359–3387.

Masson-Delmotte, V., Kageyama, M., Braconnot, P., Charbit, S., Krinner, G., Ritz, C., Guilyardi, E., Jouzel, J., Abe-Ouchi, A., Crucifix, M., Gladstone, R. M., Hewitt, C. D., Kitoh, A., LeGrande, A. N., Marti, O., Merkel, U., Motoi, T., Ohgaito, R., Otto-Bliesner, B., Peltier, W. R., Ross, I., Valdes, P. J., Vettoretti, G., Weber, S. L., Wolk, F., and Yu, Y. (2006). Past and future polar amplification of climate change: Climate model intercomparisons and ice-core constraints. *Climate Dynamics*, 26(5):513–529.

Matsikaris, A., Widmann, M., and Jungclaus, J. (2015). On-line and off-line data assimilation in palaeoclimatology: A case study. *Climate of the Past*, 11(1):81–93.

Matsuoka, K., Hindmarsh, R. C., Moholdt, G., Bentley, M. J., Pritchard, H. D., Brown, J., Conway, H., Drews, R., Durand, G., Goldberg, D., Hattermann, T., Kingslake, J., Lenaerts, J. T., Martín, C., Mulvaney, R., Nicholls, K. W., Pattyn, F., Ross, N., Scambos, T., and Whitehouse, P. L. (2015). Antarctic ice rises and rumples: Their properties and significance for ice-sheet dynamics and evolution. *Earth-Science Reviews*, 150:724–745.

Mayewski, P. A., Carleton, A. M., Birkel, S. D., Dixon, D., Kurbatov, A. V., Korotkikh, E., McConnell, J., Curran, M., Cole-Dai, J., Jiang, S., Plummer, C., Vance, T., Maasch, K. A., Sneed, S. B., and Handley, M. (2017). Ice core and climate reanalysis analogs to predict Antarctic and Southern Hemisphere climate changes. *Quaternary Science Reviews*, 155:50–66.

McConnell, J. R., Lamorey, G. W., Lambert, S. W., and Taylor, K. C. (2002). Continuous Ice-Core Chemical Analyses Using Inductively Coupled Plasma Mass Spectrometry. *Environmental Science & Technology*, 36(1):7–11.

Medley, B., Joughin, I., Smith, B. E., Das, S. B., Steig, E. J., Conway, H., Gogineni, S., Lewis, C., Criscitiello, A. S., McConnell, J. R., Van Den Broeke, M. R., Lenaerts, J. T., Bromwich, D. H., Nicolas, J. P., and Leuschen, C. (2014). Constraining the recent mass balance of pine island and thwaites glaciers, west antarctica, with airborne observations of snow accumulation. *Cryosphere*, 8(4):1375–1392.

Medley, B., McConnell, J. R., Neumann, T. A., Reijmer, C. H., Chellman, N., Sigl, M., and Kipfstuhl, S. (2018). Temperature and Snowfall in Western Queen Maud Land Increasing Faster Than Climate Model Projections. *Geophysical Research Letters*, 45(3):1472–1480.

Medley, B. and Thomas, E. R. (2019). Increased snowfall over the Antarctic Ice Sheet mitigated twentieth-century sea-level rise. *Nature Climate Change*, 9(1):34–39.

Meehl, G. A., Arblaster, J. M., Bitz, C. M., Chung, C. T., and Teng, H. (2016). Antarctic sea-ice expansion between 2000 and 2014 driven by tropical Pacific decadal climate variability. *Nature Geoscience*, 9(8):590–595.

Misson, L. (2004). MAIDEN: a model for analyzing ecosystem processes in dendroecology. *Canadian Journal of Forest Research*, 34(4):874–887.

Monaghan, A. J. and Bromwich, D. H. (2008). Advances in describing recent Antarctic climate variability. *Bulletin of the American Meteorological Society*, 89(9):1295–1306.

Monaghan, A. J., Bromwich, D. H., Fogt, R. L., Wang, S.-H., Mayewski, P. A., Dixon, D. A., Ekaykin, A., Frezzotti, M., Goodwin, I., Isaksson, E., Kaspari, S. D., Morgan, V. I., Oerter, H., Van Ommen, T. D., Van der Veen, C. J., and Wen, J. (2006). Insignificant Change in Antarctic Snowfall Since the International Geophysical Year. *Science*, 313(5788):827–831.

Nash, J. and Sutcliffe, J. (1970). River flow forecasting through conceptual models part i — a discussion of principles. *Journal of Hydrology*, 10(3):282 – 290.

Neukom, R., Barboza, L. A., Erb, M. P., Shi, F., Emile-Geay, J., Evans, M. N., Franke, J., Kaufman, D. S., Lücke, L., Rehfeld, K., Schurer, A., Zhu, F., Brönnimann, S., Hakim, G. J., Henley, B. J., Ljungqvist, F. C., McKay, N., Valler, V., von Gunten, L., and Consortium, P. k. (2019). Consistent multidecadal variability in global temperature reconstructions and simulations over the Common Era. *Nature Geoscience*, 12(8):643–649.

Neukom, R., Schurer, A. P., Steiger, N. J., and Hegerl, G. C. (2018). Possible causes of data model discrepancy in the temperature history of the last Millennium. *Scientific Reports*, 8(1):1–15.

Nicolas, J. P. and Bromwich, D. H. (2011a). Climate of West Antarctica and influence of marine air intrusions. *Journal of Climate*, 24(1):49–67.

Nicolas, J. P. and Bromwich, D. H. (2011b). Precipitation Changes in High Southern Latitudes from Global Reanalyses: A Cautionary Tale. *Surveys in Geophysics*, 32(4-5):475–494.

Nicolas, J. P. and Bromwich, D. H. (2014). New reconstruction of antarctic near-surface temperatures: Multidecadal trends and reliability of global reanalyses. *Journal of Climate*, 27(21):8070–8093.

NOAA National Geophysical Data Center (2009). ETOPO1 1 Arc-Minute Global Relief Model. NOAA National Centers for Environmental Information. .

Oerter, H., Wilhelms, F., Jung-Rothenhausler, F., Goktas, F., Miller, H., Graf, W., and Sommer, S. (2000). Accumulation rates in Dronning Maud Land, Antarctica, as revealed by dielectric-profiling measurements of shallow firn cores. *Annals of Glaciology*, 30:27–34.

Oke, P. R. and Sakov, P. (2008). Representation error of oceanic observations for data assimilation. *Journal of Atmospheric and Oceanic Technology*, 25(6):1004–1017.

Orsi, A. J., Cornuelle, B. D., and Severinghaus, J. P. (2012). Little Ice Age cold interval in West Antarctica: Evidence from borehole temperature at the West Antarctic Ice Sheet (WAIS) Divide. *Geophysical Research Letters*, 39(9).

Osborn, T. J., Jones, P. D., Lister, D. H., Morice, C. P., Simpson, I. R., Winn, J. P., Hogan, E., and Harris, I. C. (2021). Land Surface Air Temperature Variations Across the Globe Updated to 2019: The CRUTEM5 Data Set. *Journal of Geophysical Research: Atmospheres*, 126(2):e2019JD032352.

Otto-Bliesner, B. L., Brady, E. C., Fasullo, J., Jahn, A., Landrum, L., Stevenson, S., Rosenbloom, N., Mai, A., and Strand, G. (2015). Climate Variability and Change since 850 CE: An Ensemble Approach with the Community Earth System Model. *Bulletin of the American Meteorological Society*, 97(5):735–754.

Otto-Bliesner, B. L., Joussaume, S., Braconnot, P., Harrison, S. P., and Abe-Ouchi, A. (2009). Modeling and Data Syntheses of Past Climates: Paleoclimate Modelling Intercomparison Project Phase II Workshop, Eos T. Am. Geophys. Un., 90, p. 93.

PAGES 2k-PMIP3 group (2015). Continental-scale temperature variability in PMIP3 simulations and PAGES 2k regional temperature reconstructions over the past millennium. *Climate of the Past*, 11(12):1673–1699.

PAGES2k Consortium, Ahmed, M., Anchukaitis, K. J., Asrat, A., Borgaonkar, H. P., Braida, M., Buckley, B. M., Büntgen, U., Chase, B. M., Christie, D. A., Cook, E. R., Curran, M. A. J., Diaz, H. F., Esper, J., Fan, Z.-X., Gaire, N. P., Ge, Q., Gergis, J., González-Rouco, J. F., Goosse, H., Grab, S. W., Graham, N., Graham, R., Grosjean, M., Hanhijärvi, S. T., Kaufman, D. S., Kiefer, T., Kimura, K., Korhola, A. A., Krusic, P. J., Lara, A., Lézine, A.-M., Ljungqvist, F. C., Lorrey, A. M., Luterbacher, J., Masson-Delmotte, V., McCarroll, D., McConnell, J. R., McKay, N. P., Morales, M. S., Moy, A. D., Mulvaney, R., Mundo, I. A., Nakatsuka, T., Nash, D. J., Neukom, R., Nicholson, S. E., Oerter, H., Palmer, J. G., Phipps, S. J., Prieto, M. R., Rivera, A., Sano, M., Severi, M., Shanahan, T. M., Shao, X., Shi, F., Sigl, M., Smerdon, J. E., Solomina, O. N., Steig, E. J., Stenni, B., Thamban, M., Trouet, V., Turney, C. S. M., Umer, M., van Ommen, T., Verschuren, D., Viau, A. E., Villalba, R., Vinther, B. M., von Gunten, L., Wagner, S., Wahl, E. R., Wanner, H., Werner, J. P., White, J. W. C., Yasue, K., Zorita, E., and Consortium, P. k. (2013). Continental-scale temperature variability during the past two millennia. *Nature Geoscience*, 6(5):339–346.

Palerme, C., Claud, C., Dufour, A., Genthon, C., Wood, N. B., and L'Ecuyer, T. (2017a). Evaluation of Antarctic snowfall in global meteorological reanalyses. *Atmospheric Research*, 190:104–112.

Palerme, C., Genthon, C., Claud, C., Kay, J. E., Wood, N. B., and L'Ecuyer, T. (2017b). Evaluation of current and projected Antarctic precipitation in CMIP5 models. *Climate Dynamics*, 48(1-2):225–239.

Palerme, C., Kay, J. E., Genthon, C., L'Ecuyer, T., Wood, N. B., and Claud, C. (2014). How much snow falls on the antarctic ice sheet? *The Cryosphere*, 8(4):1577–1587.

Palm, S. P., Kayetha, V., and Yang, Y. (2018). Toward a Satellite-Derived Climatology of Blowing Snow Over Antarctica. *Journal of Geophysical Research: Atmospheres*, 123(18):10,301–10,313.

Palm, S. P., Kayetha, V., Yang, Y., and Pauly, R. (2017). Blowing snow sublimation and transport over antarctica from 11years of calipso observations. *The Cryosphere*, 11(6):2555–2569.

Paolo, F. S., Fricker, H. A., and Padman, L. (2015). Volume loss from Antarctic ice shelves is accelerating. *Science*, 348(6232):327–331.

Parkinson, C. L. (2019). A 40-y record reveals gradual Antarctic sea ice increases followed by decreases at rates far exceeding the rates seen in the Arctic. *Proceedings of the National Academy of Sciences of the United States of America*, 116(29):14414–14423.

Pattyn, F. and Morlighem, M. (2020). The Uncertain Future of the West Antarctic Ice Sheet. *Science*, 367(March):1331–1335.

Pendergrass, A. G., Hakim, G. J., Battisti, D. S., and Roe, G. (2012). Coupled air-mixed layer temperature predictability for climate reconstruction. *Journal of Climate*, 25(2):459–472.

Perkins, W. A. and Hakim, G. J. (2017). Reconstructing paleoclimate fields using online data assimilation with a linear inverse model. *Climate of the Past*, 13(5):421–436.

Philippe, M., Tison, J. L., Fjøsne, K., Hubbard, B., Kjær, H. A., Lenaerts, J. T., Drews, R., Sheldon, S. G., De Bondt, K., Claeys, P., and Pattyn, F. (2016). Ice core evidence for a 20th century increase in surface mass balance in coastal Dronning Maud Land, East Antarctica. *Cryosphere*, 10(5):2501–2516.

Polvani, L. M., Waugh, D. W., Correa, G. J. P., and Son, S.-W. (2011). Stratospheric ozone depletion: The main driver of twentieth-century atmospheric circulation changes in the southern hemisphere. *Journal of Climate*, 24(3):795 – 812.

Post, E., Alley, R. B., Christensen, T. R., Macias-Fauria, M., Forbes, B. C., Gooseff, M. N., Iler, A., Kerby, J. T., Laidre, K. L., Mann, M. E., Olofsson, J., Stroeve, J. C., Ulmer, F., Virginia, R. A., and Wang, M. (2019). The polar regions in a 2°C warmer world. *Science Advances*, 5(12).

Previdi, M. and Polvani, L. M. (2016). Anthropogenic impact on antarctic surface mass balance, currently masked by natural variability, to emerge by mid-century. *Environmental Research Letters*, 11(9):094001.

Pritchard, H. D., Ligtenberg, S. R., Fricker, H. A., Vaughan, D. G., Van Den Broeke, M. R., and Padman, L. (2012). Antarctic ice-sheet loss driven by basal melting of ice shelves. *Nature*, 484(7395):502–505.

Raphael, M. N. (2004). A zonal wave 3 index for the Southern Hemisphere. *Geophysical Research Letters*, 31(23):1–4.

Raphael, M. N. and Hobbs, W. (2014). The influence of the large-scale atmospheric circulation on antarctic sea ice during ice advance and retreat seasons. *Geophysical Research Letters*, 41(14):5037–5045.

Raphael, M. N., Holland, M. M., Landrum, L., and Hobbs, W. R. (2019). Links between the Amundsen Sea Low and sea ice in the Ross Sea: seasonal and interannual relationships. *Climate Dynamics*, 52(3):2333–2349.

Raphael, M. N., Marshall, G. J., Turner, J., Fogt, R. L., Schneider, D., Dixon, D. A., Hosking, J. S., Jones, J. M., and Hobbs, W. R. (2016). The Amundsen sea low: Variability, change, and impact on Antarctic climate. *Bulletin of the American Meteorological Society*, 97(1):111–121.

Rayner, N. A., Parker, E. B., Horton, C. K., Holland, C. K., Alexander, L. V., Rowell, D. P., Kent, E. C., and Kaplan, A. (2003). Global analyses of sea surface temperature, sea ice, and night marine air temperature since the late nineteenth century. *Journal of Geophysical Research*, 108(D14):4407.

Rezsöhazy, J., Goosse, H., Guiot, J., Gennaretti, F., Boucher, E., André, F., and Jonard, M. (2020). Application and evaluation of the dendroclimatic process-based model MAIDEN during the last century in Canada and Europe. *Climate of the Past*, 16(3):1043–1059.

Rhodes, R. H., Yang, X., and Wolff, E. W. (2018). Sea ice versus storms: What controls sea salt in arctic ice cores? *Geophysical Research Letters*, 45(11):5572–5580.

Rhodes, R. H., Yang, X., Wolff, E. W., McConnell, J. R., and Frey, M. M. (2017). Sea ice as a source of sea salt aerosol to greenland ice cores: a model-based study. *Atmospheric Chemistry and Physics*, 17(15):9417–9433.

Ricaud, P., Bazile, E., Del Guasta, M., Lanconelli, C., Grigioni, P., and Mahjoub, A. (2017). Genesis of diamond dust, ice fog and thick cloud episodes observed and modelled above Dome C, Antarctica. *Atmospheric Chemistry and Physics*, 17(8):5221–5237.

Rignot, E., Jacobs, S., Mouginot, J., and Scheuchl, B. (2013). Ice-shelf melting around antarctica. *Science*, 341(6143):266–270.

Rignot, E., Mouginot, J., Scheuchl, B., van den Broeke, M. R., van Wessem, M. J., and Morlighem, M. (2019). Four decades of Antarctic Ice Sheet mass balance from 1979-2017. *Proceedings of the National Academy of Sciences*, pages 1–9.

Roach, L. A., Dörr, J., Holmes, C. R., Massonnet, F., Blockley, E. W., Notz, D., Rackow, T., Raphael, M. N., O'Farrell, S. P., Bailey, D. A., and Bitz, C. M. (2020). Antarctic Sea Ice Area in CMIP6. *Geophysical Research Letters*, 47(9):1–24.

Rotstayn, L. D., Collier, M. A., Dix, M. R., Feng, Y., Gordon, H. B., O'Farrell, S. P., Smith, I. N., and Syktus, J. (2010). Improved simulation of Australian climate and ENSO-related rainfall variability in a global climate model with an interactive aerosol treatment. *International Journal of Climatology*, 30(7):1067–1088.

Roussel, M. L., Lemonnier, F., Genthon, C., and Krinner, G. (2020). Brief communication: Evaluating Antarctic precipitation in ERA5 and CMIP6 against CloudSat observations. *Cryosphere*, 14(8):2715–2727.

Rye, C. D., Marshall, J., Kelley, M., Russell, G., Nazarenko, L. S., Kostov, Y., Schmidt, G. A., and Hansen, J. (2020). Antarctic Glacial Melt as a Driver of Recent Southern Ocean Climate Trends. *Geophysical Research Letters*, 47(11):0–3.

Salinger, M., Renwick, J., and Mullan, A. (2001). Interdecadal pacific oscillation and south pacific climate. *International Journal of Climatology*, 21(14):1705–1721.

Schär, C., Vidale, P. L., Lüthi, D., Frei, C., Häberli, C., Liniger, M. A., and Appenzeller, C. (2004). The role of increasing temperature variability in European summer heatwaves. *Nature*, 427(6972):332–336.

Schlosser, E., Anschütz, H., Divine, D., Martma, T., Sinisalo, A., Altnau, S., and Isaksson, E. (2014). Recent climate tendencies on an East Antarctic ice shelf inferred from a shallow firn core network. *Journal of Geophysical Research Atmospheres*, 119:6578–6595.

Schmidt, G. A., Jungclaus, J. H., Ammann, C. M., Bard, E., Braconnot, P., Crowley, T. J., Delaygue, G., Joos, F., Krivova, N. A., Muscheler, R., Otto-Bliesner, B. L., Pongratz, J., Shindell, D. T., Solanki, S. K., Steinhilber, F., and Vieira, L. E. A. (2011). Climate forcing reconstructions for use in PMIP simulations of the Last Millennium (v1.0). *Geoscientific Model Development*, 4:33–45.

Schmidt, G. A., Jungclaus, J. H., Ammann, C. M., Bard, E., Braconnot, P., Crowley, T. J., Delaygue, G., Joos, F., Krivova, N. A., Muscheler, R., Otto-Bliesner, B. L., Pongratz, J., Shindell, D. T., Solanki, S. K., Steinhilber, F., and Vieira, L. E. A. (2012). Climate forcing reconstructions for use in PMIP simulations of the Last Millennium (v1.1). *Geoscientific Model Development*, 5(1):185–191.

Schmidt, G. A., Kelley, M., Nazarenko, L., Ruedy, R., Russell, G. L., Aleinov, I., Bauer, M., Bauer, S. E., Bhat, M. K., Bleck, R., Canuto, V., Chen, Y.-h., Cheng, Y., Clune, T. L., Genio, A. D., Fainchtein, R. D., Faluvegi, G., Hansen, J. E., Healy, R. J., Kiang, N. Y., Koch, D., Lacis, A. A., Legrande, A. N., Lerner, J., Lo, K. K., Matthews, E. E., Menon, S., Miller, R. L., Oinas, V., and Oloso, A. O. (2014). Journal of Advances in Modeling Earth Systems contributions to the CMIP5 archive. *Journal of Advances in Modeling Earth Systems*, 6:141–184.

Schneider, D. P., Deser, C., and Okumura, Y. (2012). An assessment and interpretation of the observed warming of West Antarctica in the austral spring. *Climate Dynamics*, 38(1-2):323–347.

Schneider, S. H. and Dickinson, R. E. (1974). Climate modeling. *Reviews of Geophysics*, 12(3):447–493.

Schneider, U., Becker, A., Finger, P., Meyer-Christoffer, A., Ziese, M., and Rudolf, B. (2014). GPCC's new land surface precipitation climatology based on quality-controlled in situ data and its role in quantifying the global water cycle. *Theoretical and Applied Climatology*, 115(1-2):15–40.

Schwarz, G. (1978). Estimating the Dimension of a Model. *Ann. Statist.*, 6(2):461–464.

Seager, R. and Henderson, N. (2013). Diagnostic computation of moisture budgets in the ERA-interim reanalysis with reference to analysis of CMIP-archived atmospheric model data. *Journal of Climate*, 26(20):7876–7901.

Seager, R., Naik, N., and Vecchi, G. A. (2010). Thermodynamic and dynamic mechanisms for large-scale changes in the hydrological cycle in response to global warming. *Journal of Climate*, 23(17):4651–4668.

Sheffield, J., Goteti, G., and Wood, E. F. (2006). Development of a 50-yr high-resolution global dataset of meteorological forcings for land surface modeling. *Journal of Climate*, 19(12):3088–3111.

Shepherd, A., Fricker, H. A., and Farrell, S. L. (2018a). Trends and connections across the Antarctic cryosphere. *Nature*, 558(7709):223–232.

Shepherd, A., Ivins, E., Rignot, E., Smith, B., van den Broeke, M., Velicogna, I., Whitehouse, P., Briggs, K., Joughin, I., Krinner, G., Nowicki, S., Payne, T., Scambos, T., Schlegel, N., A, G., Agosta, C., Ahlstrøm, A., Babonis, G., Barletta, V., Blazquez, A., Bonin, J., Csatho, B., Cullather, R., Felikson, D., Fettweis, X., Forsberg, R., Gallee, H., Gardner, A., Gilbert, L., Groh, A., Gunter, B., Hanna, E., Harig, C., Helm, V., Horvath, A., Horwath, M., Khan, S., Kjeldsen, K. K., Konrad, H., Langen, P., Lecavalier, B., Loomis, B., Luthcke, S., McMillan, M., Melini, D., Mernild, S., Mohajerani, Y., Moore, P., Mouginot, J., Moyano, G., Muir, A., Nagler, T., Nield, G., Nilsson, J., Noel, B., Otosaka, I., Pattle, M. E., Peltier, W. R., Pie, N., Rietbroek, R., Rott, H., Sandberg-Sørensen, L., Sasgen, I., Save, H., Scheuchl, B., Schrama, E., Schröder, L., Seo, K.-W., Simonsen, S., Slater, T., Spada, G., Sutterley, T., Talpe, M., Tarasov, L., van de Berg, W. J., van der Wal, W., van Wessem, M., Vishwakarma, B. D., Wiese, D., Wouters, B., and Team, T. I. (2018b). Mass balance of the Antarctic Ice Sheet from 1992 to 2017. *Nature*, 558(7709):219–222.

Shepherd, A., Ivins, E., Rignot, E., Smith, B., van den Broeke, M., Velicogna, I., Whitehouse, P., Briggs, K., Joughin, I., Krinner, G., Nowicki, S., Payne, T., Scambos, T., Schlegel, N., A, G., Agosta, C., Ahlstrøm, A., Babonis, G., Barletta, V. R., Bjørk, A. A., Blazquez, A., Bonin, J., Colgan, W., Csatho, B., Cullather, R., Engdahl, M. E., Felikson, D., Fettweis, X., Forsberg, R., Hogg, A. E.,

Gallee, H., Gardner, A., Gilbert, L., Gourmelen, N., Groh, A., Gunter, B., Hanna, E., Harig, C., Helm, V., Horvath, A., Horwath, M., Khan, S., Kjeldsen, K. K., Konrad, H., Langen, P. L., Lecavalier, B., Loomis, B., Luthcke, S., McMillan, M., Melini, D., Mernild, S., Mohajerani, Y., Moore, P., Mottram, R., Mouginot, J., Moyano, G., Muir, A., Nagler, T., Nield, G., Nilsson, J., Noël, B., Otosaka, I., Pattle, M. E., Peltier, W. R., Pie, N., Rietbroek, R., Rott, H., Sandberg Sørensen, L., Sasgen, I., Save, H., Scheuchl, B., Schrama, E., Schröder, L., Seo, K.-W., Simonsen, S. B., Slater, T., Spada, G., Sutterley, T., Talpe, M., Tarasov, L., van de Berg, W. J., van der Wal, W., van Wessem, M., Vishwakarma, B. D., Wiese, D., Wilton, D., Wagner, T., Wouters, B., Wuite, J., and Team, T. I. (2020). Mass balance of the Greenland Ice Sheet from 1992 to 2018. *Nature*, 579(7798):233–239.

Shepherd, A., Ivins, E. R., A, G., Barletta, V. R., Bentley, M. J., Bettadpur, S., Briggs, K. H., Bromwich, D. H., Forsberg, R., Galin, N., Horwath, M., Jacobs, S., Joughin, I., King, M. A., Lenaerts, J. T. M., Li, J., Ligtenberg, S. R. M., Luckman, A., Luthcke, S. B., McMillan, M., Meister, R., Milne, G., Mouginot, J., Muir, A., Nicolas, J. P., Paden, J., Payne, A. J., Pritchard, H., Rignot, E., Rott, H., Sørensen, L. S., Scambos, T. A., Scheuchl, B., Schrama, E. J. O., Smith, B., Sundal, A. V., van Angelen, J. H., van de Berg, W. J., van den Broeke, M. R., Vaughan, D. G., Velicogna, I., Wahr, J., Whitehouse, P. L., Wingham, D. J., Yi, D., Young, D., and Zwally, H. J. (2012). A Reconciled Estimate of Ice-Sheet Mass Balance. *Science*, 338(6111):1183–1189.

Sime, L. C., Hopcroft, P. O., and Rhodes, R. H. (2019). Impact of abrupt sea ice loss on greenland water isotopes during the last glacial period. *Proceedings of the National Academy of Sciences*, 116(10):4099–4104.

Sime, L. C., Marshall, G. J., Mulvaney, R., and Thomas, E. R. (2009). Interpreting temperature information from ice cores along the Antarctic Peninsula: ERA40 analysis. *Geophysical Research Letters*, 36(18):1–5.

Sime, L. C., Tindall, J. C., Wolff, E. W., Connolley, W. M., and Valdes, P. J. (2008). Antarctic isotopic thermometer during a CO<inf>2</inf> forced warming event. *Journal of Geophysical Research Atmospheres*, 113(24):1–16.

Sjolte, J., Sturm, C., Adolphi, F., Vinther, B. M., Werner, M., Lohmann, G., and Muscheler, R. (2018). Solar and volcanic forcing of North Atlantic climate inferred from a process-based reconstruction. *Climate of the Past Discussions*, (April):1–22.

Smith, B., Fricker, H. A., Gardner, A. S., Medley, B., Nilsson, J., Paolo, F. S., Holschuh, N., Adusumilli, S., Brunt, K., Csatho, B., Harbeck, K., Markus, T., Neumann, T., R., S. M., and Zwally, H. J. (2020). Pervasive ice sheet mass loss reflects competing ocean and atmosphere processes. *Science*, 5845(April):1–13.

Souverijns, N., Gossart, A., Gorodetskaya, I. V., Lhermitte, S., Mangold, A., Laffineur, Q., Delcloo, A., and van Lipzig, N. P. M. (2018). How does the ice sheet surface mass balance relate to snowfall? insights from a ground-based precipitation radar in east antarctica. *The Cryosphere*, 12(6):1987–2003.

Steig, E. J., Ding, Q., Battisti, D. S., and Jenkins, A. (2012). Tropical forcing of circumpolar deep water inflow and outlet glacier thinning in the amundsen sea embayment, west antarctica. *Annals of Glaciology*, 53(60):19–28.

Steig, E. J., Ding, Q., White, J. W. C., Küttel, M., Rupper, S. B., Neumann, T. A., Neff, P. D., Gallant, A. J. E., Mayewski, P. A., Taylor, K. C., Hoffmann, G., Dixon, D. A., Schoenemann, S. W., Markle, B. R., Fudge, T. J., Schneider, D. P., Schauer, A. J., Teel, R. P., Vaughn, B. H., Burgener, L., Williams, J., and Korotkikh, E. (2013). Recent climate and ice-sheet changes in West Antarctica compared with the past 2,000 years. *Nature Geoscience*, 6:372–375.

Steig, E. J. and Neff, P. D. (2018). The prescience of paleoclimatology and the future of the Antarctic ice sheet. *Nature Communications*, 9(1):11–13.

Steig, E. J., Schneider, D. P., Rutherford, S. D., Mann, M. E., Comiso, J. C., and Shindell, D. T. (2009). Warming of the Antarctic ice-sheet surface since the 1957 International Geophysical Year. *Nature*, 457(7228):459–462.

Steiger, N. J., Hakim, G. J., Steig, E. J., Battisti, D. S., and Roe, G. H. (2014). Assimilation of time-averaged pseudoproxies for climate reconstruction. *Journal of Climate*, 27(1):426–441.

Steiger, N. J., Smerdon, J. E., Cook, E. R., and Cook, B. I. (2018). A reconstruction of global hydroclimate and dynamical variables over the Common Era. *Scientific Data*, 5:1–15.

Steiger, N. J., Steig, E. J., Dee, S. G., Roe, G. H., and Hakim, G. J. (2017). Climate reconstruction using data assimilation of water isotope ratios from ice cores. *Journal of Geophysical Research: Atmospheres*, 122(3):1545–1568.

Stenni, B., Curran, M. A., Abram, N. J., Orsi, A., Goursaud, S., Masson-Delmotte, V., Neukom, R., Goosse, H., Divine, D., Van Ommen, T., Steig, E. J., Dixon, D. A., Thomas, E. R., Bertler, N. A., Isaksson, E., Ekaykin, A., Werner, M., and Frezzotti, M. (2017). Antarctic climate variability on regional and continental scales over the last 2000 years. *Climate of the Past*, 13(11):1609–1634.

Stevens, B., Giorgetta, M., Esch, M., Mauritsen, T., Crueger, T., Rast, S., Salzmann, M., Schmidt, H., Bader, J., Block, K., Brokopf, R., Fast, I., Kinne, S., Kornblueh, L., Lohmann, U., Pincus, R., Reichler, T., and Roeckner, E. (2013). Atmospheric component of the MPI-M earth system model: ECHAM6. *Journal of Advances in Modeling Earth Systems*, 5(2):146–172.

Stevenson, S., Otto-Bliesner, B. L., Brady, E. C., Nusbaumer, J., Tabor, C., Tomas, R., Noone, D. C., and Liu, Z. (2019). Volcanic Eruption Signatures in the Isotope-Enabled Last Millennium Ensemble. *Paleoceanography and Paleoclimatology*, 34(8):1534–1552.

Swart, N. C. and Fyfe, J. C. (2013). The influence of recent Antarctic ice sheet retreat on simulated sea ice area trends. *Geophysical Research Letters*, 40(16):4328–4332.

Swart, N. C., Fyfe, J. C., Gillett, N., and Marshall, G. J. (2015). Comparing trends in the southern annular mode and surface westerly jet. *Journal of Climate*, 28(22):8840–8859.

Tardif, R., Hakim, G. J., Perkins, W. A., Horlick, K. A., Erb, M. P., Emile-Geay, J., Anderson, D. M., Steig, E. J., and Noone, D. (2018). Last Millennium Reanalysis with an expanded proxy database and seasonal proxy modeling. *Climate of the Past Discussions*, pages 1–37.

Taylor, K. E., Stouffer, R. J., and Meehl, G. A. (2012). An overview of CMIP5 and the experiment design. *Bulletin of the American Meteorological Society*, 93(4):485–498.

Tetzner, D., Thomas, E., and Allen, C. (2019). A validation of era5 reanalysis data in the southern antarctic peninsula—ellsworth land region, and its implications for ice core studies. *Geosciences*, 9(7).

Thoma, M., Jenkins, A., Holland, D., and Jacobs, S. (2008). Modelling Circumpolar Deep Water intrusions on the Amundsen Sea continental shelf, Antarctica. *Geophysical Research Letters*, 35(18):2–7.

Thomas, E. R. and Abram, N. J. (2016a). Ice core reconstruction of sea ice change in the Amundsen-Ross Seas since 1702 A.D. *Geophysical Research Letters*, 43(10):5309–5317.

Thomas, E. R. and Abram, N. J. (2016b). Ice core reconstruction of sea ice change in the Amundsen-Ross Seas since 1702 A.D. *Geophysical Research Letters*, 43(10):5309–5317.

Thomas, E. R., Allen, C. S., Etourneau, J., King, A. C. F., Severi, M., Winton, V. H. L., Mueller, J., Crosta, X., and Peck, V. L. (2019). Antarctic Sea Ice Proxies from Marine and Ice Core Archives Suitable for Reconstructing Sea Ice over the past 2000 Years. *Geosciences*, pages 1–33.

Thomas, E. R. and Bracegirdle, T. J. (2015). Precipitation pathways for five new ice core sites in Ellsworth Land, West Antarctica. *Climate Dynamics*, 44(7-8):2067–2078.

Thomas, E. R., Bracegirdle, T. J., Turner, J., and Wolff, E. W. (2013). A 308 year record of climate variability in West Antarctica. *Geophysical Research Letters*, 40(20):5492–5496.

Thomas, E. R., Hosking, J. S., Tuckwell, R. R., Warren, R. A., and Ludlow, E. C. (2015). Twentieth century increase in snowfall in coastal West Antarctica. *Geophysical Research Letters*, 42(21):9387–9393.

Thomas, E. R., Marshall, G. J., and McConnell, J. R. (2008). A doubling in snow accumulation in the western Antarctic Peninsula since 1850. *Geophysical Research Letters*, 35(L01706):1–5.

Thomas, E. R., Melchior Van Wessem, J., Roberts, J., Isaksson, E., Schlosser, E., Fudge, T. J., Vallelonga, P., Medley, B., Lenaerts, J., Bertler, N., Van Den Broeke, M. R., Dixon, D. A., Frezzotti, M.,

Stenni, B., Curran, M., and Ekaykin, A. A. (2017). Regional Antarctic snow accumulation over the past 1000 years. *Climate of the Past*, 13(11):1491–1513.

Thompson, D. W., Solomon, S., Kushner, P. J., England, M. H., Grise, K. M., and Karoly, D. J. (2011a). Signatures of the Antarctic ozone hole in Southern Hemisphere surface climate change. *Nature Geoscience*, 4(11):741–749.

Thompson, D. W. J., Solomon, S., Kushner, P. J., England, M. H., Grise, K. M., and Karoly, D. J. (2011b). Signatures of the Antarctic ozone hole in Southern Hemisphere surface climate change. *Nature Geoscience*, 4(11):741–749.

Tindall, J. C., Valdes, P. J., and Sime, L. C. (2009). Stable water isotopes in HadCM3: Isotopic signature of El Niño-Southern Oscillation and the tropical amount effect. *Journal of Geophysical Research Atmospheres*, 114(4):1–12.

Trenberth, K. (1992). *Climate System Modeling*. Cambridge University Press.

Trenberth, K. E., Fasullo, J. T., and Mackaro, J. (2011). Atmospheric Moisture Transports from Ocean to Land and Global Energy Flows in Reanalyses. *Journal of Climate*, 24(18):4907–4924.

Trusel, L. D., Frey, K. E., Das, S. B., Karnauskas, K. B., Kuipers Munneke, P., Van Meijgaard, E., and Van Den Broeke, M. R. (2015). Divergent trajectories of Antarctic surface melt under two twenty-first-century climate scenarios. *Nature Geoscience*, 8(12):927–932.

Turner, J. (2004). The El Niño-Southern Oscillation and Antarctica. *International Journal of Climatology*, 24(1):1–31.

Turner, J., Colwell, S. R., Marshall, G. J., Lachlan-Cope, T. A., Carleton, A. M., Jones, P. D., Lagun, V., Reid, P. A., and Iagovkina, S. (2004). The SCAR READER project: Toward a high-quality database of mean Antarctic meteorological observations. *Journal of Climate*, 17(14):2890–2898.

Turner, J., Colwell, S. R., Marshall, G. J., Lachlan-Cope, T. A., Carleton, A. M., Jones, P. D., Lagun, V., Reid, P. A., and Iagovkina, S. (2005a). Antarctic climate change during the last 50 years. *International Journal of Climatology*, 25(3):279–294.

Turner, J., Connolley, W. M., and Marshall, G. J. (2006). The performance of the hadley centre climate model (HadCM3) in high southern latitudes. 112:91–112.

Turner, J., Lachlan-Cope, T., Colwell, S., and Marshall, G. J. (2005b). A positive trend in western Antarctic Peninsula precipitation over the last 50 years reflecting regional and Antarctic-wide atmospheric circulation changes. *Annals of Glaciology*, 41:85–91.

Turner, J., Lu, H., White, I., King, J. C., Phillips, T., Hosking, J. S., Bracegirdle, T. J., Marshall, G. J., Mulvaney, R., and Deb, P. (2016a). Absence of 21st century warming on Antarctic Peninsula consistent with natural variability. *Nature*, 535(7612):411–415.

Turner, J., Marshall, G. J., Clem, K., Colwell, S., Phillips, T., and Lu, H. (2019a). Antarctic temperature variability and change from station data. *International Journal of Climatology*, (June):1–22.

Turner, J., Orr, A., Gudmundsson, G. H., Jenkins, A., Bingham, R. G., Hillenbrand, C. D., and Bracegirdle, T. J. (2017). Atmosphere-ocean-ice interactions in the Amundsen Sea Embayment, West Antarctica. *Reviews of Geophysics*, 55(1):235–276.

Turner, J., Phillips, T., Hosking, J. S., Marshall, G. J., and Orr, A. (2013). The amundsen sea low. *International Journal of Climatology*, 33(7):1818–1829.

Turner, J., Phillips, T., Thamban, M., Rahaman, W., Marshall, G. J., Wille, J. D., Favier, V., Winton, V. H. L., Thomas, E., Wang, Z., van den Broeke, M., Hosking, J. S., and Lachlan-Cope, T. (2019b). The Dominant Role of Extreme Precipitation Events in Antarctic Snowfall Variability. *Geophysical Research Letters*, 46(6):3502–3511.

Turner, J., Scott Hosking, J., Marshall, G. J., Phillips, T., and Bracegirdle, T. J. (2016b). Antarctic sea ice increase consistent with intrinsic variability of the Amundsen sea low. *Climate Dynamics*, 46(7-8):2391–2402.

Unden, P., Rontu, L., Järvinen, H., Lynch, P., Calvo, J., Cats, G., Cuxart, J., Eerola, K., Fortelius, C., Garcia-Moya, J. A., Jones, C., Lenderlink, G., McDonald, A., McGrath, R., Navascues, B., Woetman Nielsen, N., Odegaard, V., Rodriguez, E., Rummukainen, M., Room, R., Sattler, K., Sass, B. H.,

Savijarvi, O., Wichers Schreur, B., Sigg, R., The, H., and Tijm, A. (2002). HIRLAM-5 Scientific Documentation. *Environmental Geology*, 43(1):144.

van de Berg, W. J., van den Broeke, M. R., Reijmer, C. H., and van Meijgaard, E. (2006). Reassessment of the Antarctic surface mass balance using calibrated output of a regional atmospheric climate model. *Journal of Geophysical Research: Atmospheres*, 111(D11).

van Den Broeke, M., Van De Berg, W. J., and Van Meijgaard, E. (2008). Firn depth correction along the Antarctic grounding line. *Antarctic Science*, 20(5):513–517.

Van den Broeke, M. R., Reijmer, C., Van As, D., Van de Wal, R., and Oerlemans, J. (2005). Seasonal cycles of Antarctic surface energy balance from automatic weather stations. *Annals of Glaciology*, 41:131–139.

van den Broeke, M. R. and van Lipzig, N. P. M. (2004). Changes in Antarctic temperature, wind and precipitation in response to the Antarctic Oscillation. *Annals of Glaciology*, 39:119–126.

van Kampenhout, L., Lenaerts, J. T., Lipscomb, W. H., Lhermitte, S., Noël, B., Vizcaíno, M., Sacks, W. J., and van den Broeke, M. R. (2020). Present-Day Greenland Ice Sheet Climate and Surface Mass Balance in CESM2. *Journal of Geophysical Research: Earth Surface*, 125(2):1–25.

van Kampenhout, L., Rhoades, A. M., Herrington, A. R., Zarzycki, C. M., Lenaerts, J. T. M., Sacks, W. J., and van den Broeke, M. R. (2018). Regional Grid Refinement in an Earth System Model: Impacts on the Simulated Greenland Surface Mass Balance. *The Cryosphere Discussions*, (December):1–25.

van Leeuwen, P. J. (2009). Particle Filtering in Geophysical Systems. *Monthly Weather Review*, 137(12):4089–4114.

van Lipzig, N. P. M., King, J. C., Lachlan-Cope, T. A., and van den Broeke, M. R. (2004). Precipitation, sublimation, and snow drift in the antarctic peninsula region from a regional atmospheric model. *Journal of Geophysical Research: Atmospheres*, 109(D24).

van Lipzig, N. P. M., van Meijgaard, E., and Oerlemans, J. (2002). Temperature Sensitivity of the Antarctic Surface Mass Balance in a Regional Atmospheric Climate Model. *Journal of Climate*, 15(19):2758–2774.

van Wessem, J. M., Ligtenberg, S. R., Reijmer, C. H., Van De Berg, W. J., Van Den Broeke, M. R., Barrand, N. E., Thomas, E. R., Turner, J., Wuite, J., Scambos, T. A., and Van Meijgaard, E. (2016). The modelled surface mass balance of the Antarctic Peninsula at 5.5 km horizontal resolution. *Cryosphere*, 10(1):271–285.

van Wessem, J. M., van de Berg, W. J., Noël, B. P. Y., van Meijgaard, E., Birnbaum, G., Jakobs, C. L., Krüger, K., Lenaerts, J. T. M., Lhermitte, S., Ligtenberg, S. R. M., Medley, B., Reijmer, C. H., van Tricht, K., Trusel, L. D., van Ulft, L. H., Wouters, B., Wuite, J., and van den Broeke, M. R. (2018). Modelling the climate and surface mass balance of polar ice sheets using RACMO2, part 2: Antarctica (1979–2016). *The Cryosphere*, 12:1479–1498.

Vannitsem, S., Dalaiden, Q., and Goosse, H. (2019). Testing for Dynamical Dependence: Application to the Surface Mass Balance Over Antarctica. *Geophysical Research Letters*, 46(21):12125–12135.

Vaughan, D. G., Marshall, G. J., Connolley, W. M., Parkinson, C., Mulvaney, R., Hodgson, D. A., King, J. C., Pudsey, C. J., and Turner, J. (2003). Recent rapid regional climate warming on the Antarctic Peninsula. *Climatic Change*, 60(3):243–274.

Vizcaíno, M., Lipscomb, W. H., Sacks, W. J., Van Angelen, J. H., Wouters, B., and Van Den Broeke, M. R. (2013). Greenland surface mass balance as simulated by the community earth system model. Part I: Model evaluation and 1850-2005 results. *Journal of Climate*, 26(20):7793–7812.

Wang, Y., Ding, M., van Wessem, J. M., Schlosser, E., Altnau, S., van den Broeke, M. R., Lenaerts, J. T., Thomas, E. R., Isaksson, E., Wang, J., and Sun, W. (2016). A comparison of Antarctic ice sheet surface mass balance from atmospheric climate models and in situ observations. *Journal of Climate*, 29(14):5317–5337.

Wang, Y., Huai, B., Thomas, E. R., Broeke, M. R., Wessem, J. M., and Schlosser, E. (2019). A new 200-year spatial reconstruction of West Antarctic surface mass balance. *Journal of Geophysical Research: Atmospheres*, pages 5282–5295.

Wang, Y., Thomas, E. R., Hou, S., Huai, B., Wu, S., Sun, W., Qi, S., Ding, M., and Zhang, Y. (2017). Snow Accumulation Variability Over the West Antarctic Ice Sheet Since 1900: A Comparison of Ice Core Records With ERA-20C Reanalysis. *Geophysical Research Letters*, 44(22):11,482–11,490.

Watkins, A. J. and Mardia, K. V. (1992). Maximum likelihood estimation and prediction mean square error in the spatial linear model. *Journal of Applied Statistics*, 19(1):49–59.

Widmann, M., Goosse, H., Van Der Schrier, G., Schnur, R., and Barkmeijer, J. (2010). Using data assimilation to study extratropical Northern Hemisphere climate over the last millennium. *Climate of the Past*, 6(5):627–644.

Wille, J. D., Favier, V., Dufour, A., Gorodetskaya, I. V., Turner, J., Agosta, C., and Codron, F. (2019). West Antarctic surface melt triggered by atmospheric rivers. *Nature Geoscience*, 12(11):911–916.

Wu, T., Song, L., Li, W., Wang, Z., Zhang, H., Xin, X., Zhang, Y., Zhang, L., Wu, F., Y, L., Zhang, F., Shi, X., Chu, M., Zhang, J., Fang, Y., Wang, F., Lu, Y., Liu, X., Wei, M., Liu, Q., Zhou, W., Dong, M., Zhao, Q., Ji, J., Laurent, L., and M, Z. (2014). An overview of BCC climate system model development and application for climate change studies. *Journal of Meteorological Research*, 28(1):34–56.

Yuan, X., Kaplan, M. R., and Cane, M. A. (2018). The interconnected global climate system-a review of tropical-polar teleconnections. *Journal of Climate*, 31(15):5765–5792.

Yukimoto, S., Adachi, Y., Hosaka, M., Sakami, T., Yoshimura, H., Hirabara, M., Tanaka, T. Y., Shindo, E., Tsujino, H., Deushi, M., Mizuta, R., Yabu, S., Obata, A., Nakano, H., Tsuyoshi, K., Ose, T., and Kitoh, A. (2012). A New Global Climate Model of the Meteorological Research Institute: MRI-CGCM3 – Model Description and Basic Performance –. *Journal of the Meteorological Society of Japan*, 90A(0):23–64.

Zheng, F., Li, J., Clark, R. T., and Nnamchi, H. C. (2013). Simulation and projection of the Southern Hemisphere annular mode in CMIP5 models. *Journal of Climate*, 26(24):9860–9879.

Zhu, Y. and Newell, R. E. (1994). Atmospheric rivers and bombs. *Geophysical Research Letters*, 21(18):1999–2002.

Zunz, V., Goosse, H., and Massonnet, F. (2013). How does internal variability influence the ability of CMIP5 models to reproduce the recent trend in Southern Ocean sea ice extent? *Cryosphere*, 7(2):451–468.